Justus-Liebig-Universität Gießen

Fachbereich Medizin

Aus dem Zentrum für Innere Medizin
Abteilung für Kardiologie und Angiologie
des Universitätsklinikums Gießen und Marburg GmbH, Standort Gießen
Klinikdirektor: Prof. Dr. med. Christian Hamm

Evaluation neuer Technologien für die perkutane Koronarintervention

Habilitationsschrift in kumulativer Form
zur Erlangung der Lehrbefähigung für das Fach Innere Medizin
im Fachbereich Medizin der Justus-Liebig-Universität Gießen

vorgelegt von
Dr. med. Florian Blachutzik
Gießen 2023

Bibliographische Beschreibung

Blachutzik, Florian

Evaluation neuer Technologien für die perkutane Koronarintervention

Habilitationsschrift in kumulativer Form

142 S.

Gießen 2023

Inhaltsverzeichnis Seite

Abkürzungsverzeichnis

Atm	Atmosphären
BMS	Bare-Metal Stents
BRS	Bioresorbierbare Scaffolds
Cx	Ramus circumflexus
DAPT	Duale Thrombozytenaggregationshemmung
DES	Drug-Eluting Stents
IVL	Intravaskuläre Lithoplastie
IVUS	Intravaskulärer Ultraschall
MSA	Minimale Stentfläche
NC	Non-compliant
NLI	Normalisierte Lichtintensität
OCT	Optische Kohärenztomographie
PCI	Perkutane Koronarintervention
PLLA	Poly-L-Lactid
PSLIA	Peri-strut low intensity areas
PTA	Perkutane transluminale Angioplastie
PTCA	Perkutane transluminale Koronarangioplastie
RCA	Rechte Koronararterie
RIVA	Ramus interventricularis anterior = Left anterior decending artery (LAD)

Der vorliegenden kumulativen Habilitationsschrift liegen folgende Publikationen zu Grunde:

1. **Blachutzik F**, Achenbach S, Nef H, Hamm C, Dörr O, Boeder N, Marwan M, Tröbs M, Schneider R, Röther J, Schlundt C. Optical coherence tomography: influence of contrast concentration on image quality and diagnostic confidence. Heart and Vessels 2017; 32(6): 653-659

2. **Blachutzik F**, Boeder N, Wiebe J, Mattesini A, Dörr O, Most A, Bauer T, Röther J, Tröbs M, Schlundt C, Achenbach S, Hamm CW, Nef HM. Post-dilatation after implantation of bioresorbable everolimus- and novolimus-eluting scaffolds: an observational optical coherence tomography study of acute mechanical effects. Clin Res Cardiol 2017; 106(4): 271-279

3. **Blachutzik F**, Boeder N, Wiebe J, Mattesini A, Dörr O, Most A, Bauer T, Röther J, Tröbs M, Schlundt C, Achenbach S, Hamm CW, Nef HM. Overlapping implantation of bioresorbable novolimus-eluting scaffolds: An observational optical coherence tomography study. Heart and Vessels 2017; 32(7): 781-789

4. **Blachutzik F**, Achenbach S, Marwan M, Tröbs M, Boeder N, Doerr O, Weissner M, Bauer T, Nef H, Hamm C, Schlundt C. OCT-assessment of scaffold resorption: Analysis of strut intensity by a new resorption index for poly-l-lactic acid bioresorbable vascular scaffolds. Catheter Cardiovasc Interv 2019; 94(7): 928-935

5. **Blachutzik F**, Achenbach S, Tröbs M, Marwan M, Weissner M, Nef H, Schlundt C. Effect of non-compliant balloon postdilatation on magnesium-based bioresorbable vascular scaffolds. Catheter Cardiovasc Interv 2019; 93(2): 202-207

6. **Blachutzik F**, Achenbach S, Marwan M, Röther J, Tröbs M, Schneider R, Nef H, Weissner M, Schlundt C. Major coronary evaginations following implantation of bioresorbable vascular scaffolds - Clinical and OCT characteristics. Cardiovasc Revasc Med 2019; 20(6): 485-491

7. **Blachutzik F**, Honton B, Escaned J, Hill JM, Werner N, Banning AP, Lansky AJ, Schlattner S, De Bruyne B, Di Mario C, Dörr O, Hamm C, Nef HM. Safety and effectiveness of coronary intravascular lithotripsy in eccentric calcified coronary lesions: a patient-level pooled analysis from the Disrupt CAD I and CAD II Studies. Clin Res Cardiol 2021; 110(2): 228-23
8. **Blachutzik F**, Meier S, Weissner M, Schlattner S, Gori T, Ullrich-Daub H, Gaede L, Achenbach S, Möllmann H, Chitic B, Aksoy A, Nickenig G, Weferling M, Dörr O, Boeder N, Bayer M, Elsässer A, Hamm CW, Nef N, MD on behalf of the ROTA.shock investigators. Comparison of Coronary Intravascular Lithotripsy and Rotational Atherectomy in the Modification of Severely Calcified Stenoses. Am J Cardiol 2023; accepted for publication; Reference number: AJC-D-23-00028R1

1. Einführung

1.1 Die geschichtliche Entwicklung der perkutanen Koronarintervention

Die weltweit erste perkutane Koronarintervention (PCI) wurde am 16.09.1977 durch Andreas Grüntzig am Universitätsklinikum Zürich durchgeführt. Dieser hatte zuvor umfangreiche Erfahrungen in der perkutanen transluminalen Angioplastie (PTA) mittels Ballondilatation in der Behandlung von peripheren Gefäßverschlüssen der Beinarterien sowie in tierexperimentellen Versuchen an Koronararterien gesammelt. Im Rahmen des ersten Eingriffs wurde eine erfolgreiche perkutane transluminale Koronarangioplastie (PTCA) mittels Ballonangioplastie an einer Stenose des Ramus interventricularis anterior (RIVA) durchgeführt. Nach ihren Anfängen im Jahr 1977 ist die perkutane Koronarintervention (PCI) mittlerweile, bedingt durch die hohe Prävalenz der koronaren Herzerkrankung sowie eine rasche Weiterentwicklung der angewandten Techniken und Materialien, eine der am häufigsten durchgeführten therapeutischen Prozeduren in der Medizin (1). Während die anfänglich durchgeführte alleinige Ballonangioplastie von Stenosen des Koronarsystems mit einem erheblichen Risiko für einen kompletten Gefäßverschluss durch Dissektionen und Restenosen verbunden war, sicherte die Einführung von Koronarstents ab Ende der 1980er Jahre den akuten Erfolg der Koronarintervention durch Elimination elastischer Rückstellkräfte, Senkung der Rate an Dissektionen und an Restenosen (2). Im Jahr 1999 wurden bereits bei 84% der weltweit durchgeführten PCIs Koronarstents implantiert (2). Hierbei wurden zunächst Stents aus einem Gerüst aus Metalllegierungen ohne Medikamentenbeschichtung verwendet (Bare-metal Stents, BMS). Diese führten im Vergleich zur alleinigen Ballon-PTCA bereits zu einer erheblichen Verbesserung des klinischen Outcomes nach PCI, erwiesen sich jedoch den in den frühen 2000er Jahren entwickelten und in die klinische Praxis eingeführten Stents mit antiproliferativer Medikamentenbeschichtung („Drug-Eluting Stents“, DES) hinsichtlich der Rate an Restenosen und notwendigen Revaskularisationsbehandlungen als unterlegen (3). Als ursächlich hierfür wird im Wesentlichen die Verhinderung der Intimahyperplasie durch die antiproliferative Medikamentenbeschichtung angesehen. Allerdings zieht die hierdurch verzögerte Endothelialisation der DES eine längere Dauer der dualen Thrombozytenaggregationshemmung (DAPT) nach DES- als nach BMS-Implantation nach sich (3). Aktuell sind entsprechend der klinischen Datenlage Drug-Eluting Stents der Goldstandard für die Behandlung signifikanter Koronarstenosen.

1.2 Klinische Notwendigkeit zur Weiterentwicklung aktueller DES

Obwohl DES der neuesten Generation in der Behandlung akuter Koronarsyndrome und klinisch relevanter chronischer Koronarsyndrome unverzichtbar sind, bringt ihr Einsatz, bedingt durch mögliche Stentthrombosen und Restenosen, ein nicht zu vernachlässigendes Risiko für erneute koronare Ereignisse mit sich. Während die Rate von Stentthrombosen 5 Jahre nach Implantation mit ca. 0,8-1,6% relativ niedrig ist, gilt es dennoch zu bedenken, dass Stentthrombosen zu einem kompletten Gefäßverschluss mit daraus resultierendem akutem Koronarsyndrom führen und somit mit einer hohen Mortalität assoziiert sind (4,5). Restenosen werden klinisch meist durch stabile pektanginöse Beschwerden apparent und können somit frühzeitig diagnostiziert und behandelt werden. Sie sind daher, im Gegensatz zu Stentthrombosen, auch mit einer geringeren Mortalität assoziiert. Jedoch treten Restenosen nach DE-Stentimplantation mit einer 2-Jahresinzidenz von 5-10% deutlich häufiger auf als Stentthrombosen (6,7). Es existieren verschiedene Mechanismen, die zur Ausbildung von Restenosen führen können. So kann die Polymerbeschichtung des DES Entzündungsreaktionen der Gefäßwand auslösen, die zu einer Proliferation koronarer Endothelzellen mit Ausbildung einer Restenose führen (8,9). Auch führen die Streben der Stents zu einer Reduktion der Scherspannung (engl. „shear-stress“) am Endothel, wodurch eine konsekutive Erhöhung der Konzentration von Wachstumsfaktoren induziert wird, die zu einer Intimahyperplasie und konsekutiven Restenose führt (10). Das Metallgerüst des DES verhindert die normale Vasomotion des Koronargefäßes und kann auch durch diesen Mechanismus Restenosen triggern (11). Frakturen der Stentstreben und große Strebendicken sind weitere Faktoren, die zur Ausbildung von Restenosen beitragen können (12,13). Moderne DES wurden aus diesen Gründen dahingehend weiterentwickelt, dass sie sich durch niedrige Strebendicken auszeichnen.

Weitere Verbesserungen der Stenttechnologie sind entscheidend, um die Rate an Restenosen und den damit verbundenen Folgeeingriffen sowie an potenziell lebensbedrohlichen Stentthrombosen zu reduzieren, um hierdurch das Outcome nach perkutaner Koronarintervention weiter zu verbessern.

1.3 Optimierung der PCI mit Optischer Kohärenztomographie

Die 2014 für die intrakoronare Verwendung eingeführte Optische Kohärenztomographie (OCT) bietet die Möglichkeit hochauflösende Bilder aus dem Inneren der Koronargefäße zu generieren. Die optische Auflösung ist dabei mit ca. 15µm etwa 10-mal höher als beim Intravaskulären Ultraschall (IVUS) und damit die beste, die aktuell mittels intravaskulärer Bildgebung erreicht werden kann (14). Hierdurch ist es möglich die PCI auf mehreren Wegen

zu optimieren. Zum einen kann bereits vor Stentimplantation ein genauer Eindruck von der Morphologie des Koronargefäßes und der Plaquebeschaffenheit gewonnen werden (15-17). So kann beispielsweise evaluiert werden, ob eine Vorbehandlung des Gefäßes vor Stentimplantation notwendig ist. Insbesondere das Vorhandensein von Kalzifikationen spielt hier eine entscheidende Rolle. Kalzifizierte Plaques verhindern häufig eine ausreichende Stentexpansion. Daraus resultierende Stentunterexpansionen sind wiederum ein wichtiger Prädiktor für Restenosen und notwendige Folgeeingriffe. Wenn relevante Kalzifikationen in der OCT detektiert werden, sollte eine Vorbehandlung z.B. mittels Rotablation, also unter Verwendung eines Diamant-beschichteten Bohrkopfes, oder mittels Lithoplastie, also einem Ballon, der mechanische Stoßwellen an die Gefäßwand abgibt, erfolgen, um Frakturen in den kalzifizierten Plaques zu induzieren und somit einer Stentunterexpansion vorzubeugen.

Mittels der OCT können zudem die Läsionslänge sowie der Referenzdiameter des Gefäßes genauestens bestimmt werden (14,18,19). Nach Stentimplantation kann mittels OCT die Apposition der Stentstreben, die Stentexpansion sowie das Vorhandensein von Thromben und Dissektionen evaluiert und dadurch das Ergebnis der PCI optimiert werden (18,19) (*Abbildung 1, Seite 10*).

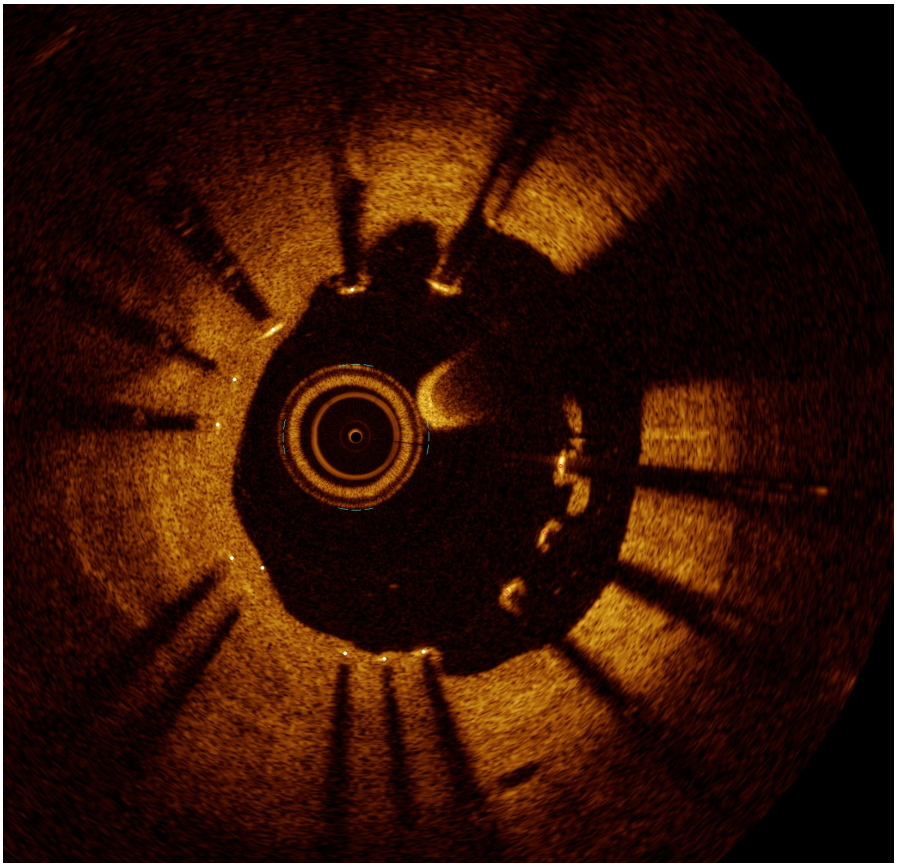

Abbildung 1: Unterexpandierter DES im OCT-Querschnittsbild

1.4 Bioresorbierbare Stenttechnologien

Bioresorbierbare Scaffolds (BRS) wurden entwickelt, um einige der Nachteile klassischer Metall-basierter Stents zu überwinden. Sie werden in Deutschland seit 2013 klinisch angewendet. Während Metallstents zur permanenten Präsenz von Fremdmaterial im Gefäßsystem führen, die Vasomotion dauerhaft verhindern und eine zukünftige Bypassversorgung eines behandelten Gefäßabschnitts unmöglich wird, sollen bioresorbierbare Scaffolds, auf Grund ihrer nur temporären Präsenz im Gefäßsystem, im Verlauf zu einer Wiederherstellung der natürlichen Gefäßstruktur und -funktion führen.

Trotz der prozeduralen Erfolge und erfolgsversprechender Outcome-Studien zu Beginn der Scaffold-Ära, haben jüngste randomisiert-kontrollierte Studien im Vergleich des ersten kommerziell verfügbaren Scaffolds ABSORB BVS™ (Abbott Vascular, Santa Clara, CA, USA) zu DES der neuesten Generation ein schlechteres klinisches Outcome gezeigt (20,21). Im German-Austrian ABSORB RegIstRy (GABI-R), der größten Registerstudie nach Scaffold-Implantation, zeigten sich signifikant erhöhte Raten an Scaffoldthrombosen. Während frühe Scaffoldthrombosen im Wesentlichen prozedural bedingt zu sein scheinen (Überdimensionierung des Stents, Gefäßschädigung), werden für das Auftreten später und sehr später Thrombosen gemeinhin Unterexpansion und Malapposition verantwortlich gemacht.

Zu berücksichtigen bleibt, dass bei konsequenter Verwendung einer Scaffold-spezifischen Implantationstechnik, die eine adäquate **P**rädilatation, korrektes **S**izing und eine konsequente **P**ostdilatation beinhaltet (sog. PSP-Technik), die Thrombose-Rate nach Scaffold-Implantation signifikant gesenkt werden kann und sich dann nicht mehr von der Eventrate moderner DES unterscheidet (22). Bioresorbierbare Scaffolds sind in Ihrer Applikationseigenschaft, wie auch in Ihrer Radialkraft den heutigen DES noch weit unterlegen. Diesen Umständen muss vor allem bei der Läsionsauswahl zwingend Rechnung getragen werden.

Auch wenn die jüngsten Studienergebnisse enttäuschend waren und der kommerzielle Vertrieb des ABSORB BVS™ gestoppt wurde, befinden sich aktuell einige erfolgversprechende Scaffolds in der Entwicklung oder werden bereits klinisch verwendet. Der Metall-basierte bioresorbierbare Scaffold Magmaris™ (Biotronik AG, Berlin, Deutschland) zeigte bisher hervorragende klinische Ergebnisse (23,24). Im klinischen Follow-up sind in den ersten 12 Monaten keine sicheren oder mutmaßlichen Devicethrombosen aufgetreten. Auch bei den Polymer-basierten Scaffolds befinden sich aktuell neue Devices in der frühen klinischen Testphase (z.B. MeRes™, Fantom™). Der Fantom™-Scaffold, der sich vor allem durch seine im Vergleich zum ABSORB BVS um 30% geringere Strebendicke auszeichnet, zeigte in der

multizentrischen Fantom II-Studie vielversprechende klinische Ergebnisse nach 6 Monaten (25).

Mit bioresorbierbaren Scaffolds können fundamentale Verbesserungen in der perkutanen Koronarintervention erreicht werden. Es ist jedoch eindeutig, dass zuvor weitreichende technische Verbesserungen dieser Devices nötig sind (Strebendicke, Resorptionszeit, Radialkraft). Hierfür braucht es Zeit sowie eine gewissenhafte Evaluation im klinischen Alltag.

2. Zielsetzung der Arbeit

Die vorliegende Habilitationsschrift beschäftigt sich mit neuen Technologien für die Verbesserung des prozeduralen und klinischen Outcomes der perkutanen Koronarintervention. Die PCI ist geprägt von einer mittlerweile fast 45-Jährigen Geschichte von raschen technologischen Fortschritten und entsprechenden Verbesserungen der Prozeduren. Als wichtiger Bestandteil der PCI-Optimierung wurde im Rahmen dieser Arbeit nach Möglichkeiten gesucht, die OCT im klinischen Alltag hinsichtlich der verwendeten Spüllösung zu optimieren und die Nephrotoxizität der Untersuchung durch Reduktion der notwendigen Kontrastmittelmenge zu reduzieren.

Weiterer wesentlicher Gegenstand dieser Arbeit war die Optimierung des prozeduralen Outcomes der PCI mit bioresorbierbaren Scaffolds. Bioresorbierbare Scaffolds bieten die Möglichkeit, Stenosen des Koronarsystems interventionell zu behandeln ohne dauerhaft Fremdmaterial im Gefäßsystem zurückzulassen. Dennoch ist es wichtig, die wesentlichen Unterschiede zu „klassischen“ DES in der Läsionsauswahl sowie in der angewandten Implantationstechnik zu berücksichtigen. Hierbei wurden grundlegend verschiedene Arten von Scaffolds (Poly-L-Lactid-Gerüst und Magnesium-Legierung) untersucht. Die vorliegende Arbeit zielte ebenfalls darauf ab, die Mechanismen der Scaffold-Resorption genauer zu evaluieren und hierdurch Verständnis dafür zu gewinnen, welche Läsion- und Patientencharakteristika eine Scaffold-Implantation begünstigen und welche Patienten somit vor allem von der Implantation bioresorbierbarer Devices profitieren. Als Ausblick in die Zukunft sollen die gewonnen Erkenntnisse helfen, zu evaluieren, in welcher Form bioresorbierbare Scaffolds weiterentwickelt werden müssen, um in der Klinik breit anwendbar zu sein.

Des Weiteren soll die intrakoronare Lithoplastie, als neue Technologie zur interventionellen Behandlung stark kalzifizierter Stenosen, hinsichtlich ihres klinischen und prozeduralen Ergebnisses untersucht werden.

3. Einfluss der Kontrastmittelkonzentration auf die Bildqualität und diagnostische Reliabilität der OCT

Zur Durchführung einer OCT ist es notwendig, den zu untersuchenden Gefäßabschnitt mit Kontrastmittel frei zu spülen, da ansonsten das Lichtsignal von den korpuskulären Blutbestandteilen erheblich abgeschwächt wird. Die notwendige Kontrastmittelgabe kann zu Einschränkungen der Nierenfunktion, insbesondere bei renal vorerkrankten Patienten, führen (26,27). Es sollte daher das Ziel sein, die für die OCT-Akquisition applizierte Kontrastmittelmenge so gering wie möglich zu halten.

Publikation Nr. 1: ***Blachutzik F****, Achenbach S, Nef H, Hamm C, Dörr O, Boeder N, Marwan M, Tröbs M, Schneider R, Röther J, Schlundt C. Optical coherence tomography: influence of contrast concentration on image quality and diagnostic confidence. Heart and Vessels 2017; 32(6): 653-659*

Im Rahmen dieser Studie wurde der Einfluss einer reduzierten Kontrastmittelkonzentration (150mg Jod/ml) auf die Bildqualität und diagnostische Genauigkeit der OCT untersucht. Hierbei wurde analysiert, ob durch die Verwendung von Kontrastmittel mit reduzierter Konzentration (150mg Jod/ml) die insgesamt notwendige Kontrastmittelmenge signifikant reduziert werden kann. Verbliebene Reste an Kontrastmittel wurden quantifiziert (*Abbildung 2, Seite 15*) und die diagnostische Genauigkeit der OCT-Untersuchung bewertet.

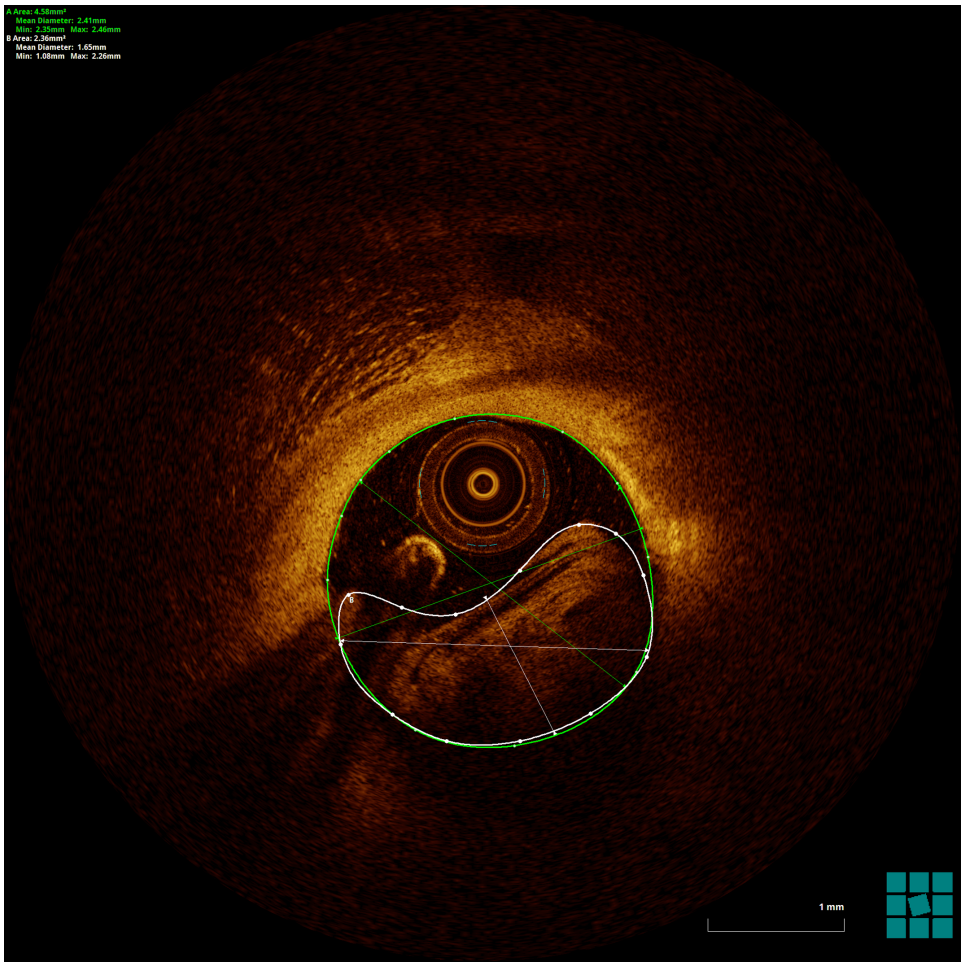

Abbildung 2: OCT Querschnittsbild einer Koronararterie mit verbliebenem Kontrastmittel. Die Fläche des Gefäßes ist in grün konturiert, die Fläche des verbliebenen Kontrastmittels in weiß. Das verbliebene Kontrastmittel und die damit unzureichende Spülung des Gefäßabschnittes macht eine sichere Diagnostik unmöglich. Im Bereich zwischen 3 und 9 Uhr der Gefäßzirkumferenz kann die Gefäßwand nicht sicher beurteilt werden.

Es zeigte sich jedoch, dass die Verminderung der Kontrastmittelkonzentration auch zu einer signifikanten Abnahme der Bildqualität und diagnostischen Genauigkeit führt und somit nicht geeignet ist, die Kontrastmittelbelastung für den Patienten relevant zu reduzieren. Das Kontrastmittel mit reduzierter Jod-Konzentration (150mg Jod/ml) ist im Vergleich zum Kontrastmittel mit Standardkonzentration (350mg Jod/ml) nicht in der Lage das Gefäß in ausreichendem Maße von Blut frei zu spülen, was mutmaßlich der geringeren Viskosität zuzuschreiben ist (*Abbildung 3, Seite 16*). Der Effekt einer reduzierten Kontrastmittel-Konzentration auf die Durchführung einer OCT-Untersuchung war zuvor nicht wissenschaftlich untersucht worden. Zwei vorhergehende Studien haben verglichen, wie sich die Verwendung von niedermolekularem Dextran oder Standard-Kontrastmittel mit einer Jod-Konzentration von 350mg/ml auf die Bildqualität der OCT auswirkt (26,27). Dextran hat ein

wesentlich geringeres nephrotoxisches Potenzial als Standard-Kontrastmittel (26,27). Jedoch bedarf es eines weit größeren Volumens an Dextran als an Kontrastmittel, um ein Gefäß suffizient zu spülen. Zudem muss eine optische Korrektur auf Grund des Refraktionsindex von Dextran erfolgen, was im klinischen Alltag kaum umzusetzen ist (27). Beide Studien kamen zu dem Ergebnis, dass Dextran zu einer vergleichbaren Bildqualität führt, wie Standardkontrastmittel. Es bleibt jedoch zu konstatieren, dass hierbei weit geringere Qualitätsmaßstäbe angelegt wurden als in der hier dargestellten Studie (*Publikation Nr. 1*). So war in beiden Studien die Sichtbarkeit der Gefäßwand in mehr als 270° der Zirkumferenz ausreichend, um die Bildqualität als gut zu deklarieren. Im Vergleich dazu wurde in der hier dargestellten Studie die Fläche an verbliebenen Blutschlieren genauestens planimetriert und erfasst. Zudem wurde die qualitative diagnostische Reliabilität mittels einer Likert-Skala evaluiert. Hierbei konnte gezeigt werden, dass die generelle Verwendung von niedrig konzentriertem Kontrastmittel (150mg Jod/ml) für die OCT-Durchführung nicht empfohlen werden kann, da sowohl Bildqualität als auch diagnostische Reliabilität signifikant schlechter sind als bei Kontrastmittel mit Standardkonzentration (350mg Jod/ml).

	150 mg/ml	**350 mg/ml**	**p-value**
Completely flushed length of pullback (%)	58.3 ± 27.3	77.6 ± 24.5	0.004
Remaining blood streaks in the cross-sections (%)	34.1 ± 25.8	19.4 ± 21.4	0.013
Likert scale (1-4)	2.1 ± 1.2	1.4 ± 0.7	<0.001
Number of runs with Likert scale 1	14/31 (45%)	27/36 (75%)	0.01

Values are mean ± standard deviation or n (%)

Abbildung 3: Ergebnisse des qualitativen Vergleichs der OCT-Durchführung mit verschiedenen Kontrastmittel-Konzentrationen

4. Evaluation der perkutanen Koronarintervention mit bioresorbierbaren Gefäßstützen („Scaffolds“)

4.1 Nachdilatation nach Implantation von bioresorbierbaren Scaffolds mit Everolimus- und Novolimus-Beschichtung: Evaluation der akuten mechanischen Effekte mittels OCT

Bioresorbierbare Scaffolds unterscheiden sich im Moment von DES der neuesten Generation durch eine größere Dicke der Gerüststreben sowie eine geringere Radialkraft. Es ist daher entscheidend, diesen strukturellen Unterschieden im Rahmen der PCI Rechnung zu tragen. Eine ausgiebige Vor- und Nachbehandlung der Läsion ist wesentlicher Bestandteil der PCI mit bioresorbierbaren Scaffolds.

*Publikation Nr. 2: **Blachutzik F**, Boeder N, Wiebe J, Mattesini A, Dörr O, Most A, Bauer T, Röther J, Tröbs M, Schlundt C, Achenbach S, Hamm CW, Nef HM. Post-dilatation after implantation of bioresorbable everolimus- and novolimus-eluting scaffolds: an observational optical coherence tomography study of acute mechanical effects. Clin Res Cardiol 2017; 106(4): 271-279*

Die Studie zielte darauf ab, den Effekt der Nachdilatation auf die beiden zum damaligen Zeitpunkt meistverwendeten bioresorbierbaren Scaffolds in der OCT zu untersuchen. Das wesentliche Ergebnis war, dass die konsequente Nachdilatation der Scaffolds die Malapposition signifikant reduziert ohne mit höheren Komplikationen wie Dissektionen oder Scaffoldfrakturen einherzugehen. Daten vorhergehender Studien zeigen, dass malappositionierte Scaffoldstreben durch die Unterbrechung des laminaren Flusses im Koronargefäß zu einem massiv erhöhten Risiko für das Auftreten von potenziell lebensbedrohlichen Scaffoldthrombosen führen (28,29). Malappositionierte Streben sind nicht in der Lage die antiproliferativen Substanzen ihrer Medikamentenbeschichtung (Novolimus oder Everolimus) in ausreichendem Maße an die Gefäßwand abzugeben, wodurch die resultierende Intimahyperplasie zum Verlust an Gefäßlumen führen kann. Nur 61% der malappositionierten Scaffold-Streben sind nach 6 Monaten mit Neointima bedeckt (30). Die direkte Korrelation zwischen einem guten mechanischen Ergebnis der Implantation in der intravaskulären Bildgebung und einem besseren klinischen Outcome wurden bisher nur für DES, nicht aber für Scaffolds gezeigt (31-33). Dennoch ist davon auszugehen, dass sich die Ergebnisse bei Scaffolds nicht wesentlich von denen bei DES unterscheiden.

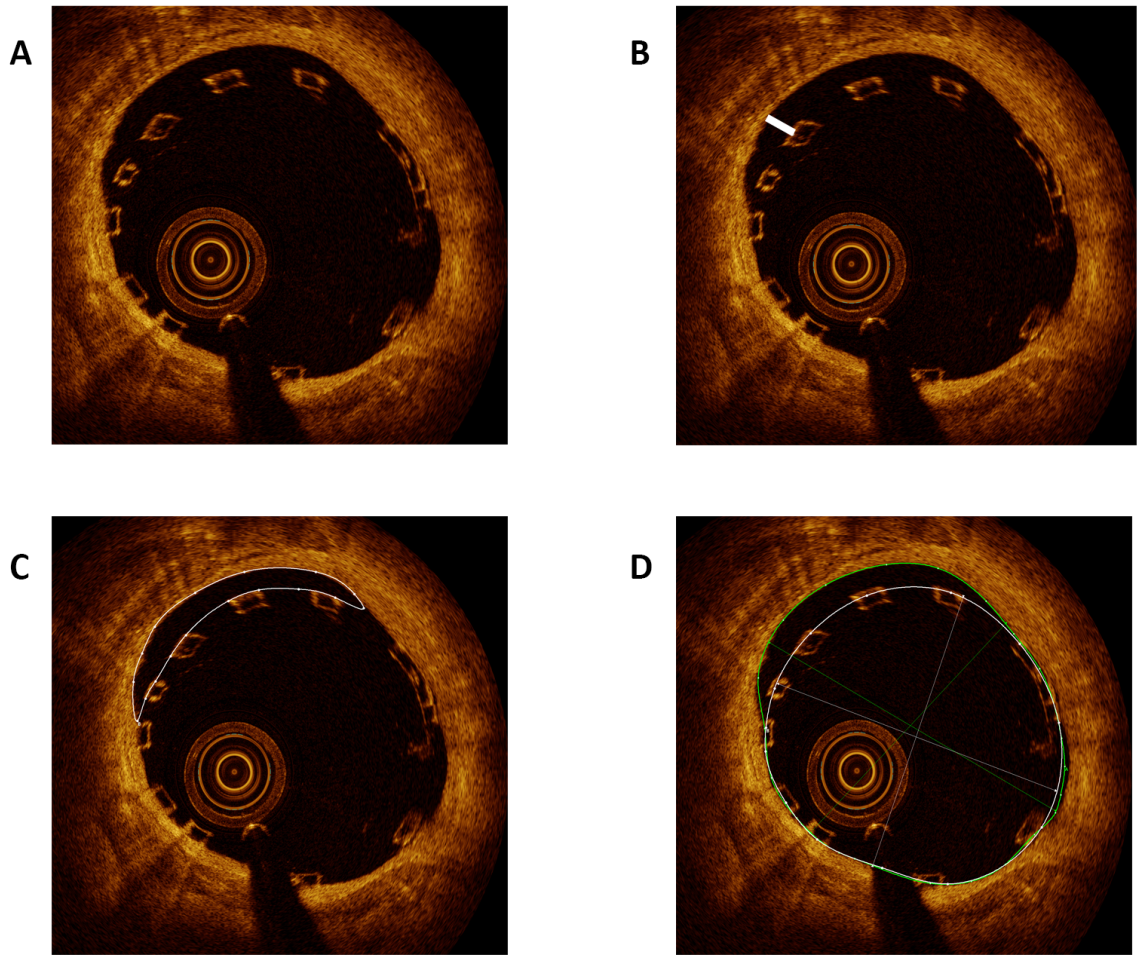

Abbildung 4: Evaluation von OCT-Parametern in Querschnittsbildern eines ABSORB™ BRS, der in den RIVA implantiert wurde. A: Vier von insgesamt 13 Streben sind malappositioniert. B: Die Distanz zwischen abluminalem Strebenende und der Gefäwand ist in weiß gemessen. Bei diesem Beispiel betrug der maximale Abstand der Strebe zur Gefäßwand 310µm. C: Messung der Malappositionsfläche (weiße Kontur). D: Scaffoldfläche (weiße Kontur) und Lumenfläche (grüne Kontur) sind eingezeichnet

Eine wichtige Limitation dieser Studie ist, dass es sich um eine retrospektive Analyse handelte. Es erfolgte keine Randomisierung hinsichtlich der Nachdilatation. Eine Nachdilatation der Scaffolds war dann erfolgt, wenn der behandelnde Arzt es für notwendig erachtete. Zudem wurden nur diejenigen PCIs in die Analyse inkludiert, im Rahmen derer eine OCT durchgeführt wurde. Hierdurch entsteht ein klarer Selektions-Bias in Bezug auf eine Kohorte mit besonders komplexen Läsionen, da in der Regel nur bei komplexen PCIs eine intravaskuläre Bildgebung durchgeführt wird.

Im Vergleich der beiden im Rahmen der Studie untersuchten Scaffold-Typen zeigte sich, dass der Novolimus-freisetzende DESolve™-Scaffold deutlich mehr Gewebsprotrusion durch die Stentmaschen aufweist als der Everolimus-freisetzende ABSORB™-Scaffold

(*Abbildung 5, Seite 19*). Dies scheint auf die unterschiedliche Struktur der Scaffolds zurückzuführen zu sein, da die Abstände zwischen den einzelnen Streben der Scaffolds beim DESolve™-Scaffold im Mittel größer sind als beim ABSORB™-Scaffold. Gewebsprotrusion, also die Vorwölbung von Gewebe der Gefäßwand ins Gefäßlumen, ist mit einem schlechteren klinischen Outcome assoziiert (34,35).

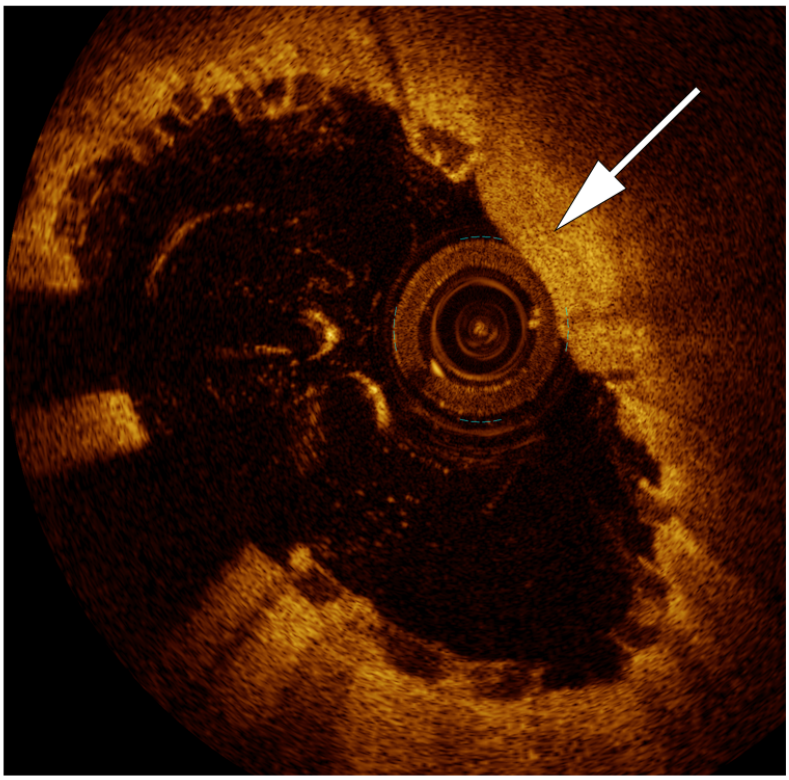

Abbildung 5: OCT-Querschnittsbilder eines DESolve™-Scaffold, der in die rechte Koronararterie (RCA) implantiert wurde, mit sichtbarer Gewebsprotrusion (weißer Pfeil)

4.2 OCT-Analyse der überlappenden Implantation von Novolimus-beschichteten Scaffolds

Die überlappende Implantation von Stents oder Scaffolds ist bei entsprechender Läsionslänge häufig notwendig. Während die überlappende Implantation von DES der neuesten Generation nicht mit einem verschlechterten klinischen Outcome assoziiert ist (36,37), gibt es zu bioresorbierbaren Scaffolds keine entsprechenden Daten. Es besteht die Sorge, dass durch die im Vergleich zu DES größere Strebendicke ein relevanter Lumenverlust im Koronargefäß induziert wird, der wiederum für Restenosen prädisponieren würde.

Publikation Nr. 3: ***Blachutzik F****, Boeder N, Wiebe J, Mattesini A, Dörr O, Most A, Bauer T, Röther J, Tröbs M, Schlundt C, Achenbach S, Hamm CW, Nef HM. Overlapping implantation of bioresorbable novolimus-eluting scaffolds: An observational optical coherence tomography study. Heart and Vessels 2017; 32(7): 781-789*

In der OCT zeigte sich, dass die überlappende Scaffoldimplantation nicht zu einer reduzierten Lumenfläche führt. Die doppelte Scaffoldschicht scheint durch eine Überexpansion nach abluminal kompensiert zu werden (*Abbildung 6, Seite 20*). Hierdurch wurde bestätigt, was in einer zuvor durchgeführten Studie bereits in Koronargefäßen des Schweins gezeigt wurde (37). Die „Überexpansions"-Fähigkeit der Grundstruktur des Novolimus-beschichteten DESolve™-Scaffold scheint in diesem Zusammenhang von Vorteil zu sein (38). Eine doppelte Lage des Scaffolds mag auf Grund der höheren Radialkraft sogar von Vorteil sein, um einem Recoil der Gefäßwand vorzubeugen, denn die Radialkraft aller bisher verfügbaren Scaffolds ist erheblich geringer, als die moderner DES mit ihrem Cobalt-Chrom-Gerüst. Zudem wurde weder eine erhöhte Rate an Frakturen der Scaffoldstreben noch eine erhöhte Rate an Dissektionen in den Überlappungsbereichen beobachtet. Es muss hierbei allerdings auch berücksichtigt werden, dass der Überlappungsbereich durch den behandelnden Interventionalisten in der Regel außerhalb der am stärksten kalzifizierten oder stenosierten Bereiche der Läsion platziert wird.

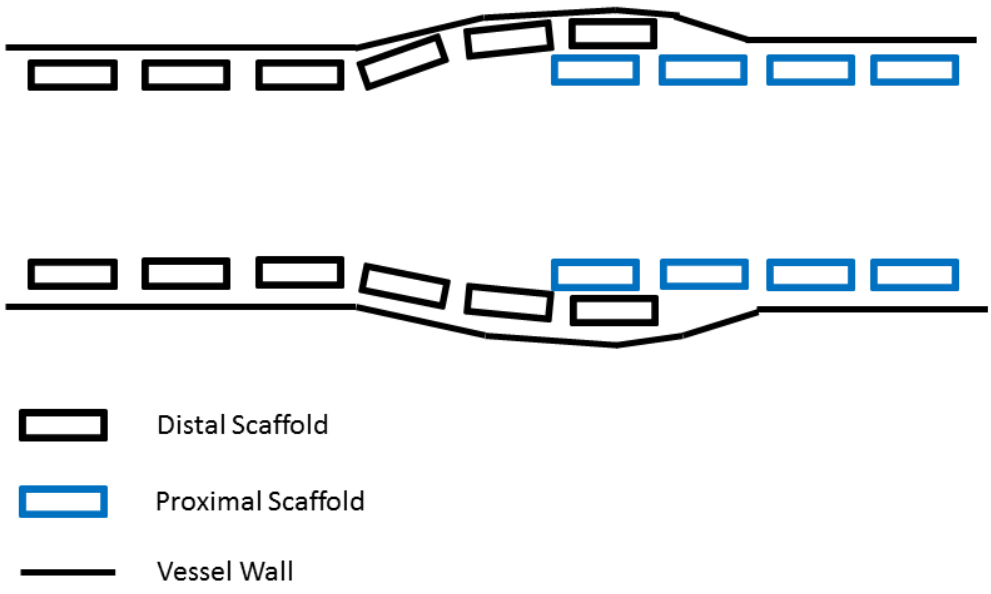

Abbildung 6: Schematische Darstellung der Überexpansion der Gefäßwand im Scaffold-Überlappungsbereich

In der Literatur war zuvor die Hypothese aufgestellt worden, dass eine überlappende Scaffold-Implantation durch Lumenverlust zu einem erhöhten Risiko für Scaffoldthrombosen führt (39-41). Dementsprechend wurde in der klinischen Praxis eine maximale Reduktion des Überlappungsbereichs empfohlen (37). Ishibashi et al. haben in einer Studie die überlappende Implantation von Scaffolds als unabhängigen Risikofaktor für periprozedurale Myokardinfarkte beschrieben (42). Im Gegensatz dazu haben Ortega-Paz et al. in einer retrospektiven Analyse keine signifikanten Unterschiede im klinischen Outcome 1 Jahr nach überlappender vs. nicht-überlappender Scaffold-Implantation gefunden (43).

Durch die größere Distanz zwischen der Gefäßwand und der inneren Scaffoldschicht bei überlappender Scaffoldimplantation ist anzunehmen, dass die Endothelialisierung dort erheblich mehr Zeit in Anspruch nimmt. Ein Punkt, der in der OCT-Auswertung nicht analysiert werden konnte, ist das Vorhandensein von Flussturbulenzen, bedingt durch die große Strebendicke der Scaffolds im Überlappungsbereich (44,45). Dies könnte potenziell zu einer höheren Rate an Scaffold-Thrombosen bei überlappender Scaffoldimplantation beitragen (42).

Nichtsdestotrotz bleibt festzuhalten, dass im Rahmen der hier dargestellten Studie keine mechanischen oder geometrischen Unterschiede zwischen überlappenden und nicht-überlappenden Scaffolds detektiert worden sind, die eine höhere Ereignisrate bei überlappender Scaffoldimplantation erklären könnten. (*Abbildung 7, Seite 22*)

	BRS without overlap ($n = 23$)	BRS with overlap ($n = 15$)	p value
Total BRS length (mm)	20 ± 6	36 ± 6	<0.001
Overlap length (mm)		3.8 ± 2.9	
OCT scaffold area (mm^2)	7.57 ± 2.18	7.90 ± 2.41	0.72
Residual area stenosis (%)	11.5 ± 10.1	10.0 ± 6.8	0.70
Reference area (mm^2)	7.95 ± 2.79	8.02 ± 2.49	0.88
Mean lumen area (mm^2)	7.36 ± 2.16	7.70 ± 2.55	0.79
Minimal lumen area (mm^2)	5.77 ± 1.72	6.41 ± 2.63	0.71
OCT ISAA† (mm^2)	0.83 ± 1.85	1.62 ± 3.25	0.72
OCT tissue prolapse area (mm^2)	7.74 ± 9.53	7.41 ± 8.68	0.95
Sum of malapposed struts (n)	5 ± 11	7 ± 13	0.72
Sum of struts (n)	246 ± 77	234 ± 85	0.72
ISA* (%)	0.03 ± 0.08	0.04 ± 0.07	0.79
Distance of malapposition‡ (mm)	0.18 ± 0.20	0.27 ± 0.32	0.58
Mean stent diameter (mm)	3.06 ± 0.42	3.03 ± 0.37	0.70
Minimum stent diameter (mm)	2.68 ± 0.38	2.71 ± 0.31	0.29
Maximum stent diameter (mm)	3.50 ± 0.51	3.38 ± 0.44	0.88
Minimum eccentricity index	0.61 ± 0.11	0.66 ± 0.06	0.08
Overlapping	0	3.33 ± 2.23	<0.001
Fracture	0.02 ± 0.08	0.36 ± 0.49	0.09
Bifurcation	0.96 ± 10.95	0.42 ± 0.67	0.20
Mean eccentricity index	0.77 ± 0.07	0.81 ± 0.03	0.07
Proximal edge dissection	0	0	>0.99
Distal edge dissection	0	1	0.87

Values are mean ± standard deviation

* Incomplete strut apposition (ratio number of malapposed struts per BRS to total number of struts per BRS)

† Incomplete scaffold apposition area

‡ Orthogonal distance between malapposed scaffold and vessel wall

Abbildung 7: Ergebnisse der OCT-Analyse im Vergleich von BRS mit und ohne überlappende Implantation

4.3 OCT-Analyse der Scaffold-Resorption: Analyse der Lichtintensität der Scaffoldstreben durch einen neuen Resorptionsindex für Poly-L-Lactid-Scaffolds

Scaffolds unterscheiden sich nicht nur in ihren mechanischen Eigenschaften grundlegend von den bisher zur Verfügung stehenden Stentplattformen. Auch der Prozess der Bioresorption an sich ist ein fundamental neues Konzept im Bereich der perkutanen Koronarintervention.

Zu Beginn der Scaffold-Ära ist man von einer durchschnittlichen Resorptionszeit von 2 Jahren für Poly-L-Lactid-Scaffolds ausgegangen. Diese Zeit resultierte im Wesentlichen aus ersten Ergebnissen nach Scaffoldimplantationen bei Tieren (41,46). Im Verlauf wurde deutlich, dass die komplette Resorptionsdauer im Menschen tatsächlich bei 4-5 Jahren liegt (46-49).

Außerdem ist in den großen randomisierten Studien deutlich geworden, dass Poly-L-Lactid-Scaffolds durch eine höhere Rate an Thrombosen mit einem schlechteren klinischen Outcome assoziiert sind als DES der neuesten Generation (20,21). Die verzögerte Resorption wiederum könnte mit zur Entstehung von Scaffoldthrombosen beitragen.

Publikation Nr. 4: ***Blachutzik F****, Achenbach S, Marwan M, Tröbs M, Boeder N, Doerr O, Weissner M, Bauer T, Nef H, Hamm C, Schlundt C. OCT-assessment of scaffold resorption: Analysis of strut intensity by a new resorption index for poly-l-lactic acid bioresorbable vascular scaffolds. Catheter Cardiovasc Interv 2019; 94(7): 928-935*

Um die Resorptionsgeschwindigkeit der Scaffolds abschätzen zu können, erfolgte die OCT-Untersuchung von Scaffolds zu verschiedenen Zeitpunkten nach der Implantation (*Abbildung 8, S.23*).

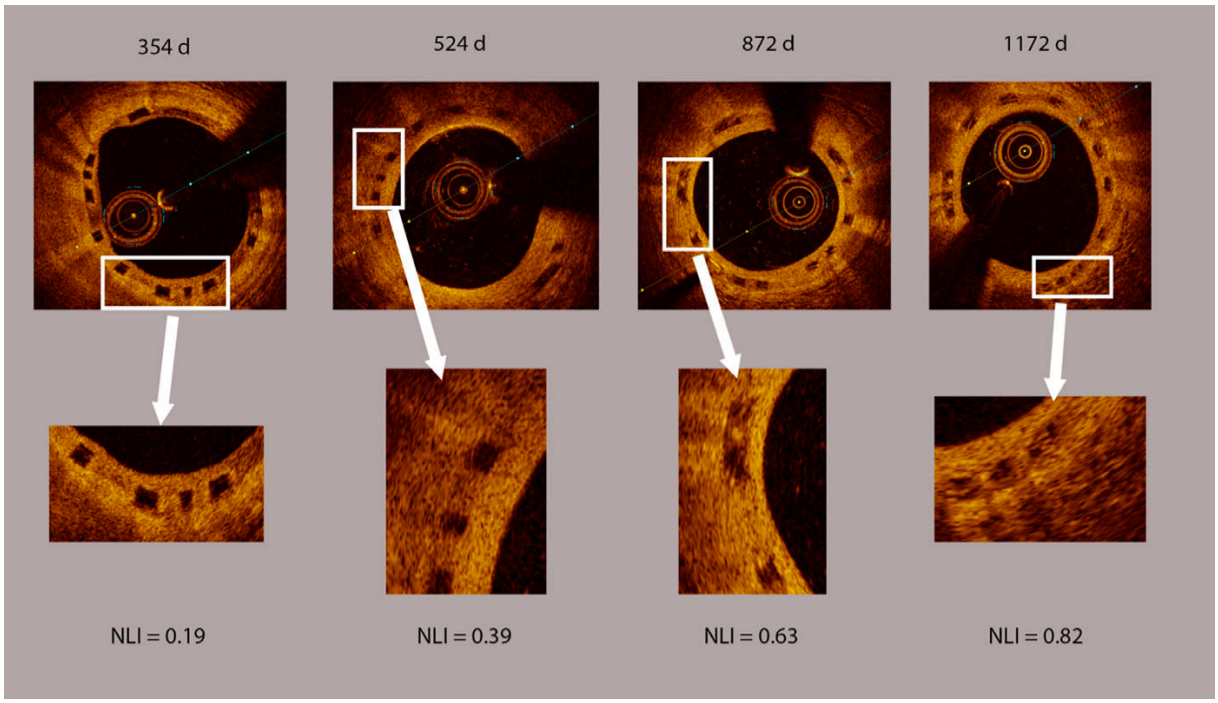

Abbildung 8: Entwicklung der normalisierten Lichtintensität (NLI) mit der Zeit (in Tagen) seit Implantation. Die Abbildung zeigt vier verschiedene Stadien der Scaffoldresorption. Mit zunehmender Zeit seit Implantation gleicht das Innere der Scaffoldstreben zunehmend dem umgebenden Gewebe und erscheint dadurch im OCT immer heller.

Hierbei zeigte sich, dass die zur umgebenden Intima normalisierte Lichtintensität linear mit der Zeit seit Implantation korreliert (*Abbildung 9, S. 24*).

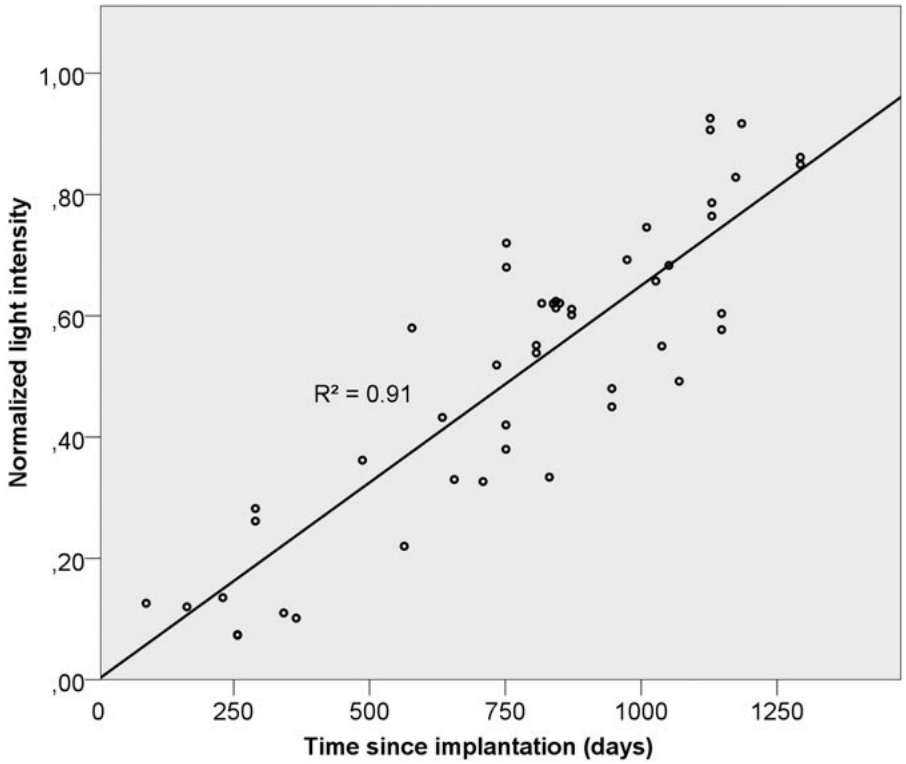

Abbildung 9: Normalisierte Lichtintensität in Abhängigkeit von der Zeit seit Scaffold-Implantation. Die normalisierte Lichtintensität korreliert linear mit der Zeit seit Scaffoldimplantation. R^2 = Spearman-Korrelationskoeffizient

Auf Grund der linearen Korrelation der normalisierten Lichtintensität mit der Zeit seit der Implantation wurde der BRS-RESORB-Index eingeführt. Dieser wird berechnet als:

$$\frac{Normalisierte\ Lichtintensität \times 1000}{Zeit\ seit\ Scaffoldimplantation\ (Tagen)}$$

Über den BRS-RESORB-Index kann der Grad der Degradation des Scaffolds abgeschätzt werden. Es zeigte sich, dass der Resorptionsprozess durch verschiedene Patienten-spezifische Faktoren signifikant beeinflusst wird. Nach Implantation werden die Poly-L-Lactid-Streben zunehmend durch Hydrolyse abgebaut (50). Sobald die Polymerketten klein genug sind, diffundieren sie in das umgebende Gewebe und werden zunächst durch Komponenten der extrazellulären Matrix ersetzt. Die Matrixbestandteile sind zunächst zellfrei und werden Schritt für Schritt durch Bindegewebszellen ersetzt (50,51). Nakatani et al. haben bereits in einer vorherigen Studie gezeigt, dass die Lichtintensität in der OCT mit dem histologischen

Resorptionsprozess von Scaffolds in Koronarien des Schweins korreliert (48). Allerdings wurde hierbei beschrieben, dass sich die Lichtintensität im Strebenzentrum zwischen 3 und 18 Monaten nach Implantation nicht ändert, während sie zwischen 18 und 30 Monaten kontinuierlich ansteigt. Im Gegensatz dazu zeigten die Daten aus *Publikation Nr. 4* eine kontinuierliche und lineare Zunahme der Lichtintensität mit der Zeit, wobei dieser Gegensatz durch prozedurale und methodische Unterschiede bedingt zu sein scheint. Die Scaffoldimplantation ist bei Nakatani et al. ohne Nachdilatation erfolgt, was eine schlechtere Einbettung der Scaffoldstreben in die Gefäßwand nach sich ziehen kann und somit den Resorptionsprozess potenziell verzögert (48). Zudem wurde die Lichtintensität nur im Zentrum der Strebe, nicht wie in unserer Studie in der kompletten Fläche aller Streben gemessen. Die Resorption beginnt an den Rändern der Scaffoldstreben, sodass es einige Zeit dauert bis der Prozess das Zentrum der Strebe erreicht. Dementsprechend führt die Analyse der kompletten Streben, wie in unserer Studie, zu einer wesentlich genaueren visuellen Abschätzung der Scaffold-Degradation.

Der BRS-RESORB-Index wurde eingeführt, um die Geschwindigkeit der Scaffoldresorption abschätzen zu können. Wenn zwei oder mehr Scaffolds im gleichen Patienten implantiert wurde, war der BRS-RESORB-Index für die verschiedenen Scaffolds stets sehr ähnlich, was den Schluss zulässt, dass individuelle Patientenfaktoren den Resorptionsprozess stärker beeinflussen als prozedurale oder Läsions-Charakteristika.

Im Rahmen einer multivariablen Analyse konnte das Vorhandensein eines Diabetes mellitus oder von Peri-strut low intensity areas (PSLIA) als unabhängige Risikofaktoren für eine verzögerte Scaffoldresorption identifiziert werden. Diabetes mellitus ist mit persistierenden vaskulären Entzündungsprozessen assoziiert, die mit den Resorptionsprozessen von Scaffolds interferieren können. PSLIA in der OCT korrelierten in der Histologie von Koronararterien des Schweins mit perivaskulären Entzündungsprozessen (52). Lokale Inflammationsprozesse tragen wiederum ebenfalls zu einem verlangsamten Resorptionsprozess bei. Bei Patienten mit akutem Koronarsyndrom war die Resorptionsgeschwindigkeit signifikant höher als bei solchen mit stabiler koronarer Herzerkrankung.

Die Analyse des BRS-RESORB-Index macht deutlich, dass individuelle Patientenfaktoren den Resorptionsprozess von Scaffolds beeinflussen und somit bei deren Implantation berücksichtigt werden sollten. Auch die Dauer der dualen Thrombozytenaggregationshemmung sollte abhängig von der zu erwartenden Resorptionszeit ausgewählt und ggfs. verlängert werden. Denn in der Literatur ist ein verlängerter Resorptionsprozess und das damit einhergehende Remodelling der Gefäßwand als potenzieller

Risikofaktor für die bei bioresorbierbaren Scaffolds beobachtete höhere Rate an Device-Thrombosen diskutiert worden (20,21).

4.4 Effekt der Nachdilatation mit non-compliant Ballons auf metallische bioresorbierbare Scaffolds

Die klinischen Outcome-Ergebnisse nach PCI mit bioresorbierbaren Poly-L-Lactid-Scaffolds waren, wie oben dargestellt, signifikant schlechter als nach Implantation von modernen DES. Der kommerzielle Vertrieb dieser Devices wurde daher 2017 eingestellt (20,21). Von metallischen Scaffolds, wie dem Magnesium-basierten Magmaris™ (Biotronik AG, Berlin, Deutschland), erhoffte man sich die Überwindung einiger Nachteile der Erst-Generations-Scaffolds mit ihrem Poly-L-Lactid-Zuckergerüst. Im Wesentlichen ging es hierbei um eine größere Radialkraft, einen kleineren Footprint, eine geringere Strebendicke sowie eine schnellere Resorption (53,54). Der Magmaris™-Scaffold erhielt 2016 seine CE-Zulassung wobei die initialen Implantationsempfehlungen allein auf einem Experten-Konsensus beruhten (55). Wie bei jedem neuen Device, war es auch hier entscheidend in ersten Studien zu untersuchen, auf welche Art und Weise die Implantation am besten erfolgen sollte.

Publikation Nr. 5: Blachutzik F, Achenbach S, Tröbs M, Marwan M, Weissner M, Nef H, Schlundt C. Effect of non-compliant balloon postdilatation on magnesium-based bioresorbable vascular scaffolds. Catheter Cardiovasc Interv 2019; 93(2): 202-207

Im Rahmen dieser Publikation wurde der Effekt der Nachdilatation mit non-compliant Ballons auf Magnesium-Scaffolds standardisiert untersucht. Im Gegensatz zur vorhergehenden Studie zur Untersuchung der Nachdilatation auf Absorb™-und DESolve™-Scaffolds (*Publikation Nr. 2*) wurde hierbei der Effekt vor und nach Nachdilatation während der gleichen Prozedur mittels OCT untersucht. Bei der Untersuchung der Absorb™- und DESolve™-Scaffolds waren die OCTs retrospektiv nach Implantation mit oder ohne Nachdilatation ausgewertet worden.

Die Ergebnisse dieser Studie zeigten, dass die non-compliant Nachdilatation des Magmaris™-Scaffold die Apposition der Streben sowie die Scaffoldexpansion signifikant verbessert ohne höhere Raten an Strebenfrakturen und Dissektionen zu induzieren (*Abbildung 10, Seite 27*). Die Lumen- und Scaffoldexpansion konnte dagegen in Gefäßabschnitten mit

kalzifizierten Plaques nicht verbessert werden. Auch konnte eine signifikante Verbesserung der Scaffold-Symmetrie durch die Nachdilatation erreicht werden (*Abbildung 11, Seite 27-28*). Die höhere Symmetrie wiederum kann das klinische Outcome positiv beeinflussen, da niedrige Scaffold-Symmetrien mit einem schlechteren klinischen Outcome assoziiert sind (34, 35).

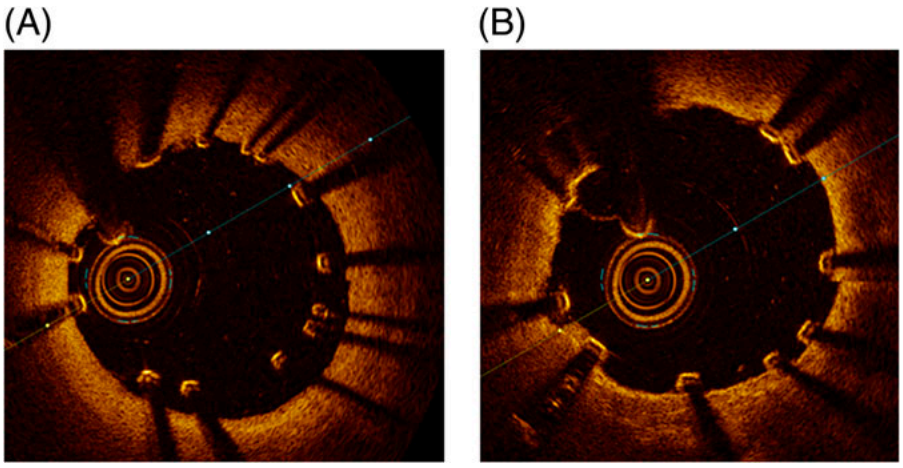

Abbildung 10: Effekt der Nachdilatation auf die Apposition der Streben eines metallischen Scaffolds: 3.0/20mm Magmaris™-Scaffold vor (A) und nach (B) non-compliant Nachdilatation

Variable	Before post-dilatation	After post-dilatation	p-value
Mean BRS diameter (mm)	2.80±0.39	3.21±0.32	<0.001
Minimum BRS diameter (mm)	2.44±0.41	2.62±0.29	0.003
Maximum BRS diameter (mm)	3.08±0.33	3.45±0.39	<0.001
Abluminal scaffold area (mm^2)	6.72±1.28	7.92±1.43	<0.001
Adluminal scaffold area (mm^2)	5.82±1.31	6.94±1.22	<0.001
Lumen area (mm^2)	6.83±1.12	7.58±1.09	<0.001
Minimum lumen area	5.44±1.88	6.11±1.62	0.002

(mm²)			
Incomplete scaffold apposition area (mm²)	0.17±0.11	0.01±0.04	<0.001
Mean eccentricity index	0.82±0.05	0.91±0.07	0.01
Proximal edge dissection	0	0	>0.99
Distal edge dissection	1	1	>0.99

Values are mean ± standard deviation or n (%)
[*] *Optical coherence tomography*

Abbildung 11: Ergebnisse der OCT-Analyse von metallischen Magmaris™-Scaffolds vor und nach NC-Ballon Nachdilatation

Obwohl primär nur Läsionen ohne angiographisch sichtbare Kalzifikationen eingeschlossen wurden, zeigte die OCT kalzifizierte Plaques, die mehr als 25% der Gefäßzirkumferenz betrafen, verteilt über 9,2% der gesamten Läsionslänge. Die fehlende Möglichkeit, die Lumen- und Scaffoldexpansion im Bereich von kalzifizierten Plaques durch Nachdilatation zu verbessern, macht deutlich, wie wichtig eine sorgfältige Läsionsauswahl und -präparation ist. Die Implantation in kalzifizierte Läsionen sollte dementsprechend vermieden werden. Zum sicheren Ausschluss, dass eine Läsion kalzifiziert ist, sollte eine intravaskuläre Bildgebung vor geplanter Scaffoldimplantation stets erwogen werden.

Während des 6-Monats Follow-up stellten sich 2 von 35 Patienten mit Zielläsionsversagen auf Grund von Restenosen im Magmaris™-Scaffold vor. In der OCT zeigte sich hierbei bei beiden Patienten eine homogene Restenose, die mittels DES-Implantation behandelt wurde. Scaffoldstreben waren zum Zeitpunkt der Restenose nur noch teilweise sichtbar. Der im Vergleich zu Poly-L-Lactid-Scaffolds schnellere Resorptionsprozess (6-12 Monate) und der damit einhergehende frühe Verlust der Radialkraft könnte in beiden Fällen zur Restenose beigetragen haben.

Auf Basis der im Rahmen dieser Studie erhobenen Daten erscheint die standardmäßige non-compliant Nachdilatation für metallische Magmaris™-Scaffolds ebenso notwendig wie für Poly-L-Lactid -Scaffolds, um Malappositionen vorzubeugen und eine optimale Expansion des Devices zu erreichen.

4.5 Besonderheiten nach Implantation von bioresorbierbaren Poly-L-Lactid Scaffolds

Eine Besonderheit nach Implantation von bioresorbierbaren Poly-L-Lactid Scaffolds war das gehäufte Auftreten koronarer Evaginationen (*Abbildung 12, Seite 30-31*). Hierbei handelt es sich um „Aussackungen" der Gefäßwand. Diese scheinen eine Folge von Gefäßverletzungen im Rahmen der PCI sowie von positivem Remodelling der Gefäßwand im weiteren Verlauf zu sein. Das Auftreten von Evaginationen korreliert mit Frakturen der Streben, Malappositionen und nicht-endothelialisierten Streben (56-59). Koronare Evaginationen unterbrechen den laminaren Fluss und werden als potenzieller Risikofaktor für späte Stentthrombosen angesehen (60,61). Evaginationen treten nach Implantation von modernen DES fast nicht mehr auf, was mutmaßlich zu der im Vergleich zu DES der ersten Generation geringeren Rate an späten Stentthrombosen mit beigetragen hat (56). Die zur Verfügung stehenden Daten legen den Schluss nahe, dass koronare Evaginationen und Aneurysmata nach Implantation von Scaffolds deutlich häufiger vorkommen, als nach Implantation moderner DES (62-64).

*Publikation Nr. 6: **Blachutzik F**, Achenbach S, Marwan M, Röther J, Tröbs M, Schneider R, Nef H, Weissner M, Schlundt C. Major coronary evaginations following implantation of bioresorbable vascular scaffolds - Clinical and OCT characteristics. Cardiovasc Revasc Med 2019; 20(6): 485-491*

Ziel dieser Studie war es, die morphologischen und klinischen Charakteristika von Evaginationen nach Scaffold-Implantation zu analysieren. Scaffolds mit Evaginationen sind mit signifikant größeren Scaffoldflächen und -diametern assoziiert als solche ohne Evaginationen. Zudem sind Scaffolds mit Evaginationen mit höheren Raten an Scaffoldfrakturen und malappositionierten Streben assoziiert. Ein wesentlicher Aspekt, der sich in der OCT-Analyse zeigte, war, dass obwohl Evaginationen sich nur lokal begrenzt im Scaffold zeigen, die Überexpansion des Gefäßes und des Scaffolds die komplette Scaffoldlänge betrifft. Außerdem zeigte sich, dass die Zunahme der Gefäß- und Scaffolddimensionen umso größer ist je länger der Implantationszeitpunkt zurückliegt (*Abbildung 13, Seite 31-32*). Der Prozess scheint dementsprechend kontinuierlich voranzuschreiten, wobei die Überexpansion des Gefäßes den Scaffold mitzuziehen scheint und konsekutiv in einer Überexpansion des Scaffolds selbst resultiert. In die Gefäßwand inkorporierte Scaffoldstreben und die Degradation

der Poly-L-Lactid-Matrix erlaubt den Scaffoldstreben der Gefäßexpansion zu folgen (*Abbildung 12, Seite 30-31*).

Gori et al. haben im Rahmen einer Studie 102 Scaffolds 12 Monate nach Implantation mittels OCT analysiert und hierbei in ungefähr 54% der Scaffolds Evaginationen identifiziert (65). Im Gegensatz hierzu wurden in unsere Untersuchung nur Scaffolds eingeschlossen, die im Rahmen von Koronarangiographien auffällig und dann mittels OCT untersucht wurden. Es besteht somit ein klarer Selektions-Bias für Patienten mit großen Evaginationen. Die beobachtete Assoziation zwischen Frakturen der Scaffoldstreben und Malapposition mit dem Auftreten von Evaginationen war ebenso von Gori et al. beschrieben worden (65). Die positive Korrelation zwischen den Lumen- und Scaffolddimensionen mit der vergangenen Zeit seit Implantation war jedoch eine komplett neue Erkenntnis der hier dargestellten Studie. Koronare Aneurysmata, wie sie als Spätfolge nach Scaffoldimplantation beschrieben wurden, könnten der Endpunkt dieser kontinuierlichen Zunahme der Gefäß-und Scaffolddimensionen sein (62-64).

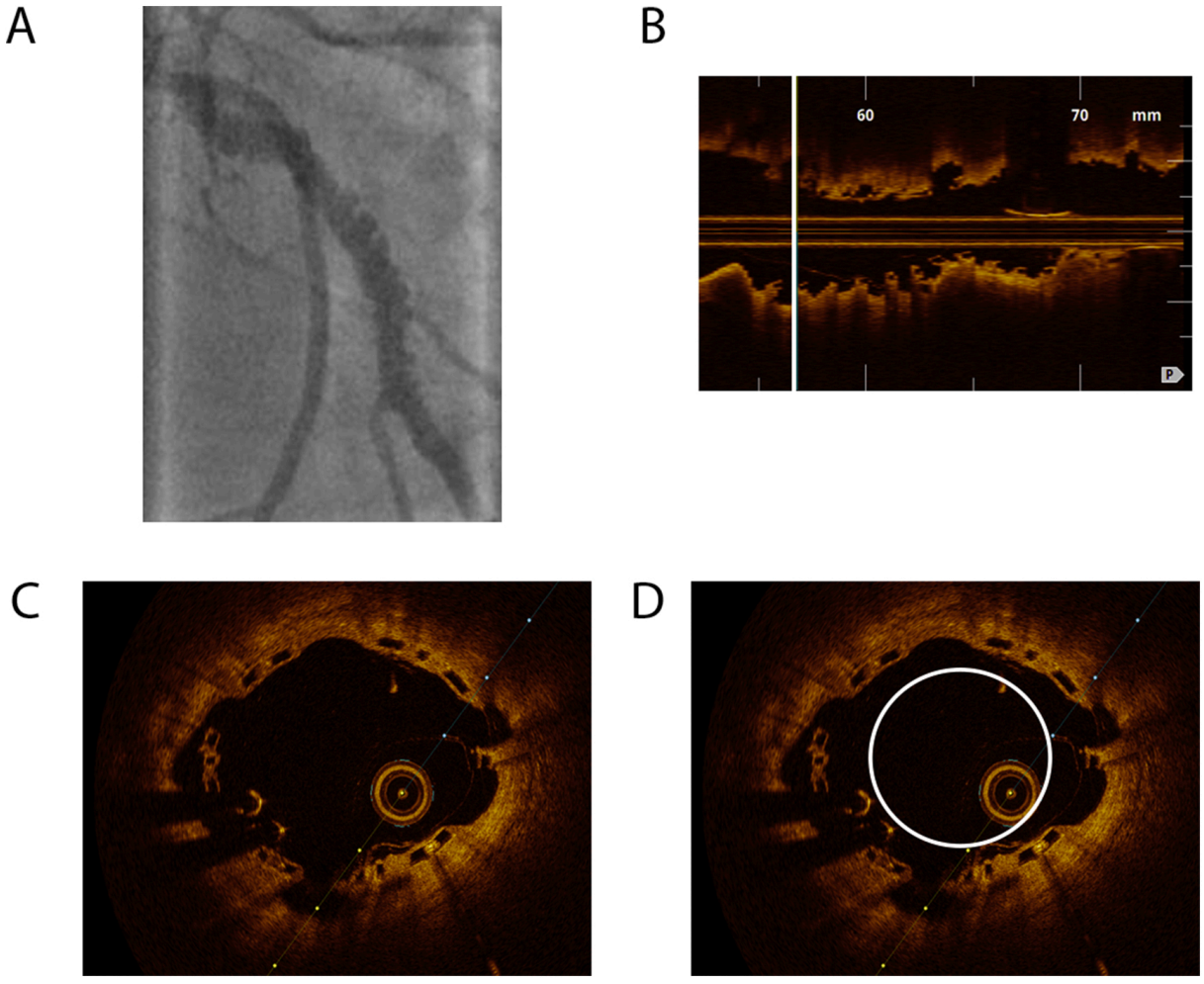

Abbildung 12: Koronare Evaginationen eines Poly-L-Lactid Scaffolds
A: Koronarangiographie eines 3.0/28mm Absorb™-Scaffold 33 Monate nach Implantation in die Circumflexarterie. B: Längsschnitt des Scaffolds in der OCT. C: Querschnitt in der OCT (Position: weiße Markierung in B); D: die nominale Scaffoldgröße bei Implantation ist in weiß eingezeichnet. Der mittlere Scaffolddiameter (4,16mm) 33 Monate nach Implantation liegt ungefähr 40% über der nominalen Größe bei Implantation (3,0mm)

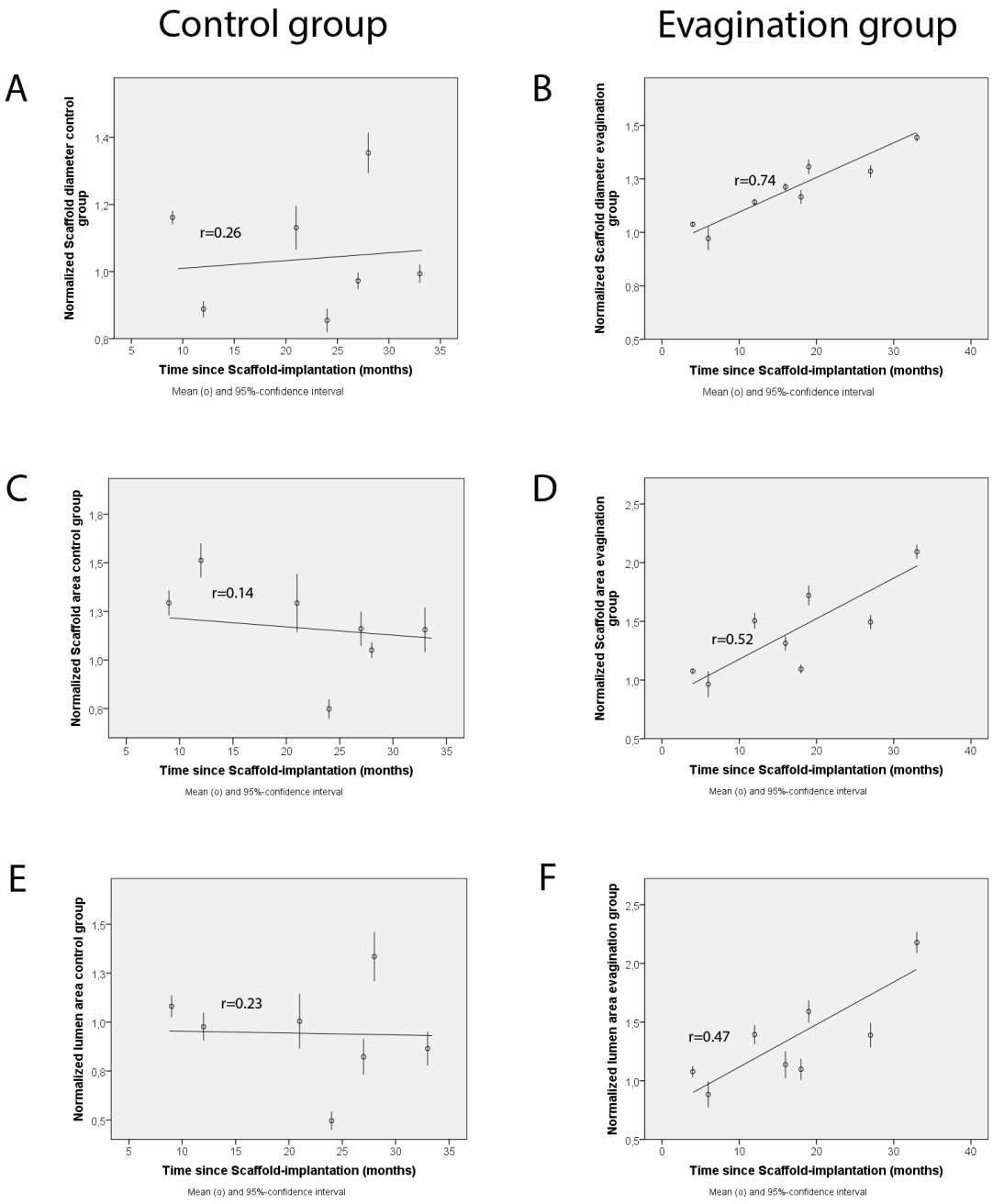

Abbildung 13: Korrelation der Scaffold- und Gefäßdimensionen mit der Zeit seit Implantation.

A und B: Normalisierte Scaffolddiameter der Kontroll- (A) und Evaginationsgruppe (B) in Relation zur Zeit seit Implantation. B und C: Normalisierte Scaffoldfläche der Kontroll- (C) und Evaginationsgruppe (D) in Relation zur Zeit seit Implantation. E und F: Normalisierte Lumenfläche der Kontroll- (E) und Evaginationsgruppe (F) in Relation zur Zeit seit Implantation. Die Werte sind angegeben als Mittelwert (o) und 95%-Konfidenzintervall. Die Ausgleichsgerade ist für jeden Graph angegeben; r = Pearson Korrelationskoeffizient

4.6 Ausblick

Die enttäuschenden klinischen Ergebnisse nach Implantation von bioresorbierbaren Scaffolds der ersten Generation haben dazu geführt, dass Poly-L-Lactid-Scaffolds mittlerweile komplett vom Markt verschwunden sind. Geplante Optimierungen, wie Poly-L-Lactid-Devices mit deutlich geringer Strebendicke, sind nicht mehr bis zur Marktreife entwickelt worden. Dahingegen sind Metall-basierte Scaffolds, wie etwa der Magmaris™, der bisher im Vergleich zu modernen DES gute klinische Ergebnisse gezeigt hat, weiterhin auf dem Markt. Auch bei den Polymer-basierten Scaffolds befinden sich aktuell neue Devices in der klinischen Testphase (z.B. MeRes™, Fantom™). Der Fantom™-Scaffold, der sich vor allem durch seine im Vergleich zum ABSORB BVS um 30% geringere Strebendicke auszeichnet, zeigte in der multizentrischen Fantom II-Studie exzellente klinische Ergebnisse nach 6 Monaten (25).

Im Jahr 2020 wurde zudem der erste bioadaptive Stent, der Elixir Bioadaptor ELX1805J™ (Elixir Medical, Milpitas, CA, USA) auf den Markt gebracht, welcher Eigenschaften von DES und von bioresorbierbaren Scaffolds in sich vereinigt. Dieses Device zeichnet sich durch ein klassisches Cobalt-Chrom-Gerüst mit hoher Radialkraft wie bei modernen DES aus, das bioresorbierbare Gelenkstellen beinhaltet. Nach ca. 6 Monaten werden die Gelenke freigegeben und das Gefäß kann danach die physiologische Vasomotion in gewissem Maße wieder nachvollziehen (66).

Mit bioresorbierbaren Scaffolds können fundamentale Verbesserungen in der perkutanen Koronarintervention erreicht werden. Es ist jedoch eindeutig, dass zuvor weitreichende technische Verbesserungen der Devices nötig sind. Hierzu zählt eine geringere Strebendicke, adäquate Resorptionszeiten, eine ausreichende Radialkraft sowie das Verhindern von vaskulären Entzündungsreaktionen durch den Prozess der Bioresorption mit eventuell resultierender Ausbildung von Evaginationen. Sollten diese Probleme gelöst werden können, könnten in Zukunft bioresorbierbare Devices die herkömmlichen DES im Rahmen der perkutanen Koronarintervention als Standarddevice ablösen.

5. Die koronare Lithoplastie für die Behandlung stark verkalkter Koronarstenosen

5.1 Klinische Evaluation der intrakoronaren Lithoplastie

Neben der Weiterentwicklung der Stenttechnologien hat es auch im Bereich der zur Verfügung stehenden Ballons für die PCI neue Entwicklungen gegeben. So steht die Lithoplastie, die im Bereich der Zertrümmerung von Nieren-, Gallen- und Harnleitersteinen bereits seit langer Anwendung findet, seit 2018 auch für den intrakoronaren Einsatz zur Verfügung (67). Der Lithoplastie-Ballon wird im Rahmen der PCI in den Bereich der zu behandelnden Läsion vorgeführt, auf 4atm inflatiert und sodann die Stoßwellentherapie gestartet. Hierbei werden durch die Bildung einer rasch expandierenden und dann kollabierenden Gasblase im Ballon pulsatile Stoßwellenwellen an das umgebende Gewebe abgegeben. Die mechanische Energie entspricht dabei in etwa 50-60atm. Die Technologie der intravaskulären Lithoplastie (IVL) eignet sich im Rahmen der PCI vor allem für die Behandlung stark kalzifizierter koronarer Plaques (67-71). Stark verkalkte Koronarstenosen stellen für die perkutane Koronarintervention (PCI) nach wie vor eine Herausforderung dar. Vor Stentimplantation ist es zwingend erforderlich einen ausreichenden Lumengewinn zu erzielen, um einer Unterexpansion des Stents vorzubeugen, die mit einem deutlich verschlechterten klinischen Outcome assoziiert ist (72,73). Die intrakoronare Lithoplastie induziert durch die abgegeben Stoßwellen Brüche im kalzifizierten Plaque und ermöglicht dadurch den notwendigen Lumengewinn (*Abbildung 14, Seite 34*). Da die IVL für den intrakoronaren Einsatz jedoch erst relativ kurz zur Verfügung steht, existieren bisher bezüglich dieser Technologie nur wenige wissenschaftliche Daten.

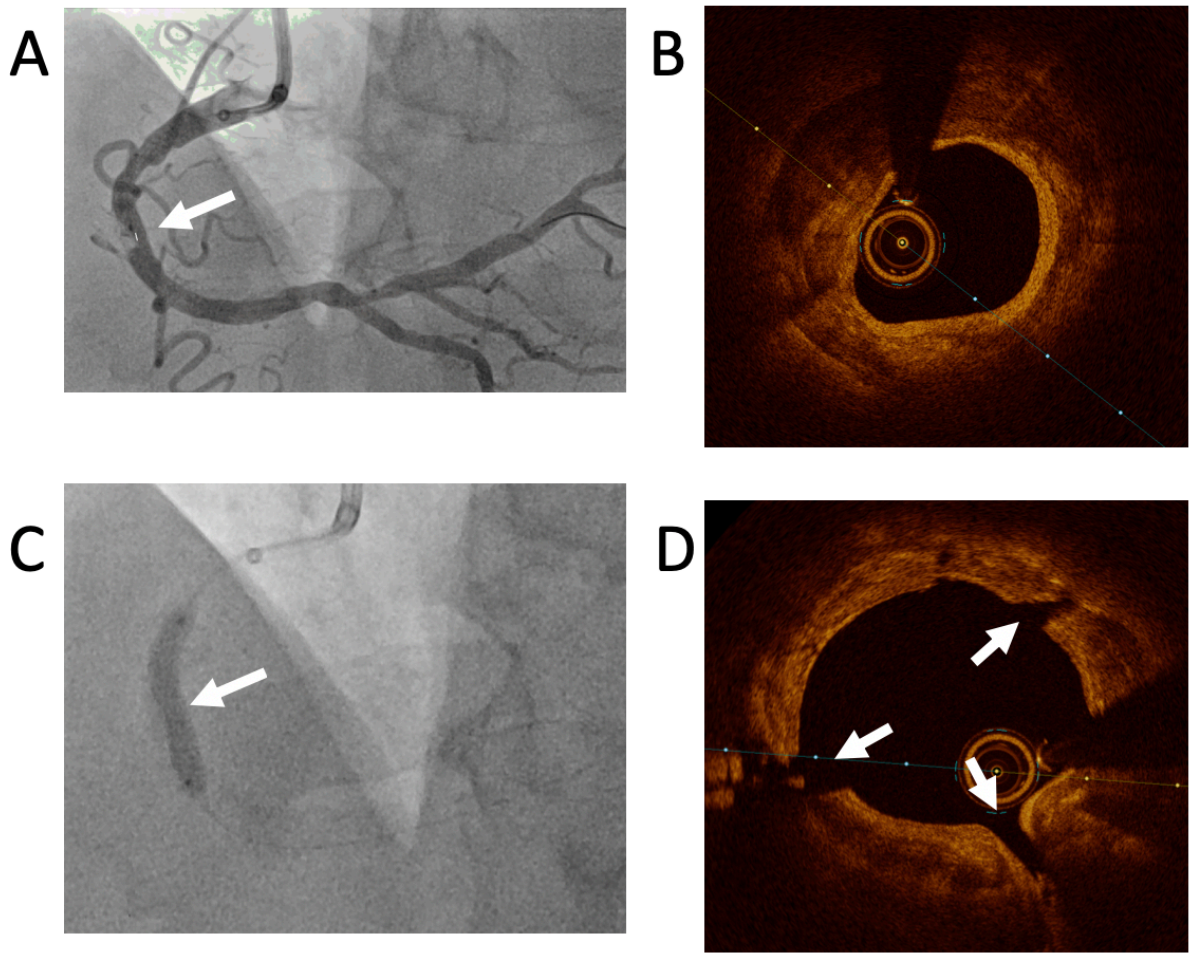

Abbildung 14: Intrakoronare Lithoplastie einer stark verkalkten Stenose der rechten Koronararterie. A: Koronarangiographie der RCA mit hochgradiger Stenose im mittleren Abschnitt (weißer Pfeil). B: OCT Querschnittsbild aus dem Bereich der Stenose mit sichtbarer zirkumferenzieller Verkalkung. C: Nach Lithoplastie ist der Ballon im Bereich der vormaligen Stenose suffizient entfaltet (weißer Pfeil). D: OCT Querschnittsbild mit aus dem Bereich der vormaligen Stenose mit den IVL-charakteristischen Frakturen des kalzifizierten Plaques (weiße Pfeile)

*Publikation Nr. 7: **Blachutzik F**, Honton B, Escaned J, Hill JM, Werner N, Banning AP, Lansky AJ, Schlattner S, De Bruyne B, Di Mario C, Dörr O, Hamm C, Nef HM. Safety and effectiveness of coronary intravascular lithotripsy in eccentric calcified coronary lesions: a patient-level pooled analysis from the Disrupt CAD I and CAD II Studies. Clin Res Cardiol 2021; 110(2): 228-23*

Ziel dieser Arbeit war es daher, die Sicherheit und Effektivität der IVL im intrakoronaren Einsatz zur Behandlung exzentrischer und konzentrischer kalzifizierter Stenosen zu untersuchen. Exzentrizität bedeutet hierbei, dass ein großer Unterschied zwischen minimalem und maximalem Gefäßdurchmesser besteht (*Abbildung 5* zeigt beispielsweise einen implantierten Scaffold mit hoher Exzentrizität). Mit insgesamt 180 eingeschlossenen Patienten aus 19 Zentren in 10 Ländern handelte es sich hierbei bis dato um die größte klinische Studie zur Evaluation der intrakoronaren Lithoplastie. Im Rahmen der Analyse wurden 47 exzentrische (26%) und 133 konzentrische (74%) kalzifizierte Läsionen identifiziert. Es zeigte sich eine hohe prozedurale Erfolgsrate der IVL sowohl in der Behandlung exzentrischer als auch in der Behandlung konzentrischer kalzifizierter Stenosen (93.6% vs. 93.2%; p=1.0). In keiner der Gruppen traten Perforationen, Fluss-relevante Dissektionen oder slow-/no-reflow-Phänomene auf. Die finale Residualstenose von 8.6 ± 9.8% in exzentrischen und 10.0 ± 9.0% (p = 0.56) in konzentrischen kalzifizierten Stenosen bestätigt den signifikanten Effekt der IVL auf koronare kalzifizierte Stenosen (*Abbildung 15, Seite 35*).

	Overall ($n=180$)	Eccentric ($n=47$)	Concentric ($n=133$)	p value
Clinical success	168 (93.3)	44 (93.6)	124 (93.2)	1.0
Angiographic success	178 (98.9)	47 (100.0)	131 (98.5)	1.0
Stent delivery	180 (100.0)	47 (100.0)	133 (100.0)	
Final in-stent angiographic outcomes				
MSD[a] (mm)	2.8 ± 0.5	3.0 ± 0.5	2.7 ± 0.5	0.004
Residual stenosis (%)	9.7 ± 9.2	8.6 ± 9.8	10.0 ± 9.0	0.56
Acute gain (mm)	1.7 ± 0.5	1.8 ± 0.5	1.7 ± 0.5	0.47
Residual stenosis < 50%	180 (100.0)	47 (100.0)	133 (100.0)	
Residual stenosis < 30%	175 (97.2)	46 (97.9)	129 (97.0)	0.84

Values are mean ± standard deviation or *n* (%)

[a]*MSD* minimum stent diameter

Abbildung 15: Prozedurales Ergebnis nach IVL exzentrischer und konzentrischer kalzifizierter koronarer Läsionen

Durch das zunehmende Patientenalter in den letzten Jahren hat auch die Häufigkeit komplexer Koronarstenosen zugenommen. Diese stellen sich häufiger kalzifiziert und mit ausgeprägter Exzentrizität dar, was die interventionelle Behandlung im Rahmen der PCI erschwert (74). Dies macht es notwendig, verlässliche interventionelle Techniken zur Verfügung zu haben, mit deren Hilfe auch entsprechend komplexe Läsionen erfolgreich behandelt werden können. Die

erhobenen Daten legen den Schluss nahe, dass die IVL eine erfolgversprechende Technik hierfür ist.

5.2 Vergleich von koronarer Lithoplastie und Rotablation für die Behandlung stark kalzifizierter Koronarstenosen – ROTA.shock Studie

Bisher ist die Rotablation der Goldstandard zur Behandlung stark kalzifizierter Koronarstenosen im Rahmen der PCI. Hierbei wird ein Diamant-beschichteter Bohrkopf verwendet, um mit hoher Drehzahl eine Modifikation des kalzifizierten Plaques zu erreichen. Im Rahmen der prospektiv randomisierten multi-zentrischen ROTA.shock-Studie (75) wurde die koronare Lithoplastie mit der Rotablation hinsichtlich der minimalen Stentfläche (MSA) am Prozedurende verglichen. Patienten mit vordiagnostizierter stark kalzifizierter Koronarstenose, die eine entsprechende Plaquemodifikation notwendig macht, wurden entweder zur Behandlung mit Rotablation oder mit koronarer Lithoplastie vor Stentimplantation randomisiert. Insgesamt wurden zwischen Juli 2019 und November 2021 70 Patienten an sechs Zentren in Deutschland (Justus Liebig Universität Gießen, Medizinische Klinik I, Gießen; Kerckhoff-Klinik, Abteilung für Kardiologie, Bad Nauheim; Universitätsmedizin Mainz, Kardiologie 1, Mainz; Universitätsklinikum Erlangen, Medizinische Klinik 2, Erlangen; St. Johannes-Hospital, Innere Medizin 1, Dortmund; Universitätsklinikum Bonn, Medizinische Klinik 2, Bonn) in die Studie eingeschlossen. Die ROTA.shock-Studie ist die erste wissenschaftliche Arbeit, die die intrakoronare Lithoplastie randomisiert mit dem bisherigen Goldstandard für die Behandlung stark kalzifizierter Koronarstenosen, der Rotablation, verglichen hat. Analysiert wurden die Gefäß-, Plaque- und Stentdimensionen mittels OCT zu Beginn der Prozedur, nach Rotablation oder Lithoplastie sowie am Prozedurende. Die Auswertung der intravaskulären Bilder erfolgte unter Verwendung einer speziellen OCT-Analysesoftware (QIVUS™ OCT Software, Medis, Leiden, Niederlande).

Der primäre Endpunkt der Studie war die Nicht-Unterlegenheit der koronaren Lithoplastie im Vergleich zur Rotablation hinsichtlich der MSA im finalen OCT am Prozedurende. Die MSA ist der prognostisch wichtigste Marker bzgl. zukünftiger koronarer Ereignisse nach der Implantation von DES ist (76-78). Aus der biometrischen Fallzahlplanung ergab sich eine Stichprobengröße von 28 Patienten pro Gruppe, die auf Grund der Möglichkeit von Exklusionen auf 35 Patienten pro Gruppe gesteigert wurde.

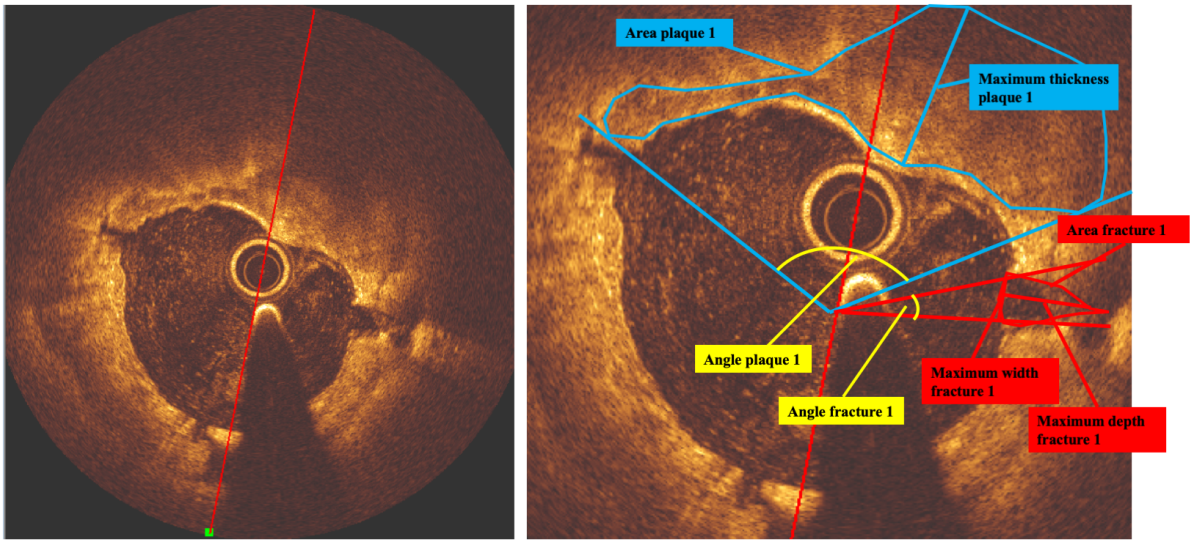

Abbildung 16: Beispielhafte Auswertung eines OCT-Querschnittbilds direkt nach koronarer Lithoplastie. Links ist das native Bild dargestellt, rechts sind Flächen, Längen und Winkel eines kalzifizierten Plaques sowie einer Fraktur im kalzifizierten Plaque für die Auswertung markiert.

Eine erste Subgruppenanalyse der Daten zielte darauf ab, die Effekte der Plaquemodulation durch Rotablation und Lithoplastie detailliert miteinander zu vergleichen. Hierfür wurden 21 der insgesamt 70 Patienten eingeschlossen, da bei diesen Patienten eine intravaskuläre Bildgebung mittels OCT vor und unmittelbar nach Rotablation und Lithoplastie zur Verfügung stand. Eine beispielhafte Auswertung der OCT-Daten ist in *Abbildung 16, Seite 37* dargestellt.

*Publikation Nr. 8: **Blachutzik F**, Meier S, Weissner M, Schlattner S, Gori T, Ullrich-Daub H, Gaede L, Achenbach S, Möllmann H, Chitic B, Aksoy A, Nickenig G, Weferling M, Dörr O, Boeder N, Bayer M, Elsässer A, Hamm CW, Nef N, MD on behalf of the ROTA.shock investigators. Comparison of Coronary Intravascular Lithotripsy and Rotational Atherectomy in the Modification of Severely Calcified Stenoses. Am J Cardiol 2023; accepted for publication; Reference number: AJC-D-23-00028R1*

Nach durchgeführter Rotablation oder Lithoplastie waren Frakturen des kalzifizierten Plaques in 14 der 21 Patienten sichtbar (66,7%), wobei nach Lithoplastie (3.23± 0.49) signifikant mehr Frakturen pro Plaque zu sehen waren als nach Rotablation (1.67 ± 0.52; $p<0.001$). Zudem waren die Plaquefrakturen nach Lithoplastie länger als nach Rotablation (Lithoplastie: 1.67 ± 0.43 mm vs. Rotablation: 0.57 ± 0.55 mm; $p=0.01$) was sich auch in einem

insgesamt größeren Volumen der Frakturen widerspiegelte (Lithoplastie: 1.47 ± 0.40mm^3 vs. Rotablation: 0.48 ± 0.27mm^3; p=0.003). Nach Rotablation war im Vergleich zur Lithoplastie ein deutlich größerer akuter Lumengewinn zu verzeichnen als nach Lithoplastie (Rotablation: 0.46 ± 0.16mm^2 vs. Lithoplastie: 0.17 ± 0.14mm^2; p=0.03). Dissektionen waren in 16 der 21 Patienten nach Plaquemodulation sichtbar, wobei diese nach Lithoplastie oder Rotablation in etwa gleicher Häufigkeit zu beobachten waren.

Beide Techniken modulieren den kalzifizierten Plaque derart, dass ein akuter Lumengewinn entsteht, der jedoch nach Rotablation deutlich größer ist als nach Lithoplastie. Hierdurch könnte die Rotablation bei der Behandlung stark exzentrischer Stenosen besser geeignet sein als die Lithoplastie, da sie die folgende Ballon- und Stentpositionierung durch den direkten Atherektomie-Effekt in größerem Maße vereinfachen kann.

Die Lithoplastie könnte im Gegensatz dazu bei Stenosen mit langen und zirkumferenziellen Kalzifikationen besser geeignet sein als die Rotablation, da sie eine größere Anzahl und auch längere Frakturen im kalzifizierten Plaque generiert.

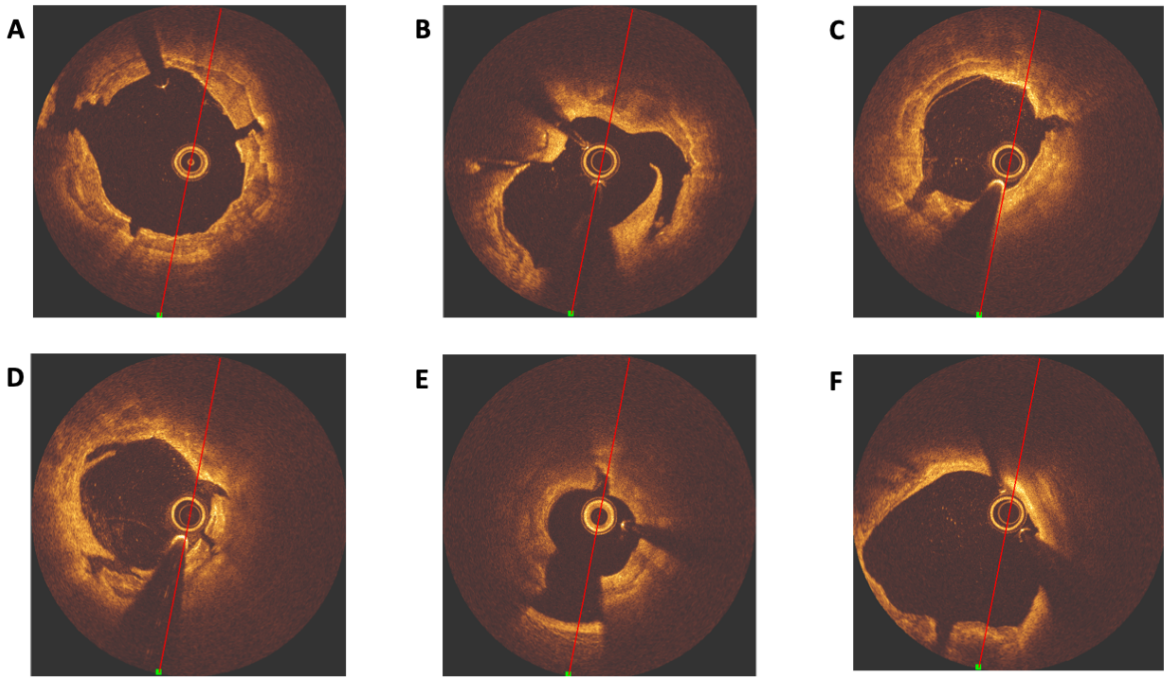

Abbildung 17: A, B und C zeigen OCT-Querschnittsbilder stark kalzifizierter Koronarläsionen nach Behandlung mit Lithoplastie. D, E, F zeigen OCT-Querschnittsbilder stark kalzifizierter Koronarläsionen nach Rotablation.

Mit beiden Techniken lässt sich eine deutliche Modulation kalzifizierter Koronarstenosen erzielen (*Abbildung 17, Seite 38*). Im Rahmen der Planung des interventionellen Vorgehens sollten die Unterschiede der beiden Techniken bedacht werden, um ein optimales Ergebnis zu gewährleisten. Die Ergebnisse der ROTA.shock-Hauptstudie sind aktuell zur Publikation eingereicht.

6. Diskussion

Da die Koronarangiographie und die PCI zu den am häufigsten durchgeführten Prozeduren in der modernen Medizin gehören, ergibt sich die Notwendigkeit alle Maßnahmen zur Verbesserung der zu Grunde liegenden Techniken zu ergreifen (1). Die intravaskuläre Bildgebung unter Verwendung der OCT bietet die beste Auflösung für Bilder aus dem Inneren des Koronargefäßes, die aktuell technisch erreicht werden kann, dennoch stellt die notwendige Kontrastmittelgabe eine potenzielle Limitation, insbesondere bei Patienten mit Niereninsuffizienz, dar. Die notwendige Kontrastmittelmenge so weit, wie möglich zu reduzieren war daher das Ziel der in Publikation Nr. 1 dargestellten Arbeit. Hierbei wurde versucht Kontrastmittel mit niedrigerer als der Standardkonzentration zu verwenden. Vergleichbare Studien wurde bis dato nicht durchgeführt, lediglich das Kontrastmittel durch Dextran zu ersetzen ist zuvor wissenschaftlich untersucht worden (26,27). Hier hatte sich jedoch eine notwendige optische Korrektur als erhebliche Limitation erwiesen, die vor allem die Größen- und Längenmessungen auf Grund erschwerter Skalierung verkomplizierten. In der in *Publikation Nr. 1* dargestellten Arbeit zeigte sich jedoch, dass die Reduktion der Kontrastmittelkonzentration durch die dadurch auch reduzierte Viskosität eine signifikante Verschlechterung der Bildqualität nach sich zieht und die diagnostische Qualität somit generell erheblich leidet. Lediglich für kurze Gefäßabschnitte oder Gefäße mit geringem Durchmesser zeigte sich in einer Subgruppenanalyse kein signifikanter Unterschied in der diagnostischen Genauigkeit zwischen Kontrastmittel mit normaler und solchem mit reduzierter Konzentration. Auf Grund der geringen Fallzahl in der Subgruppenanalyse (=10) könnte der fehlende signifikante Unterschied jedoch allein auf die geringe Stichprobengröße zurückzuführen sein und bedarf weiterer Analysen mit darauf ausgerichteter Power.

Im Rahmen weiterer Studien wurden verschiedene bioresorbierbare Stentsysteme mittels hochauflösender intravaskulärer Bildgebung unter Verwendung der OCT untersucht. Die Untersuchungen zielten hierbei vor allem darauf ab, die Implantationstechnik dieser Devices zu optimieren. Dies ist erforderlich, da sich bioresorbierbare Stentsysteme grundlegend von den üblichen Metall-basierten Stents unterscheiden und vor allem eine nicht an die neuen Devices adaptierte Implantationstechnik für das schlechtere klinische Outcome im Vergleich zu Metall-basierten Stents verantwortlich gemacht wird (20-22). In den *Publikationen Nr. 2 und Nr. 5* zeigte sich, dass eine konsequente Nachdilatation von bioresorbierbaren Poly-L-Lactid- und auch Magnesium-basierten Scaffolds erforderlich ist, um eine optimale Deviceexpansion zu erreichen. Vor allem diese unzureichende Expansion der Devices und

damit häufig auftretende malappositionierte Scaffoldstreben können durch Flussturbulenzen Gerinnungsprozesse induzieren, die wiederum zu potenziell lebensbedrohlichen Devicethrombosen führen (28,29). Bei allen drei untersuchten Typen von bioresorbierbaren Scaffolds (Zwei auf Poly-L-Lactid-Basis: Everolimus-freisetzender ABSORB™-Scaffold und Novolimus-freisetzender DESolve™-Scaffold; Einer auf Magnesium-Basis: Magmaris™-Scaffold) zeigte sich in der intravaskulären Bildgebung nach Nachdilatation ein gutes Ergebnis ohne relevante Malappositionen. Zudem wurden bei keinem der Devices vermehrt Komplikationen durch die Nachdilatation induziert. Die oben genannten Scaffold-Typen wurden für die Analysen ausgewählt, da es sich bei Ihnen um die im klinischen Alltag am häufigsten verwendeten handelte. Sowohl die Poly-L-Lactid, als auch die Magnesium-basierten Devices gleichen sich hinsichtlich der umsichtigen Implantationstechnik inklusive Nachdilatation, die angewendet werden sollte, um ein gutes klinisches Ergebnis zu erzielen. Neben der Reduktion der Malapposition verbessert die Nachdilatation bei den genannten bioresorbierbaren Scaffolds zudem die Symmetrie des implantieren Devices. Eine höhere Symmetrie ist wiederum mit einem besseren klinischen Outcome assoziiert (34,35). Dies scheint vor allem dem durch symmetrische Implantation und optimales „Anmodellieren“ des Scaffolds an die Gefäßwand verbesserten laminarem Blutfluss geschuldet zu sein. Die Ergebnisse der Analyse des Magnesium-basierten Magmaris™-Scaffolds in *Publikation Nr. 5* unterstreichen nochmal die Bedeutung der intravaskulären Bildgebung bei der Implantation bioresorbierbarer Devices. Obwohl nur Läsionen ohne angiographisch sichtbare Kalzifikation eingeschlossen wurden, zeigte sich in der intravaskulären Bildgebung über fast 10% der mittels Scaffold-behandelten Läsionslänge eine relevante Kalzifikation der Gefäßwand. Hierbei zeigt sich eindeutig der positive Effekt der höheren optischen Auflösung durch intravaskuläre Bildgebung, der gerade bei bioresorbierbaren Scaffolds entscheidend für den prozeduralen Erfolg sein kann, da im Bereich relevanter Kalzifikationen auch mittels Nachdilatation keine bessere Expansion und Apposition der Scaffolds erreicht werden kann. Als Konsequenz hieraus ist zu konstatieren, dass vor der Implantation bioresorbierbarer Scaffolds, eine intravaskuläre Bildgebung des zu behandelnden Gefäßabschnittes zwingend erfolgen sollte, um Kalzifikationen der Gefäßwand sicher auszuschließen. Gerade den strukturellen Unterschieden der bioresorbierbaren Devices im Vergleich zu den klassischen Metall-basierten Stents, die sich auch in einer geänderten Implantationstechnik mit vorhergehender intravaskulärer Bildgebung und sorgsamer Läsionsauswahl, -präparation und Nachdilatation abbilden müssen ist in der Frühphase zu wenig Rechnung getragen worden. Bei klassischen Metall-basierten Stents ist eine regelhafte Nachdilatation nämlich nicht notwendig. Auch ist durch ihre im Vergleich zu

Scaffolds deutlich höhere Radialkraft und strukturelle Stabilität eine derart extensive Läsionsvorbereitung und Devicenachbehandlung selten indiziert. In Teilen hat somit sicherlich auch eine nicht an Scaffolds adaptierte Implantationstechnik mit zu den im Vergleich zu modernen DES schlechteren klinischen Outcome beigetragen (20,21).

Ein weiterer Punkt, dem Rechnung getragen werden muss, ist die überlappende Implantation von Stents oder Scaffolds, die bei langen Läsionen oder edge dissections (= Dissektionen der Gefäßwand am Stenteingang/-ausgag) notwendig ist. Vor allem auf Grund der geringen Strebendicke moderner DES (ca. 50-70µm) stellt die überlappende Implantation dieser Devices in der Regel kein Problem dar (36, 37). Bei bioresorbierbarer Scaffolds mit ihrer Strebendicke von meist ca. 150µm bestand die Sorge, dass der starke Lumenverlust durch dann überlappende Strebendicken von ca. 300µm für Restenose oder Stentthrombosen prädisponieren würde, da es zu erheblichen Flusslimitationen im Blutstrom kommen könnte. Die überlappende Implantation von Scaffolds wurde daher anfangs, wann immer möglich, vermieden. In der unter *Publikation Nr. 3* dargestellten Studie, in der erstmals überlappend implantierte Scaffolds mittels intravaskulärer Bildgebung untersucht wurden zeigte sich jedoch entgegen der Befürchtungen, dass die doppelte Schicht an Scaffoldstreben nicht zu einer Reduktion des Gefäßlumens führt, sondern durch eine Überexpansion des Gefäßes im Überlappungsbereich nach abluminal kompensiert wird. Hinsichtlich des klinischen Outcomes nach überlappender Scaffold-Implantation sind die Daten widersprüchlich. Während Ishibashi et al. die überlappende Scaffold-Implantation als unabhängigen Risikofaktor für periprozedurale Myokardinfarkte beschreiben (42), haben Ortega-Paz et al. keine signifikanten Unterschiede im klinischen 1-Jahres-Outcome nach überlappender vs. nicht-überlappender Scaffold-Implantation gefunden (43). Während in der Analyse mittels OCT keine Unterschiede im Gefäßlumen identifiziert werden konnten, bleibt dennoch die Möglichkeit zu konstatieren, dass die großen Strebendicken von ca. 300µm im Überlappungsbereich zu Flussturbulenzen und somit zu Scaffoldthrombosen beitragen können. Somit sollte die überlappende Implantation dieser Devices auf Grund der aktuell widersprüchlichen Datenlage bis zum Vorliegen großer randomisierter Studien nach Möglichkeit vermieden werden.

Der komplette Prozess der Bioresorption bei Scaffolds war ein fundamental neuer Ansatz in der Behandlung der koronaren Herzerkrankung, da alle bis dahin verfügbaren Stentdevices auf eine dauerhafte Präsenz im Koronargefäß ausgelegt waren. Im Rahmen der unter *Publikation Nr. 4* dargestellten Analyse zeigte sich, dass die Dauer des Resorptionsprozesses von individuellen Patientenfaktoren entscheidend beeinflusst wird. So zeigte sich in Patienten mit Diabetes mellitus eine deutlich verzögerte Scaffoldresorption.

Ebenso wurde das Vorhandensein von Peri-strut low intensity areas (PSLIA) als Ausdruck perivaskulärer Entzündungsprozesse in der OCT als unabhängiger Risikofaktor für eine längere Resorptionsdauer identifiziert. Lokale Inflammationsprozesse scheinen also mit der Bioresorption der Scaffolds zu interferieren. Dagegen zeigte sich in Patienten mit akutem Koronarsyndrom eine signifikant höhere Resorptionsgeschwindigkeit als in Patienten mit stabiler koronarer Herzerkrankung. Während sich die Resorptionsgeschwindigkeiten bei verschiedenen Patienten deutlich unterschieden, aber bei mehreren implantierten Scaffolds im selben Patienten stets sehr ähnlich waren, liegt der Schluss nahe, dass es vor allem Patientencharakteristika sind, die den Resorptionsprozess beeinflussen und denen bei der Auswahl des Devices Rechnung getragen werden sollte. Die dargestellte Analyse war die erste, die die Resorptionseigenschaften der Scaffolds im Menschen genauer beleuchtete. Da eine verlängerte Resorptionsdauer ebenfalls als Risikofaktor für die erhöhte Devicethromboserate von Scaffolds im Vergleich zu modernen DES diskutiert wird, sollte auf die Implantation von Scaffolds bei Patienten mit Diabetes mellitus verzichtet werden (20-22). Der protrahierte Abbauprozess scheint auf Grund des anhaltenden Gefäßremodellings für Thrombosen zu prädisponieren. Die erhobenen Daten machen deutlich, wie wichtig neben einem speziell adaptierten Implantationsprotokoll auch die sorgsame Patientenauswahl bei der Implantation von Scaffolds ist.

Ein weiteres Phänomen, das bei der Implantation von modernen DES so gut wie nicht mehr auftrat, war die vermehrte Entstehung von koronaren Evaginationen nach Scaffold-Implantation, die im Rahmen der *Publikation Nr. 6* mittels OCT genauer analysiert wurde. Hierbei wurde erstmals gezeigt, dass es im Rahmen der Ausbildung von Evaginationen zu einer mit der Zeit kontinuierlichen Zunahme von Gefäß- und Scaffoldgröße kommt. Als Endergebnis kann es dadurch zur Ausbildung koronarer Aneurysmata kommen (62-64). Als ursächlich für die Ausbildung von Evaginationen werden anhaltende vaskuläre Entzündungsprozesse mit resultierendem positivem Remodelling der Gefäßwand gesehen (62-65). Koronare Evaginationen unterbrechen, ebenso wie malappositionierte Streben, den laminaren Blutfluss und führen zu Flussturbulenzen, was wiederum das Risiko für Scaffoldthrombosen erhöht. Zudem stellen koronare Aneurysmata eine besondere Herausforderung für eine eventuell notwendige erneute PCI dar, da die Gefäßdiameter eine Größe erreichen können, die mit den herkömmlichen Stentdevices nicht zu behandeln sind.

Zusammenfassend macht die Analyse der bioresorbierbaren Scaffolds deutlich, dass eine spezielle und sorgfältige Läsions-, wie auch Patientenauswahl bei der Anwendung dieser

Devices von entscheidender Bedeutung ist, um potenziell fatalen Scaffoldthrombosen vorzubeugen.

Zur ausreichenden Vorbehandlung stark kalzifizierter Koronarläsionen stellt die vor Kurzem neu eingeführte koronare Lithoplastie eine vielversprechende Therapieoption dar. In der bisher größten durchgeführten Studie (*Publikation Nr. 7*) zur Evaluation dieser Technologie im klinischen Alltag, zeigte sich eine hohe prozedurale Erfolgsrate ohne Induktion relevanter klinischer Komplikationen. Gerade vor dem Hintergrund eines zunehmenden Patientenalters mit entsprechend höherem Maß an interventionell zu behandelnden kalzifizierten Koronarstenosen stellt die koronare Lithoplastie auch eine gute Alternative zum bisherigen Goldstandard, der Rotablation, dar. Um den Stellenwert der Lithoplastie im Vergleich zur Rotablation weiter zu evaluieren wurde mit der ROTA.shock-Studie die weltweit erste randomisierte Vergleichsstudie durchgeführt. Alle bisherigen großen Studien zum Thema Lithoplastie (DISRUPT CAD I-IV) zielten auf die Marktzulassung der Technologie ab und waren daher als Einzelarmstudien mit den Endpunkten Sicherheit und Effektivität ausgelegt (79-82). Für den täglichen klinischen Einsatz spielt jedoch auch vor allem der Vergleich mit bereits etablierten Technologien, wie in diesem Fall der Rotablation, eine entscheidende Rolle. Die ersten Ergebnisse einer Subgruppenanalyse (*Publikation Nr.8*) zeigten das sich mit beiden Techniken eine deutliche Modulation kalzifizierter Koronarstenosen erzielen lässt. Es wurden jedoch auch Unterschiede deutlich, die im Rahmen der perkutanen Koronarintervention solcher Läsionen bedacht werden sollten. Durch die koronare Lithoplastie scheinen mehr und größere Frakturen im kalzifizierten Plaque induziert zu werden als durch dir Rotablation. Dies legt den Schluss nahe, dass Läsionen mit zirkumferenzieller und langer Kalzifikation besser mit dieser Technik adressiert werden sollten. Im Gegensatz dazu ist er mit Anwendung der Rotablation möglich einen größeren akuten Lumengewinn zu erzielen als durch koronare Lithoplastie. Dieser größere „Arbeitskanal“ kann die im weiteren Verlauf der Koronarintervention notwendige Positionierung von Ballons oder Stents deutlich erleichtern. Dementsprechend könnte es bei stark exzentrischen Kalzifikationen zielführender sein, eine Rotablation durchzuführen.

Bedacht werden sollte indes stets, dass die Lithoplastie auf Grund ihrer einfacheren Anwendbarkeit als Ballon-basierte Technik dafür geeignet scheint, eine effektive Möglichkeit zur Modulation stark kalzifizierter Koronarstenosen einem breiteren Patientenkollektiv zugänglich zu machen. Die Rotablation findet im Gegensatz dazu auf Grund ihrer höheren technischen Komplexität und dem Komplikationsrisiko (Koronarperforation, Okklusion des Koronargefäßes, No-Flow/Slow-Flow) in der großen Mehrzahl der Herzkatheterlabore keine

regelhafte Anwendung. In der interventionellen Therapie stark kalzifizierter Koronarstenosen ist es jedoch von entscheidender Bedeutung bereits vor Implantation des Stents eine ausreichende Plaquemodulation zu erreichen, um einer Unterexpansion des Stents mit entsprechend schlechterem klinischem Outcome vorzubeugen (72,73).

Eine bedeutende Limitation der Lithoplastie bleibt jedoch der Umstand, dass der Lithoplastie-Ballon in manchen Situationen trotz vorheriger Prädilatation nicht in die Zielläsion vorgebracht werden kann und somit nur die Möglichkeit zur direkten Atherektomie bleibt.

Die im Rahmen dieser Arbeit dargestellten Projekte verdeutlichen, dass die in der perkutanen Koronarintervention Anwendung findenden Techniken in den letzten Jahren weiterhin innovative Verbesserungen erfahren haben. Insbesondere der verstärkte Einsatz intravaskulärer Bildgebung, wie dem IVUS oder der OCT, erlaubt die Durchführung einer optimalen interventionellen Therapie durch die hochauflösende Darstellung des Gefäßes wie auch der Stents. Hiermit konnten auch potenzielle Ursachen für das schlechtere klinische Outcome bioresorbierbarer Stenttechnologien im Vergleich zu modernen DES auf Metallbasis ermittelt werden. Es wurde deutlich, dass bei der Verwendung bioresorbierbarer Stents eine sorgsame Läsionsauswahl wie auch -präparation von entscheidender Bedeutung sind und eine an das Device angepasste Implantationstechnik angewandt werden muss. Auf Grund des enttäuschenden klinischen Outcomes sind bioresorbierbare Stents zum jetzigen Zeitpunkt nahezu komplett vom Markt verschwunden, bleiben jedoch eine für die Zukunft vielversprechende Option, sobald Verbesserungen der Devices, wie etwa geringere Strebendicken und stärkere Radialkraft, erreicht werden konnten. Gerade vor dem Hintergrund eines alternden Patientenkollektivs und der zunehmenden Häufigkeit stark kalzifizierter Koronarstenosen, die einer interventionellen Therapie zugeführt werden müssen, ist die im Rahmen dieser Arbeit genauer evaluierte koronare Lithoplastie ein bedeutender Baustein, der das vorhandene Therapieportfolio um eine weitere effektive Methode ergänzt. Hier werden in den nächsten Jahren mit Sicherheit weitere Studien folgen, die das klinische Outcome dieser und weiterer Techniken zur Behandlung stark kalzifizierter Koronarstenosen, wie beispielsweise die orbitale Atherektomie, evaluieren und uns somit aufzeigen können, von welcher Technik Patienten bei möglichst geringem Komplikationsrisiko am meisten profitieren.

7. Zusammenfassende Darstellung

Bioresorbierbare Gefäßstützen („Scaffolds“) wurden entwickelt, um einige Nachteile klassischer Drug-Eluting Stents (DES) zu überwinden. Durch ihre zeitlich begrenzte Präsenz im Gefäßsystem kommt es nach Abschluss der Resorption zur Restitution der physiologischen Vasomotion. Zudem bleibt kein Fremdmaterial im Gefäßsystem zurück. Die wissenschaftlichen Arbeiten beschäftigten sich im Wesentlichen mit der Analyse bioresorbierbarer Scaffolds unter Verwendung intravaskulärer Bildgebung mittels hochauflösender Optischer Kohärenztomographie (OCT). Im Rahmen einer ersten Studie wurde untersucht, ob sich die für die Durchführung einer OCT notwendige Kontrastmittelmenge durch eine geringere Kontrastmittelkonzentration reduzieren lässt. Hierbei zeigte sich im Vergleich zur Standard-Kontrastmittelkonzentration jedoch, dass eine entsprechende Reduktion leider auch zu einem erheblichen Verlust an Bildqualität und diagnostischer Verlässlichkeit führt, womit die OCT-Durchführung mittels reduzierter Kontrastmittelkonzentration keine Möglichkeit bietet, die Gesamtmenge an notwendigem Kontrastmittel signifikant zu reduzieren. Im Weiteren wurde der Effekt der Nachdilatation mittels non-compliant Ballons auf die gängigsten Typen bioresorbierbarer Scaffolds untersucht. Es zeigte sich, dass eine regelhafte Nachdilatation der Devices erfolgen sollte, da nur so eine optimale Apposition der Streben und Expansion des Scaffolds erreicht werden kann, ohne dass höhere Raten an Dissektionen oder Strebenfrakturen induziert werden. Die Länge koronarer Läsionen macht in manchen Fällen die überlappende Implantation von bioresorbierbaren Scaffolds notwendig. Aufgrund der hohen Strebendicke dieser Devices bestand jedoch die große Sorge, dass dies zu relevanten Lumenverlusten führen könnte. Im Rahmen einer OCT-Analyse von Scaffolds mit überlappender Implantation konnte gezeigt werden, dass diese nicht mit einer verminderten Lumen- und Scaffoldfläche assoziiert ist, sondern die doppelte Strebendicke tendenziell zu einer Überexpansion des entsprechenden Gefäßabschnittes mit einer im Vergleich zum übrigen Scaffold stabilen Lumenfläche führt. Da sich die anfängliche Annahme, dass Poly-L-Lactid Scaffolds nach 2 Jahren komplett resorbiert sein würden nicht bestätigte und die tatsächliche Resorptionsdauer in vivo bei ca. 4-5 Jahren lag, wurde eine Analyse der Resorptionsgeschwindigkeit nach Scaffoldimplantation durchgeführt. In der OCT-gestützten Analyse der Resorption über die Lichtintensität der Streben zu verschiedenen Zeitpunkten nach Implantation konnte ermittelt werden, dass Diabetes mellitus sowie lokale Entzündungsprozesse der Gefäßwand mit einer verzögerten Resorption einhergehen, wohingegen die Degradation bei Patienten, die den Scaffold im Rahmen eines akuten

Koronarsyndroms implantiert bekamen, eine deutlich höhere Resorptionsgeschwindigkeit zeigte. Es konnte damit dargelegt werden, dass individuelle Patientenfaktoren einen erheblichen Einfluss auf den Abbauprozess haben und bei der Implantation berücksichtigt werden sollten. Koronare Evaginationen können nach Scaffoldimplantation auftreten und stellen einen weiteren Risikofaktor für ein reduziertes klinisches Outcome dar. In der OCT-Analyse von Evaginationen zeigte sich, dass diese umso größer zu sein scheinen, je länger der Zeitpunkt der Implantation zurückliegt. Den Endpunkt dieser Entwicklung stellen möglicherweise koronare Aneurysmata dar. Evaginationen können den laminaren Fluss unterbrechen und zu späten Scaffoldthrombosen führen.

In der Analyse der durchgeführten bioresorbierbaren Devices wurde deutlich, wie wichtig sowohl eine sorgsame Läsionsauswahl und -vorbereitung wie auch die Scaffoldnachdilatation sind. Es konnten einige Mechanismen dargestellt werden, die potenzielle Erklärungen für das im Vergleich zu modernen DES schlechtere klinische Outcome nach Implantation eines Poly-L-Lactid Scaffolds liefern.

Als weitere neue Technologie in der perkutanen Koronarintervention wurde die intrakoronare Lithoplastie zur Behandlung stark kalzifizierter Koronarstenosen in der mit 180 Patienten bisher größten Studie hinsichtlich ihres klinischen und prozeduralen Outcomes analysiert. Es zeigten sich exzellente Prozedurergebnisse, die einen breiteren Einsatz der intrakoronaren Lithoplastie rechtfertigen. Im Rahmen der ROTA.shock-Studie wurde die koronare Lithoplastie weltweit erstmals randomisiert mit dem bisherigen Goldstandard zur Behandlung stark kalzifizierter Koronarstenosen, der Rotablation, verglichen. Hier zeigte sich, dass die koronare Lithoplastie durch eine im Vergleich zur Rotablation höhere Anzahl induzierter Frakturen im kalzifizierten Plaque bei Läsionen mit zirkumferenzieller Verkalkung besser geeignet zu sein scheint, wohingegen die Rotablation mit einem größeren akuten Lumengewinn assoziiert ist, der bei kalzifizierten Läsionen mit starker Exzentrizität von Vorteil sein kann. Da die Lithoplastie im Gegensatz zur technisch aufwendigeren Rotablation eine Ballon-basierte Technik ist, kann sie einfach in den Ablauf der meisten Herzkatheterlabore implementiert werden und stellt eine effektive und sichere Therapieoption bei Patienten mit stark kalzifizierten Koronarstenosen dar.

7.1 Summarized Presentation

Bioresorbable scaffolds have been developed to overcome some disadvantages of classical drug-eluting stents (DES). Due to their only temporary presence in the vascular system, there is a restitution of physiological vasomotion after resorption is complete. In addition, no foreign material remains in the vascular system. The scientific work was mainly concerned with the analysis of bioresorbable scaffolds using intravascular imaging by high-resolution optical coherence tomography (OCT). In an initial study, we investigated whether the amount of contrast agent required to perform OCT could be reduced by using a lower contrast agent concentration. However, compared to the standard contrast agent concentration, it was shown that a corresponding reduction unfortunately also leads to a considerable loss of image quality and diagnostic reliability, so that OCT performance by means of reduced contrast agent concentration does not offer the possibility of significantly reducing the total amount of contrast agent required. Furthermore, the effect of post-dilation using non-compliant balloons on the most common types of bioresorbable scaffolds was investigated. It was shown that regular postdilatation of the devices should be performed, as this is the only way to achieve optimal apposition of the struts and expansion of the scaffold without inducing higher rates of dissection or strut fracture. The length of coronary lesions in some cases necessitates the overlapping implantation of bioresorbable scaffolds. However, due to the high strut thickness of these devices, there was a major concern that this could lead to relevant lumen loss. OCT analysis of scaffolds with overlapping implantation showed that this was not associated with decreased lumen and scaffold area, but that the double strut thickness tended to lead to overexpansion of the corresponding vessel section with a stable lumen area compared with the rest of the scaffold. Because the initial assumption that poly-L-lactide scaffolds would be completely resorbed after 2 years was not confirmed and the actual resorption time in vivo was approximately 4-5 years, an analysis of the resorption rate after scaffold implantation was performed. OCT-based analysis of resorption via light intensity of the struts at different time points after implantation revealed that diabetes mellitus as well as local inflammatory processes of the vessel wall were associated with delayed resorption, whereas degradation in patients who had the scaffold implanted in the context of an acute coronary syndrome showed a significantly higher resorption rate. Thus, it could be clearly demonstrated that individual patient factors have a significant influence on the degradation process and should be considered during implantation. Coronary evaginations may occur after scaffold implantation and represent another risk factor for reduced clinical outcome. OCT analysis of evaginations showed that the longer the time of

implantation, the greater they appear to be. Coronary aneurysms may represent the end point of this evolution. Evaginations may interrupt laminar flow and lead to late scaffold thrombosis. In the analysis of the bioresorbable devices performed, the importance of both careful lesion selection and preparation as well as scaffold postdilation became clear. Some mechanisms were presented that provide potential explanations for the poorer clinical outcome after implantation of a poly-lactide scaffold compared with modern DES.

As another new technology in percutaneous coronary intervention, intracoronary lithoplasty for the treatment of severely calcified coronary stenoses was analyzed with respect to its clinical and procedural outcome in the largest study to date with 180 patients. Excellent procedural results were shown, justifying a wider use of intracoronary lithoplasty. In the ROTA.shock study, coronary lithoplasty was compared for the first time worldwide in a randomized fashion with the previous gold standard for the treatment of severely calcified coronary stenoses, rotablation. Whereas RA leads to a larger acute lumen gain, IVL induces more and longer fractures of the calcified plaque. These differences should be considered when planning a PCI strategy. Because lithoplasty is a balloon-based technique, in contrast to the more technically complex rotablation, it can be easily implemented into the workflow of most cardiac catheterization laboratories and represents an effective and safe therapeutic option in patients with severely calcified coronary stenoses.

8. Referenzen

1. Nabel EG, Braunwald E. A tale of coronary artery disease and myocardial infarction. *N Engl J Med* 2012; 366(1): 54-63
2. Sigwart U, Puel J, Mirkovitch V, Joffre F, Kappenberger L. Intravascular stents to prevent occlusion and restenosis after transluminal angioplasty. *N Engl J Med* 1987; 316(12): 701-706
3. Stefanini GG, Holmes DR Jr. Drug-eluting coronary-artery stents. *N Engl J Med* 2013; 368(3): 254-265
4. Bønaa KH, Mannsverk J, Wiseth R, Aaberge L, Myreng Y, Nygård O, Nilsen DW, Kløw NE, Uchto M, Trovik T, Bendz B, Stavnes S, Bjørnerheim R, Larsen AI, Slette M, Steigen T, Jakobsen OJ, Bleie Ø, Fossum E, Hanssen TA, Dahl-Eriksen Ø, Njølstad I, Rasmussen K, Wilsgaard T, Nordrehaug JE; NORSTENT Investigators. Drug-Eluting or Bare-Metal Stents for Coronary Artery Disease. *N Engl J Med* 2016; 375(13): 1242-1252
5. Iqbal J, Serruys PW, Silber S, Kelbaek H, Richardt G, Morel MA, Negoita M, Buszman PE, Windecker S. Comparison of zotarolimus- and everolimus-eluting coronary stents: final 5-year report of the RESOLUTE all-comers trial. *Circ Cardiovasc Interv* 2015; 8(6): e002230
6. Haude M, Ince H, Abizaid A, Toelg R, Lemos PA, von Birgelen C, Christiansen EH, Wijns W, Neumann FJ, Kaiser C, Eeckhout E, Lim ST, Escaned J, Onuma Y, Garcia-Garcia HM, Waksman R. Sustained safety and performance of the second-generation drug-eluting absorbable metal scaffold in patients with de novo coronary lesions: 12-month clinical results and angiographic findings of the BIOSOLVE-II first-in-man trial. *Eur Heart J* 2016; 37(35): 2701-2709
7. Garg S, Serruys PW. Coronary stents: current status. *J Am Coll Cardiol* 2010; 56: S1–S42
8. Nakazawa G, Finn AV, Ladich E, Ribichini F, Coleman L, Kolodgie FD, Virmani R. Drug-eluting stent safety: findings from preclinical studies. *Expert Rev Cardiovasc Ther* 2008; 6: 1379–1391
9. Wilson GJ, Nakazawa G, Schwartz RS, Huibregtse B, Poff B, Herbst TJ, Baim DS, Virmani R. Comparison of inflammatory response after implantation of sirolimus- and paclitaxel-eluting stents in porcine coronary arteries. *Circulation* 2009; 120: 141–149
10. Papafaklis MI, Bourantas CV, Theodorakis PE, Katsouras CS, Naka KK, Fotiadis DI, Michalis LK. The effect of shear stress on neointimal response following sirolimus- and

paclitaxel-eluting stent implantation compared with bare-metal stents in humans. *J Am Coll Cardiol Intv* 2010; 3: 1181–1189.

11. Spanos V, Stankovic G, Tobis J, Colombo A. The challenge of in-stent restenosis: insights from intravascular ultrasound. *Eur Heart J* 2003; 24: 138–150
12. Frobert O, Lagerqvist B, Carlsson J, Lindback J, Stenestrand U, James SK. Differences in restenosis rate with different drug-eluting stents in patients with and without diabetes mellitus: a report from the SCAAR (Swedish Angiography and Angioplasty Registry). *J Am Coll Cardiol* 2009; 53: 1660–1667
13. Canan T, Lee MS. Drug-eluting stent fracture: incidence, contributing factors, and clinical implications. Catheter Cardiovasc Interv 2010; 75: 237–245
14. Alfonso F, Prati F. Optical coherence tomography or intravascular ultrasound to optimize coronary stent implantation. *Eur Heart J* 2017; 38(42): 3148-3151
15. Jang IK, Arbustini E, Bezerra HG, Ozaki Y, Bruining N, Dudek D, Radu M, Erglis A, Motreff P, Alfonso F, Toutouzas K, Gonzalo N, Tamburino C, Adriaenssens T, Pinto F, Serruys PW, Di Mario C; Expert's OCT Review Document. Expert review document part 2: methodology, terminology and clinical applications of optical co- herence tomography for the assessment of interventional procedures. Eur Heart J 2012; 33: 2513–2520
16. Di Vito L, Yoon JH, Kato K, Yonetsu T, Vergallo R, Costa M, Bezerra HG, Arbustini E, Narula J, Crea F, Prati F, Jang IK; COICO group (Consortium of Inves- tigators for Coronary OCT). Comprehensive overview of definitions for optical coherence tomography-based plaque and stent analyses. Coron Artery Dis 2014; 25: 172–185
17. Wijns W, Shite J, Jones MR, Lee SW, Price MJ, Fabbiocchi F, Barbato E, Akasaka T, Bezerra H, Holmes D. Optical coherence tomography imaging during percutaneous coronary intervention impacts physician decision-making: ILUMIEN I study. *Eur Heart J* 2015; 36(47): 3346-3355
18. Maehara A, Ben-Yehuda O, Ali Z, Wijns W, Bezerra HG, Shite J, Généreux P, Nichols M, Jenkins P, Witzenbichler B, Mintz GS, Stone GW. Comparison of Stent Expansion Guided by Optical Coherence Tomography Versus Intravascular Ultrasound: The ILUMIEN II Study (Observational Study of Optical Coherence Tomography [OCT] in Patients Undergoing Fractional Flow Reserve [FFR] and Percutaneous Coronary Intervention). *JACC Cardiovasc Interv* 2015; 8(13): 1704-1714
19. Ali ZA, Maehara A, Généreux P, Shlofmitz RA, Fabbiocchi F, Nazif TM, Guagliumi G, Meraj PM, Alfonso F, Samady H, Akasaka T, Carlson EB, Leesar MA, Matsumura M, Ozan MO, Mintz GS, Ben-Yehuda O, Stone GW; ILUMIEN III: OPTIMIZE PCI Investigators.

Optical coherence tomography compared with intravascular ultrasound and with angiography to guide coronary stent implantation (ILUMIEN III: OPTIMIZE PCI): a randomised controlled trial. *Lancet* 2016; 388(10060): 2618-2628

20. Wykrzykowska JJ, Kraak RP, Hofma SH, van der Schaaf RJ, Arkenbout EK, IJsselmuiden AJ, Elias J, van Dongen IM, Tijssen RYG, Koch KT, Baan J Jr, Vis MM, de Winter RJ, Piek JJ, Tijssen JGP, Henriques JPS; AIDA Investigators. Bioresorbable Scaffolds versus Metallic Stents in Routine PCI. *N Engl J Med* 2017; 376(24): 2319-2328
21. Ali ZA, Serruys PW, Kimura T, Gao R, Ellis SG, Kereiakes DJ, Onuma Y, Simonton C, Zhang Z, Stone GW. 2-year outcomes with the Absorb bioresorbable scaffold for treatment of coronary artery disease: a systematic review and meta-analysis of seven randomised trials with an individual patient data substudy. *Lancet* 2017; 390(10096): 760-772
22. Ortega-Paz L, Capodanno D, Gori T, Nef H, Latib A, Caramanno G, Di Mario C, Naber C, Lesiak M, Capranzano P, Wiebe J, Mehilli J, Araszkiewicz A, Pyxaras S, Mattesini A, Geraci S, Naganuma T, Colombo A, Münzel T, Sabaté M, Tamburino C, Brugaletta S. Predilation, sizing and post-dilation scoring in patients undergoing everolimus-eluting bioresorbable scaffold implantation for prediction of cardiac adverse events: development and internal validation of the PSP score. *EuroIntervention* 2017; 12(17): 2110-2117
23. Haude M, Ince H, Abizaid A, Toelg R, Lemos PA, von Birgelen C, Christiansen EH, Wijns W, Neumann FJ, Kaiser C, Eeckhout E, Lim ST, Escaned J, Onuma Y, Garcia-Garcia HM, Waksman R. Sustained safety and performance of the second-generation drug-eluting absorbable metalscaffold in patients with de novo coronary lesions: 12-month clinical results and angiographicfindings of the BIOSOLVE-II first-in-man trial. *Eur Heart J* 2016; 37(35): 2701-2709
24. Haude M, Ince H, Abizaid A, Toelg R, Lemos PA, von Birgelen C, Christiansen EH, Wijns W, Neumann FJ, Kaiser C, Eeckhout E, Lim ST, Escaned J, Garcia-Garcia HM, Waksman R. Safety and performance of the second-generation drug-eluting absorbable metal scaffold in patients with de-novo coronary artery lesions (BIOSOLVE-II): 6 month results of a prospective, multicentre, non-randomised, first-in-man trial. *Lancet* 2016; 387(10013): 31-39
25. Abizaid A, Carrié D, Frey N, Lutz M, Weber-Albers J, Dudek D, Chevalier B, Weng SC, Costa RA, Anderson J, Stone GW; FANTOM II Clinical Investigators. 6-Month Clinical and Angiographic Outcomes of a Novel Radiopaque Sirolimus-Eluting

Bioresorbable Vascular Scaffold: The FANTOM II Study. *JACC Cardiovasc Interv* 2017; 10(18): 1832-1838

26. Frick K, Michael TT, Alomar M, Mohammed A, Rangan BV, Abdullah S, Grodin J, Hastings JL, Banerjee S, Brilakis ES. Low molecular weight dextran provides similar optical coherence tomography coronary imaging compared to radiographic contrast media. *Catheter Cardiovasc Interv* 2014; 84(5): 727–731
27. Ozaki Y, Kitabata H, Tsujioka H, Hosokawa S, Kashiwagi M, Ishibashi K, Komukai K, Tanimoto T, Ino Y, Takarada S, Kubo T, Kimura K, Tanaka A, Hirata K, Mizukoshi M, Imanishi T, Akasaka T. Comparison of contrast media and low-molecularweight dextran for frequency-domain optical coherence tomography. *Circ J* 2012; 76(4): 922–927
28. Cuculi F, Puricel S, Jamshidi P, Valentin J, Kallinikou Z, Toggweiler S, Weissner M, Münzel T, Cook S, Gori T. Optical coherence tomography findings in bioresorbable vascular scaffolds thrombosis. *Circ Cardiovasc Interv* 2015; 8(10): e002518
29. Karanasos A, Van Mieghem N, van Ditzhuijzen N, Felix C, Daemen J, Autar A, Onuma Y, Kurata M, Diletti R, Valgimigli M, Kauer F, van Beusekom H, de Jaegere P, Zijlstra F, van Geuns RJ, Regar E. Angiographic and optical coherence tomography insights into bioresorbable scaffold thrombosis: single-center experience. *Circ Cardiovasc Interv* 2015; 8(5); pii: e002369
30. Gutiérrez-Chico JL, Gijsen F, Regar E, Wentzel J, de Bruyne B, Thuesen L, Ormiston J, McClean DR, Windecker S, Chevalier B, Dudek D, Whitbourn R, Brugaletta S, Onuma Y, Serruys PW. Differences in neointimal thickness between the adluminal and the abluminal sides of malapposed and side-branch struts in a polylactide bioresorbable scaffold: evidence in vivo about the abluminal healing process. *JACC Cardiovasc Interv* 2012; 5(4): 428-435
31. Sonoda S, Morino Y, Ako J, Terashima M, Hassan AH, Bonneau HN, Leon MB, Moses JW, Yock PG, Honda Y, Kuntz RE, Fitzgerald PJ, SIRIUS Investigators. Impact of final stent dimensions on long-term results following sirolimus-eluting stent implantation: serial intravascular ultrasound analysis from the sirius trial. *J Am Coll Cardiol* 2004; 43: 1959–1963
32. Costa MA, Angiolillo DJ, Tannenbaum M, Driesman M, Chu A, Patterson J, Kuehl W, Battaglia J, Dabbons S, Shamoon F, Flieshman B, Niederman A, Bass TA, STLLR Investigators. Impact of stent deployment procedural factors on longterm effectiveness and safety of sirolimus-eluting stents (final results of the multicenter prospective STLLR trial). *Am J Cardiol* 2008; 101: 1704–1711

33. Doi H, Maehara A, Mintz GS, Yu A, Wang H, Mandinov L, Popma JJ, Ellis SG, Grube E, Dawkins KD, Weissman NJ, Turco MA, Ormiston JA, Stone GW. Impact of post-intervention minimal stent area on 9-month follow-up patency of paclitaxeleluting stents: an integrated intravascular ultrasound analysis from the TAXUS IV, V, and VI and TAXUS ATLAS Workhorse, Long Lesion, and Direct Stent Trials. *J Am Coll Cardiol Interv* 2009; 2: 1269–1275
34. Suwannasom P, Sotomi Y, Ishibashi Y, Cavalcante R, Albuquerque FN, Macaya C, Ormiston JA, Hill J, Lang IM, Egred M, Fajadet J, Lesiak M, Tijssen JG, Wykrzykowska JJ, de Winter RJ, Chevalier B, Serruys PW, Onuma Y. The impact of postprocedural asymmetry, expansion, and eccentricity of bioresorbable everolimus-eluting scaffold and metallic everolimuseluting stent on clinical outcomes in the ABSORB II Trial. *J Am Coll Cardiol Interv* 2016*;* 9(12): 1231–1242
35. Rivero F, Bastante T, Cuesta J, Benedicto A, Restrepo JA, Alfonso F. Treatment of in-stent restenosis with bioresorbable vascular scaffolds: optical coherence tomography insights. *Can J Cardiol* 2015 31(3):255–259
36. O'Sullivan CJ, Stefanini GG, Räber L, Heg D, Taniwaki M, Kalesan B, Pilgrim T, Zanchin T, Moschovitis A, Büllesfeld L, Khattab AA, Meier B, Wenaweser P, Jüni P, Windecker S. Impact of stent overlap on long-term clinical outcomes in patients treated with newer-generation drug-eluting stents. *Euro-Intervention* 2014; 9: 1076–1084
37. Farooq V, Vranckx P, Mauri L, Cutlip DE, Belardi J, Silber S, Widimsky P, Leon M, Windecker S, Meredith I, Negoita M, van Leeuwen F, Neumann FJ, Yeung AC, Garcia-Garcia HM, Serruys PW. Impact of overlapping newer generation drug-eluting stents on clinical and angiographic outcomes: pooled analysis of five trials from the international Global RESOLUTE Program. *Heart* 2013; 99: 626–633
38. Verheye S, Ormiston JA, Stewart J, Webster M, Sanidas E, Costa R, Costa JR Jr, Chamie D, Abizaid AS, Pinto I, Morrison L, Toyloy S, Bhat V, Yan J, Abizaid A. A next-generation bioresorbable coronary scaffold system: from bench to first clinical evaluation: 6- and 12-month clinical and multimodality imaging results. *JACC Cardiovasc Interv* 2014 7: 89–99
39. Everaert B, Felix C, Koolen J, den Heijer P, Henriques J, Wykrzykowska J, van der Schaaf R, de Smet B, Hofma S, Diletti R, Van Mieghem N, Regar E, Smits P, van Geuns RJ. Appropriate use of bioresorbable vascular scaffolds in percutaneous coronary interventions: a recommendation from experienced users: a position statement on the use of bioresorbable vascular scaffolds in the Netherlands. *Neth Heart J* 2015; 23: 161–165

40. Tamburino C, Latib A, van Geuns RJ, Sabate M, Mehilli J, Gori T, Achenbach S, Alvarez MP, Nef H, Lesiak M, Di Mario C, Colombo A, Naber CK, Caramanno G, Capranzano P, Brugaletta S, Geraci S, Araszkiewicz A, Mattesini A, Pyxaras SA, Rzeszutko L, Depukat R, Diletti R, Boone E, Capodanno D, Dudek D. Contemporary practice and technical aspects in coronary intervention with bioresorbable scaffolds: a European perspective. *EuroIntervention* 2015 11: 45–52
41. Wiebe J, Nef HM, Hamm CW. Current status of bioresorbable scaffolds in the treatment of coronary artery disease. *J Am Coll Cardiol* 2014; 64: 2541–2551B
42. Ishibashi Y, Muramatsu T, Nakatani S, Sotomi Y, Suwannasom P, Grundeken MJ, Cho YK, Garcia-Garcia HM, van Boven AJ, Piek JJ, Sabaté M, Helqvist S, Baumbach A, McClean D, de Sousa Almeida M, Wasungu L, Miquel-Hebert K, Dudek D, Chevalier B, Onuma Y, Serruys PW. Incidence and potential mechanism(s) of post-procedural rise of cardiac biomarker in patients with coronary artery narrowing after implantation of an everolimus-eluting bioresorbable vascular scaffold or everolimus-eluting metallic stent. *JACC Cardiovasc Interv* 2015; 8: 1053–1063
43. Ortega-Paz L, Capodanno D, Giacchi G, Gori T, Nef H, Latib A, Caramanno G, Di Mario C, Naber C, Lesiak M, Capranzano P, Wiebe J, Mehilli J, Araszkiewicz A, Pyxaras S, Mattesini A, Geraci S, Naganuma T, Colombo A, Münzel T, Sabaté M, Tamburino C, Brugaletta S. Impact of overlapping on 1-year clinical outcomes in patients undergoing everolimus-eluting bioresorbable scaffolds implantation in routine clinical practice: Insights from the European multicenter GHOST-EU registry. *Catheter Cardiovasc Interv* 2017; 89(5): 812-818
44. Bourantas CV, Papafaklis MI, Kotsia A, Farooq V, Muramatsu T, Gomez-Lara J, Zhang YJ, Iqbal J, Kalatzis FG, Naka KK, Fotiadis DI, Dorange C, Wang J, Rapoza R, Garcia-Garcia HM, Onuma Y, Michalis LK, Serruys PW. Effect of the endothelial shear stress patterns on neointimal proliferation following drug-eluting bioresorbable vascular scaffold implantation: an optical coherence tomography study. *JACC Cardiovasc Interv* 2014; 7: 315–324
45. Bourantas CV, Papafaklis MI, Lakkas L, Sakellarios A, Onuma Y, Zhang YJ, Muramatsu T, Diletti R, Bizopoulos P, Kalatzis F, Naka KK, Fotiadis DI, Wang J, Garcia Garcia HM, Kimura T, Michalis LK, Serruys PW. Fusion of optical coherence tomographic and angiographic data for more accurate evaluation of the endothelial shear stress patterns and neointimal distribution after bioresorbable scaffold implantation: comparison with

intravascular ultrasound-derived reconstructions. *Int J Cardiovasc Imaging* 2014; 30: 485–494

46. Sotomi Y, Onuma Y, Collet C, Tenekecioglu E, Virmani R, Kleiman NS, Serruys PW. Bioresorbable scaffold: the emerging reality and future directions. *Circ Res* 2017; 120(8): 1341-1352
47. Gogas BD, Radu M, Onuma Y, Perkins L, Powers JC, Gomez-Lara J, Farooq V, Garcia-Garcia HM, Diletti R, Rapoza R, Virmani R, Serruys PW. Evaluation with in vivo optical coherence tomography and histology of the vascular effects of the everolimus-eluting bioresorbable vascular scaffold at two years following implantation in a healthy porcine coronary artery model: implications of pilot results for future pre-clinical studies. *Int J Cardiovasc Imaging* 2012; 28(3): 499-511
48. Nakatani S, Ishibashi Y, Sotomi Y, Perkins L, Eggermont J, Grundeken MJ, Dijkstra J, Rapoza R, Virmani R, Serruys PW, Onuma Y. Bioresorption and vessel wall integration of a fully bioresorbable polymeric everolimus-eluting scaffold: optical coherence tomography, intravascular ultrasound, and histological study in a porcine model with 4-year follow-up. *JACC Cardiovasc Interv* 2016; 9(8): 838-851
49. Zhang YJ, Iqbal J, Nakatani S, Bourantas CV, Campos CM, Ishibashi Y, Cho YK, Veldhof S, Wang J, Onuma Y, Garcia-Garcia HM, Dudek D, van Geuns RJ, Serruys PW; ABSORB Cohort B Study Investigators. Scaffold and edge vascular response following implantation of everolimus-eluting bioresorbable vascular scaffold: a 3-year serial optical coherence tomography study. *JACC Cardiovasc Interv* 2014; 7(12): 1361-1369
50. Otsuka F, Pacheco E, Perkins LE, Lane JP, Wang Q, Kamberi M, Frie M, Wang J, Sakakura K, Yahagi K, Ladich E, Rapoza RJ, Kolodgie FD, Virmani R. Long-term safety of an everolimus-eluting bioresorbable vascular scaffold and the cobaltchromium XIENCE V stent in a porcine coronary artery model. *Circ Cardiovasc Interv* 2014; 7(3): 330-342
51. Vorpahl M, Finn AV, Nakano M, Virmani R. The bioabsorption process: tissue and cellular mechanisms and outcomes. *EuroIntervention* 2009; 5 Suppl F: F28-35
52. Tellez A, Afari ME, Buszman PP, Seifert P, Cheng Y, Milewski K, McGregor JC, Garza JA, Roberts MB, Yi GH, Kaluza GL, Granada JF. Peri-strut low-intensity areas in optical coherence tomography correlate with peri-strut inflammation and neointimal proliferation: an in-vivo correlation study in the familial hypercholesterolemic coronary swine model of in-stent restenosis. *Coron Artery Dis* 2014; 25(7): 595-601

53. Ormiston JA, Webber B, Ubod B, Darremont O, Webster MW. An independent bench comparison of two bioresorbable drug-eluting coronary scaffolds (absorb and DESolve) with a durable metallic drug-eluting stent (ML8/Xpedition). *EuroIntervention* 2015; 11(1): 60-67
54. Schmidt W, Behrens P, Brandt-Wunderlich C, Siewert S, Grabow N, Schmitz KP. In vitro performance investigation of bioresorbable scaffolds – Standard tests for vascular stents and beyond. *Cardiovasc Revasc Med* 2016; 17(6): 375-383
55. Everaert B, Wykrzykowska JJ, Koolen J, van der Harst P, den Heijer P, Henriques JP, van der Schaaf R, de Smet B, Hofma SH, Diletti R, Weevers A, Hoorntje J, Smits P, van Geuns RJ. Recommendations for the use of bioresorbable vascular scaffolds in percutaneous coronary interventions: 2017 revision. *Neth Heart J* 2017; 25(7-8): 419-428
56. Radu MD, Räber L, Kalesan B, Muramatsu T, Kelbæk H, Heo J, Jørgensen E, Helqvist S, Farooq V, Brugaletta S, Garcia-Garcia HM, Jüni P, Saunamäki K, Windecker S, Serruys PW. Coronary evaginations are associated with positive vessel remodelling and are nearly absent following implantation of newer-generation drug-eluting stents: an optical coherence tomography and intravascular ultrasound study. Eur Heart J 2014; 35(12): 795-807
57. Joner M, Finn AV, Farb A, Mont EK, Kolodgie FD, Ladich E, Kutys R, Skorija K, Gold HK, Virmani R. Pathology of drug-eluting stents in humans: delayed healing and late thrombotic risk. *J Am Coll Cardiol* 2006; 48(1): 193-202
58. Cook S, Windecker S. Early stent thrombosis: past, present, and future. *Circulation* 2009; 119(5): 657-659
59. Guagliumi G, Sirbu V, Musumeci G, Gerber R, Biondi-Zoccai G, Ikejima H, Ladich E, Lortkipanidze N, Matiashvili A, Valsecchi O, Virmani R, Stone GW. Examination of the in vivo mechanism of late drug-eluting stent thrombosis: findings from optical coherence tomography and intravascular ultrasound imaging. *JACC Cardiovasc Interv* 2012; 5(1): 12-20
60. Räber L, Baumgartner S, Garcia-Garcia HM, Kalesan B, Justiz J, Pilgrim T, Moschovitis A, Khattab AA, Buellesfeld L, Wenaweser P, Meier B, Serruys PW, Jüni P, Windecker S. Long-term vascular healing in response to sirolimus- and paclitaxel-eluting stents: an optical coherence tomography study. *JACC Cardiovasc Interv* 2012; 5(9): 946-957
61. Radu MD, Pfenniger A, Räber L, de Marchi SF, Obrist D, Kelbæk H, Windecker S, Serruys PW, Vogel R. Flow disturbances in stent-related coronary evaginations: a computational fluid-dynamicsimulation study. *EuroIntervention* 2014; 10(1): 113-123

62. Cortese B, Silva Orrego P, Virmani R. Late coronary BVS malapposition and aneurysm: A Time for Appraisal. *Catheter Cardiovasc Interv* 2015; 86(4): 678-681
63. Timmers L, Lim YC, Tan HC, Low AF. Coronary aneurysm without malapposition after bioresorbable vascular scaffold implantation. *EuroIntervention* 2016; 12(1): 60
64. O'Gallagher K, Nerla R, Hill J, Byrne J. Acquired coronary artery aneurysm following treatment with bioresorbable vascular scaffolds. *EuroIntervention* 2016; 12(9): 1174
65. Gori T, Jansen T, Weissner M, Foin N, Wenzel P, Schulz E, Cook S, Münzel T. Coronary evaginations and peri-scaffold aneurysms following implantation of bioresorbable scaffolds: incidence, outcome, and optical coherence tomography analysis of possible mechanisms. *Eur Heart J* 2016; 37(26): 2040-2049
66. https://clinicaltrials.gov/ct2/show/NCT04192747
67. Tovar Forero MN, Wilschut J, Van Mieghem NM, Daemen J. Coronary lithoplasty: a novel treatment for stent underexpansion. Eur Heart J 2018; doi: 10.1093/eurheartj/ehy593
68. Morabito G, Tripolino C, Tassone EJ, Grillo P, Missiroli B. A Case of Stent Under-Expansion due to Calcified Plaque Treated with Shockwave Lithoplasty. Cardiology 2018; 141(2): 75-77
69. Chen G, Zrenner B, Pyxaras SA. Combined rotational atherectomy and intravascular lithotripsy for the treatment of severely calcified in-stent neoatherosclerosis: A mini-review. Cardiovasc Revasc Med 2018; doi: 10.1016/j.carrev.2018.10.007
70. Ali ZA, Brinton TJ, Hill JM, Maehara A, Matsumura M, Karimi Galougahi K, Illindala U, Götberg M, Whitbourn R, Van Mieghem N, Meredith IT, Di Mario C, Fajadet J. Optical Coherence Tomography Characterization of Coronary Lithoplasty for Treatment of Calcified Lesions: First Description. JACC Cardiovasc Imaging 2017; 10(8): 897-906
71. Serruys PW, Katagiri Y, Onuma Y. Shaking and Breaking Calcified Plaque: Lithoplasty, a Breakthrough in Interventional Armamentarium? JACC Cardiovasc Imaging 2017; 10(8): 907-911
72. Goto K, Zhao Z, Matsumura M, Dohi T, Kobayashi N, Kirtane AJ, Rabbani LE, Collins MB, Parikh MA, Kodali SK, Leon MB, Moses JW, Mintz GS, Maehara A. Mechanisms and Patterns of Intravascular Ultrasound In-Stent Restenosis Among Bare Metal Stents and First- and Second-Generation Drug-Eluting Stents. Am J Cardiol 2015; 116(9): 1351-1357
73. West NE, Ruygrok PN, Disco CM, Webster MW, Lindeboom WK, O'Neill WW, Mercado NF, Serruys PW. Clinical and angiographic predictors of restenosis after stent deployment in diabetic patients. Circulation 2004; 109(7): 867-873

74. Räber L, Mintz GS, Koskinas K, Johnson T, Holm NR, Onuma Y, Radu MD, Joner M, Yu B, Jia H, Meneveau N, de la Torre Hernandez JM, Escaned J, Hill J, Prati F, Colombo A, di Mario C, Regar E, Capodanno D, Wijns W, Byrne RA, Guagliumi G. Clinical use of intracoronary imaging. Part 1: guidance and optimization of coronary interventions. An expert consensus document of the European Association of Percutaneous Cardiovascular Interventions. Eur Heart J 2018; 39: 3281–3300
75. https://clinicaltrials.gov/ct2/show/NCT04047368; ClinicalTrials.gov Identifier: NCT04047368
76. Zahn R, Hamm CW, Schneider S, Zeymer U, Nienaber CA, Richardt G, Kelm M, Levenson B, Bonzel T, Tebbe U, Sabin G, Senges J; German Cypher StentRegistry. Incidence and predictors of target vessel revascularization and clinical event rates of the sirolimus-eluting coronary stent (results from the prospective multicenter German Cypher Stent Registry). Am J Cardiol 2005; 95(11): 1302-1308.
77. Zahn R, Hamm CW, Schneider S, Richardt G, Kelm M, Levenson B, Bonzel T, Tebbe U, Sabin G, Nienaber CA; German Cypher Stent Registry. Coronary stenting with the sirolimus-eluting stent in clinical practice: final results from the prospective multicenter German Cypher Stent Registry. J Interv Cardiol 2010; 23(1): 18-25.
78. Kastrati A, Dibra A, Mehilli J, Mayer S, Pinieck S, Pache J, Dirschinger J, Schömig A. Predictive factors of restenosis after coronary implantation of sirolimus- or paclitaxel-eluting stents. Circulation 2006; 113(19): 2293-2300
79. Brinton TJ, Ali ZA, Hill JM, Meredith IT, Maehara A, Illindala U, Lansky A, Götberg M, Van Mieghem NM, Whitbourn R, Fajadet J, Di Mario C. Feasibility of Shockwave Coronary Intravascular Lithotripsy for the Treatment of Calcified Coronary Stenoses. Circulation 2019; 139(6): 834-836
80. Ali ZA, Nef H, Escaned J, Werner N, Banning AP, Hill JM, De Bruyne B, Montorfano M, Lefevre T, Stone GW, Crowley A, Matsumura M, Maehara A, Lansky AJ, Fajadet J, Di Mario C. Safety and Effectiveness of Coronary Intravascular Lithotripsy for Treatment of Severely Calcified Coronary Stenoses: The Disrupt CAD II Study. Circ Cardiovasc Interv 2019; 12(10): e008434
81. Hill JM, Kereiakes DJ, Shlofmitz RA, Klein AJ, Riley RF, Price MJ, Herrmann HC, Bachinsky W, Waksman R, Stone GW; Disrupt CAD III Investigators. Intravascular Lithotripsy for Treatment of Severely Calcified Coronary Artery Disease. J Am Coll Cardiol 2020; 76(22): 2635-2646

82. Saito S, Yamazaki S, Takahashi A, Namiki A, Kawasaki T, Otsuji S, Nakamura S, Shibata Y; Disrupt CAD IV Investigators. Intravascular Lithotripsy for Vessel Preparation in Severely Calcified Coronary Arteries Prior to Stent Placement - Primary Outcomes From the Japanese Disrupt CAD IV Study. Circ J 2021; 85(6): 826-833

9. Schriftenverzeichnis des Verfassers

Erstautorenschaften

1. **Blachutzik F**, Honton B, Escaned J, Hill JM, Werner N, Banning AP, Lansky AJ, Schlattner S, De Bruyne B, Di Mario C, Dörr O, Hamm C, Nef HM. Safety and effectiveness of coronary intravascular lithotripsy in eccentric calcified coronary lesions: a patient-level pooled analysis from the Disrupt CAD I and CAD II Studies. Clin Res Cardiol 2021; 110(2): 228-236

2. **Blachutzik F**, Achenbach S, Marwan M, Tröbs M, Boeder N, Doerr O, Weissner M, Bauer T, Nef H, Hamm C, Schlundt C. OCT-assessment of scaffold resorption: Analysis of strut intensity by a new resorption index for poly-l-lactic acid bioresorbable vascular scaffolds. Catheter Cardiovasc Interv 2019; 94(7): 928-935

3. **Blachutzik F**, Achenbach S, Tröbs M, Marwan M, Weissner M, Nef H, Schlundt C. Effect of non-compliant balloon postdilatation on magnesium-based bioresorbable vascular scaffolds. Catheter Cardiovasc Interv 2019; 93(2): 202-207

4. **Blachutzik F**, Achenbach S, Marwan M, Röther J, Tröbs M, Schneider R, Nef H, Weissner M, Schlundt C. Major coronary evaginations following implantation of bioresorbable vascular scaffolds - Clinical and OCT characteristics. Cardiovasc Revasc Med 2019; 20(6): 485-491

5. **Blachutzik F**, Achenbach S, Röther J, Tröbs M, Schneider R, Marwan M, Schlundt C. Percutaneous coronary intervention of unprotected left main stenoses - Procedural data and outcome depending on SYNTAX I Score. Cardiovasc Revasc Med 2018; 7 Pt A:740-743

6. **Blachutzik F**, Boeder N, Wiebe J, Mattesini A, Dörr O, Most A, Bauer T, Röther J, Tröbs M, Schlundt C, Achenbach S, Hamm CW, Nef HM. Overlapping implantation of bioresorbable novolimus-eluting scaffolds: An observational optical coherence tomography study. Heart and Vessels 2017; 32(7): 781-789

7. **Blachutzik F**, Achenbach S, Nef H, Hamm C, Dörr O, Boeder N, Marwan M, Tröbs M, Schneider R, Röther J, Schlundt C. Optical coherence tomography: influence of contrast concentration on image quality and diagnostic confidence. Heart and Vessels 2017; 32(6): 653-659

8. **Blachutzik F**, Boeder N, Wiebe J, Mattesini A, Dörr O, Most A, Bauer T, Röther J, Tröbs M, Schlundt C, Achenbach S, Hamm CW, Nef HM. Post-dilatation after implantation of bioresorbable everolimus- and novolimus-eluting scaffolds: an observational optical coherence tomography study of acute mechanical effects. Clin Res Cardiol 2017; 106(4): 271-279

9. **Blachutzik F**, Achenbach S, Troebs M, Roether J, Nef H, Hamm C, Schlundt C. Angiographic Findings and Revascularization Success in Patients With Acute Myocardial Infarction and Previous Coronary Bypass Grafting. Am J Cardiol 2016; 118(4): 473-6

10. **Blachutzik F**, Meier S, Weissner M, Schlattner S, Gori T, Ullrich-Daub H, Gaede L, Achenbach S, Möllmann H, Chitic B, Aksoy A, Nickenig G, Weferling M, Dörr O, Boeder N, Bayer M, Elsässer A, Hamm CW, Nef N, MD on behalf of the ROTA.shock investigators. Comparison of Coronary Intravascular Lithotripsy and Rotational Atherectomy in the Modification of Severely Calcified Stenoses. Am J Cardiol 2023; accepted for publication; Reference number: AJC-D-23-00028R1

Co-Autorenschaften

1. Rai H, Harzer F, Otsuka T, Abdelwahed YS, Antuña P, **Blachutzik F**, Koppara T, Räber L, Leistner DM, Alfonso F, Nef H, Seguchi M, Aytekin A, Xhepa E, Kufner S, Cassese S, Laugwitz KL, Byrne RA, Kastrati A, Joner M. Stent Optimization Using Optical Coherence Tomography and Its Prognostic Implications After Percutaneous Coronary Intervention. J Am Heart Assoc. 2022; 11(9): e023493

2. Boeder NF, Dörr O, Gaderer R, **Blachutzik F**, Achenbach S, Elsässer A, Hamm C, Nef HM. Clinical presentation does not affect acute mechanical performance of the

Novolimus-eluting bioresorbable vascular scaffold as assessed by optical coherence tomography. Postepy Kardiol Interwencyjnej 2021; 17(3): 272-280

3. Boeder NF, Dörr O, Koepp T, **Blachutzik F**, Achenbach S, Elsässer A, Hamm CW, Nef HM. Acute Mechanical Performance of Magmaris vs. DESolve Bioresorbable Scaffolds in a Real-World Scenario. Front Cardiovasc Med 2021; 8: 696287

4. Schochlow K, Weissner M, **Blachutzik F**, Boeder NF, Tröbs M, Lorenz L, Dijkstra J, Münzel T, Achenbach S, Nef H, Gori T. Coronary Stent Strut Fractures: Classification, Prevalence and Clinical Associations. J. Clin. Med 2021; 10(8), 1765

5. Hell MM, Gilg MD, Röther J, **Blachutzik F**, Achenbach S, Schlundt C. Dual-axis rotational coronary angiography versus conventional coronary angiography: a randomized comparison. Clin Res Cardiol 2021; 110(2): 258-269

6. Wiebe J, Hofmann FJ, Dörr O, Bauer T, Boeder N, Liebetrau C, **Blachutzik F**, Möllmann H, Elsässer A, Achenbach S, Hamm CW, Nef HM. Five-year follow-up of patients who underwent everolimus-eluting bioresorbable scaffold implantation. Catheter Cardiovasc Interv 2021; 97(1): 56-62

7. Wiebe J, Baquet M, Dörr O, Hoppmann P, Jochheim D, Rheude T, Boeder N, Grundmann D, **Blachutzik F**, Theiss H, Cassese S, Hofmann FJ, Gschwendtner S, Elsässer A, Massberg S, Hamm C, Laugwitz KL, Byrne RA, Mehilli J, Kastrati A, Nef H. Long-term follow-up and predictors of target lesion failure after implantation of everolimus-eluting bioresorbable scaffolds in real-world practice. Int J Cardiol. 2020; 312: 42-47

8. Dörr O, Liebetrau C, Weferling M, Hoffmann F, Forderer N, Keller T, Boeder N, **Blachutzik F**, Keranov S, Bauer P, Bauer T, Hamm CW, Nef H. Fractional flow reserve and frequency of PCI in patients with coronary artery disease. Herz 2020; 45(8): 752-758

9. Boeder NF, Weissner M, **Blachutzik F**, Ullrich H, Anadol R, Tröbs M, Münzel T, Hamm CW, Dijkstra J, Achenbach S, Nef HM, Gori T. Incidental Finding of Strut

Malapposition Is a Predictor of Late and Very Late Thrombosis in Coronary Bioresorbable Scaffolds. J Clin Med 2019; 8(5): 580. doi: 10.3390/jcm8050580

10. Röther J, Moshage M, Dey D, Schwemmer C, Tröbs M, **Blachutzik F**, Achenbach S, Schlundt C, Marwan M. Comparison of invasively measured FFR with FFR derived from coronary CT angiography for detection of lesion-specific ischemia: Results from a PC-based prototype algorithm. J Cardiovasc Comput Tomogr 2018; 12(2): 101-107

11. Tröbs M, Achenbach S, Plank PM, Marwan M, Röther J, Klinghammer L, **Blachutzik F**, Schlundt C. Predictors of Technical Failure in Transradial Coronary Angiography and Intervention. Am J Cardiol 2017; 120(9): 1508-1513

12. Hell MM, Achenbach S, Yoo IS, Franke J, **Blachutzik F**, Roether J, Graf V, Raaz-Schrauder D, Marwan M, Schlundt C. 3D printing for sizing left atrial appendage closure device: Head-to-head comparison with computed tomography and transesophageal echocardiography. EuroIntervention 2017; 3(10): 1234-1241

13. Boeder NF, Koepp T, Dörr O, Bauer T, Mattesini A, Elsässer A, Möllmann H, **Blachutzik F**, Achenbach S, Ghanem A, Hamm CW, Nef HM. A new novolimus-eluting bioresorbable scaffold for large coronary arteries: an OCT study of acute mechanical performance. Int J Cardiol 2016; 220: 706-710

14. Röther J, Achenbach S, Tröbs M, **Blachutzik F**, Nef H, Marwan M, Schlundt C. Comparison of standard- and high-dose intracoronary adenosine for the measurement of coronary fractional flow reserve (FFR). Clin Res Cardiol 2016; 105(12): 1003-1010

15. Groener JB, **Blachutzik F**, Oikonomou D, Kliemank E, Fleming T, Nawroth PP. Altered methylglyoxal metabolism identifies patients with late diabetic complications. Exp Clin Endocrinol Diabetes 2014; 122 - P011

Übersichtsartikel

1. Hofmann FJ, Dörr O, **Blachutzik F**, Boeder N, Elsässer A, Keranov S, Köhne A, Hofmann S, Möllmann H, Hamm C, Nef HM. Latest Developments in Robotic Percutaneous Coronary Intervention. Surg Technol Int 2021; 38: 325-330

2. Nef H, Wiebe J, Foin N, **Blachutzik F**, Dörr O, Toyloy S, Hamm C. A new novolimus-eluting bioresorbable coronary scaffold: present status and future clinical perspectives. Int J Cardiol 2017; 227: 127-133

Buchbeiträge

1. OCT-Kompendium 2. Auflage, 2019, Co-Autor und Redakteur

Fallberichte

1. Habermehl D, **Blachutzik F**, Ecker S, Dittmar JO, Rieken S, Debus J, Welzel T, Combs SE. Early treatment response of a rare papillary tumor of the pineal region after primary proton-beam therapy using the raster-scanning technique at HIT. Tumori 2012; 98(5): 122e-125e

10. Abbildungsverzeichnis

11. Danksagung

Ich möchte mich hiermit bei allen Personen bedanken, die mich in der Erstellung der vorliegenden Arbeit unterstützt und mir die Voraussetzungen für die Habilitation ermöglicht haben.

In erster Linie sei an dieser Stelle Herrn Prof. Dr. Christian Hamm gedankt unter dessen Leitung ich einen wesentlichen Teil der zugrunde liegenden Arbeiten durchführen konnte und der mir stets mit Rat und Tat zur Seite stand.

Ebenso möchte ich mich bei Herrn Prof. Dr. Achenbach ganz herzlich bedanken, der mir während meiner Tätigkeit in Erlangen die ersten wissenschaftlichen Arbeiten ermöglicht hat und mich bei der Durchführung zu jeder Zeit in vollem Umfang unterstützt hat.

Mein besonderer Dank gilt auch Herrn PD Dr. Schlundt mit dem zusammen ich die wesentlichen ersten Arbeiten in Erlangen zusammen durchführen konnte.

Bei Herrn Prof. Dr. Nef möchte ich mich für seine großartigen Impulse und die umfassende Unterstützung bei den jüngsten wissenschaftlichen Projekten in aller Form herzlichst bedanken.

Großer Dank gilt ebenso meiner Familie und hier insbesondere meinen Eltern, Herrn Dr. Christoph Blachutzik und Frau Dr. Martina Blachutzik, die mir die Voraussetzungen für meine persönliche und berufliche Entwicklung gegeben haben und mir im Leben stets zur Seite standen.

In ganz besonderem Maße möchte ich auch meiner Ehefrau, Frau Dr. Melissa Blachutzik, für ihre immerwährende Unterstützung danken.

12. Erklärung der Habilitationsleistung

Hiermit erkläre ich, dass ich die vorliegende Arbeit bzw. die mir zuzuordnenden Teile im Rahmen einer kumulativen Habilitationsschrift, selbstständig und ohne unzulässige Hilfe oder Benutzung anderer als der angegebenen Hilfsmittel angefertigt habe. Alle Textstellen, die wörtlich oder sinngemäß aus veröffentlichten oder nichtveröffentlichten Schriften entnommen sind, und alle Angaben, die auf mündlichen Auskünften beruhen, sind als solche kenntlich gemacht. Ich versichere, dass ich für die nach §2 (3) der Habilitationsordnung angeführten bereits veröffentlichten Originalarbeiten als Erst-oder Seniorautor fungiere, da ich den größten Teil der Daten selbst erhoben habe, für das Design der Arbeiten verantwortlich bin und die Manuskripte maßgeblich gestaltet habe. Für alle von mir erwähnten Untersuchungen habe ich die in der „Satzung der Justus-Liebig-Universität zur Sicherung guter wissenschaftlicher Praxis“ niedergelegten Grundsätze befolgt. Ich versichere, dass alle an der Finanzierung der Arbeiten beteiligten Geldgeber in den jeweiligen Publikationen genannt worden sind. Ich versichere außerdem, dass die vorgelegte Arbeit weder im Inland noch im Ausland in gleicher oder ähnlicher Weise einer anderen Prüfungsbehörde vorgelegt wurde oder Gegenstand eines anderen Prüfungsverfahrens war. Mit der Überprüfung meiner Arbeit durch eine Plagiatserkennungssoftware bzw. ein internetbasiertes Softwareprogramm erkläre ich mich einverstanden.

Gießen, den 01. März 2023

Dr. med. Florian Blachutzik
Medizinische Klinik 1 – Kardiologie und Angiologie
Universitätsklinikum Gießen
Klinikstraße 33
35392 Gießen

13. Erklärung zu anderweitigen Habilitationen oder Habilitationsversuchen

Hiermit erkläre ich, dass ich bisher keine Habilitationsversuche unternommen habe. Zudem versichere ich, dass ich mich nicht an anderer Stelle zur Habilitation gemeldet habe und vor Abschluss dieses Verfahrens auch nicht zur Habilitation an anderer Stelle melden werde.

Gießen, den 01. März 2023

Dr. med. Florian Blachutzik
Medizinische Klinik 1 – Kardiologie und Angiologie
Universitätsklinikum Gießen
Klinikstraße 33
35392 Gießen

14. Publikationen

Nr. 1: Optical coherence tomography: influence of contrast concentration on image quality and diagnostic confidence

Heart Vessels
DOI 10.1007/s00380-016-0918-7

ORIGINAL ARTICLE

Optical coherence tomography: influence of contrast concentration on image quality and diagnostic confidence

Florian Blachutzik[1] · Stephan Achenbach[1] · Holger Nef[2] · Christian Hamm[2] · Oliver Dörr[2] · Niklas Boeder[2] · Mohamed Marwan[1] · Monique Tröbs[1] · Reinhard Schneider[1] · Jens Röther[1] · Christian Schlundt[1]

Received: 17 August 2016 / Accepted: 4 November 2016

Abstract OCT requires intracoronary injection of contrast agent to remove blood from the coronary lumen during data acquisition, which is a possible limitation of this method. Aim of this study was to analyze the influence of iodine concentration on image quality and diagnostic certainty of optical coherence tomography (OCT). OCT sequences acquired using contrast agent with a reduced concentration of 150 mg iodine/ml and a standard concentration of 350 mg iodine/ml were analyzed. Cross-sectional images with a spacing of 10 mm were evaluated regarding image quality and diagnostic confidence. A total of 67 OCT sequences acquired in 24 patients were analyzed. 31 sequences were acquired using contrast agent with a concentration of 150 mg iodine/ml and 36 sequences with a concentration of 350 mg iodine/ml. The percentage of remaining blood streaks in the cross sections was significantly lower for 350 mg iodine/ml compared to 150 mg iodine/ml (19 ± 21 vs. 34 ± 26%, $p = 0.013$). Contrast with 350 mg iodine/ml showed a significantly higher percentage of completely flushed pullback length as compared to 150 mg iodine/ml (78 ± 24 vs. 58 ± 27%, $p = 0.004$). Diagnostic certainty was significantly higher for 350 mg iodine/ml than for 150 mg iodine/ml (Likert scale average 1.4 ± 0.7 vs. 2.1 ± 1.2, $p < 0.001$; Likert scale: 1 = absolutely confident, 2 = confident with slight doubts, 3 = doubtful/not confident, 4 = non-diagnostic). Regarding image quality and diagnostic certainty, contrast agent with a concentration of 350 mg iodine/ml is superior to 150 mg iodine/ml.

Keywords Optical coherence tomography · Coronary angiography · Percutaneous coronary intervention

Introduction

Optical coherence tomography (OCT) has gained increasing importance to supplement coronary angiography, especially in the context of percutaneous coronary interventions (PCI) [1–7]. It enables cross-sectional visualization of endothelial and intraluminal structures with high spatial resolution [1–4, 8]. Recent data suggest that the use OCT during PCI can improve clinical outcome by identifying non-optimal stent deployment, edge dissections or intra-stent plaque and thrombus protrusion more sensitively than coronary angiography alone [1, 9, 10]. OCT acquisition requires a blood-free environment. Hence, the coronary lumen is flushed with contrast agent during pullback of the OCT device, either by manual or machine injection. Especially with repeated OCT imaging during a coronary intervention, this can contribute substantially to the amount of contrast that is used for the procedure. Renal impairment is, therefore, a potential consequence and it is desirable to limit the amount of injected iodine to the greatest possible extent [11–14]. Lowering iodine concentration of the contrast agent used for flushing would translate into a linear reduction of iodine load. We, therefore, analyzed the effect of standard (350 mg iodine/ml) versus low iodine concentration contrast agent (150 mg iodine/ml) on the image quality and diagnostic certainty of OCT pullback sequences acquired during coronary angiography and PCI.

✉ Florian Blachutzik
florian.blachutzik@uk-erlangen.de

[1] Department of Cardiology, Friedrich-Alexander-Universität Erlangen-Nürnberg (FAU), University Hospital Erlangen, Ulmenweg 18, 91054 Erlangen, Germany

[2] Department of Cardiology, University Hospital Giessen, Giessen, Germany

Published online: 09 November 2016

Materials and methods

Patients

Consecutive patients undergoing clinically indicated coronary angiography or percutaneous coronary intervention with OCT imaging between July and October 2015 were included. Exclusion criteria were hemodynamic instability, known contrast agent allergy, renal impairment (creatinine >1.5 mg/dl) and acute myocardial infarction (troponin I >0.5 mg/dl). The study complied with the Declaration of Helsinki. The Ethics Committee of the Justus-Liebig-University Hospital (Giessen, Germany; Ethics votum number 203/14) approved the study protocol. Written informed consent was obtained from each patient before inclusion.

Coronary angiography or intervention

Coronary angiography was performed via a femoral or radial access. For OCT, a 6-F guiding catheter and standard coronary guidewire (Runthrough™, Terumo Europe NV, Leuven, Belgium) was used. Patients received intravenous heparin and intracoronary nitrates. Further medication, technique and equipment for percutaneous coronary intervention were according to clinical requirements and at the discretion of the operator.

Optical coherence tomography

OCT was performed using a 2.7-F Dragonfly™ intravascular imaging catheter (St. Jude Medical, Saint Paul, Mn, USA) at a mechanical pullback speed of 18 mm/s over a distance of 54 or 75 mm. For acquisition, 20 ml of contrast agent (Imeron, Bracco Imaging, Konstanz, Germany) were injected manually. A contrast media concentration of 350 mg iodine/ml or 150 mg iodine/ml was used in random order.

OCT image analysis was performed offline using the ILUMIEN™ OPTIS system (St. Jude Medical, Saint Paul, Mn, US) with manual calibration before each measurement. For evaluation of image quality, the following parameters were obtained: planimetry of remaining blood streaks in the cross section (Figs. 1, 2) of the vessel at intervals of 10 mm over the complete pullback length (from the first acquired frame over the complete maximum length of 75 mm or until entry into the guiding catheter) and determination of the percentage of streak-free cross sections, as well as the percentage of completely flushed pullback length (Figs. 3, 4) in relation to the complete length of pullback. OCT image analysis was performed by two experienced interventional cardiologists blinded to the OCT acquisition and the procedural data, especially regarding the iodine concentration used. Nevertheless, the two investigators were informed about the specific clinical question

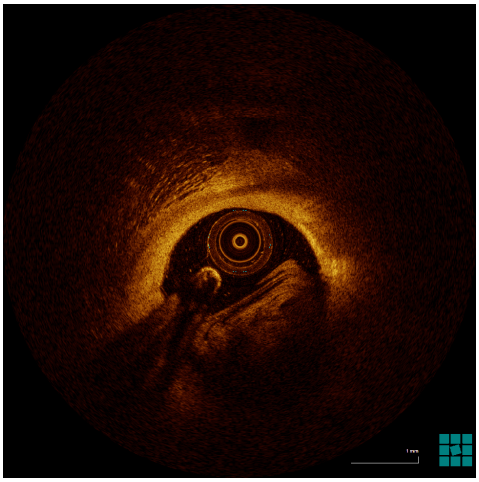

Fig. 1 OCT raw image with remaining blood streaks

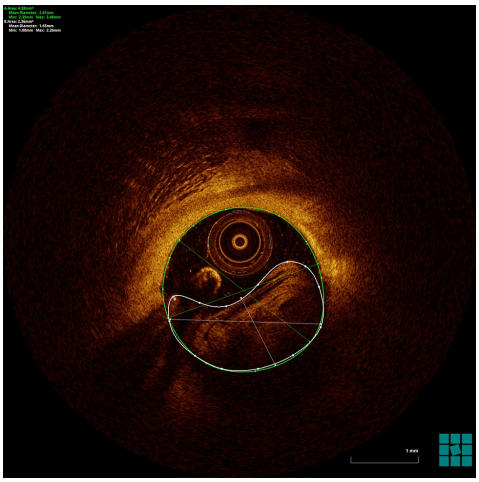

Fig. 2 Planimetry of remaining blood streaks in the cross section (*green mark* lumen area, *white mark* remaining blood streaks)

that should be answered by performing the OCT. When mixed with optically transparent contrast media, blood may form many different patterns within the artery lumen, but usually can be identified because of its high superficial backscattering and the high OCT signal attenuation below the surface [15]. Finally, diagnostic certainty regarding to the specific clinical question was rated using a four-point

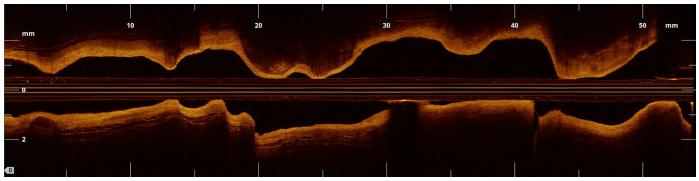

Fig. 3 54-mm OCT run (*longitudinal view*) complete pullback length flushed

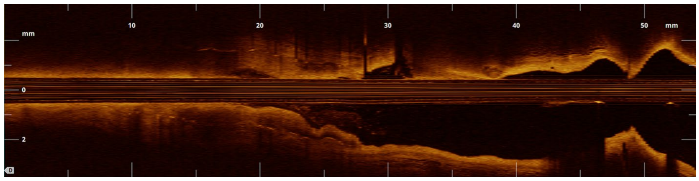

Fig. 4 54-mm OCT run (*longitudinal view*) not flushed from 0 to 18 mm of pullback length

Likert scale (1 = absolutely confident, 2 = confident with slight doubts, 3 = doubtful/not confident, 4 = non-diagnostic). Sequences which showed absolutely no flushed area due to technical problems with contrast agent application were excluded from analysis and data acquisition was repeated ($n = 7$).

Statistical analysis

Continuous variables were summarized as mean ± standard deviation and compared using the *t* test for unpaired samples. Categorical variables are quoted as *n* (%). Kolmogorov–Smirnov test was used to test for normal distribution. Since results for percentage of completely flushed pullback length, percentage of remaining streaks in the cross section and diagnostic certainty (Likert scale) showed no normal distribution, the Mann–Whitney *U* test or Chi-square test was used. To investigate whether the use of low iodine concentration contrast agent with manual injection may be suitable if a very short region of the coronary vessels were to be evaluated, we additionally compared the 10 shortest pullbacks of both groups as a subanalysis. Statistical analysis was performed using SPSS version 21.0 (IBM SPSS Statistics, IBM Corporation, Armonk, New York, USA) and a two-sided $p < 0.05$ was considered significant.

Results

Patients

A total of 67 OCT sequences, performed in the course of coronary angiography or intervention in 24 patients (17 male, 7 female), were analyzed. 31 sequences were performed with a contrast media concentration of 150 mg iodine/ml, 36 sequences were performed with a contrast media concentration of 350 mg iodine/ml. Mean patient age was 62 ± 10 years and mean body mass index was 28.3 ± 5.4 kg/m^2. No significant differences existed between the two groups regarding weight, body mass index, indication for OCT imaging or average length of pullback (Table 1). OCT sequences were acquired from the following vessels: left main (LM) ($n = 9$, 13%), left anterior descending artery (LAD) ($n = 35$, 52%), circumflex (Cx) ($n = 10$, 15%), right coronary artery (RCA) ($n = 13$, 20%) (Table 1). There were no complications due to OCT or contrast agent application.

OCT analysis

A total of 402 cross sections were analyzed, 184 cross sections with a contrast agent concentration of 150 mg iodine/ml and 218 cross sections with a concentration of 350 mg iodine/ml. The percentage of completely flushed pullback length (Figs. 3, 4) was significantly higher for 350 mg iodine/ml as compared to 150 mg iodine/ml (78 ± 24 vs. 58 ± 27%, $p = 0.004$; Table 2).

The percentage of remaining streaks in the cross section (Figs. 1, 2) was significantly lower if a concentration of 350 mg iodine/ml compared to a concentration of 150 mg iodine/ml was injected (19 ± 21 vs. 34 ± 26%, $p = 0.013$; Table 2). Diagnostic confidence was significantly higher for 350 mg iodine/ml than for 150 mg iodine/ml (average score 1.4 ± 0.7 vs. 2.1 ± 1.2, $p < 0.001$; Table 2).

75% (27/36) of the pullbacks with an iodine concentration of 350 mg/ml allowed an absolutely confident diagnosis (Likert scale 1) compared to only 45% (14/31) with an iodine concentration of 150 mg/ml ($p = 0.01$, Table 2).

Table 1 Patient characteristics

	Iodine concentration 150 mg/ml	Iodine concentration 350 mg/ml	*P* value
Number of runs	31 (46%)	36 (54%)	
Age (years)	62 ± 9	60 ± 9	0.33
Body mass index (kg/m^2)	28.3 ± 5.0	27.8 ± 4.9	0.53
Length of pullback (mm)	58 ± 15	59 ± 16	0.83
Vessel			
LM	4 (13%)	5 (13%)	0.94
LAD	16 (52%)	19 (53%)	
Cx	4 (13%)	6 (17%)	
RCA	7 (22%)	6 (17%)	
Indication			
Vessel dimension	4 (13%)	4 (11%)	0.86
Stent deployment BMS	1 (3%)	1 (2%)	
Stent deployment DES	17 (54%)	20 (56%)	
Stent deployment Scaffold	6 (18%)	6 (16%)	
Dissection	0 (0%)	0 (0%)	
Mechanism In-Stent-Stenosis	2 (6%)	4 (11%)	
Plaque rupture/thrombus	1 (3%)	1 (2%)	
Other	1 (3%)	1 (2%)	

Values are mean ± standard deviation or *n* (%)

BMS bare metal stent, *DES* drug eluting stent, length of pullback until inside the guiding catheter

Table 2 Results

	150 mg/ml	350 mg/ml	*p* value
Completely flushed length of pullback (%)	58.3 ± 27.3	77.6 ± 24.5	0.004
Remaining blood streaks in the cross sections (%)	34.1 ± 25.8	19.4 ± 21.4	0.013
Likert scale (1–4)	2.1 ± 1.2	1.4 ± 0.7	<0.001
Number of runs with Likert scale 1	14/31 (45%)	27/36 (75%)	0.01

Values are mean ± standard deviation or *n* (%)

OCT analysis short pullback length

When comparing the ten shortest OCT pullbacks for both iodine concentrations, there were no differences between the two groups regarding baseline characteristics (Table 3). Average pullback length was 41.4 ± 6.5 for 150 mg iodine/ml and 38.4 ± 7.1 for 350 mg iodine/ml. No significant differences regarding completely flushed pullback length, remaining blood streaks or diagnostic confidence were present (Table 4). A Likert scale 1 for diagnostic confidence was achieved in 60% (6/10) of pullbacks with an iodine concentration of 350 mg/ml as compared to 40% (4/10) with 150 mg/ml. This difference, however, was not significant ($p = 0.33$).

Discussion

We evaluated the influence of reduced contrast media concentration on OCT image quality and diagnostic certainty. OCT provides more detailed information regarding vessel, stent and plaque morphology than any other intravascular imaging system [16–18]. Several studies have reported a significant benefit of OCT for intraprocedural decision-making during PCI and suboptimal stent deployment as documented by quantitative OCT criteria has been shown to be associated with an increased risk of major adverse cardiac and cerebrovascular events during follow-up [9, 10]. In spite of its potential benefit, OCT is not widely used in the context of coronary intervention and one of the potential reasons is the fact that OCT requires flushing of the imaging field since OCT signals are attenuated by erythrocytes. This flushing is usually achieved by injection of iodinated contrast agent during image acquisition which, in turn, could have a negative impact on renal function, especially in individuals with pre-existing renal impairment.

The main intention for this study was to analyze whether a reduction of the contrast agent concentration would constitute a simple way to reduce the iodine burden associated

Table 3 Patient characteristics for short pullback length

	Iodine concentration 150 mg/ml	Iodine concentration 350 mg/ml	*P* value
Number of runs	10 (50%)	10 (50%)	
Age (years)	59 ± 12	53 ± 7	0.44
Body mass index (kg/m^2)	28.0 ± 4.5	28.9 ± 5.8	0.67
Length of pullback (mm)	41 ± 7	38 ± 7	0.39
Vessel			
LM	2 (20%)	4 (40%)	0.56
LAD	2 (20%)	1 (10%)	
Cx	5 (50%)	4 (40%)	
RCA	1 (10%)	1 (10%)	
Indication			
Vessel dimension	2 (20%)	2 (20%)	>0.99
Stent deployment BMS	0 (0%)	0 (0%)	
Stent deployment DES	6 (60%)	6 (60%)	
Stent deployment Scaffold	0 (0%)	0 (0%)	
Dissection	0 (0%)	0 (0%)	
Mechanism In-Stent-Stenosis	1 (10%)	0 (0%)	
Plaque rupture/thrombus	0 (0%)	1 (10%)	
Other	1 (10%)	1 (10%)	

Values are mean ± standard deviation or *n* (%)

BMS bare metal stent, *DES* drug eluting stent, length of pullback until inside the guiding catheter

Table 4 Results for short pullback length

	150 mg/ml	350 mg/ml	*p* value
Pullback length (mm)	41.4 ± 6.5	38.4 ± 7.1	0.39
Completely flushed length of pullback (%)	56.4 ± 24.5	66.8 ± 39.1	0.17
Remaining blood streaks in the cross sections (%)	34.0 ± 21.0	34.8 ± 30.6	0.28
Likert scale (1–4)	2.1 ± 0.9	1.9 ± 1.1	0.32
Number of runs with Likert scale 1	4/10 (40%)	6/10 (60%)	0.33

Values are mean ± standard deviation or *n* (%)

with OCT and hence, possibly to reduce the risk of contrast agent-associated complications [13, 14]. Contrast-induced nephropathy frequently complicates primary PCI, even in patients with initially normal renal function and is associated with higher in-hospital complication rate and mortality [13]. Accordingly, iodine application should be reduced as far as possible.

However, our results show that a reduced contrast media concentration of 150 mg/ml iodine (as compared to a standard concentration of 350 mg iodine/ml) is associated with significantly inferior results regarding image quality and diagnostic certainty of OCT performed in the context of coronary intervention. Most likely, the lower viscosity is the underlying reason for the significantly inferior results of reduced contrast concentration (150 mg/ml) regarding both quantitative parameters of image quality as well as subjective diagnostic confidence as determined by OCT. Based on these findings, application of contrast media with iodine concentrations as low as used here is no promising way to reduce iodine burden during OCT. The reduced iodine concentration of 150 mg/ml has been selected because it presents a relevant reduction of iodine load compared to the standard concentration of 350 mg/ml.

No previous studies have addressed the effect of contrast concentration on image quality or diagnostic confidence of intracoronary OCT. Two previous studies compared standard concentration contrast agents with iodine contents of 320 mg/ml [19] and 350 mg/ml [20] to low molecular weight dextran regarding OCT image quality [19, 20]. Dextran has much lower nephrotoxic potential than standard radiographic contrast agent [14]. However, dextran requires an optical correction because of its refractive index [20] and a significantly higher volume of dextran has to be injected as compared to standard contrast agent, likely because of its lower viscosity. In the two published studies, image quality during OCT acquisition was similar for dextran and

standard contrast [19, 20]. In the study of Ozaki et al., a total number of approximately 1000 cross sections acquired within stents was analyzed [20], while 3418 OCT cross sections were analyzed in the study of Frick et al. [19] In both studies, OCT images were analyzed in 1-mm intervals regarding image clarity, and an evaluable image was defined as a cross section with a visible lumen border over an arc >270°. We used stricter criteria for image quality, since there is some concern that relevant findings may be missed even if 25% or less of vessel contours is obscured. We, therefore, additionally analyzed the completely flushed pullback length, the amount of remaining blood streaks, and we also used a subjective scale to rate diagnostic confidence. With these criteria, image quality of low iodine concentration contrast agent was determined to not be sufficient for routine use during OCT. There are some possible exceptions, such as very small vessels or very short pullbacks, especially since no significant difference regarding image quality or diagnostic confidence was observed in a subanalysis of the 10 shortest pullbacks in each group, but the lack of a significant difference may fully be attributable to small numbers, so that this would need to be investigated in specific trials.

Limitations

Our study has a number of limitations. It was a single-center study with a relatively small number of OCT sequences, but results were statistically significant. Image analysis was performed without active knowledge of the injected contrast, but image appearance would provide the reader with information about what contrast had been injected. As a technical specification, we used manual injection of contrast media as frequently done in clinical practice. It is conceivable, albeit not very likely, that results would be different had machine injection been used. One aspect we did not analyze in our present study was whether other iodine concentrations in between 150 and 350 mg/ml would provide adequate image quality. However, a slight reduction of iodine concentration might result in proper image quality, but would not be associated with a clinically relevant reduction of iodine load.

Our results suggest that the general use of contrast agent with an iodine concentration of 150 mg/ml does not result in sufficiently stable image quality to serve as a feasible strategy to limit the total amount of iodine for intracoronary OCT imaging in the context of coronary interventions.

Compliance with ethical standards

Conflict of interest The authors declare that they have no conflict of interest.

References

1. Prati F, Kodama T, Romagnoli E, Gatto L, Di Vito L, Ramazzotti V, Chisari A, Marco V, Cremonesi A, Parodi G, Albertucci M, Alfonso F (2015) Suboptimal stent deployment is associated with subacute stent thrombosis: optical coherence tomography insights from a multicenter matched study. From the CLI Foundation investigators: the CLI-THRO study. Am Heart J 169(2):249–256
2. Guagliumi G, Sirbu V, Musumeci G, Gerber R, Biondi-Zoccai G, Ikejima H, Ladich E, Lortkipanidze N, Matiashvili A, Valsecchi O, Virmani R, Stone GW (2012) Examination of the in vivo mechanisms of late drug-eluting stent thrombosis: findings from optical coherence tomography and intravascular ultrasound imaging. JACC Cardiovasc Interv 5(1):12–20
3. Alfonso F, Dutary J, Paulo M, Gonzalo N, Pérez-Vizcayno MJ, Jiménez-Quevedo P, Escaned J, Bañuelos C, Hernández R, Macaya C (2012) Combined use of optical coherence tomography and intravascular ultrasound imaging in patients undergoing coronary interventions for stent thrombosis. Heart 98(16):1213–1220
4. Prati F, Regar E, Mintz GS, Arbustini E, Di Mario C, Jang IK, Akasaka T, Costa M, Guagliumi G, Grube E, Ozaki Y, Pinto F, Serruys PW (2010) Expert review document on methodology, terminology, and clinical applications of optical coherence tomography: physical principles, methodology of image acquisition, and clinical application for assessment of coronary arteries and atherosclerosis. Eur Heart J 31(4):401–415
5. Yabushita H, Bouma BE, Houser SL, Aretz HT, Jang IK, Schlendorf KH, Kauffman CR, Shishkov M, Kang DH, Halpern EF, Tearney GJ (2002) Characterization of human atherosclerosis by optical coherence tomography. Circulation 106(13):1640–1645
6. Suter MJ, Nadkarni SK, Weisz G, Tanaka A, Jaffer FA, Bouma BE, Tearney GJ (2011) Intravascular optical imaging technology for investigating the coronary artery. JACC Cardiovasc Imaging 4(9):1022–1039
7. Nakao F, Okamura T, Suetomi T, Yamada J, Nakamura T, Ueda T, Oda T, Kanemoto M, Ikeda Y, Fujii T, Yano M (2016) Differences of side branch jailing between left main-left anterior descending artery stenting and left main-left circumflex artery stenting with Nobori biolimus-eluting stent. Heart Vessels. doi:10.1007/s00380-016-0812-3 **(Epub ahead of print)**
8. Sakaguchi M, Hasegawa T, Ehara S, Matsumoto K, Mizutani K, Iguchi T, Ishii H, Nakagawa M, Shimada K, Yoshiyama M (2016) New insights into spotty calcification and plaque rupture in acute coronary syndrome: an optical coherence tomography study. Heart Vessels. doi:10.1007/s00380-016-0820-3 **(Epub ahead of print)**
9. Prati F, Romagnoli E, Burzotta F, Limbruno U, Gatto L, La Manna A, Versaci F, Marco V, Di Vito L, Imola F, Paoletti G, Trani C, Tamburino C, Tavazzi L, Mintz GS (2015) Clinical impact of OCT findings during PCI: the CLI-OPCI II study. JACC Cardiovasc Imaging 8(11):1297–1305
10. Wijns W, Shite J, Jones MR, Lee SW, Price MJ, Fabbiocchi F, Barbato E, Akasaka T, Bezerra H, Holmes D (2015) Optical coherence tomography imaging during percutaneous coronary intervention impacts physician decision-making: ILUMIEN I study. Eur Heart J 36(47):3346–3355
11. McCullough PA (2008) Contrast-induced acute kidney injury. J Am Coll Cardiol 51(15):1419–1428
12. Brown JR, Solomon RJ, Sarnak MJ, McCullough PA, Splaine ME, Davies L, Ross CS, Dauerman HL, Stender JL, Conley SM, Robb JF, Chaisson K, Boss R, Lambert P, Goldberg DJ, Lucier D, Fedele FA, Kellett MA, Horton S, Phillips WJ, Downs C, Wiseman A, MacKenzie TA, Malenka DJ, Northern New

England Cardiovascular Disease Study Group (2014) Reducing contrast-induced acute kidney injury using a regional multicenter quality improvement intervention. Circulation 7(5):693–700
13. Marenzi G, Lauri G, Assanelli E, Campodonico J, De Metrio M, Marana I, Grazi M, Veglia F, Bartorelli AL (2004) Contrast-induced nephropathy in patients undergoing primary angioplasty for acute myocardial infarction. J Am Coll Cardiol 44(9):1780–1785
14. Bottinor W, Polkampally P, Jovin I (2013) Adverse reactions to iodinated contrast media. Int J Angiol 22(3):149–154
15. Tearney GJ, Regar E, Akasaka T, Adriaenssens T, Barlis P, Bezerra HG, Bouma B, Bruining N, Cho JM, Chowdhary S, Costa MA, de Silva R, Dijkstra J, Di Mario C, Dudek D, Falk E, Feldman MD, Fitzgerald P, Garcia-Garcia HM, Gonzalo N, Granada JF, Guagliumi G, Holm NR, Honda Y, Ikeno F, Kawasaki M, Kochman J, Koltowski L, Kubo T, Kume T, Kyono H, Lam CC, Lamouche G, Lee DP, Leon MB, Maehara A, Manfrini O, Mintz GS, Mizuno K, Morel MA, Nadkarni S, Okura H, Otake H, Pietrasik A, Prati F, Räber L, Radu MD, Rieber J, Riga M, Rollins A, Rosenberg M, Sirbu V, Serruys PW, Shimada K, Shinke T, Shite J, Siegel E, Sonoda S, Suter M, Takarada S, Tanaka A, Terashima M, Thim T, Uemura S, Ughi GJ, van Beusekom HM, van der Steen AF, van Es GA, van Soest G, Virmani R, Waxman S, Weissman NJ, Weisz G, International Working Group for Intravascular Optical Coherence Tomography (IWG-IVOCT) (2012) Consensus standards for acquisition, measurement, and reporting of intravascular optical coherence tomography studies: a report from the International Working Group for Intravascular Optical Coherence Tomography Standardization and Validation. J Am Coll Cardiol 59(12):1058–1072
16. Bouma BE, Tearney GJ, Yabushita H, Shishkov M, Kauffman CR, DeJoseph Gauthier D, MacNeill BD, Houser SL, Aretz HT, Halpern EF, Jang IK (2003) Evaluation of intracoronary stenting by intravascular optical coherence tomography. Heart 89(3):317–320
17. Terashima M, Kaneda H, Suzuki T (2012) The role of optical coherence tomography in coronary intervention. Korean J Intern Med 27(1):1–12
18. Waksman R, Kitabata H, Prati F, Albertucci M, Mintz GS (2013) Intravascular ultrasound versus optical coherence tomography guidance. J Am Coll Cardiol 62(17 Suppl):S32–S40
19. Frick K, Michael TT, Alomar M, Mohammed A, Rangan BV, Abdullah S, Grodin J, Hastings JL, Banerjee S, Brilakis ES (2014) Low molecular weight dextran provides similar optical coherence tomography coronary imaging compared to radiographic contrast media. Catheter Cardiovasc Interv 84(5):727–731
20. Ozaki Y, Kitabata H, Tsujioka H, Hosokawa S, Kashiwagi M, Ishibashi K, Komukai K, Tanimoto T, Ino Y, Takarada S, Kubo T, Kimura K, Tanaka A, Hirata K, Mizukoshi M, Imanishi T, Akasaka T (2012) Comparison of contrast media and low-molecular-weight dextran for frequency-domain optical coherence tomography. Circ J 76(4):922–927

Nr. 2: Post-dilatation after implantation of bioresorbable everolimus- and novolimus-eluting scaffolds: an observational optical coherence tomography study of acute mechanical effects

Clin Res Cardiol
DOI 10.1007/s00392-016-1048-z

ORIGINAL PAPER

Post-dilatation after implantation of bioresorbable everolimus- and novolimus-eluting scaffolds: an observational optical coherence tomography study of acute mechanical effects

Florian Blachutzik[1] · Niklas Boeder[2] · Jens Wiebe[3] · Alessio Mattesini[4] · Oliver Dörr[2] · Astrid Most[2] · Timm Bauer[2] · Jens Röther[1] · Monique Tröbs[1] · Christian Schlundt[1] · Stephan Achenbach[1] · Christian W. Hamm[2] · Holger M. Nef[2]

Received: 22 July 2016 / Accepted: 12 October 2016

Abstract
Objectives The objective was to investigate the acute mechanical effects of post-dilatation on bioresorbable scaffolds (BRS) as determined by optical coherence tomography (OCT).
Background Post-dilatation with high-pressure balloons is regarded as a key component of BRS implantation for treatment of coronary artery stenoses. However, the impact of post-dilatation on BRS in vivo has not been thoroughly investigated.
Methods OCT was performed after the implantation procedure of 51 everolimus-eluting or novolimus-eluting polylactic acid-based BRS with ($n = 27$) or without non-compliant balloon post-dilatation ($n = 24$). The number of malapposed struts, strut fractures, edge dissections, residual in-scaffold area stenosis, and incomplete scaffold apposition area was analyzed over the complete length of each BRS with a spacing of 1 mm.
Results OCT revealed a significantly lower incomplete scaffold apposition area if post-dilatation was performed (0.16 ± 0.49 mm^2 with post-dilatation vs. 2.65 ± 2.78 mm^2 without post-dilatation, $p < 0.001$), as well as a significantly lower absolute number of malapposed struts (1 ± 2 with post-dilatation vs. 13 ± 13 without post-dilatation, $p < 0.001$). No significant differences regarding residual in-scaffold area stenosis, strut fracture, edge dissection, symmetry index, or eccentricity index were observed in patients with vs. without post-dilatation.
Conclusion Post-dilatation of BRS with non-compliant balloons significantly reduces the number of malapposed struts and incomplete scaffold apposition area without inducing higher rates of edge dissection or strut fracture.

Keywords Bioresorbable vascular scaffolds · Coronary artery disease · Optical coherence tomography · Percutaneous coronary intervention (PCI)

Introduction

The implantation of bioresorbable scaffolds (BRS) is a new concept for the treatment of coronary artery disease. Similar to metal stents, BRS initially provide mechanical scaffolding that prevents acute occlusion and early recoil after percutaneous transluminal coronary angioplasty (PTCA) and release everolimus or novolimus to prevent neointima proliferation. In contrast to metallic stents, which indefinitely impair physiological vascular biomechanics, future percutaneous coronary interventions (PCI), or grafting of the stented segment, BRS are subsequently resorbed, thus restoring pulsatility, cyclical strain, physiological shear stress, and mechanotransduction [1, 2].

Post-dilatation with an appropriately sized non-compliant (NC) balloon is considered essential for successful BRS implantation [3, 4], since underexpansion and strut malapposition might result in an increased rate of BRS

F. Blachutzik and N. Boeder contributed equally.

✉ Florian Blachutzik
florian.blachutzik@uk-erlangen.de

[1] Department of Cardiology, Friedrich-Alexander University Erlangen-Nürnberg (FAU), Erlangen, Germany

[2] Department of Cardiology and Angiology, University of Giessen, Giessen, Germany

[3] Deutsches Herzzentrum München, Technische Universität München, Munich, Germany

[4] Department of Heart and Vessels, Azienda Ospedaliero Universitaria Careggi, Florence, Italy

Published online: 18 October 2016

restenosis and thrombosis [5–7]. The impact of post-dilatation, however, has not been thoroughly investigated in a clinical patient cohort. Thus, the aim of this study was to analyze the acute mechanical effects of post-dilatation on BRS expansion, geometry, and apposition as determined by optical coherence tomography (OCT), which enables cross-sectional visualization of endothelial and intraluminal structures with high spatial resolution [8–11].

Materials and methods

Study design and population

We retrospectively analyzed the data of all patients undergoing implantation of everolimus-eluting Absorb BVS™ (Abbott Vascular, Santa Clara, California, USA) between March 2013 and June 2015 or of novolimus-eluting DESolve™ (Elixir Medical Corporation, Sunnyvale, California, USA) between January 2014 and June 2015 in a single center. All consecutive patients in whom OCT was performed after completion of the implantation procedure were included. The final OCT pullbacks were digitally stored and used for offline analysis. Exclusion criteria for BRS implantation were severe lesion calcification, ostial involvement, left main stem lesion, and vessel diameters for which appropriate BRS sizes are not available. OCT was not performed in the case of hemodynamic instability or renal impairment (creatinine >1.5 mg/dl). A total of 73 patients were identified to meet these criteria (Absorb 33 patients, DESolve 40 patients). Cases were excluded from this analysis if OCT quality was inadequate as assessed by two independent experienced interventional cardiologists. OCT quality was inadequate if parts of the vessel wall were invisible due to remaining blood streaks. There were no significant differences regarding baseline characteristics or procedural data between the patients excluded due to inadequate OCT quality and the patients included. The final study included 47 patients receiving 51 BRS (24 Absorb and 27 DESolve). Twenty-seven BRS were treated with post-dilatation, while in 24 BRS, no post-dilatation was performed (see Table 1).

Baseline patient characteristics, including medical history as well as clinical, angiographic, and procedural data, were collected in a standardized fashion. All patients gave written informed consent for evaluation of clinical, angiographic, procedural, and OCT data. The study was performed in accordance with the Declaration of Helsinki. The Ethics Committee of the Justus Liebig University Hospital (Giessen, Germany) approved the study protocol (reference number 203/14).

Percutaneous coronary intervention

PCI was performed via the radial or femoral approach using a 6 French guiding catheter and standard coronary guidewire (Runthrough™, Terumo Europe NV, Leuven, Belgium). Patients received intravenous heparin and intracoronary nitrates. Pre-dilatation with an NC balloon was performed in all lesions. Balloon size was selected based on visual estimation of the angiogram to achieve a 1:1 ratio of vessel and balloon diameter. Lesions were treated with either an everolimus-eluting BRS (Absorb BVS™, Abbott Vascular, Santa Clara, CA, USA) or a novolimus-eluting BRS (DESolve™, Elixir Medical Corporation, Sunnyvale, CA, USA). Absorb BRS were implanted with an initial pressure of 2 bar and increasing pressure in increments of 2 bar every 5 s until fully deployed (minimum 8 bar), and maximum pressure was maintained for 30 s. DESolve BRS were implanted starting at 1 bar for 10 s, continuing at 2 bar for 10 s, and subsequently increasing pressure in increments of 1 bar every 2 s until fully deployed, and maximum pressure was maintained for 20–30 s (minimum pressure 10 bar). Further medication, techniques, and equipment for PCI were used in accordance with the current clinical guidelines and were left to the responsible physician's discretion. If post-dilatation was performed, a non-compliant (NC) balloon (NC Trek™, Abbott Vascular, Santa Clara, CA, USA) was used at a pressure of 16 ± 9 bar (minimum pressure 10 bar; maximum pressure 26 bar). Post-dilatation was at the discretion of the operator.

Optical coherence tomography image acquisition

OCT was performed after the last step of the implantation procedure using a 2.7 French Dragonfly™ intravascular imaging catheter (St. Jude Medical, Saint Paul, MN, USA) at a mechanical pullback speed of 18 or 36 mm/s over a distance of 54 or 75 mm. Injection of 20 ml standard contrast agent (Ultravist™ 370, Bayer AG, Leverkusen, Germany) was performed at 4 ml/s with a maximum pressure of 600 psi (ACIST CVi™, ACIST Medical Systems, Eden Prairie, MN, USA). The OCT catheter was inserted distally to the treated segment and the pullback continued until either the guiding catheter was reached or the maximal pullback length (75 mm) was completed. In 25 patients (11 without and 14 with post-dilatation), pre-PCI OCT had been performed. In three patients with post-dilatation, an additional OCT pullback had been performed immediately after BRS deployment and before post-dilatation.

Table 1 Baseline characteristics

	All patients	No post-dilatation	Post-dilatation	*p* value
Number of patients	47	22	25	0.77
Number of scaffolds	51	24	27	0.78
Number of lesions	49	23	26	0.78
Age (years)	63 ± 8	63 ± 8	62 ± 7	0.66
Male gender (%)	79	78	80	0.58
BMI (kg/m^2)	29.3 ± 5.9	29.2 ± 3.5	28.1 ± 3.6	0.15
Previous MI (%)	12 (26)	6 (27)	6 (24)	0.80
Previous PCI (%)	22 (47)	13 (59)	9 (36)	0.12
Previous CABG (%)	2 (4)	1 (5)	1 (4)	0.93
LVEF (%)	56 ± 12	57 ± 12	56 ± 12	0.74
Presentation				
STEMI	8 (17)	3 (14)	5 (20)	0.58
NSTEMI	4 (9)	1 (5)	3 (12)	
Unstable AP	5 (11)	2 (10)	3 (12)	
Stable AP	21 (44)	10 (45)	11 (44)	
No complaints/atypical complaints	9 (19)	6 (27)	3 (12)	
NC pre-dilatation				
Performed (%)	100	100	100	>0.99
Pressure (bar)	15 ± 5	16 ± 5	14 ± 5	0.25
Diameter (mm)	2.9 ± 0.4	2.8 ± 0.4	3.0 ± 0.4	0.31
Length (mm)	15 ± 3	16 ± 5	16 ± 3	0.45
Scaffold				
Diameter (mm)	3.1 ± 0.3	3.1 ± 0.3	3.1 ± 0.3	0.89
Length (mm)	22 ± 6	23 ± 6	21 ± 6	0.21
Implantation pressure (bar)	13 ± 4	13 ± 3	13 ± 3	0.77
NC post-dilatation				
Diameter (mm)	3.3 ± 1.8		3.3 ± 1.8	
Pressure (bar)	16.0 ± 9.0		16.0 ± 9.0	
Number of NC balloons	2.2 ± 1.4	1.3 ± 0.4	2.8 ± 1.0	<0.001
Fluoroscopy time (min)	16 ± 9	15 ± 9	16 ± 8	0.74
Contrast volume (ml)	173 ± 82	169 ± 77	175 ± 80	0.58

Values are mean ± standard deviation or *n*

AP angina pectoris, *BMI* body mass index, *CABG* coronary artery bypass graft surgery, *LVEF* left ventricular ejection fraction, *NC* non-compliant balloon, *MI* myocardial infarction, *PCI* percutaneous coronary intervention

Optical coherence tomography image analysis

OCT image analysis was performed offline using the LightLab Imaging workstation (St. Jude Medical, Saint Paul, MN, USA) with manual calibration before each measurement. All images were digitally recorded, stored, and analyzed by two independent experienced investigators blinded to clinical characteristics and procedural data. OCT cross sections were analyzed over the complete length of implanted BRS with a spacing of 1 mm, starting 5 mm distal to the BRS, and ending 5 mm proximally. Malapposition was defined as the distance between the abluminal strut edge and the vessel wall being greater than 170 μm, which is the sum of strut and polymer thickness (150 μm) and the minimal axial resolution of the OCT (20 μm). Proximal and distal lumen reference areas were defined as the maximum area with physiological vessel structure visible at more than 180° of circumference within 5 mm proximal and distal to the BRS. In the cases without appropriate reference on both proximal and distal ends due to a large sidebranch, only a proximal or a distal reference was used.

The following parameters were manually contoured and measured for each cross section:

- Lumen area (mm^2) (see Fig. 1d).

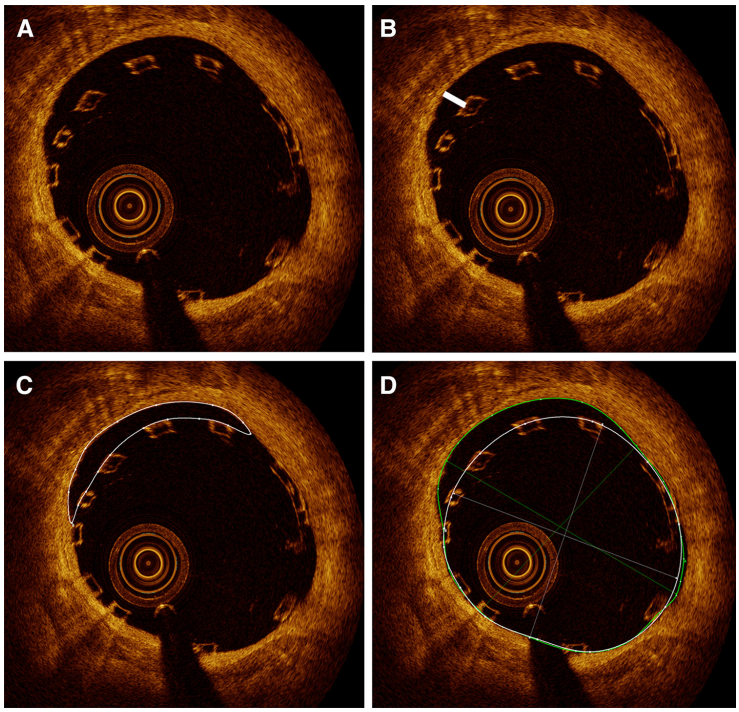

Fig. 1 Evaluation of OCT parameters in a cross section of an Absorb BRS implanted into the left anterior descending coronary artery. **a** Four malapposed struts and a total of 13 visible struts. **b** Distance between abluminal strut edge and vessel wall (*white line*) was measured. In this example, the maximum length of stent malapposition was 310 µm. **c** Measurement of incomplete scaffold apposition area (*white contour*). **d** Scaffold area (*white contour*) and total lumen area (*green contour*) are shown

- Scaffold area (mm^2): measured at abluminal strut edge (see Fig. 1d).
- Maximum/minimum/mean scaffold diameter (mm).
- Number of struts.
- Number of malapposed struts (see Fig. 1a).
- Maximum distance of malapposition (mm^2): maximum orthogonal distance between abluminal BRS strut and vessel wall (see Fig. 1b).
- Incomplete scaffold apposition area (mm^2): area between abluminal edge of BRS struts and vessel wall (see Fig. 1c).
- Tissue prolapse area (mm^2): the presence of tissue protruding between struts into the lumen as a circular arc connecting adjacent struts (see Fig. 2a and [12]).
- Overlapping scaffolds: defined as the visibility of more than one BRS.
- Strut fracture: struts lying isolated in the lumen or the presence of one strut on another.
- Proximal edge dissection: flap visible within 5 mm proximal to BRS.
- Distal edge dissection: flap visible within 5 mm distal to BRS.
- Bifurcation.

The following parameters were calculated (adapted from [13, 14]):

- Increment = (proximal lumen reference area − distal lumen reference area)/length in mm.
- Reference area (mm^2) = distal lumen reference area + (x × incremental), where x is the distance between distal end of BRS and actual cross section in mm.
- In-scaffold residual area stenosis (%) = 100 − (scaffold area/reference area) × 100; calculated for each cross section.
- Incomplete strut apposition (ISA) (%) = (number of malapposed struts per cross section/total number of visible struts per cross section) × 100.
- BRS eccentricity index = (minimum scaffold diameter/maximum scaffold diameter); calculated for each cross section analyzed (see Fig. 2).
- BRS symmetry index = (largest maximum scaffold diameter − smallest minimum scaffold diameter)/largest scaffold diameter; calculated for each cross section analyzed.
- Mean lumen area (mm^2).
- Minimal lumen area (mm^2).

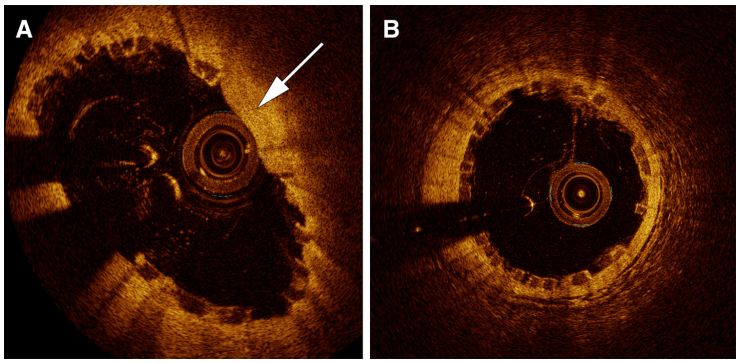

Fig. 2 DESolve BRS with low versus high eccentricity index. **a** Eccentricity index of 0.73. **b** Eccentricity index of 0.88. A lower eccentricity index is the result of greater differences between minimum and maximum scaffold diameter. In **a**, tissue protrusion is visible (*white arrow*)

Statistical analysis

Continuous variables are summarized as mean ± standard deviation; categorical variables are quoted as *n* (%). The Kolmogorov–Smirnov test was performed to test for parametric distribution. To test for statistical differences between two groups for comparison of continuous variables, either a *t* test for unpaired samples (parametric distribution) or a Mann–Whitney *U* test (non-parametric distribution) was performed. For categorical variables, a Chi-squared or Fischer's exact test was carried out to test for significant differences. Statistical analysis was performed using SPSS version 21.0 (IBM SPSS Statistics, IBM Corporation, Armonk, New York, USA). A two-sided $p < 0.05$ was considered significant.

Results

Patients

A total of 51 BRS implanted in 49 lesions of 47 patients (37 male, 10 female) who were treated with either Absorb or DESolve BRS with or without post-dilatation were analyzed. Four patients were treated with two BRS, whereas 43 patients were treated with only one. Of those patients receiving more than one BRS, two received two Absorb BRS and two were treated with two DESolve BRS. In two of the patients (1 Absorb, 1 DESolve), two different lesions were treated, whereas in the other two patients (1 Absorb, 1 DESolve), lesion length required sequential overlapping implantation of BRS.

24 BRS were implanted without post-dilatation, and 27 BRS were treated with post-dilatation. There were no significant differences in baseline characteristics between the groups with and without post-dilatation performed (Table 1). Most of the patients presented with stable angina (44 %). The target lesion was located in the left anterior descending coronary artery (LAD) in 38 % of cases, in the circumflex artery (Cx) in 19 %, and in the right coronary artery (RCA) in 43 %.

Percutaneous coronary intervention

Pre-dilatation with an NC balloon was performed in all the cases. The mean inflation pressure was 15 ± 5 bar (maximum pressure used: 22 bar), the mean balloon diameter was 2.9 ± 0.4 mm, and the mean balloon length was 15 ± 3 mm. As shown in Table 1, there were no significant differences in BRS length, diameter, or implantation pressure between the groups with or without post-dilatation (mean post-dilatation pressure: 16 ± 9 bar; maximum pressure: 20 bar; mean diameter of NC balloon: 3.3 ± 1.8 mm).

Optical coherence tomography: post-dilatation vs. no post-dilatation

A total of 1654 OCT cross sections were analyzed to obtain the data, as shown in Table 2. Incomplete scaffold apposition area was significantly smaller with post-dilatation than without post-dilatation (0.16 ± 0.49 vs. 2.65 ± 2.78 mm^2; $p < 0.001$). In addition, the absolute number of malapposed struts per scaffold was significantly lower with post-dilatation (1 ± 2 vs. 13 ± 13; $p < 0.001$). The malapposed struts' mean orthogonal distance to the vessel wall was significantly larger without post-dilatation (0.36 ± 0.23 mm vs. 0.09 ± 0.17 mm; $p < 0.001$). Mean, minimum, and maximum scaffold diameters as well as mean and minimal lumen areas were similar between the groups with and without post-dilatation. In addition, there were no significant differences in terms of eccentricity index or symmetry index. While mean tissue prolapse area

Table 2 OCT findings with vs. without post-dilatation

	All patients ($n = 51$)	No post-dilatation ($n = 24$)	Post-dilatation ($n = 27$)	p value
OCT scaffold area (mm^2)	7.47 ± 1.70	7.38 ± 1.63	7.55 ± 1.79	0.68
Residual in-scaffold area stenosis (%)	20.7 ± 15.5	25.2 ± 14.0	18.5 ± 12.4	0.14
Reference area (mm^2)	7.69 ± 1.97	8.02 ± 2.14	7.40 ± 1.79	0.35
Mean lumen area (mm^2)	7.35 ± 1.74	7.40 ± 1.78	7.30 ± 1.73	0.90
Minimal lumen area (mm^2)	5.81 ± 1.57	5.77 ± 1.41	5.84 ± 1.73	0.96
OCT ISAA (mm^2)	1.33 ± 2.30	2.65 ± 2.78	0.16 ± 0.49	<0.001
OCT tissue prolapse area (mm^2)	5.05 ± 8.49	3.44 ± 6.84	6.47 ± 9.63	0.16
Sum of malapposed struts (n)	6 ± 11	13 ± 13	1 ± 2	<0.001
Sum of struts (n)	227 ± 66	228 ± 66	226 ± 66	0.95
ISA (%)	0.04 ± 0.07	0.06 ± 0.06	0.02 ± 0.07	<0.001
Distance[a] (mm)	0.22 ± 0.24	0.36 ± 0.23	0.09 ± 0.17	<0.001
Mean stent diameter (mm)	3.05 ± 0.35	3.03 ± 0.33	3.06 ± 0.37	0.72
Minimum stent diameter (mm)	2.73 ± 0.32	2.72 ± 0.31	2.74 ± 0.32	0.79
Maximum stent diameter (mm)	3.39 ± 0.43	3.37 ± 0.39	3.41 ± 0.47	0.85
Minimum eccentricity index	0.66 ± 0.10	0.65 ± 0.09	0.67 ± 0.11	0.50
Overlapping	0.75 ± 1.70	0.88 ± 1.94	0.63 ± 1.47	0.62
Fracture	0.078 ± 0.28	0.13 ± 0.34	0.04 ± 0.19	0.25
Bifurcation	0.94 ± 1.03	0.75 ± 0.99	1.11 ± 1.05	0.19
Mean eccentricity index	0.81 ± 0.06	0.81 ± 0.06	0.79 ± 0.07	0.94
Symmetry index	0.41 ± 0.11	0.43 ± 0.11	0.39 ± 0.10	0.20
Proximal edge dissection	0	0	0	>0.99
Distal edge dissection	0	0	0	>0.99

Values are mean ± standard deviation

ISA incomplete strut apposition (ratio of number of malapposed struts per BRS to total number of struts per BRS), *ISAA* incomplete scaffold apposition area (area between abluminal edge of malapposed struts and vessel wall)

[a] Distance: orthogonal distance between malapposed scaffold and vessel wall

was larger with post-dilatation, this difference was not significant (6.47 ± 9.63 vs. 3.44 ± 6.84 mm^2; $p = 0.16$). Residual in-scaffold area stenosis was lower with post-dilatation, but also in this case, not significantly (18.5 ± 12.4 vs. 25.2 ± 14.0 %; $p = 0.14$). Post-dilatation used with BRS was not associated with a higher frequency of proximal or distal edge dissections or strut fractures.

When comparing all everolimus-eluting BRS (with and without post-dilatation) and all novolimus-eluting BRS (with and without post-dilatation), there were no significant differences regarding incomplete scaffold apposition area (1.17 ± 1.85 vs. 1.47 ± 2.66 mm^2; $p = 0.63$) or the absolute number of malapposed struts per scaffold (5 ± 9 vs. 8 ± 13; $p = 0.33$). Nevertheless, mean tissue prolapse area (8.53 ± 10.44 vs. 1.13 ± 1.81 mm^2; $p = 0.005$) was significantly larger and eccentricity was significantly higher, as displayed in a lower eccentricity index (mean eccentricity index: 0.78 ± 0.07 vs. 0.85 ± 0.04) in novolimus-eluting BRS as compared to everolimus-eluting BRS.

Discussion

Post-dilatation vs. no post-dilatation

The principal finding of this study is that post-dilatation after implantation of contemporary bioresorbable vascular scaffolds significantly reduces the incomplete scaffold apposition area and the number of malapposed struts without inducing more edge dissections or strut fractures. Previous studies have demonstrated that malapposed struts are associated with very late thrombosis of DES, most likely due to disruption of laminar flow [6, 15]. Stent thrombosis leads to myocardial infarction and has an extremely high mortality rate [16, 17]. Similar to the conventional stents, available data suggest an association of BRS underexpansion and malapposition with BRS thrombosis [5, 18]. Malapposed BRS struts do not sufficiently supply the vessel wall with novolimus or everolimus, and lumen loss due to intima proliferation is likely to occur. Furthermore, only approximately 61 % of

malapposed BRS struts are covered with neointima after 6 months [17]. On the other hand, one must keep in mind that malapposition is theoretically limited in time with BRS due to their eventual dissolution.

Clinical implications

Our data suggest that post-dilatation after implantation of Absorb or DESolve with an adequately sized NC balloon significantly improves acute deployment as evidenced by the reduced number of malapposed struts and reduced incomplete scaffold apposition area without higher rates of strut fractures or edge dissections. This may result in improved clinical outcome. Common and accepted criteria for appropriate BRS deployment were used to define the quality of the acute mechanical results [19–21]. Nevertheless, a correlation between these criteria and long-term outcome is mainly derived from previous studies comparing outcome after bare metal stents or first-generation DES using intravascular ultrasound [22–24]. Data regarding long-term outcome with BRS are very limited. De Ribamar Costa et al. reported that using post-dilatation with the Absorb device did not influence 1-year clinical outcome and concluded that post-dilatation should be performed whenever possible; however, no routine intravascular assessment was performed to evaluate the acute mechanical effects of post-dilatation and, in contrast to our study, only lesions with low-to-moderate complexity were included [25].

Whether the improvement in acute performance of BRS achieved by post-dilatation that we observed is really associated with a better clinical outcome still needs to be evaluated in controlled, randomized studies with the long-term follow-up to confirm the value of post-dilatation after BRS implantation and establish it as standard of care.

Interestingly, tissue prolapse area was significantly larger and eccentricity was significantly higher in novolimus-eluting scaffolds as compared to everolimus-eluting scaffolds. This could be due to structural differences between those two BRS, especially due to the larger scaffold cells of novolimus-eluting BRS [26]. Higher BRS eccentricity and larger tissue prolapse area have been reported to be associated with an impaired clinical outcome [27, 28].

Limitations

This is a non-randomized, retrospective, single-center study that compared acute mechanical effects of post-dilatation for two types of BRS. With 47 patients and 51 scaffolds, the sample size is relatively small. Therefore, results may have been influenced by differences in baseline characteristics, although no significant differences could be observed. A paired analysis with OCT performed immediately after BRS deployment, and then, again, after NC balloon, post-dilatation would have been superior to our study design. Furthermore, PCI procedures were not all performed by the same operator, and therefore, we cannot exclude the possibility that individual differences in procedural approach may have influenced the results. In three patients, OCT was performed after BRS implantation and before post-dilatation. It is possible that post-implantation OCT influenced the decision to perform post-dilatation. This, however, would emphasize our results, since the effect would be to mitigate the difference between BRS with and without post-dilatation (no post-dilatation done if OCT shows a good implantation result, yet we can still demonstrate significantly more malapposition if post-dilatation is not performed).

It should also be noted that our results are not generally applicable to all PCI procedures performed with BRS implantation. The selection of cases that included the use of OCT for clinical reasons likely resulted in a cohort of more complex lesions than those typically treated with BRS. In addition, the lack of clinical outcome data is an important limitation of our study.

Conclusion

Post-dilatation of either Absorb or DESolve BRS with non-compliant balloons significantly reduces the number of malapposed struts as well as the area of incomplete scaffold apposition without inducing higher rates of edge dissection or strut fracture.

Compliance with ethical standards

Ethical standards All patients gave written informed consent for the evaluation of clinical, angiographic, procedural, and OCT data. The study was performed in accordance with the ethical standards laid down in the 1964 Declaration of Helsinki and its later amendments. The Ethics Committee of the Justus Liebig University Hospital (Giessen, Germany) approved the study protocol (reference number 203/14).

Conflict of interest Christian Hamm and Holger Nef received speaking honoraria from Abbott Vascular. Stephan Achenbach and Holger Nef have received research grants (to institution) from Abbott Vascular. Holger Nef also received a research grant (to institution) from Elixir Medical. All the other authors have no potential conflict of interest.

References

1. Iqbal J, Onuma Y, Ormiston J, Abizaid A, Waksman R, Serruys P (2014) Bioresorbable scaffolds: rationale, current status, challenges, and future. Eur Heart J 35:765–776
2. Simsek C, Karanasos A, Magro M, Garcia-Garcia HM, Onuma Y, Regar E, Boersma E, Serruys PW, van Geuns RJ (2016) Long-

term invasive follow-up of the everolimus-eluting bioresorbable vascular scaffold: five-year results of multiple invasive imaging modalities. EuroIntervention 11:996–1003
3. Everaert B, Felix C, Koolen J, den Heijer P, Henriques J, Wykrzykowska J, van der Schaaf R, de Smet B, Hofma S, Diletti R, Van Mieghem N, Regar E, Smits P, van Geuns RJ (2015) Appropriate use of bioresorbable vascular scaffolds in percutaneous coronary interventions: a recommendation from experienced users. A position statement on the use of bioresorbable vascular scaffolds in the Netherlands. Neth Heart J 23:161–165
4. Tamburino C, Latib A, van Geuns RJ, Sabate M, Mehilli J, Gori T, Achenbach S, Alvarez MP, Nef H, Lesiak M, Di Mario C, Colombo A, Naber CK, Caramanno G, Capranzano P, Brugaletta S, Geraci S, Araszkiewicz A, Mattesini A, Pyxaras SA, Rzeszutko L, Depukat R, Diletti R, Boone E, Capodanno D, Dudek D (2015) Contemporary practice and technical aspects in coronary intervention with bioresorbable scaffolds: a European perspective. EuroIntervention 11:45–52
5. Cuculi F, Puricel S, Jamshidi P, Valentin J, Kallinikou Z, Toggweiler S, Weissner M, Münzel T, Cook S, Gori T (2015) Optical coherence tomography findings in bioresorbable vascular scaffolds thrombosis. Circ Cardiovasc Interv 8(10):e002518. doi:10.1161/CIRCINTERVENTIONS.114.002518 **(Epub ahead of print)**
6. Taniwaki M, Radu MD, Zaugg S, Amabile N, Garcia-Garcia HM, Yamaji K, Jørgensen E, Kelbæk H, Pilgrim T, Caussin C, Zanchin T, Veugeois A, Abildgaard U, Jüni P, Cook S, Koskinas KC, Windecker S, Räber L (2016) Mechanisms of very late drug-eluting stent thrombosis assessed by optical coherence tomography. Circulation. doi:10.1161/CIRCULATIONAHA.115.019071 **(Epub ahead of print)**
7. Souteyrand G, Amabile N, Mangin L, Chabin X, Meneveau N, Cayla G, Vanzetto G, Barnay P, Trouillet C, Rioufol G, Rangé G, Teiger E, Delaunay R, Dubreuil O, Lhermusier T, Mulliez A, Levesque S, Belle L, Caussin C, Motreff P; PESTO Investigators (2016) Mechanisms of stent thrombosis analysed by optical coherence tomography: insights from the national PESTO French registry. Eur Heart J. doi:10.1093/eurheartj/ehv711 **(Epub ahead of print)**
8. Prati F, Kodama T, Romagnoli E, Gatto L, Di Vito L, Ramazzotti V, Chisari A, Marco V, Cremonesi A, Parodi G, Albertucci M, Alfonso F (2015) Suboptimal stent deployment is associated with subacute stent thrombosis: optical coherence tomography insights from a multicenter matched study. From the CLI Foundation investigators: the CLI-THRO study. Am Heart J 169:249–256
9. Guagliumi G, Sirbu V, Musumeci G, Gerber R, Biondi-Zoccai G, Ikejima H, Ladich E, Lortkipanidze N, Matiashvili A, Valsecchi O, Virmani R, Stone GW (2012) Examination of the in vivo mechanisms of late drug-eluting stent thrombosis: findings from optical coherence tomography and intravascular ultrasound imaging. J Am Coll Cardiol Interv 5:12–20
10. Alfonso F, Dutary J, Paulo M, Gonzalo N, Pérez-Vizcayno MJ, Jiménez-Quevedo P, Escaned J, Bañuelos C, Hernández R, Macaya C (2012) Combined use of optical coherence tomography and intravascular ultrasound imaging in patients undergoing coronary interventions for stent thrombosis. Heart 98:1213–1220
11. Prati F, Regar E, Mintz GS, Arbustini E, Di Mario C, Jang IK, Akasaka T, Costa M, Guagliumi G, Grube E, Ozaki Y, Pinto F, Serruys PW (2010) Expert review document on methodology, terminology, and clinical applications of optical coherence tomography: physical principles, methodology of image acquisition, and clinical application for assessment of coronary arteries and atherosclerosis. Eur Heart J 31:401–415
12. Serruys PW, Onuma Y, Ormiston JA, de Bruyne B, Regar E, Dudek D, Thuesen L, Smits PC, Chevalier B, McClean D, Koolen J, Windecker S, Whitbourn R, Meredith I, Dorange C, Veldhof S, Miquel-Hebert K, Rapoza R, García-García HM (2010) Evaluation of the second generation of a bioresorbable everolimus drug-eluting vascular scaffold for treatment of de novo coronary artery stenosis: six-month clinical and imaging outcomes. Circulation 122:2301–2312
13. Mattesini A, Boeder N, Löblich K, Valente S, Foin N, Caiazzo G, Ghione M, Gensini GF, Italo P, Di Mario C, Nef H (2015) TCT-514 Absorb vs DESolve: an optical coherence tomography comparison of acute mechanical performances. J Am Coll Cardiol 66(15_S). doi:10.1016/j.jacc.2015.08.531 **(Epub ahead of print)**
14. Mattesini A, Secco GG, Dall'Ara G, Ghione M, Rama-Merchan JC, Lupi A, Viceconte N, Lindsay AC, De Silva R, Foin N, Naganuma T, Valente S, Colombo A, Di Mario C (2014) ABSORB biodegradable stents versus second-generation metal stents: a comparison study of 100 complex lesions treated under OCT guidance. J Am Coll Cardiol Interv 7:741–750
15 Kimura T, Morimoto T, Kozuma K, Honda Y, Kume T, Aizawa T, Mitsudo K, Miyazaki S, Yamaguchi T, Hiyoshi E, Nishimura E, Isshiki T, RESTART Investigators (2010) Comparisons of baseline demographics, clinical presentation, and long-term outcome among patients with early, late, and very late stent thrombosis of sirolimus-eluting stents. Circulation 122:52–61
16 van Werkum JW, Heestermans AA, de Korte FI, Kelder JC, Suttorp MJ, Rensing BJ, Zwart B, Brueren BR, Koolen JJ, Dambrink JH, van't Hof AW, Verheugt FW, ten Berg JM (2009) Long-term clinical outcome after a first angiographically confirmed coronary stent thrombosis: an analysis of 431 cases. Circulation 119:828–834
17 Gutiérrez-Chico JL, Gijsen F, Regar E, Wentzel J, de Bruyne B, Thuesen L, Ormiston J, McClean DR, Windecker S, Chevalier B, Dudek D, Whitbourn R, Brugaletta S, Onuma Y, Serruys PW (2012) Differences in neointimal thickness between the adluminal and the abluminal sides of malapposed and side-branch struts in a polylactide bioresorbable scaffold: evidence in vivo about the abluminal healing process. J Am Coll Cardiol Interv 5:428–435
18 Karanasos A, Van Mieghem N, van Ditzhuijzen N, Felix C, Daemen J, Autar A, Onuma Y, Kurata M, Diletti R, Valgimigli M, Kauer F, van Beusekom H, de Jaegere P, Zijlstra F, van Geuns RJ, Regar E (2015) Angiographic and optical coherence tomography insights into bioresorbable scaffold thrombosis: single-center experience. Circ Cardiovasc Interv 8(5). doi:10.1161/CIRCINTERVENTIONS.114.002369
19 Tearney GJ, Regar E, Akasaka T, Adriaenssens T, Barlis P, Bezerra HG, Bouma B, Bruining N, Cho JM, Chowdhary S, Costa MA, de Silva R, Dijkstra J, Di Mario C, Dudek D, Falk E, Feldman MD, Fitzgerald P, Garcia-Garcia HM, Gonzalo N, Granada JF, Guagliumi G, Holm NR, Honda Y, Ikeno F, Kawasaki M, Kochman J, Koltowski L, Kubo T, Kume T, Kyono H, Lam CC, Lamouche G, Lee DP, Leon MB, Maehara A, Manfrini O, Mintz GS, Mizuno K, Morel MA, Nadkarni S, Okura H, Otake H, Pietrasik A, Prati F, Räber L, Radu MD, Rieber J, Riga M, Rollins A, Rosenberg M, Sirbu V, Serruys PW, Shimada K, Shinke T, Shite J, Siegel E, Sonoda S, Suter M, Takarada S, Tanaka A, Terashima M, Thim T, Uemura S, Ughi GJ, van Beusekom HM, van der Steen AF, van Es GA, van Soest G, Virmani R, Waxman S, Weissman NJ, Weisz G; International Working Group for Intravascular Optical Coherence Tomography (IWG-IVOCT) (2012) Consensus standards for acquisition, measurement, and reporting of intravascular optical coherence tomography studies: a report from the International Working Group for Intravascular Optical Coherence Tomography Standardization and Validation. J Am Coll Cardiol 59:1058–1072
20 Uren NG, Schwarzacher SP, Metz JA, Lee DP, Honda Y, Yeung AC, Fitzgerald PJ, Yock PG, POST Registry Investigators (2002)

Predictors and outcomes of stent thrombosis: an intravascular ultrasound registry. Eur Heart J 23:124–132

21 Gomez-Lara J, Diletti R, Brugaletta S, Onuma Y, Farooq V, Thuesen L, McClean D, Koolen J, Ormiston JA, Windecker S, Whitbourn R, Dudek D, Dorange C, Veldhof S, Rapoza R, Regar E, Garcia-Garcia HM, Serruys PW (2012) Angiographic maximal luminal diameter and appropriate deployment of the everolimus-eluting bioresorbable vascular scaffold as assessed by optical coherence tomography: an ABSORB cohort B trial sub-study. EuroIntervention 8:214–224

22 Sonoda S, Morino Y, Ako J, Terashima M, Hassan AH, Bonneau HN, Leon MB, Moses JW, Yock PG, Honda Y, Kuntz RE, Fitzgerald PJ, SIRIUS Investigators (2004) Impact of final stent dimensions on long-term results following sirolimus-eluting stent implantation: serial intravascular ultrasound analysis from the sirius trial. J Am Coll Cardiol 43:1959–1963

23 Costa MA, Angiolillo DJ, Tannenbaum M, Driesman M, Chu A, Patterson J, Kuehl W, Battaglia J, Dabbons S, Shamoon F, Flieshman B, Niederman A, Bass TA, STLLR Investigators (2008) Impact of stent deployment procedural factors on long-term effectiveness and safety of sirolimus-eluting stents (final results of the multicenter prospective STLLR trial). Am J Cardiol 101:1704–1711

24 Doi H, Maehara A, Mintz GS, Yu A, Wang H, Mandinov L, Popma JJ, Ellis SG, Grube E, Dawkins KD, Weissman NJ, Turco MA, Ormiston JA, Stone GW (2009) Impact of post-intervention minimal stent area on 9-month follow-up patency of paclitaxel-eluting stents: an integrated intravascular ultrasound analysis from the TAXUS IV, V, and VI and TAXUS ATLAS Workhorse, Long Lesion, and Direct Stent Trials. J Am Coll Cardiol Interv 2:1269–1275

25 De Ribamar Costa Jr J, Abizaid A, Bartorelli AL, Whitbourn R, van Geuns RJ, Chevalier B, Perin M, Seth A, Botelho R, Serruys PW; ABSORB EXTEND Investigators (2015) Impact of post-dilation on the acute and one-year clinical outcomes of a large cohort of patients treated solely with the Absorb bioresorbable vascular scaffold. EuroIntervention 11:141–148

26 Ormiston JA, Webber B, Ubod B, Darremont O, Webster MW (2015) An independent bench comparison of two bioresorbable drug-eluting coronary scaffolds (Absorb and DESolve) with a durable metallic drug-eluting stent (ML8/Xpedition). EuroIntervention 11(1):60–67

27 Suwannasom P, Sotomi Y, Ishibashi Y, Cavalcante R, Albuquerque FN, Macaya C, Ormiston JA, Hill J, Lang IM, Egred M, Fajadet J, Lesiak M, Tijssen JG, Wykrzykowska JJ, de Winter RJ, Chevalier B, Serruys PW, Onuma Y (2016) The impact of post-procedural asymmetry, expansion, and eccentricity of bioresorbable everolimus-eluting scaffold and metallic everolimus-eluting stent on clinical outcomes in the ABSORB II Trial. J Am Coll Cardiol Interv 9(12):1231–1242

28 Rivero F, Bastante T, Cuesta J, Benedicto A, Restrepo JA, Alfonso F (2015) Treatment of in-stent restenosis with bioresorbable vascular scaffolds: optical coherence tomography insights. Can J Cardiol 31(3):255–259

Nr. 3: Overlapping implantation of bioresorbable novolimus-eluting scaffolds: An observational optical coherence tomography study

Heart Vessels
DOI 10.1007/s00380-016-0932-9

ORIGINAL ARTICLE

Overlapping implantation of bioresorbable novolimus-eluting scaffolds: an observational optical coherence tomography study

Florian Blachutzik[1] · Niklas Boeder[2] · Jens Wiebe[3] · Alessio Mattesini[4] · Oliver Dörr[2] · Astrid Most[2] · Timm Bauer[2] · Monique Tröbs[1] · Jens Röther[1] · Christian Schlundt[1] · Stephan Achenbach[1] · Christian Hamm[2] · Holger Nef[2]

Received: 7 August 2016 / Accepted: 9 December 2016

Abstract Overlapping implantation of bioresorbable vascular scaffolds is frequently necessary, but its influence on vessel and scaffold structure has not been thoroughly analyzed previously. The aim of this study was to analyze the acute effects of overlapping implantation on BRS as determined by optical coherence tomography (OCT). A total of 38 patients with de novo coronary artery stenoses who underwent OCT in the context of implantation of novolimus-eluting BRS (DESolve, Elixir Medical Corporation, Sunnyvale, California, USA) were investigated. In 15 patients, overlapping implantation of two BRS was performed, while 23 patients with implantation of one single BRS served as the control group. OCT data were retrospectively analyzed regarding acute scaffold implantation results. There were no significant differences between the overlap and control group in terms of residual in-scaffold area stenosis, scaffold area, mean or minimal lumen area, eccentricity index, incomplete scaffold apposition area or malapposition. While strut fracture was slightly more frequent in BRS with overlap its incidence was low overall. In patients with overlapping BRS, overlap segments did not display smaller lumen areas than segments without overlap (mean lumen area overlap: 8.16 ± 2.97 mm^2 vs. no overlap: 7.70 ± 2.55 mm^2; $p = 0.71$; minimal lumen area overlap: 6.83 ± 2.71 mm^2 vs. no overlap: 6.17 ± 2.58 mm^2; $p = 0.37$). Acute mechanical performance of novolimus-eluting BRS is not impaired by overlapping implantation. It can be assumed that vessel expansion compensates for the double scaffold layer in the overlap area resulting in a similar lumen area in overlap areas and in those with a single strut layer.

Keywords Percutaneous coronary intervention · Optical coherence tomography · Bioresorbable Scaffold

Introduction

While overlapping implantation of coronary stents was usually avoided for bare metal stents (BMS), given a higher frequency of target vessel revascularization and impaired clinical outcome [1], stent overlap has been used more liberally with drug eluting stents (DES). Overlapping implantation of first-generation DES remained associated with impaired angiographic and clinical outcome [2, 3], but data for second-generation DES revealed that overlapping implantation of these devices is safe without increased rates of target vessel revascularization or impaired clinical outcome [2, 4]. Bioresorbable vascular scaffolds (BRS) are a novel approach for treatment of coronary artery stenoses. They promise to overcome some limitations of DES, mainly because of their biodegradation within a period of 2–4 years. Several studies have reported non-inferiority as compared to DES [5–9], with the potential exception of very small vessels [10]. All the same, research regarding optimal use of BRS is still under progress. Notably, all randomized trials published to date have excluded the

F. Blachutzik and N. Boeder contributed equally.

✉ Florian Blachutzik
florian.blachutzik@uk-erlangen.de

[1] Friedrich-Alexander Universität Erlangen-Nürnberg (FAU), Department of Medicine 2-Cardiology, University Hospital Erlangen, Ulmenweg 18, 91054 Erlangen, Germany

[2] Justus Liebig Universität Giessen, University Hospital Giessen, Medical Clinic I, Giessen, Germany

[3] German Heart Centre Munich, Munich, Germany

[4] Careggi Hospital, Florence, Italy

Published online: 21 December 2016

implantation of overlapping BRS. Hence, only limited data exist regarding the performance and outcome of BRS in long lesions with overlapping device implantation. We analyzed the acute mechanical effects of overlapping BRS implantation as well as the differences between overlap areas and areas with a single BRS layer by optical coherence tomography (OCT) in vivo.

Materials and methods

Study design and population

Between July 2014 and August 2015, 46 patients were treated using novolimus-eluting BRS at the University Hospital of Giessen. Post-procedural OCT was pre-specified to be performed in case of a difficult implantation process due to lesion calcification, fibrosis or tortuosity in 40 patients. Two of these 40 patients displayed inadequate OCT image quality as assessed by two independent experienced interventional cardiologists. Out of the remaining 38 patients, 15 patients received two overlapping novolimus-eluting BRS and formed the study group, while 23 patients received one single novolimus-eluting BRS and constitute the control group. Overlapping BRS implantation was performed if one BRS was insufficient to cover the entire lesion length. A priori exclusion criteria for BRS implantation included severe lesion calcification, ostial involvement, lesion location in the left main coronary artery, and a reference vessel diameter exceeding 4.0 mm. OCT was not performed in case of hemodynamic instability, known contrast agent allergy or renal impairment (creatinine > 1.5 mg/dl).

Baseline characteristics of the patients including medical history, clinical, angiographic and procedural data were prospectively collected in a standardized form. Our aim was to analyze whether overlapping of novolimus-eluting BRS is associated with acute mechanical alterations in BRS structure that are different from those implanted without overlap and whether the overlap of two BRS layers results in a significantly smaller vessel lumen area compared to lesion segments without BRS overlap. The study complied with the Declaration of Helsinki. The Ethics Committee of the Justus-Liebig-University Hospital (Giessen, Germany) approved the study protocol (Reference number 203/14). Written informed consent for evaluation of clinical, procedural and OCT data was obtained from each patient before inclusion.

Percutaneous coronary intervention

Percutaneous coronary intervention (PCI) was performed via a radial or femoral approach, using 6 French guiding catheters and standard coronary guidewires (Runthrough™, Terumo Europe NV, Leuven, Belgium). All patients received intravenous heparin and intracoronary nitrates. Pre-dilatation with an appropriately sized NC (non-compliant) balloon was performed in all lesions applying a maximal implantation pressure of 20 bar. While lesions in the control group were treated with one single novolimus-eluting BRS (DESolve™ or DESolve XL™, Elixir Medical Corporation, Sunnyvale, California, USA), lesions in the 15 patients with overlap were treated by sequential implantation of two novolimus-eluting BRS using the "marker-to-marker" method. Novolimus-eluting BRS were available with a length of 14, 18 or 28 mm and a diameter of 2.5, 3.0, 3.5 or 4.0 mm. BRS were deployed with slow balloon implantation (2 bar each 5 s keeping the delivery balloon inflated at least 30 s, if possible). Post-dilatation with an appropriately sized NC balloon (NC Trek™, Abbott Vascular, Santa Clara, California, USA) was mandatory (mean pressure: 17 ± 5 bar; mean diameter: 3.5 ± 0.6 mm). Further medication, technique and equipment for percutaneous coronary intervention were according to clinical requirements and at the discretion of the operator.

Optical coherence tomography image acquisition

After completion of the implantation procedure (including post-dilatation), OCT was performed using a 2.7 F Dragonfly™ intravascular imaging catheter (St. Jude Medical, Saint Paul, MN, USA) at a mechanical pullback speed of 18 mm/s over a distance of 54 or 36 mm/s over 75 mm. Contrast agent (20 ml, Ultravist™ 370, Bayer AG, Leverkusen, Germany) was injected through the guiding catheter at 4 ml/s with a maximum pressure of 600 psi using machine injection (ACIST CVi™, ACIST Medical Systems, Eden Prairie, MN, USA). The OCT catheter was positioned distally to the treated segment before starting the pullback. Additional OCT runs were performed in eight cases because the treated segment was not completely captured by one single pullback.

Optical coherence tomography image analysis

Offline OCT image analysis was performed using the LightLab Imaging workstation (St. Jude Medical, Saint Paul, MN, US) with manual calibration before each measurement. All images were recorded digitally, stored and analyzed by two experienced investigators blinded to clinical and procedural data. OCT cross sections were analyzed starting 5 mm distal to the BRS and ending 5 mm proximal to the BRS with a spacing of 1 mm between consecutive images. Struts were defined as malapposed if the distance between the outer strut edge and vessel wall was larger than 170 μm [equal to the sum of strut and polymer thickness (150 μm) plus the minimal axial resolution of OCT

(20 µm)]. Proximal and distal lumen reference areas were defined as maximum area with a three-layered vessel wall visible at more than 180° of circumference within 5 mm proximal and distal to the BRS. In case of absence of any appropriate proximal or distal lumen reference because of ostial location or a large side branch, only one reference was used.

The following parameters were manually traced and measured for each OCT cross section:

- Lumen area (mm^2): contoured by following the area filled with contrast media (Fig. 1: green mark)
- Scaffold area (mm^2): measured at the outer strut edge of each scaffold (Fig. 1: white mark).
- Maximum/minimum/mean scaffold diameter (mm).
- Number of struts.
- Number of malapposed struts (Fig. 2).
- Maximum malapposition distance (mm): maximum orthogonal distance between outer BRS strut and vessel wall (Fig. 3).
- Incomplete scaffold apposition area (mm^2): area between outer edge of BRS struts and vessel wall (Fig. 4: white mark).
- Tissue prolapse area (mm^2): presence of tissue protruding between struts into the lumen as a circular arc connecting adjacent struts [11].
- Overlapping (Yes/No): struts of more than one BRS visible in one cross section (Fig. 1).
- Strut fracture (Yes/No): isolated struts in the vessel lumen or visible discontinuity of a strut edge (Fig. 5).
- Maximum distance inner strut edge to vessel wall for overlapping BRS.

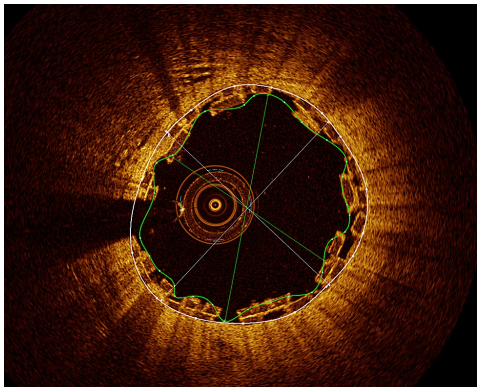

Fig. 1 Overlapping BRS OCT cross section showing two overlapping DESolve BRS. Lumen area (*green mark*) and scaffold area of the outer BRS (*white mark*) are contoured (color figure online)

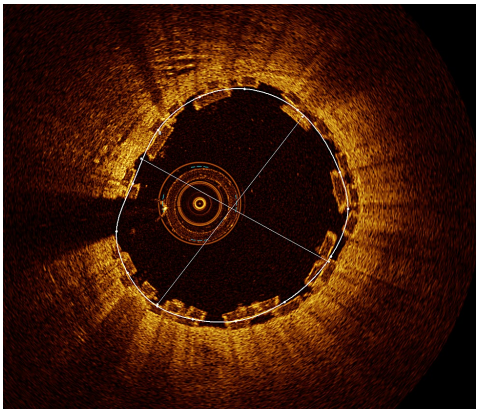

Fig. 2 BRS malapposition. OCT cross section showing six malapposed BRS struts

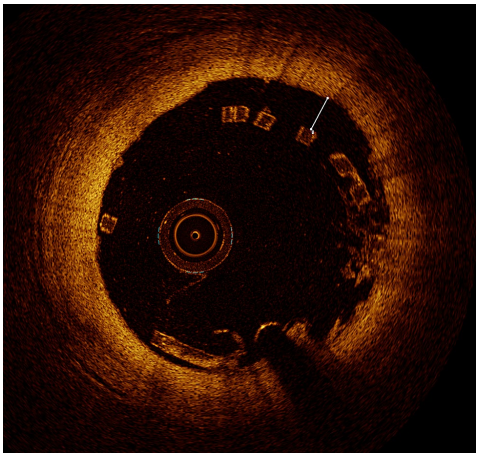

Fig. 3 Distance of malapposition. This figure shows a malapposed DESolve BRS with six malapposed struts. The malapposition distance is marked as maximum orthogonal distance between outer BRS strut and vessel wall (*white mark*)

- Proximal edge dissection (Yes/No): visible flap within 5 mm proximal of BRS.
- Distal edge dissection (Yes/No): visible flap within 5 mm distal of BRS.
- Bifurcation (Yes/No).

The following parameters were calculated (adopted from [12, 13]:

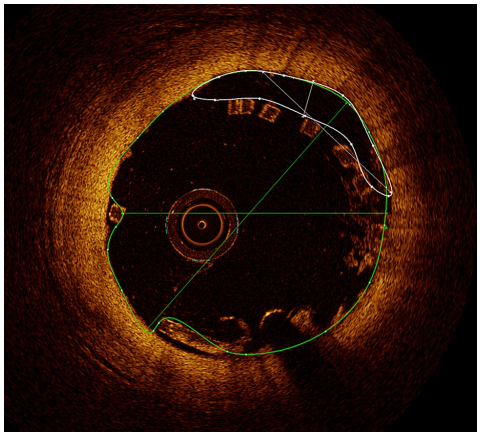

Fig. 4 Incomplete scaffold apposition area. Malapposed DESolve BRS with contoured lumen profile (*green mark*) and incomplete scaffold apposition area (*green mark*) (color figure online)

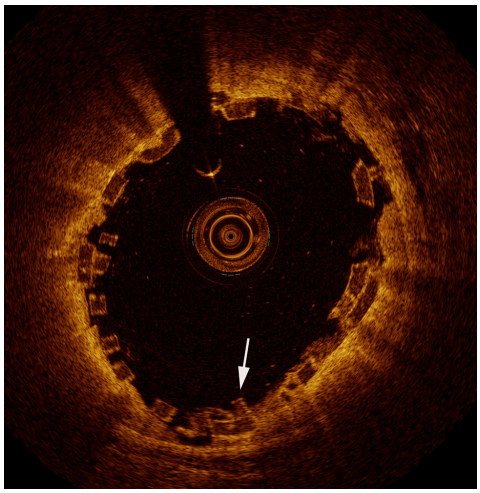

Fig. 5 Strut fracture. A strut fractures located in an overlap segment of two DESolve BRS is visible (*white arrow*). On the *left side* of the broken strut, no coating polymer is visible

- Increment = (proximal lumen reference area – distal lumen reference area)/length (mm).
- Reference area (mm^2) = distal lumen reference area + (x × Increment) x = distance between distal end of BRS and actual cross section in mm.
- In-scaffold residual area stenosis (%) = 100 − (Lumen area/Reference area) × 100 calculated for each cross section.
- Incomplete strut apposition (ISA) (%) = (number of malapposed struts per cross section/total number of visible struts per cross section) × 100.
- Eccentricity index = (minimum scaffold diameter/maximum scaffold diameter); calculated for each cross section analyzed.
- Mean lumen area.
- Minimal lumen area.

Follow-up

Clinical follow-up was obtained at 1, 6 and 12 months using a standardized protocol by direct clinical examination or by phone.

Statistical analysis

Continuous variables were summarized as mean ± standard deviation; categorical variables are quoted as n (%).Test for binomial distribution was used to measure deviations of expected frequencies. Kolmogorov–Smirnov test was performed to test for parametric distribution. To test for statistical differences between two groups for comparison of continuous variables either t test for unpaired samples (parametric distribution) or Mann–Whitney U test (non-parametric distribution) was performed. For categorical variables, Chi-square or Fischer exact tests were carried out to test for significant differences. Statistical analysis was performed using SPSS version 21.0 (IBM SPSS Statistics, IBM Corporation, Armonk, New York, USA) and a two-sided $p < 0.05$ was considered significant.

Results

Patients and procedure

A total of 38 patients (26 male, 12 female) were included. 23 patients received one novolimus-eluting BRS for treating a single native lesion, 15 patients with 17 native lesions were treated with two overlapping novolimus-eluting BRS. In two cases, overlapping implantation was performed to cover two sequential lesions. In four cases, proximal BRS diameter was 0.5 mm larger than the diameter of the distal scaffold. Except for lesion length, which was significantly larger in the overlap group (16.8 ± 5.9 vs. 10.8 ± 5.2 mm; $p < 0.001$), no significant differences regarding baseline characteristics existed between the groups. Most patients presented with stable angina (no overlap: 52%, overlap: 60%). Pre-procedural OCT was performed in 27 patients

[control group: 15 patients (65%) vs. overlap group: 12 patients (80%); $p = 0.46$], additional intra-procedural OCT was performed in 9 patients [control group: 5 patients (22%) vs. overlap group: 4 patients (27%); $p = 0.46$]. Predilatation was conducted in all cases and the length of the NC balloon applied was significantly larger in the overlap group as compared to the control group (14 ± 3 mm vs. 16 ± 3 mm; $p = 0.007$). A cutting balloon was used for lesion preparation in three cases [control group: 2 patients (9%) vs. overlap group: 1 patient (7%); $p = 0.93$]. NC balloon post-dilatation was performed in all cases, mean pressure was 17 bar. Mean BRS diameter was significantly smaller than the diameter of the NC balloon for post-dilatation (3.2 ± 0.3 vs. 3.6 ± 0.6 mm; $p < 0.001$). For detailed information regarding baseline characteristics and procedural data see Table 1.

OCT findings

Total BRS length was significantly longer in the overlap group as compared to the control group (36 ± 6 vs. 20 ± 6 mm; $p < 0.001$) and the mean overlap length determined by OCT was 3.8 ± 2.9 mm. Mean lumen area (overlap group: 7.70 ± 2.55 mm^2 vs. control group: 7.36 ± 2.16 mm^2; $p = 0.79$) and mean residual in-scaffold area stenosis (overlap group: 10.0 ± 6.8% vs. control group: 11.5 ± 10.1%; $p = 0.70$) were not different between lesions treated with and without overlapping BRS. Furthermore, there were no significant differences in terms of minimal lumen area, incomplete scaffold apposition area (ISAA), ISA, tissue prolapse area, sum of malapposed struts and stent diameters. There was a trend towards higher eccentricity in the control group compared to the overlap group (0.77 ± 0.07 vs. 0.81 ± 0.03; $p = 0.07$). The frequency of strut fractures (mean number of visible strut fractures per cross section along the entire scaffold length) was higher in cases of overlapping implantation, even though the difference failed to reach statistical significance (overlap group: 0.36 ± 0.49 vs. control group: 0.02 ± 0.08; $p = 0.09$) (for detailed results see Table 2).

OCT findings within novolimus-eluting BRS implanted with overlap

Mean and minimal lumen area was not smaller in the overlapping segment as compared to the BRS segments without overlap (mean lumen area overlap: 8.16 ± 2.97 mm^2 vs. no overlap: 7.70 ± 2.55 mm^2; $p = 0.71$; minimal lumen area overlap: 6.83 ± 2.71 mm^2 vs. no overlap: 6.17 ± 2.58 mm^2; $p = 0.37$). Due to the double stent layer, the maximum distance between the inner strut edge to the vessel wall was significantly higher in the overlap area compared to the BRS area with single layer (349 ± 27 vs. 182 ± 21 µm; $p < 0.001$; see Table 3) Additionally, there were no significant differences between the overlap and the adjacent scaffold area (3 mm proximal and distal to the overlap area; see Table 4).

Clinical follow-up

Median follow-up time was 9 months. One patient (3%) out of the overlap group was lost to follow-up. One rehospitalization in the overlap group was observed. The patient presented with atypical thoracic complaints. Coronary angiography revealed no progress of coronary artery disease. No events were observed in the control group.

Discussion

The main finding of this study is that overlapping implantation of novolimus-eluting BRS does not result in a reduced luminal area. Much rather the double strut layer seems to be compensated for by outward overexpansion of the vessel. Hence, we were able to confirm in atherosclerotic coronary artery lesions what Farooq et al. [14] observed after implantation of overlapping everolimus-eluting BRS in porcine coronary arteries. The "overexpansion" capabilities of the DESolve novolimus-eluting BRS [15] may be advantageous in this context. In fact, a double strut layer may increase radial force and may to some extent prevent recoil. At the same time, neither was disintegrity of the BRS observed significantly more frequently, nor was vessel wall injury (dissection) observed more often in lesions treated with overlapping BRS. However, it has to be kept in mind that overlap areas in most cases will be located outside the most severely obstructed and calcified parts of a lesion by intention of the operator.

Clinical implications

Although clinical safety and efficacy of everolimus-eluting BRS have been reported to be comparable with those of second-generation DES [6, 13], a non-negligible rate of BRS thrombosis occurs and several authors have hypothesized that BRS overlap may contribute to a higher risk of scaffold thrombosis, especially because of large lumen loss due to the double layer of BRS struts [16–18]. Accordingly, trying to minimize BRS overlap length is widely recommended and standard in clinical practice [14, 19, 20].

On the one hand, data from Ishibashi et al. suggest that overlapping implantation of BRS is an independent risk factor for peri-procedural myocardial infarction [21]. On the other hand, Ortega-Paz et al. recently reported in a retrospective analysis that there were no significant differences in 1-year clinical outcome if comparing overlap

Table 1 Baseline characteristics

	BRS without overlap	BRS with overlap	*p* value
Number of patients	23	15	0.26
Number of scaffolds	23	30	0.41
Number of treated lesions	23	15	0.26
Age (years)	62 ± 9	62 ± 10	0.86
Male gender	19 (83%)	7 (47%)	0.14
BMI† (kg/m^2)	25.6 ± 10.8	28.0 ± 3.8	0.84
Previous MI# (%)	5 (22%)	6 (40%)	0.36
Previous PCI†† (%)	7 (30%)	8 (53%)	0.25
Previous CABG§ (%)	2 (9%)	1 (7)	0.93
LVEF¶ (%)	57 ± 10	55 ± 11	0.62
Presentation			
STEMI	5 (22%)	2 (13%)	0.63
NSTEMI	3 (13%)	1 (7%)	
Unstable AP*	2 (9%)	3 (20%)	
Stable AP*	12 (52%)	9 (60%)	
No complaints/atypical complaints	1 (4%)	0 (0%)	
Vessel			
LAD‖	12 (52%)	3 (20%)	0.09
Cx‡	4 (17%)	4 (27%)	
RCA‡‡	7 (31%)	8 (53%)	
Lesion length (mm)	10.8 ± 5.2	16.8 ± 5.9	<0.001
NC** pre-dilatation			
Performed (%)	100	100	>0.99
Cutting balloon (%)	2 (9%)	1 (7%)	0.93
Pressure (bar)	14 ± 4	15 ± 4	0.59
Diameter (mm)	3.1 ± 0.4	2.9 ± 0.4	0.36
Length (mm)	14 ± 3	16 ± 3	0.007
Scaffold			
Diameter (mm)	3.2 ± 0.3	3.2 ± 0.3	0.43
Length (mm)	20 ± 6	20 ± 6	0.94
Implantation pressure (bar)	14 ± 3	13 ± 2	0.17
NC** post-dilatation			
Performed (%)	100	100	>0.99
Diameter (mm)	3.7 ± 0.6	3.4 ± 0.5	0.12
Pressure (bar)	17 ± 4	17 ± 6	0.22

Values are mean ± standard deviation or *n* (%)

* Angina pectoris

† Body mass index

‡ Circumflex artery

§ Coronary artery bypass graft surgery

‖ Left anterior descending artery

¶ Left ventricular ejection fraction

Myocardial infarction

** Non-compliant balloon

†† Percutaneous coronary intervention

‡‡ Right coronary artery

and non-overlap everolimus-eluting BRS [22]. In fact, we found no mechanical or geometric differences in novolimus-eluting BRS overlap areas that might be responsible for a higher event rate. Especially, there were no significant differences regarding lumen area, stent diameter, residual area stenosis, eccentricity, malapposition and rate of strut

Table 2 OCT findings

	BRS without overlap ($n = 23$)	BRS with overlap ($n = 15$)	p value
Total BRS length (mm)	20 ± 6	36 ± 6	<0.001
Overlap length (mm)		3.8 ± 2.9	
OCT scaffold area (mm^2)	7.57 ± 2.18	7.90 ± 2.41	0.72
Residual area stenosis (%)	11.5 ± 10.1	10.0 ± 6.8	0.70
Reference area (mm^2)	7.95 ± 2.79	8.02 ± 2.49	0.88
Mean lumen area (mm^2)	7.36 ± 2.16	7.70 ± 2.55	0.79
Minimal lumen area (mm^2)	5.77 ± 1.72	6.41 ± 2.63	0.71
OCT ISAA[†] (mm^2)	0.83 ± 1.85	1.62 ± 3.25	0.72
OCT tissue prolapse area (mm^2)	7.74 ± 9.53	7.41 ± 8.68	0.95
Sum of malapposed struts (n)	5 ± 11	7 ± 13	0.72
Sum of struts (n)	246 ± 77	234 ± 85	0.72
ISA* (%)	0.03 ± 0.08	0.04 ± 0.07	0.79
Distance of malapposition[‡] (mm)	0.18 ± 0.20	0.27 ± 0.32	0.58
Mean stent diameter (mm)	3.06 ± 0.42	3.03 ± 0.37	0.70
Minimum stent diameter (mm)	2.68 ± 0.38	2.71 ± 0.31	0.29
Maximum stent diameter (mm)	3.50 ± 0.51	3.38 ± 0.44	0.88
Minimum eccentricity index	0.61 ± 0.11	0.66 ± 0.06	0.08
Overlapping	0	3.33 ± 2.23	<0.001
Fracture	0.02 ± 0.08	0.36 ± 0.49	0.09
Bifurcation	0.96 ± 10.95	0.42 ± 0.67	0.20
Mean eccentricity index	0.77 ± 0.07	0.81 ± 0.03	0.07
Proximal edge dissection	0	0	>0.99
Distal edge dissection	0	1	0.87

Values are mean ± standard deviation

* Incomplete strut apposition (ratio number of malapposed struts per BRS to total number of struts per BRS)

[†] Incomplete scaffold apposition area

[‡] Orthogonal distance between malapposed scaffold and vessel wall

Table 3 OCT findings inside BRS with overlap

	Area without overlap	Overlap area	p value
Minimal lumen area (mm^2)	6.17 ± 2.58	6.83 ± 2.71	0.37
Location of minimal lumen area	11 (73%)	4 (27%)	0.12
Fracture	0.28 ± 0.44	0.40 ± 0.31	0.33
Maximum distance inner strut edge to vessel wall (μm)	182 ± 21	349 ± 27	<0.001
Residual area stenosis (%)	10.56 ± 6.63	9.31 ± 5.28	0.60
Mean lumen area (mm^2)	7.70 ± 2.55	8.16 ± 2.97	0.71

Values are mean ± standard deviation or n (%)

Table 4 OCT findings: comparison of overlap and adjacent area (3 mm on each side)

	Adjacent area	Overlap area	p value
Minimal lumen area (mm^2)	6.62 ± 2.44	6.83 ± 2.71	0.54
Fracture	0.48 ± 0.38	0.40 ± 0.31	0.58
Residual area stenosis (%)	10.26 ± 5.81	9.31 ± 5.28	0.67
Mean lumen area (mm^2)	7.68 ± 3.11	8.16 ± 2.97	0.47

Values are mean ± standard deviation or n (%)

fractures when comparing BRS implanted with overlap to those without. Nevertheless, due to the longer distance between the vessel wall and the inner struts in overlap areas, endothelialization of these struts will hardly be sufficient leading to an increased risk for an impaired clinical outcome [14, 22]. One aspect we could not analyze in our study was the presence of turbulent flow or shear stress which may be increased in areas with particularly inhomogeneous surface patterns caused by thick BRS struts [23, 24]. Especially the double scaffold layer in overlap

segments can possibly interrupt laminar flow. This might be an explanation for the higher frequency of scaffold thrombosis if overlapping implantation of BRS is performed [21].

Our results suggest that overlapping implantation of BRS can be safely performed in terms of acute mechanical outcome. Nevertheless, reliable data regarding long-term clinical outcome after overlapping implantation of BRS are very limited so far. Hence, randomized controlled studies on long-term clinical outcome are required to analyze the effect of overlap implantation of BRS. Additionally, we have to mention that results for everolimus-eluting BRS are not completely adaptable to novolimus-eluting BRS since mechanical specifications are somewhat different. It has to be kept in mind that effects of overlap might be influenced by overlap length. However, the number of analyzed cases for this study was too low to perform a reliable sub-analysis for effect of different overlap lengths.

Limitations

This was a single-center, non-randomized retrospective observational analysis with all its limitations. Clearly there may be bias in lesion selection. However, OCT was preferentially used in complex lesions so that even more benign effects of overlapping BRS implantation should be expected in less complex lesion subsets. It has to be emphasized that BRS implantation was performed carefully, with thorough lesion preparation and mandatory post-dilatation using appropriately sized NC balloons, so that results may not be comparable when less standardized implantation protocols are used. Finally, patient numbers were small, and the lack of observed differences may be attributable to a lack of statistical power. Especially the systematic evaluation of clinical outcome would require substantially larger patient numbers.

Conclusion

Acute mechanical performance of novolimus-eluting BRS is not impaired by overlapping implantation. In particular, overlapping BRS segments do not display a smaller lumen area as compared to segments with a single layer. This would suggest that overlap implantation can be safely performed, but long-term clinical outcome remains to be investigated in future trials.

Compliance with ethical standards

Conflict of interest Holger Nef received speaking honoraria and a research grant (to institution) from Elixir Medical. All other authors have no potential conflict of interest. There are no relationships with industry regarding this study.

References

1. Kereiakes DJ, Wang H, Popma JJ, Kuntz RE, Donohoe DJ, Schofer J, Schampaert E, Meier B, Leon MB, Moses JW (2006) Periprocedural and late consequences of overlapping Cypher sirolimus-eluting stents: pooled analysis of five clinical trials. J Am Coll Cardiol 48:21–31
2. O'Sullivan CJ, Stefanini GG, Räber L, Heg D, Taniwaki M, Kalesan B, Pilgrim T, Zanchin T, Moschovitis A, Büllesfeld L, Khattab AA, Meier B, Wenaweser P, Jüni P, Windecker S (2014) Impact of stent overlap on long-term clinical outcomes in patients treated with newer-generation drug-eluting stents. EuroIntervention 9:1076–1084
3. Räber L, Jüni P, Löffel L, Wandel S, Cook S, Wenaweser P, Togni M, Vogel R, Seiler C, Eberli F, Lüscher T, Meier B, Windecker S (2010) Impact of stent overlap on angiographic and long-term clinical outcome in patients undergoing drug-eluting stent implantation. J Am Coll Cardiol 55:1178–1188
4. Farooq V, Vranckx P, Mauri L, Cutlip DE, Belardi J, Silber S, Widimsky P, Leon M, Windecker S, Meredith I, Negoita M, van Leeuwen F, Neumann FJ, Yeung AC, Garcia-Garcia HM, Serruys PW (2013) Impact of overlapping newer generation drug-eluting stents on clinical and angiographic outcomes: pooled analysis of five trials from the international Global RESOLUTE Program. Heart 99:626–633
5. Kimura T, Kozuma K, Tanabe K, Nakamura S, Yamane M, Muramatsu T, Saito S, Yajima J, Hagiwara N, Mitsudo K, Popma JJ, Serruys PW, Onuma Y, Ying S, Cao S, Staehr P, Cheong WF, Kusano H, Stone GW, Japan Investigators ABSORB (2015) A randomized trial evaluating everolimus-eluting Absorb bioresorbable scaffolds vs. everolimus-eluting metallic stents in patients with coronary artery disease: ABSORB Japan. Eur Heart J 36:3332–3342
6. Serruys PW, Chevalier B, Dudek D, Cequier A, Carrié D, Iniguez A, Dominici M, van der Schaaf RJ, Haude M, Wasungu L, Veldhof S, Peng L, Staehr P, Grundeken MJ, Ishibashi Y, Garcia-Garcia HM, Onuma Y (2015) A bioresorbable everolimus-eluting scaffold versus a metallic everolimus-eluting stent for ischaemic heart disease caused by de-novo native coronary artery lesions (ABSORB II): an interim 1-year analysis of clinical and procedural secondary outcomes from a randomised controlled trial. Lancet 385:43–54
7. Sabaté M, Windecker S, Iñiguez A, Okkels-Jensen L, Cequier A, Brugaletta S, Hofma SH, Räber L, Christiansen EH, Suttorp M, Pilgrim T, Anne van Es G, Sotomi Y, García-García HM, Onuma Y, Serruys PW (2016) Everolimus-eluting bioresorbable stent vs. durable polymer everolimus-eluting metallic stent in patients with ST-segment elevation myocardial infarction: results of the randomized ABSORB ST-segment elevation myocardial infarction-TROFI II trial. Eur Heart J 37:229–240
8. Dörr O, Liebetrau C, Wiebe J, Hecker F, Rixe J, Möllmann H, Hamm C, Nef H (2015) Bioresorbable scaffolds for the treatment of in-stent restenosis. Heart Vessels 30:265–269
9. Toušek P, Kočka V, Malý M, Lisa L, Buděšínský T, Widimský P (2016) Neointimal coverage and late apposition of everolimus-eluting bioresorbable scaffolds implanted in the acute phase of myocardial infarction: OCT data from the PRAGUE-19 study. Heart Vessels 31:841–845
10. Ishibashi Y, Nakatani S, Sotomi Y, Suwannasom P, Grundeken MJ, Garcia-Garcia HM, Bartorelli AL, Whitbourn R, Chevalier B, Abizaid A, Ormiston JA, Rapoza RJ, Veldhof S, Onuma Y, Serruys PW (2015) Relation between bioresorbable scaffold sizing using QCA-Dmax and clinical outcomes at 1 year in 1,232 patients from 3 study cohorts (ABSORB Cohort B,

ABSORB EXTEND, and ABSORB II). JACC Cardiovasc Interv 8:1715–1726
11. Serruys PW, Onuma Y, Ormiston JA, de Bruyne B, Regar E, Dudek D, Thuesen L, Smits PC, Chevalier B, McClean D, Koolen J, Windecker S, Whitbourn R, Meredith I, Dorange C, Veldhof S, Miquel-Hebert K, Rapoza R, García-García HM (2010) Evaluation of the second generation of a bioresorbable everolimus drug-eluting vascular scaffold for treatment of de novo coronary artery stenosis: six-month clinical and imaging outcomes. Circulation 122:2301–2312
12. Mattesini A, Boeder N, Löblich K, Valente S, Foin N, Caiazzo G, Ghione M, Gensini GF, Italo P, Di Mario C, Nef H (2016) Absorb Vs DESolve: an optical coherence tomography comparison of acute mechanical performances. EuroIntervention 12:566–573
13. Mattesini A, Secco GG, Dall'Ara G, Ghione M, Rama-Merchan JC, Lupi A, Viceconte N, Lindsay AC, De Silva R, Foin N, Naganuma T, Valente S, Colombo A, Di Mario C (2014) ABSORB biodegradable stents versus second-generation metal stents: a comparison study of 100 complex lesions treated under OCT guidance. JACC Cardiovasc Interv 7:741–750
14. Farooq V, Serruys PW, Heo JH, Gogas BD, Onuma Y, Perkins LE, Diletti R, Radu MD, Räber L, Bourantas CV, Zhang Y, van Remortel E, Pawar R, Rapoza RJ, Powers JC, van Beusekom HM, Garcìa-Garcìa HM, Virmani R (2013) Intracoronary optical coherence tomography and histology of overlapping everolimus-eluting bioresorbable vascular scaffolds in a porcine coronary artery model: the potential implications for clinical practice. JACC Cardiovasc Interv 6:523–532
15. Verheye S, Ormiston JA, Stewart J, Webster M, Sanidas E, Costa R, Costa JR Jr, Chamie D, Abizaid AS, Pinto I, Morrison L, Toyloy S, Bhat V, Yan J, Abizaid A (2014) A next-generation bioresorbable coronary scaffold system: from bench to first clinical evaluation: 6- and 12-month clinical and multimodality imaging results. JACC Cardiovasc Interv 7:89–99
16. Everaert B, Felix C, Koolen J, den Heijer P, Henriques J, Wykrzykowska J, van der Schaaf R, de Smet B, Hofma S, Diletti R, Van Mieghem N, Regar E, Smits P, van Geuns RJ (2015) Appropriate use of bioresorbable vascular scaffolds in percutaneous coronary interventions: a recommendation from experienced users: a position statement on the use of bioresorbable vascular scaffolds in the Netherlands. Neth Heart J 23:161–165
17. Tamburino C, Latib A, van Geuns RJ, Sabate M, Mehilli J, Gori T, Achenbach S, Alvarez MP, Nef H, Lesiak M, Di Mario C, Colombo A, Naber CK, Caramanno G, Capranzano P, Brugaletta S, Geraci S, Araszkiewicz A, Mattesini A, Pyxaras SA, Rzeszutko L, Depukat R, Diletti R, Boone E, Capodanno D, Dudek D (2015) Contemporary practice and technical aspects in coronary intervention with bioresorbable scaffolds: a European perspective. EuroIntervention 11:45–52
18. Wiebe J, Nef HM, Hamm CW (2014) Current status of bioresorbable scaffolds in the treatment of coronary artery disease. J Am Coll Cardiol 64:2541–2551B
19. Biscaglia S, Secco GG, Tumscitz C, Di Mario C, Campo G (2015) Optical coherence tomography evaluation of overlapping everolimus-eluting bioresorbable vascular scaffold implantation guided by enhanced stent visualization system. Int J Cardiol 182:1–3
20. Biscaglia S, Campo G, Tebaldi M, Tumscitz C, Pavasini R, Fileti L, Secco GG, Di Mario C, Ferrari R (2016) Bioresorbable vascular scaffold overlap evaluation with optical coherence tomography after implantation with or without enhanced stent visualization system (WOLFIE study): a two-centre prospective comparison. Int J Cardiovasc Imaging 32:211–223
21. Ishibashi Y, Muramatsu T, Nakatani S, Sotomi Y, Suwannasom P, Grundeken MJ, Cho YK, Garcia-Garcia HM, van Boven AJ, Piek JJ, Sabaté M, Helqvist S, Baumbach A, McClean D, de Sousa Almeida M, Wasungu L, Miquel-Hebert K, Dudek D, Chevalier B, Onuma Y, Serruys PW (2015) Incidence and potential mechanism(s) of post-procedural rise of cardiac biomarker in patients with coronary artery narrowing after implantation of an everolimus-eluting bioresorbable vascular scaffold or everolimus-eluting metallic stent. JACC Cardiovasc Interv 8:1053–1063
22. Ortega-Paz L, Capodanno D, Giacchi G, Gori T, Nef H, Latib A, Caramanno G, Di Mario C, Naber C, Lesiak M, Capranzano P, Wiebe J, Mehilli J, Araszkiewicz A, Pyxaras S, Mattesini A, Geraci S, Naganuma T, Colombo A, Münzel T, Sabaté M, Tamburino C, Brugaletta S (2016) Impact of overlapping on 1-year clinical outcomes in patients undergoing everolimus-eluting bioresorbable scaffolds implantation in routine clinical practice: Insights from the European multicenter GHOST-EU registry. Catheter Cardiovasc Interv. doi:10.1002/ccd.26674. **[Epub ahead of print]**
23. Bourantas CV, Papafaklis MI, Kotsia A, Farooq V, Muramatsu T, Gomez-Lara J, Zhang YJ, Iqbal J, Kalatzis FG, Naka KK, Fotiadis DI, Dorange C, Wang J, Rapoza R, Garcia-Garcia HM, Onuma Y, Michalis LK, Serruys PW (2014) Effect of the endothelial shear stress patterns on neointimal proliferation following drug-eluting bioresorbable vascular scaffold implantation: an optical coherence tomography study. JACC Cardiovasc Interv 7:315–324
24. Bourantas CV, Papafaklis MI, Lakkas L, Sakellarios A, Onuma Y, Zhang YJ, Muramatsu T, Diletti R, Bizopoulos P, Kalatzis F, Naka KK, Fotiadis DI, Wang J, Garcia Garcia HM, Kimura T, Michalis LK, Serruys PW (2014) Fusion of optical coherence tomographic and angiographic data for more accurate evaluation of the endothelial shear stress patterns and neointimal distribution after bioresorbable scaffold implantation: comparison with intravascular ultrasound-derived reconstructions. Int J Cardiovasc Imaging 30:485–494

Nr. 4: OCT-assessment of scaffold resorption: Analysis of strut intensity by a new resorption index for poly-L-lactic acid bioresorbable vascular scaffolds

Received: 20 November 2018 | Revised: 9 February 2019 | Accepted: 23 March 2019
DOI: 10.1002/ccd.28223

WILEY

ORIGINAL STUDIES

OCT-assessment of scaffold resorption: Analysis of strut intensity by a new resorption index for poly-L-lactic acid bioresorbable vascular scaffolds

Florian Blachutzik[1,2] | Stephan Achenbach[1] | Mohamed Marwan[1] | Monique Tröbs[1] | Niklas Boeder[2] | Oliver Doerr[2] | Melissa Weissner[3,4] | Timm Bauer[2] | Holger Nef[2] | Christian Hamm[2] | Christian Schlundt[1]

[1]Department of Cardiology, Friedrich-Alexander Universität (FAU) Erlangen-Nürnberg, University Hospital Erlangen, Erlangen, Germany

[2]Department of Cardiology, Justus-Liebig University Giessen, Giessen, Germany

[3]Zentrum für Kardiologie, University Hospital Mainz, Mainz, Germany

[4]German Center for Cardiac and Vascular Research (DZHK), Mainz, Germany

Correspondence
Florian Blachutzik, University of Giessen – Department of Cardiology and Angiology, Klinikstrasse 33, 35392 Giessen, Germany.
Email: florian.blachutzik@innere.med.uni-giessen.de

Abstract

Background: The aim of this study was to analyze individual differences in resorption of bioresorbable vascular scaffolds (BRS) through optical coherence tomography (OCT) analysis and to identify factors potentially influencing the resorption process.

Methods: Between April 2016 and July 2017 clinically driven invasive coronary angiography and OCT examinations were performed in 36 patients who had previously been treated with a total of 48 BRS (ABSORB BVS, Abbott Vascular, Santa Clara, CA). For each scaffold, a new BRS-RESORB-INDEX (BRI) was calculated.

Results: The mean time interval since implantation was 789 ± 321 days. In OCT, BRS struts remained detectable in all 48 BRS. Normalized light intensity as a marker for the resorption of BRS struts increased with time in a linear fashion (Spearman Rho: $p < .001$, correlation coefficient = .90; R^2 [linear] = .91). Multivariable analysis identified diabetes (BRI of patients with diabetes vs. patients without diabetes: 0.34 ± 0.13 vs. 0.58 ± 0.22; $p = .002$) and presence of Peri-strut low intensity areas (PSLIA, BRI of 10 patients with PSLIA vs. 26 patients without PSLIA: 0.44 ± 0.21 vs. 0.61 ± 18; $p = .027$) as independent predictors for a prolonged BRS resorption, whereas the resorption rate in ACS patients (STEMI, NSTEMI, and unstable angina; $n = 13$) was significantly higher as compared to patients without ACS (0.62 ± 0.17 vs. 0.43 ± 0.24; $p = .012$).

Conclusion: In humans, BRS resorption rate is significantly influenced by numerous factors. Our data suggest that diabetes and PSLIA are associated with a prolonged resorption process, whereas in ACS patients, BRS resorption appears to be significantly faster.

KEYWORDS
bioresorbable vascular scaffolds, optical coherence tomography, percutaneous coronary intervention

Abbreviations: BMI, body-mass index; BRI, BRS-RESORB-INDEX; BRS, bioresorbable vascular scaffolds; DES, drug-eluting stent; NC balloon, noncompliant balloon; NLI, normalized light intensity; NSTEMI, non-ST-segment elevation myocardial infarction; OCT, optical coherence tomography; PCI, percutaneous coronary intervention; PLLA, poly-L-lactic acid; PTCA, percutaneous transluminal coronary angioplasty.

1 | INTRODUCTION

Bioresorbable vascular scaffolds (BRS) have been developed to overcome some disadvantages of permanent metallic coronary stents, such as the risk of target lesion revascularization, neoatherosclerosis, and indefinite impairment of vasomotion. So far, the most commonly used BRS are the Absorb BVS™ (Abbott Vascular, Santa Clara, CA) and the DESolve™ (Elixir Medical Corporation, Sunnyvale, CA).[1,2] Both of these devices have a poly-L-lactic acid polymeric structure. The best studied BRS is the Absorb BVS™ with several randomized controlled studies and registries published as well as >100,000 patients treated.[2] It had initially been assumed that this device would be completely resorbed after about 2 years,[1,2] but recent data demonstrated that complete resorption and cellularization requires about 4–5 years.[2–5] The latest data from randomized controlled studies have raised concerns about the safety of BRS, with a higher rate of device thrombosis and target lesion failure when compared to second-generation Drug-eluting stents (DES).[6,7] The timing and homogeneity of the resorption process may be an important factor for events following BRS implantation. Former studies showed that acute scaffold thrombosis correlates well with procedural problems during implantation. However, the reason for very late scaffold thrombosis is questionable. Whether dismantling or different resorption processes might be responsible has to be elucidated. Thus, it was the aim of this study to analyze interindividual differences in BRS resorption and to identify factors potentially influencing the resorption process through optical coherence tomography (OCT) analysis.

2 | MATERIALS AND METHODS

2.1 | Study design and population

We collected the data of all patients who underwent coronary angiography between April 2016 and July 2017 for clinical reasons and who had undergone prior percutaneous coronary intervention (PCI) with implantation of at least one Absorb BVS™. Intravascular imaging using OCT is mandatory per institutional protocol when patients represent after previous BRS implantation.

Baseline patient characteristics, including medical history as well as clinical, angiographic, and procedural data, were collected from the department's database.

2.2 | Percutaneous coronary intervention

Baseline PCI with implantation of a BRS had been performed via transradial or transfemoral approach using six French guiding catheters and standard coronary guidewires (Runthrough™, Terumo Europe NV, Leuven, Belgium). All patients had received intravenous heparin and intracoronary nitrates. Predilatation with a noncompliant balloon (NC balloon) had been performed in all lesions, with balloon size selected based on visual angiographic estimation to achieve a 1:1 ratio of vessel and balloon diameter. Lesions had been treated with everolimus-eluting BRS (Absorb BVS™, Abbott Vascular, Santa Clara, CA). Deployment of Absorb BVS™ had been performed with an initial pressure of 2 bar and increasing pressure in increments of 2 bar every 10 s until fully deployed (minimum 8 bar). NC balloon (NC Trek™, Abbott Vascular, Santa Clara, CA) postdilatation at a pressure of 16 bar was mandatory per institutional protocol and had been performed in all lesions. Further medication, techniques, and equipment for PCI were used in accordance with current clinical guidelines and were left to the responsible physician's discretion.

2.3 | OCT image acquisition

At follow-up, OCT was performed as part of the diagnostic angiogram and before any PCI. A 2.7 French Dragonfly™ intravascular imaging catheter (St. Jude Medical, Saint Paul, MN) was used with a mechanical pullback speed of 18 mm/s over a distance of 54 mm. During pullback, 25 mL contrast agent (Ultravist™ 370, Bayer AG, Leverkusen, Germany) were injected at 4 mL/s with a maximum pressure of 400 psi using machine injection (Liebel-Flarsheim 903300 G, Liebel-Flarsheim Co, Cincinnati, OH).

2.4 | OCT image analysis

All OCT data sets were digitally recorded, stored, and analyzed. OCT image analysis was performed offline using QCU-CMS v4.69 OCT analysis software (Leiden University Medical Center, Leiden, Netherlands). Strut fractures were defined as struts lying isolated in the lumen or the presence of one strut on top of another. OCT analysis was performed in accordance with previous publications.[8,9] The light intensity of each BRS strut was defined as number of color pixels per strut which were measured using ImageJ 1.51j8 (National Institutes of Health). Afterwards, BRS strut light intensity was normalized for the light intensity in an equally sized area of the surrounding intima to eliminate intensity fluctuations (see Figure 1). Normalized light intensity (NLI) per strut was calculated as:

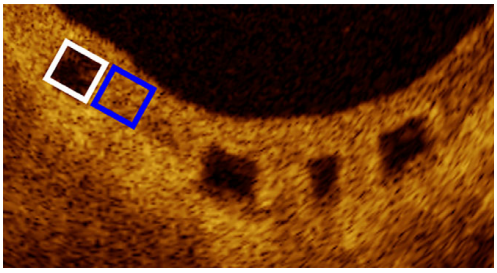

FIGURE 1 Measurement of normalized light intensity. Four struts of an Absorb BVS™ are visible. Normalized light intensity of the left strut is calculated as number of color pixels of the strut (white rectangle) divided by number of color pixels of an equivalent area in the intima (blue rectangle). The equivalent area is always selected directly adjacent to the strut [Color figure can be viewed at wileyonlinelibrary.com]

$$\frac{\text{Number of color pixels per BRS strut}}{\text{Number of color pixels per equivalent area in the adjacent intima}}.$$

Equal light intensity to the surrounding intima is the assumed endpoint of BRS resorption. Hence, if the scaffold was resorbed and the former volume completely cellularized, its light intensity would be equivalent to the surrounding intima. NLI per BRS was calculated as:

$$\frac{\sum \text{Number of color pixels per BRS strut}}{\text{Number of struts per BRS}}.$$

The BRS-RESORB-INDEX (BRI) as a marker for the speed of scaffold resorption was calculated as:

$$\frac{\text{Normalized light intensity} \times 1000}{\text{Time since BRS implantation (days)}}.$$

2.5 | Statistical analysis

Continuous variables are summarized as mean ± *SD*; categorical variables are provided as *n* (%). The Kolmogorov–Smirnov test was performed to test for nonparametric distribution. The Pearson correlation coefficient was calculated to test for linear relationships. To test for statistical differences between two groups for comparison of continuous variables, either a *t* test for unpaired samples (parametric distribution) or a Mann–Whitney-*U* test (nonparametric distribution) was used. To analyze the relevant factors, influencing the BRI, multivariable regression analysis was performed per scaffold, including all covariates with a $p < .2$ in univariable analysis. Statistical analyses were performed using SPSS version 21.0 (IBM SPSS Statistics, IBM Corporation, Armonk, NY). A two-sided $p < .05$ was considered significant.

3 | RESULTS

3.1 | Baseline data

Between April 2016 and July 2017, 36 patients with previous implantation of a total of 48 BRS presented at our department because of clinically suspected progression of coronary artery disease. The mean time interval since BRS implantation was 789 ± 321 days, with a minimum of 89 and a maximum of 1,293 days. The index procedure with initial BRS implantation had been performed because of stable angina in 23 patients (64%) and because of acute coronary syndrome (STEMI, NSTEMI, unstable angina) in 13 patients (36%). For detailed patient characteristics see Table 1. Procedural data of the initial BRS implantation are summarized in Table 2. All BRS had been implanted according to manufacturer recommendations and pertinent guidelines. Appropriate predilatation and postdilatation with noncompliant balloons had been performed in all lesions.

3.2 | Clinical presentation

Stable angina was the most common reason for patient presentation at our department after previous BRS implantation (35 of 36 patients).

TABLE 1 Patient characteristics

Patients	36
Scaffolds	48
Lesions	39
Time since scaffold implantation (days)	789 ± 321
Age (years)	66 ± 10
BMI (kg/m^2)	25.8 ± 7.1
Male gender	25 (69%)
Previous CABG	4 (11%)
Previous PCI	12 (33%)
Hypertension	29 (81%)
Diabetes	12 (33%)
Hyperlipidemia	25 (69%)
Active smoking	6 (17%)
Family history for coronary artery disease	14 (39%)
Left ventricular ejection fraction (%)	52 ± 10
Presentation	
STEMI	4 (11%)
NSTEMI	6 (17%)
Unstable angina	3 (8%)
Stable angina	23 (64%)
Target vessel	
LAD	29 (60%)
Cx	10 (21%)
RCA	9 (19%)
CTO	4 (10%)

Note. Values are mean ± *SD*, *n* or *n* (%).
Abbreviations: BMI, body-mass-index; CABG, coronary artery bypass grafting; CTO, chronic total occlusion; Cx, circumflex artery; LAD, left-anterior descending artery; PCI, percutaneous coronary intervention; RCA, right coronary artery.

Coronary angiography including intravascular OCT of the previously implanted scaffolds was performed in all cases. Repeat PCI was necessary in 16 patients (44%). Target-vessel revascularization without target lesion revascularization was performed in six patients (17%). PCI of another but the former target vessel was performed in four patients (11%). In six patients (17%), target lesion revascularization was required, in all cases due to in-scaffold-restenosis. For more details, see Table 3.

3.3 | OCT results at representation

Scaffold struts were still discernible in all 48 BRS. Mean scaffold diameter at follow-up was 3.02 ± 0.46 mm, mean scaffold area was 7.40 ± 2.24 mm^2. Lumen dimensions were smaller, with a mean lumen diameter of 2.50 ± 0.43 mm and a mean lumen area 5.16 ± 1.91 mm^2. Lumen dimensions were smaller than scaffold dimensions mainly due to in-scaffold restenosis (mean in-scaffold restenosis: 2.12 ± 0.83 mm^2). In-scaffold restenosis was formed of homogenous neointima in all cases. Peri-strut low intensity areas (PSLIA; Figure 2) were present in 13 of 48 scaffolds (27%). See also Table 4.

TABLE 2 Procedural characteristics

Predilatation	
Pressure (atm)	14 ± 4
Balloon diameter (mm)	2.9 ± 0.6
Balloon length (mm)	19 ± 5
NC balloon	46 (96%)
Compliant balloon	2 (4%)
Cutting/scoring balloon	7 (15%)
Scaffold implantation	
Pressure (atm)	12 ± 3
Diameter (mm)	3.0 ± 0.4
Length (mm)	21 ± 6
Postdilatation	
Pressure (atm)	17 ± 7
Diameter (mm)	3.4 ± 1.8
Length (mm)	18 ± 4
NC balloon	48 (100%)
Intravascular imaging (IVUS or OCT)	10 (28%)

Note. Values are mean ± *SD* or *n* (%).
Abbreviations: IVUS, intravascular ultrasound; NC, noncompliant; OCT, optical coherence tomography.

3.4 | Normalized light intensity

NLI was calculated for all BRS. Pearson correlation coefficient showed that NLI and time since scaffold implantation correlate in a linear fashion (Spearman Rho: $p < .001$, correlation coefficient = .91; see Figures 3 and 4).

3.5 | BRS-RESORB-INDEX

Since NLI correlates in a linear fashion with the time since scaffold implantation, the BRI was introduced as a marker of BRS resorption.

TABLE 3 Clinical representation

Presentation	
STEMI	0 (0)
NSTEMI	0 (0)
Unstable angina	1 (3%)
Stable angina	35 (97%)
PCI	
Performed	16 (44%)
TVR	6 (17%)
TLR	6 (17%)
Scaffold-thrombosis	0 (0%)
In-scaffold-restenosis	6 (17%)
Treatment in-scaffold restenosis	
DES	6 (100%)

Note. Values are mean ± *SD* or *n* (%).
Abbreviations: DES, drug-eluting stent; PCI, percutaneous coronary intervention; TLR, target lesion revascularization; TVR, target vessel revascularization.

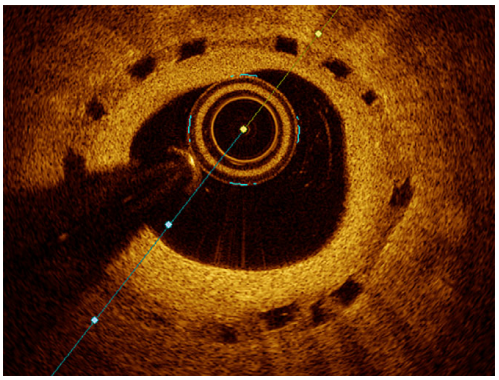

FIGURE 2 Absorb BVS™ 13 months after implantation. Peri-strut low intensity areas are visible as attenuation of the light signal in between the scaffold struts [Color figure can be viewed at wileyonlinelibrary.com]

BRS resorption, as measured by the BRI, varies widely between different individuals (range: 0.09–0.85) but is always very similar in different BRS implanted in one patient (interpatient variance: 0.32 ± 0.38, intrapatient variance: 0.02 ± 0.06; $p < .001$). For results of univariate analysis see Table 5. Multivariable analysis, including diabetes, clinical presentation (ACS vs. stable coronary artery disease), chronic total occlusion, and PSLIA, identified diabetes (mean BRI of patients with diabetes vs. patients without diabetes: 0.34 ± 0.13 vs. 0.58 ± 0.22; $p = .002$; see also Figure 5) and presence of PSLIA (Mean BRI of patients with PSLIA vs. patients without PSLIA: 0.44 ± 0.21 vs. 0.61 ± 18; $p = .027$) as independent risk factors for prolonged BRS resorption, whereas the resorption rate in ACS patients (STEMI, NSTEMI,

TABLE 4 OCT results

Scaffold	
Mean diameter (mm)	3.02 ± 0.46
Minimum diameter (mm)	2.80 ± 0.43
Maximum diameter (mm)	3.26 ± 0.51
Area (mm^2)	7.40 ± 2.24
Lumen	
Mean diameter (mm)	2.50 ± 0.43
Minimum diameter (mm)	2.26 ± 0.44
Maximum diameter (mm)	2.75 ± 0.54
Area (mm^2)	5.16 ± 1.91
Scaffold struts per OCT cross-section	9 ± 2
Strut fractures per scaffold	5 ± 2
In-scaffold restenosis (mm^2)	2.12 ± 0.83
PSLIA present	13/48 (27%)

Note. Values are mean ± *SD* or *n* (%).
Abbreviations: OCT, optical coherence tomography; PSLIA, peri-strut low intensity areas.

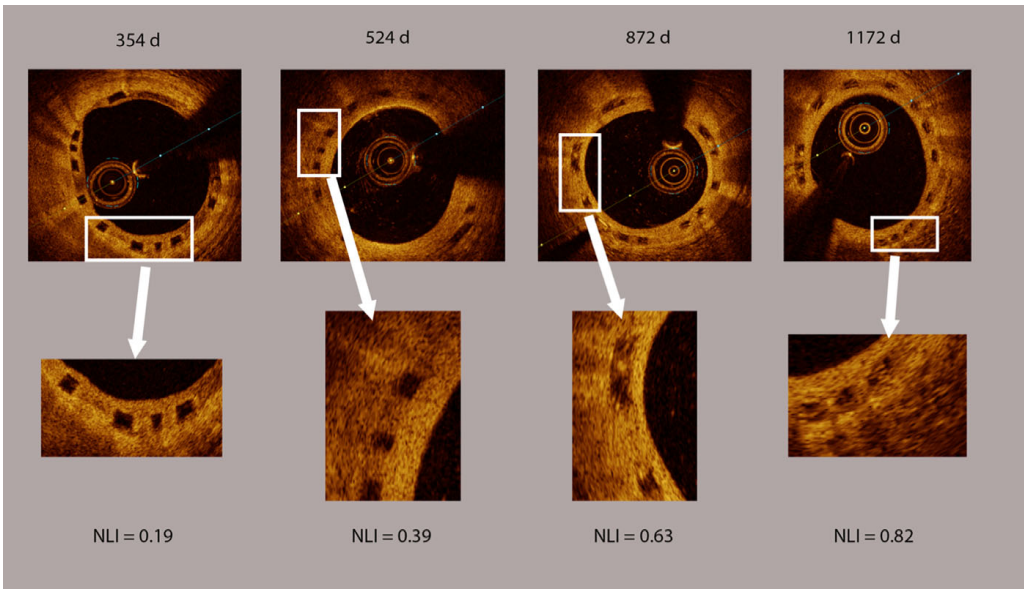

FIGURE 3 Development of normalized light intensity (NLI) in the course of time. This figure shows four examples of BRS at different stages of resorption. The time since implantation in days is written on top of each OCT image, the calculated NLI is written beneath the OCT images. BRS, bioresorbable vascular scaffolds; OCT, optical coherence tomography [Color figure can be viewed at wileyonlinelibrary.com]

and unstable angina; n = 13) was significantly higher as compared to patients without ACS (Mean BRI of patients with ACS vs. patients without ACS: 0.62 ± 0.17 vs. 0.43 ± 0.24; p = .012). For detailed BRI results see also Table 6.

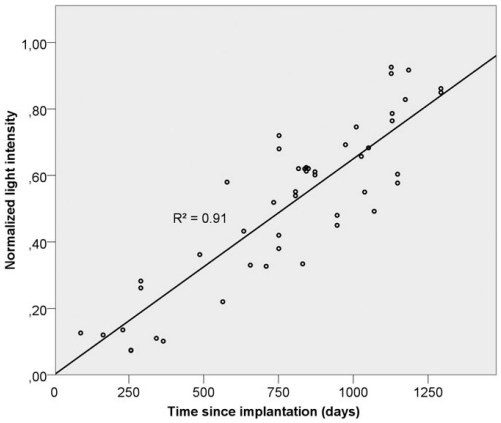

FIGURE 4 Normalized light intensity in dependence of time since BRS implantation (days). Normalized light intensity correlates with the time since scaffold implantation in a linear fashion. R^2 = Spearman correlation coefficient. BRS, bioresorbable vascular scaffolds

4 | DISCUSSION

The primary findings of this study are the following: (a) NLI of BRS struts correlates in a linear fashion with the time since scaffold implantation; (b) the BRI is a marker to estimate the degree of strut degradation; and (c) the BRS resorption process is influenced by patient-specific factors.

It is evident from recent studies, as well as our present data, that complete Absorb BVS™ resorption takes significantly more time than the initially proposed 2 years.[2,3,10,11] The everolimus-eluting Absorb BVS™ consists of a poly-L-lactic acid backbone. After implantation, the poly-L-lactic acid strut progressively degrades by hydrolysis.[12] Once the polymeric chains become small enough, they diffuse into the surrounding tissue and are progressively replaced by a provisional matrix initially composed of a milieu of extracellular matrix components. The

TABLE 5 Multivariate analysis of BRS-RESORB-INDEX

Variable	Yes	No	*p*-value
Diabetes	0.30 ± 0.21	0.54 ± 0.24	.002
PSLIA	0.46 ± 0.28	0.63 ± 24	.027
ACS	0.65 ± 0.24	0.40 ± 0.26	.012
Chronic total occlusion	0.57 ± 0.25	0.49 ± 0.24	.245

Note. Values are median ± 95%-confidence interval.
Abbreviation: PSLIA, peri-strut low intensity areas.

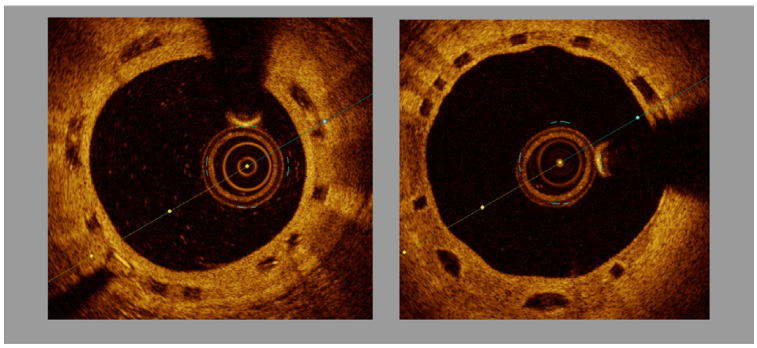

FIGURE 5 BRS-RESORB-INDEX as a marker for BRS resorption. On the left there is shown an OCT picture of an ABSORB BVS™ in a patient without diabetes 17 months after implantation. The BRI for this scaffold is 0.67. On the right there is shown an OCT picture of an ABSORB BVS™ in a patient with diabetes 17 months after implantation. The BRI for this scaffold is 0.34. BRS resorption in patients with diabetes takes more time as compared to patients without diabetes. BRS, bioresorbable vascular scaffolds; OCT, optical coherence tomography [Color figure can be viewed at wileyonlinelibrary.com]

provisional matrix is initially acellular and gradually cellularized with connective tissues. A full integration into the surrounding intima is the suspected endpoint of this resorption process.[12,13] Nakatani et al demonstrated in their previous study that OCT light intensity significantly correlates with the histological resorption process of BRS in porcine coronary arteries.[4] They reported that NLI of strut cores did not change between 3 and 18 months, while thereafter it gradually increased from 18 to 30 months. Our data showed a continuous increase of NLI with time since BRS implantation. Actually, our analysis even revealed a linear relationship between NLI and time. In the study of Nakatani et al there was no linear relationship between OCT light intensity and time since implantation which might be due to procedural and methodical differences. BRS implantation in this previous study was performed without postdilatation and an impaired embedding of the struts into the vessel wall could possibly have delayed the resorption process. In contrast to our present study, light intensity was only measured in the strut center, whereas we analyzed the light intensity of each strut completely. Resorption begins at the edge of each strut and needs some time until reaching the very center of the strut. Hence, analyzing the light intensity of each strut completely may lead to a more accurate visual estimation of the stage of resorption.

TABLE 6 Univariate analysis of BRS-RESORB-INDEX

Variable	Yes	No	*p*-value
Previous revascularization	0.48 ± 0.24	0.55 ± 0.18	.45
Male gender	0.51 ± 0.22	0.61 ± 0.34	.30
Hypertension	0.53 ± 0.24	0.48 ± 0.17	.67
Diabetes	0.34 ± 0.13	0.58 ± 0.22	<.001
Hyperlipidemia	0.50 ± 0.23	0.58 ± 0.19	.56
PSLIA	0.44 ± 0.21	0.61 ± 18	<.001
Smoking	0.52 ± 0.25	0.61 ± 0.1	.56
ACS	0.62 ± 0.17	0.43 ± 0.24	<.001
Chronic total occlusion	0.55 ± 0.17	0.46 ± 0.19	.184
Family history for coronary artery disease	0.49 ± 0.20	0.53 ± 0.22	.49

Note. Values are mean ± *SD* or *n* (%).
Abbreviation: PSLIA, peri-strut low intensity areas.

Multivariable analysis identified diabetes and presence of PSLIA as independent risk factors for a lower BRI indicating a prolonged resorption process. Diabetes is associated with persisting vascular inflammation processes. These inflammation processes may interfere with the degradation of BRS. Accordingly, we observed a prolonged BRS resorption process in patients with diabetes compared to patients without diabetes. In porcine coronary arteries, PSLIA correlated with peri strut inflammation in histology.[14] Local inflammation processes may also interfere with the resorption. On the other hand, patients presenting with ACS had a significantly higher BRI as compared to patients presenting without ACS. Since our data showed a wide variation for BRI between different patients, but was always very similar in BRS implanted in the same patient, we can assume, that the resorption process of poly-L-lactic acid BRS is mainly influenced by patient specific characteristics.

BRI was introduced as a marker to measure the speed of the BRS resorption process. If two or more BRS were implanted in the same patient, BRI was always very similar when calculating it for the different BRS, suggesting that individual patient factors influence the resorption process more likely than procedural factors or the characteristics of the lesion a BRS was implanted in.

4.1 | Limitations

This study has some important limitations. First of all, it is a retrospective single-center analysis with a small number of patients and BRS. Only patients who required coronary angiography for clinical reasons

were included in this analysis, resulting in a clear selection bias toward restenosis. For the basis of our analysis we used the NLI as measured by OCT, which is only an indirect marker for the resorption and cellularization process of poly-L-lactic acid based BRS. An association between OCT light intensity and resorption has so far only been shown after BRS implantation in porcine coronary arteries.[4] Nevertheless, it can be assumed that due to the similar metabolism, this association is adoptable to human subjects. Light intensity of each scaffold strut was normalized for the surrounding intima. Especially in atherosclerotic coronary segments, composition of the intima might be heterogeneous to some extent. Hence, light intensity of the adjacent intima might not be exactly what light intensity of completely cellularized BRS strut should be at the end of resorption. Finally, it is not clear to what extent partially resorbed scaffold struts still contain poly-L-lactic acid or extracellular matrix components.[4] Nevertheless, if BRS struts are still discernible on OCT images, it is reasonable to assume that the resorption process has not been completed.

4.2 | Clinical implications

Analysis of the BRI revealed that individual factors significantly influence the speed of BRS resorption. These factors may need to be taken into account when considering the use of BRS and when deciding about the duration of post-PCI dual antiplatelet therapy. Progressive vessel remodeling has been reported to be present during the whole resorption process.[15] It has been suspected that the higher rate of device thrombosis and target lesion failure that has been reported in latest randomized controlled trials when comparing ABSORB BVS™ and second-generation DES might be caused by a prolonged resorption process in some extent.[6,7,16,17] This might also explain why the DESolve BRS™, which is characterized by an early degradation at 6 months, showed lower rates of scaffold thrombosis and target lesion failure as compared to the values reported for the ABSORB BVS™ in a first study including 126 patients.[18]

Future clinical trials are needed to evaluate the reliability of the BRI in an all-comers patient cohort, not only in patients with restenosis after implantation of poly-L-lactic acid based BRS. Additionally, the BRI could be evaluated for newer generation BRS.

5 | CONCLUSION

The resorption rate of BRS is influenced by numerous individual factors. Our data indicate that diabetes and the presence of PSLIA are associated with a prolonged BRS resorption process, whereas in ACS patients, BRS resorption appears to be significantly faster. The BRI provides the possibility to estimate the degree of strut degradation in a quantitative fashion and might also be applicable for newer generation BRS.

CONFLICT OF INTEREST

Christian Hamm received consulting and speakers fee from Abbott Vascular. All other authors declare that there are no potential conflicts of interest. There is no relation with industry regarding this study.

ORCID

Florian Blachutzik https://orcid.org/0000-0002-7695-3663
Stephan Achenbach https://orcid.org/0000-0002-7596-095X
Niklas Boeder https://orcid.org/0000-0002-2802-3533
Oliver Doerr https://orcid.org/0000-0003-4526-6956
Timm Bauer https://orcid.org/0000-0001-7862-5789

REFERENCES

1. Wiebe J, Nef HM, Hamm CW. Current status of bioresorbable scaffolds in the treatment of coronary artery disease. J Am Coll Cardiol. 2014;64:2541-2525.
2. Sotomi Y, Onuma Y, Collet C, et al. Bioresorbable scaffold: the emerging reality and future directions. Circ Res. 2017;120(8):1341-1352.
3. Gogas BD, Radu M, Onuma Y, et al. Evaluation with in vivo optical coherence tomography and histology of the vascular effects of the everolimus-eluting bioresorbable vascular scaffold at two years following implantation in a healthy porcine coronary artery model: implications of pilot results for future pre-clinical studies. Int J Cardiovasc Imaging. 2012;28(3):499-511.
4. Nakatani S, Ishibashi Y, Sotomi Y, et al. Bioresorption and vessel wall integration of a fully bioresorbable polymeric everolimus-eluting scaffold: optical coherence tomography, intravascular ultrasound, and histological study in a porcine model with 4-year follow-up. J Am Coll Cardiol Intv. 2016;9(8):838-851.
5. Zhang YJ, Iqbal J, Nakatani S, et al. Scaffold and edge vascular response following implantation of everolimus-eluting bioresorbable vascular scaffold: a 3-year serial optical coherence tomography study. J Am Coll Cardiol Intv. 2014;7(12):1361-1369.
6. Wykrzykowska JJ, Kraak RP, Hofma SH, et al. Bioresorbable scaffolds versus metallic stents in routine PCI. N Engl J Med. 2017;376(24):2319-2328.
7. Ali ZA, Serruys PW, Kimura T, et al. 2-year outcomes with the absorb bioresorbable scaffold for treatment of coronary artery disease: a systematic review and meta-analysis of seven randomised trials with an individual patient data substudy. Lancet. 2017;390:760-772. https://doi.org/10.1016/S0140-6736(17)31470-8.
8. Gori T, Jansen T, Weissner M, et al. Coronary evaginations and peri-scaffold aneurysms following implantation of bioresorbable scaffolds: incidence, outcome, and optical coherence tomography analysis of possible mechanisms. Eur Heart J. 2016;37(26):2040-2049.
9. Gori T, Schulz E, Hink U, et al. Clinical, angiographic, functional, and imaging outcomes 12 months after implantation of drug-eluting bioresorbable vascular scaffolds in acute coronary syndromes. J Am Coll Cardiol Intv. 2015;8(6):770-777.
10. Karanasos A, Simsek C, Gnanadesigan M, et al. OCT assessment of the long-term vascular healing response 5 years after everolimus-eluting bioresorbable vascular scaffold. J Am Coll Cardiol. 2014;64(22):2343-2356.
11. Onuma Y, Serruys PW, Muramatsu T, et al. Incidence and imaging outcomes of acute scaffold disruption and late structural discontinuity after implantation of the absorb everolimus-eluting fully bioresorbable vascular scaffold: optical coherence tomography assessment in the ABSORB cohort B Trial (a clinical evaluation of the bioabsorbable everolimus eluting coronary stent system in the treatment of patients with de novo native coronary artery lesions). J Am Coll Cardiol Intv. 2014;7(12):1400-1411.
12. Otsuka F, Pacheco E, Perkins LE, et al. Long-term safety of an everolimus-eluting bioresorbable vascular scaffold and the cobalt-chromium XIENCE V stent in a porcine coronary artery model. Circ Cardiovasc Interv. 2014;7(3):330-342.

13. Vorpahl M, Finn AV, Nakano M, Virmani R. The bioabsorption process: tissue and cellular mechanisms and outcomes. EuroIntervention. 2009;5(suppl F):F28-F35.
14. Tellez A, Afari ME, Buszman PP, et al. Peri-strut low-intensity areas in optical coherence tomography correlate with peri-strut inflammation and neointimal proliferation: an in-vivo correlation study in the familial hypercholesterolemic coronary swine model of in-stent restenosis. Coron Artery Dis. 2014;25(7):595-601.
15. Serruys PW, Katagiri Y, Sotomi Y, et al. Arterial remodeling after bioresorbable scaffolds and metallic stents. J Am Coll Cardiol. 2017;70(1):60-74.
16. Sorrentino S, Giustino G, Mehran R, et al. Everolimus-eluting bioresorbable scaffolds versus everolimus-eluting metallic stents. J Am Coll Cardiol. 2017;69(25):3055-3066.
17. Serruys PW, Katsikis A, Onuma Y. Long-term data of BRS presented at EuroPCR 2017 (Friday, 19 May). EuroIntervention. 2017;13(5):e515-e521.
18. Abizaid A, Costa RA, Schofer J, et al. Serial multimodality imaging and 2-year clinical outcomes of the novel DESolve Novolimus-eluting bioresorbable coronary scaffold system for the treatment of single de novo coronary lesions. J Am Coll Cardiol Intv. 2016;9:565-574.

How to cite this article: Blachutzik F, Achenbach S, Marwan M, et al. OCT-assessment of scaffold resorption: Analysis of strut intensity by a new resorption index for poly-L-lactic acid bioresorbable vascular scaffolds. *Catheter Cardiovasc Interv*. 2019;1–8. https://doi.org/10.1002/ccd.28223

Nr. 5: Effect of non-compliant balloon postdilatation on magnesium-based bioresorbable vascular scaffolds

Received: 3 April 2018 | Revised: 31 May 2018 | Accepted: 24 June 2018
DOI: 10.1002/ccd.27794

WILEY

ORIGINAL STUDIES

Effect of non-compliant balloon postdilatation on magnesium-based bioresorbable vascular scaffolds

Florian Blachutzik MD[1,2] | Stephan Achenbach MD[1] | Monique Tröbs MD[1] | Mohamed Marwan MD[1] | Melissa Weissner[3,4] | Holger Nef MD[2] | Christian Schlundt MD[1]

[1]Department of Cardiology, Friedrich-Alexander Universität Erlangen-Nürnberg, Erlangen, Germany

[2]Department of Cardiology and Angiology, Justus-Liebig Universität Giessen, Medical Clinic I, Germany

[3]Zentrum für Kardiologie, University Hospital Mainz, Mainz, Germany

[4]German Center for Cardiac and Vascular Research (DZHK), Mainz, Germany

Correspondence
Florian Blachutzik, MD, Department of Cardiology and Angiology, University of Giessen, Klinikstrasse 33, 35392 Giessen, Germany.
Email: dr.blachutzik@t-online.de

Abstract

Background: Optimal implantation results of bioresorbable scaffolds (BRS) are typically assumed to require postdilatation with non-compliant (NC) balloons to achieve full scaffold apposition and minimize event rates. We systematically evaluated the mechanical effect of NC balloon postdilatation on magnesium-based BRS (Magmaris®, Biotronik AG, Bülach, Switzerland) in vivo.

Methods: In 35 patients, 40 Magmaris® BRS were implanted to treat 37 de novo coronary artery stenoses. A systematic implantation protocol was followed. After appropriately sized NC balloon predilatation (1:1:1 vessel:balloon:scaffold ratio), Magmaris® BRS were implanted with a pressure of 10 atm, followed by NC balloon postdilatation at nominal BRS size (standardized at 16 atm). OCT was performed before and after postdilatation and OCT images were analyzed at a spacing of 0.2 mm to measure BRS dimensions and determine apposition as well as to detect strut fractures.

Results: PCI with Magmaris® BRS (mean diameter: 3.21 ± 0.32 mm; mean length: 20 ± 4 mm) was successful in all cases, in one case a non-flow-limiting distal edge dissection occurred after implantation and before postdilatation. NC balloon postdilatation led to significantly larger mean scaffold diameter (3.21 ± 0.32 mm vs. 2.80 ± 0.39 mm, $P < 0.001$), abluminal scaffold area (7.92 ± 1.43 mm^2 vs. 6.72 ± 1.28 mm^2, $P < 0.001$) and lumen area (7.58 ± 1.1 mm^2 vs. 6.83 ± 1.12 mm^2, $P < 0.001$). Incomplete scaffold apposition area was significantly lower if postdilatation was performed (0.01 ± 0.04 mm^2 vs. 0.17 ± 0.11 mm^2, $P < 0.001$). Strut fractures could neither be observed before nor after postdilatation.

Conclusion: NC balloon postdilatation of Magmaris® BRS is required to achieve optimal expansion. It significantly reduces malapposition and can safely be performed without relevant rates of strut fracture.

KEYWORDS

bioabsorbable stent, optical coherence tomography, percutaneous coronary intervention

1 | INTRODUCTION

Bioresorbable scaffolds (BRS) have been developed to secure the acute results of percutaneous coronary intervention (PCI) while avoiding long-term complications, such as very late thrombosis. Despite high procedural success rates and favorable early outcome studies, recent large-scale randomized controlled trials showed an increased rate of early and late device thrombosis when comparing first-generation polymer-based Absorb BVS™ (Abbott Vascular, Santa Clara, CA, USA) to 2nd generation DES [1–5]. It is commonly assumed that the high event rate may be partially explained by the fact that in initial studies, operators were not aware of the importance of following a strictly standardized implantation protocol that mandates thorough lesion preparation and high-pressure postdilatation with appropriately sized balloons [6–8]. Also, the avoidance of lesions with a

Abbreviations: BMI, body mass index; BMS, bare-metal stent; BRS, bioresorbable scaffold; DES, drug-eluting stent; NC balloon, non-compliant balloon; NSTEMI, non-ST-segment elevation myocardial infarction; OCT, optical coherence tomography; PCI, percutaneous coronary intervention; PTCA, percutaneous transluminal coronary angioplasty.

small reference diameter was postulated to improve results [9]. However, even in the most recent randomized ABSORB IV trial, ischemia-driven target vessel revascularization at 1 month follow-up was significantly more frequent for the Absorb BVS™ as compared to DES (1.2% vs. 0.2%, $P = 0.003$) [10]. A recently published analysis of AIDA trial did not show any effect on clinical outcome after a median follow-up of 707 days, if strict predilatation, sizing and postdilatation (PSP) technique was performed in the course of Absorb BVS™ implantation when comparing it with Absorb BVS™ implantation without performing PSP technique [11].

Metallic BRS might be able to overcome some of the disadvantages of first-generation polymer-based BRS by providing a higher radial force, smaller footprint and lower strut thickness as well as faster resorption [12,13]. Magnesium-based Magmaris™ BRS (Biotronik AG, Bülach, Switzerland) received CE approval in Europe in June 2016. Implantation recommendations for this device are based on expert consensus [14]. Hence, clinical studies are required to identify the optimal implantation technique. Accordingly, the aim of our study was to analyze the effect of non-compliant (NC) balloon postdilatation on Magmaris™ BRS.

2 | METHODS

2.1 | Study design and population

A series of 35 consecutive patients who underwent PCI with implantation of magnesium-based Magmaris™ BRS were included in this study. Intravascular imaging using optical coherence tomography (OCT) was mandated per institutional protocol when implanting Magmaris™ BRS.

Baseline characteristics of the patients, including medical history as well as clinical, angiographic, and procedural data were collected. Six-month clinical follow-up was obtained by telephone interview. The study was performed in accordance with the Declaration of Helsinki. The study protocol was approved by the Internal Review Board of the Medical Faculty, Friedrich-Alexander-University Erlangen-Nürnberg (Number: 351_16 Bc).

2.2 | Percutaneous coronary intervention

PCI with implantation of Magmaris™ BRS was performed via a transradial ($n = 33$) or transfemoral approach ($n = 2$) using six French guiding catheters and standard coronary guidewires (Runthrough™, Terumo Europe NV, Leuven, Belgium). All patients had received intravenous heparin and intracoronary nitrates. Target lesions were required to have a reference vessel diameter based on visual estimation between 2.7 and 3.7 mm. Exclusion criteria, as suggested by expert consensus, included a left ventricular ejection fraction of less than 30%, thrombus in the target vessel, severe calcification, three-vessel disease, ostial lesion, target lesions involving a side branch of more than 2.0 mm in diameter, target lesions located in an arterial or venous bypass graft, in-stent restenosis and unsuccessful predilatation [13,14].

Predilatation was performed in all lesions, with balloon size based on visual angiographic estimation to achieve a 1:1 ratio of vessel and balloon diameter. Successful predilatation was mandatory to proceed with scaffold implantation and was defined as a residual stenosis of less than 80%. Lesions were treated using sirolimus-eluting Magmaris™ BRS (Biotronik AG, Bülach, Switzerland) with diameters of 3.0 or 3.5 mm and lengths of 15, 20 or 25 mm. Deployment of Magmaris™ was performed with a pressure of 10 atm for at least 20 seconds. NC balloon (NC Trek™, Abbott Vascular, Santa Clara, CA, USA) postdilatation at a pressure of 16 atm was mandatory per institutional protocol and was systematically performed in all lesions. NC balloon diameter was selected according to the diameter of the scaffold balloon at a 1:1 ratio. Further medication, techniques, and equipment for PCI were used in accordance with current clinical guidelines and were left to the responsible physician's discretion.

2.3 | Optical coherence tomography image acquisition

OCT was performed immediately after device implantation as well as after postdilatation. A 2.7 French Dragonfly™ intravascular imaging catheter (St. Jude Medical, Saint Paul, MN, USA) was used with a mechanical pullback speed of 18 mm/s over a distance of 54 mm. During pullback, 25 ml contrast agent (Ultravist™ 370, Bayer AG, Leverkusen, Germany) were injected at 4 ml/s with a maximum pressure of 400 psi using machine injection (Liebel-Flarsheim 903300G, Liebel-Flarsheim Co, Cincinnati, OH, USA).

2.4 | Optical coherence tomography image analysis

All OCT data sets were digitally recorded, stored, and analyzed. OCT image analysis was performed offline using QCU-CMS v4.69 OCT analysis software (Leiden University Medical Center, Leiden, Netherlands) at a spacing of 200 μm. OCT analysis was performed in accordance with previous publications [15–18]. Strut fractures were defined as struts lying isolated in the lumen or the presence of one strut on top of another. Malapposition was defined as present when the measured distance between the inner contour of the strut and the vessel wall was greater than the strut thickness (150 μm including polymer matrix). The eccentricity index was defined as minimum scaffold diameter divided by maximum scaffold diameter [19]. Calcification was defined as "present" if calcified plaque was visible in more than one quarter of the vessel wall.

2.5 | Statistical analysis

Continuous variables are summarized as mean ± standard deviation; categorical variables are provided as *n* (%). The Kolmogorov–Smirnov test was performed to test for non-parametric distribution. To test for statistical differences between two groups for comparison of continuous variables, either a *t*-test for unpaired samples (parametric distribution) or a Mann–Whitney *U*-test (non-parametric distribution) was used. For categorical variables, a Chi-squared or Fisher's exact test was carried out. Statistical analyses were performed using SPSS

version 21.0 (IBM SPSS Statistics, IBM Corporation, Armonk, NY, USA). A two-sided $P < 0.05$ was considered significant.

3 | RESULTS

3.1 | Patient and procedural data

Between June 2016 and October 2017, 35 patients with implantation of 40 Magmaris™ BRS were included. Thirty patients presented with stable angina (86%), five patients with NSTEMI (14%). For detailed patient characteristics, see Table 1. Predilatation was successfully performed in all lesions, increasing the balloon size or the use of debulking devices was not necessary in any of the lesions. In four patients lesion length required sequential implantation of two BRS, in one patient, two different lesions in one target vessel were treated with two single BRS. Magmaris™ implantation was successful in all cases. Mean nominal BRS length was 20 ± 4 mm, mean nominal diameter was 3.2 ± 0.2 mm. Procedural data are summarized in Table 2.

3.2 | OCT results

Mean BRS diameter was 2.80 ± 0.39 mm after implantation at 10 atm and was significantly larger after NC postdilatation (3.21 ± 0.32 mm; $P < 0.001$). Accordingly, ab- and adluminal scaffold areas were significantly larger after postdilatation was performed (7.92 ± 1.43 mm^2 vs. 6.72 ± 1.28 mm^2; $P < 0.001$ and 6.94 ± 1.22 mm^2 vs. 5.82 ± 1.31 mm^2; $P < 0.001$) (Figure 1). Lumen dimensions were also significantly larger following postdilatation (7.58 ± 1.09 mm^2 vs. 6.83 ± 1.12 mm^2; $P < 0.001$). Twenty eight scaffolds showed complete apposition after implantation and 37 scaffolds showed complete apposition after NC balloon postdilatation ($P = 0.01$). Incomplete scaffold apposition area was significantly smaller after postdilatation (0.01 ± 0.04 mm^2 vs. 0.17 ± 0.11 mm^2; $P < 0.001$) (Figure 1). Strut fractures could neither be observed before nor after NC postdilatation. One distal non flow-limiting edge dissection occurred after Magmaris™-implantation, it was thus not induced by postdilatation. Symmetry of Magmaris™ BRS was significantly improved by postdilatation (0.91 ± 0.07 vs. 0.82 ± 0.05; $P = 0.01$). In OCT, calcification was visible over 9.2% of the total scaffold length.

Postdilatation did not lead to significantly larger ab- or adluminal scaffold area (6.92 ± 1.13 mm^2 vs. 6.84 ± 1.11 mm^2; $P = 0.61$ and 5.94 ± 1.03 m^2 vs. 5.78 ± 1.29 mm^2; $P = 0.25$) or lumen area (6.90 ± 0.92 mm^2 vs. 6.79 ± 1.12 mm^2; $P = 0.46$) in calcified segments. Additionally, incomplete scaffold apposition area could not be

TABLE 1 Patient characteristics

Patients	35
Magmaris™ BRS	40
Lesions	36
Age (years)	66 ± 12
BMI[a] (kg/m^2)	24.3 ± 6.7
Male gender	25 (71%)
Previous CABG[b]	1 (3%)
Previous PCI[e]	7 (20%)
Hypertension	22 (63%)
Diabetes	9 (26%)
Hyperlipidemia	18 (52%)
Active smoking	6 (17%)
Family history for coronary artery disease	12 (34%)
Left ventricular ejection fraction (%)	51 ± 10
Presentation	
STEMI	0 (0%)
NSTEMI	5 (14%)
Unstable angina	0 (0%)
Table angina	30 (86%)
Target vessel	
LAD[d]	17 (48%)
Cx[c]	10 (29%)
RCA[f]	8 (23%)

Values are mean ± standard deviation, *n* or *n* (%).
[a] Body mass index.
[b] Coronary artery bypass grafting.
[c] Circumflex artery.
[d] Left-anterior descending artery.
[e] Percutaneous coronary intervention.
[f] Right coronary artery.

TABLE 2 Procedural characteristics

Predilatation	
Pressure (atm)	14 ± 3
Balloon diameter (mm)	3.1 ± 0.3
Balloon length (mm)	16 ± 4
NC[a] balloon	35 (87%)
Compliant balloon	5 (13%)
Magmaris™ implantation	
Pressure (atm)	10 ± 1
Diameter (mm)	3.2 ± 0.2
Length (mm)	20 ± 4
Postdilatation	
Pressure (atm)	16 ± 2
Diameter (mm)	3.2 ± 0.2
Length (mm)	14 ± 3
NC[a] balloon	40 (100%)

Values are mean ± standard deviation or *n* (%).
[a] Non-compliant.

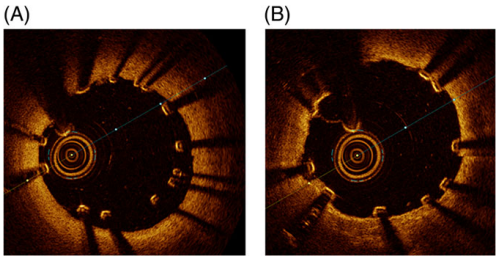

FIGURE 1 Effect of NC postdilatation on Magmaris™ BRS. OCT cross sections showing a 3.0/20 mm Magmaris™ BRS before (A) and after (B) non-compliant balloon postdilatation. The apposition of the BRS is significantly improved by postdilatation [Color figure can be viewed at wileyonlinelibrary.com]

TABLE 3 OCT[a] results

Variable	Before postdilatation	After postdilatation	*P*-value
Mean BRS diameter (mm)	2.80 ± 0.39	3.21 ± 0.32	<0.001
Minimum BRS diameter (mm)	2.44 ± 0.41	2.62 ± 0.29	0.003
Maximum BRS diameter (mm)	3.08 ± 0.33	3.45 ± 0.39	<0.001
Abluminal scaffold area (mm^2)	6.72 ± 1.28	7.92 ± 1.43	<0.001
Adluminal scaffold area (mm^2)	5.82 ± 1.31	6.94 ± 1.22	<0.001
Lumen area (mm^2)	6.83 ± 1.12	7.58 ± 1.09	<0.001
Minimum lumen area (mm^2)	5.44 ± 1.88	6.11 ± 1.62	0.002
Incomplete scaffold apposition area (mm^2)	0.17 ± 0.11	0.01 ± 0.04	<0.001
Mean eccentricity index	0.82 ± 0.05	0.91 ± 0.07	0.01
Proximal edge dissection	0	0	>0.99
Distal edge dissection	1	1	>0.99

Values are mean ± standard deviation or *n* (%).
[a] Optical coherence tomography.

reduced significantly in these vessel segments (0.10 ± 0.07 mm^2 after postdilatation vs. 0.11 ± 0.05 mm^2 before postdilatation; $P = 0.40$). For more details, see Tables 3 and 4.

3.3 | Follow-up

Clinical follow-up after 6 months can be provided for all 35 patients. Repeat revascularization was necessary in two patients 3 and 4 months after Magmaris™-implantation. In both cases, patients presented with stable angina. Invasive coronary angiography including OCT was performed and showed a high-grade restenosis in the vessel segment previously treated with Magmaris™. Restenosis was treated in both patients with implantation of DES. For follow-up data, see also Table 5.

4 | DISCUSSION

The main findings of our study are the following: (1) NC balloon postdilatation of Magmaris™ BRS significantly improves strut apposition and results in a larger scaffold area without inducing higher rates of strut fractures or edge dissections, (2) lumen and scaffold dimensions cannot be improved by NC postdilatation in vessel segments with calcified plaque, and (3) Magmaris™ symmetry can be enhanced by NC postdilatation.

TABLE 4 Effect of NC postdilatation of Magmaris™ in calcified vessel segments

Variable	Before postdilatation	After postdilatation	*P*-value
Abluminal scaffold area (mm^2)	6.84 ± 1.11	6.92 ± 1.13	0.61
Adluminal scaffold area (mm^2)	5.78 ± 1.29	5.94 ± 1.03	0.25
Lumen area (mm^2)	6.79 ± 1.12	6.90 ± 0.92	0.46
Mean eccentricity index	0.82 ± 0.05	0.84 ± 0.08	0.52
Incomplete scaffold apposition area (mm^2)	0.11 ± 0.05	0.10 ± 0.07	0.40

Values are mean ± standard deviation or *n* (%).

Metallic BRS may be able to overcome some limitations of first generation polymer-based BRS by providing stronger radial force and better deliverability. The prospective, multi-center, first-in-man BIOSOLVE-II trial, enrolling 123 patients with Magmaris™-implantation, showed a favorable safety profile up to 12 months and stable angiographic parameters between 6 and 12 months [20,21]. No definite or probable scaffold thrombosis was observed with Magmaris™. Previous generations of magnesium-based scaffolds showed no scaffold thrombosis up to 3 years [16,22]. However, the patient cohorts included in these studies are relatively small.

For the successful use of polymer-based BRS, two things seem to be very important: (1) a scaffold-specific implantation technique with high pressure postdilatation and (2) an adequate lesion preparation [6,8,23,24]. Accordingly, when following these recommendations, clinical results are not significantly inferior when comparing ABSORB BVS™ and DES [6,8,23,24]. It is unknown, if these results would be the same for Magmaris™. Nevertheless, one could assume that things are quite similar with metal-based BRS. Our study demonstrated that scaffold apposition and expansion can be significantly improved by high pressure NC postdilatation of Magmaris™. However, high pressure NC postdilatation is unable to optimize the results in calcified vessel segments. Hence, adequate lesion selection and, possibly, preparation are essential. Postdilatation cannot solve the problems induced by inadequate lesion selection or preparation.

During 6-month follow-up, two patients represented due to restenosis in the vessel segment previously treated with Magmaris™. OCT showed a homogeneous restenosis. Scaffold struts were only partially discernible at follow-up. Maybe the fast resorption process of Magmaris™ and its early loss of radial force contributed to the restenosis in these two cases.

4.1 | Limitations

This study has some important limitations. First of all, it is a retrospective single-center analysis with a small number of patients and BRS. Nevertheless, interventions were standardized since implantation strictly adhered to the study protocol. We used an NC balloon for high pressure postdilatation and could not compare the effect to high-

TABLE 5 Clinical outcome after 6 months

Follow-up obtained	35/35 (100)
Periprocedural death	0 (0)
Myocardial infarction	0 (0)
Repeat revascularization	2 (6)
Target vessel failure	2 (6)
Target lesion failure	2 (6)
Scaffold restenosis	2 (6)
Scaffold thrombosis	0 (0)
Mortality	0 (0)

Values are *n* (%).

pressure dilatation performed with the implantation balloon itself. Another important limitation is the lack of long-term follow-up data for the patients. However, the aim of this study was to analyze the acute effect of NC postdilatation on Magmaris™ BRS.

Despite carefully selecting only lesions without angiographically visible calcification, calcified plaque exceeding one quadrant of the vessel wall was visible in OCT over 9.2% of total lesion length. Calcified plaques exceeding one quarter of vessel wall were visible in all lesions, most likely due to the high resolution of OCT analysis at a spacing of 200 μm. NC balloon postdilatation did not lead to a significant improvement of scaffold or lumen dimensions in these areas, suggesting that implantation of Magmaris™ should be avoided in calcified lesions, despite providing a higher radial force compared to polymer-based ABSORB BVS™. It has to be kept in mind, that metallic BRS can only provide 20% of the radial force of new generation metallic DES [25]. To avoid scaffold failure or inadequate expansion of Magmaris™, intravascular imaging with OCT may need to be performed before implanting this device.

4.2 | Clinical implications

Following a BRS-specific implantation protocol, as in this study, leads to high success rates when implanting Magmaris™. Adequate NC balloon postdilatation should always be performed since it leads to a significant improvement of scaffold and lumen dimensions as well as to a significant reduction of malapposition without inducing negative side effects as strut fractures or edge dissections. Additionally, scaffold symmetry can be significantly improved, which may positively influence clinical outcome since lower BRS symmetry has been reported to be associated with an impaired clinical outcome [26,27]. Implantation of Magmaris™ in calcified lesions should be avoided since radial force is still lower than of metallic DES and NC postdilatation is unable to optimize BRS apposition and expansion in calcified vessel segments.

Future clinical trials are needed to analyze proper lesion and patient selection, lesion preparation and to evaluate the long-term outcome after Magmaris™ implantation.

5 | CONCLUSION

NC balloon postdilatation of Magmaris® BRS is required to achieve optimal expansion. It significantly reduces malapposition and can safely be performed without relevant rates of strut fracture. Implantation in calcified lesions should be avoided since lumen and scaffold dimensions cannot be improved by NC postdilatation if relevant calcification is present.

CONFLICT OF INTEREST

The authors declare that there are no potential conflicts of interest.

ORCID

Florian Blachutzik http://orcid.org/0000-0002-7695-3663
Stephan Achenbach http://orcid.org/0000-0002-7596-095X

REFERENCES

1. Wykrzykowska JJ, Kraak RP, Hofma SH, et al. Bioresorbable scaffolds versus metallic stents in routine PCI. *N Engl J Med*. 2017;*376*(24):2319-2328.
2. Ali ZA, Serruys PW, Kimura T, et al. 2-Year outcomes with the absorb bioresorbable scaffold for treatment of coronary artery disease: A systematic review and meta-analysis of seven randomised trials with an individual patient data substudy. *Lancet*. 2017;*390*(10096):760-772.
3. Ishibashi Y, Onuma Y, Muramatsu T, et al. Lessons learned from acute and late scaffold failures in the ABSORB EXTEND trial. *EuroIntervention*. 2014;*10*(4):449-457.
4. Lipinski MJ, Escarcega RO, Baker NC, et al. Scaffold thrombosis after percutaneous coronary intervention with ABSORB Bioresorbable vascular scaffold: A systematic review and meta-analysis. *J Am Coll Cardiol Interv*. 2016;*9*(1):12-24.
5. Capodanno D, Gori T, Nef H, et al. Percutaneous coronary intervention with everolimus-eluting bioresorbable vascular scaffolds in routine clinical practice: Early and midterm outcomes from the European multicentre GHOST-EU registry. *EuroIntervention*. 2015;*10*(10):1144-1153.
6. Polimeni A, Weissner M, Schochlow K, et al. Incidence, clinical presentation, and predictors of clinical restenosis in coronary bioresorbable scaffolds. *J Am Coll Cardiol Interv*. 2017;*10*(18):1819-1827.
7. Markovic S, Kugler C, Rottbauer W, Wöhrle J. Long-term clinical results of bioresorbable absorb scaffolds using the PSP-technique in patients with and without diabetes. *J Interv Cardiol*. 2017;*30*(4):325-330.
8. Ortega-Paz L, Capodanno D, Gori T, et al. Predilation, sizing and post-dilation scoring in patients undergoing everolimus-eluting bioresorbable scaffold implantation for prediction of cardiac adverse events: Development and internal validation of the PSP score. *EuroIntervention*. 2017;*12*(17):2110-2117.
9. Kereiakes DJ, Ellis SG, Metzger C, et al. 3-Year clinical outcomes with everolimus-eluting bioresorbable coronary scaffolds: The ABSORB III trial. *J Am Coll Cardiol*. 2017;*70*:2852-2862.
10. Stone GW. Preliminary data of ABSORB IV trial. Paper presented at TCT 2017, Denver, CO, USA.
11. Tijssen RYG, Kraak RP, Elias J, van Dongen IM, Kalkman DN, Nassif M, Sotomi Y, Asano T, Katagiri Y, Collet C, Piek JJ, Henriques JPS, de Winter RJ, Tijssen JG, Onuma Y, Serruys PW, Wykrzykowska JJ. Implantation techniques (pre-dilatation, sizing, and post-dilatation) and the incidence of scaffold thrombosis and revascularization in lesions treated with an everolimus-eluting bioresorbable vascular scaffold: Insights from the AIDA-trial. *EuroIntervention* 2018;*14*(4):e434-e442.
12. Ormiston JA, Webber B, Ubod B, Darremont O, Webster MW. An independent bench comparison of two bioresorbable drug-eluting coronary scaffolds (absorb and DESolve) with a durable metallic drug-eluting stent (ML8/Xpedition). *EuroIntervention*. 2015;*11*(1):60-67.
13. Schmidt W, Behrens P, Brandt-Wunderlich C, Siewert S, Grabow N, Schmitz KP. In vitro performance investigation of bioresorbable scaffolds – Standard tests for vascular stents and beyond. *Cardiovasc Revasc Med*. 2016;*17*(6):375-383.
14. Everaert B, Wykrzykowska JJ, Koolen J, et al. Recommendations for the use of bioresorbable vascular scaffolds in percutaneous coronary interventions: 2017 revision. *Neth Heart J*. 2017;*25*(7–8):419-428.
15. Fajadet J, Haude M, Joner M, et al. Magmaris preliminary recommendation upon commercial launch: A consensus from the expert panel on 14 April 2016. *EuroIntervention*. 2016;*12*(7):828-833.
16. Haude M, Erbel R, Erne P, et al. Safety and performance of the drug-eluting absorbable metal scaffold (DREAMS) in patients with de novo coronary lesions: 3-Year results of the prospective, multicentre, first-in-man BIOSOLVE-I trial. *EuroIntervention*. 2016;*12*(2):e160-e166.
17. Waksman R, Zumstein P, Pritsch M, et al. Second-generation magnesium scaffold Magmaris: Device design and preclinical evaluation in a porcine coronary artery model. *EuroIntervention*. 2017;*13*(4):440-449.
18. Bennett J, Vanhaverbeke M, Vanden Driessche N, et al. The drug-eluting absorbable magnesium vascular scaffold in complex coronary bifurcations: Insights from an in-vivo multimodality imaging study. *EuroIntervention*. 2017;*13*:2036-2046.

19. Boeder NF, Dörr O, Bauer T, et al. Impact of strut thickness on acute mechanical performance: A comparison study using optical coherence tomography between DESolve 150 and DESolve 100. *Int J Cardiol*. 2017;*246*:74-79.
20. Haude M, Ince H, Abizaid A, et al. Sustained safety and performance of the second-generation drug-eluting absorbable metal scaffold in patients with de novo coronary lesions: 12-Month clinical results and angiographic findings of the BIOSOLVE-II first-in-man trial. *Eur Heart J*. 2016;*37*(35):2701-2709.
21. Haude M, Ince H, Abizaid A, et al. Safety and performance of the second-generation drug-eluting absorbable metal scaffold in patients with de-novo coronary artery lesions (BIOSOLVE-II): 6 Month results of a prospective, multicentre, non-randomised, first-in-man trial. *Lancet*. 2016;*387*(10013):31-39.
22. Waksman R, Prati F, Bruining N, et al. Serial observation of drug-eluting absorbable metal scaffold: Multi-imaging modality assessment. *Circ Cardiovasc Interv*. 2013;*6*(6):644-653.
23. Sotomi Y, Onuma Y, Dijkstra J, et al. Impact of implantation technique and plaque morphology on strut embedment and scaffold expansion of Polylactide Bioresorbable scaffold – Insights from ABSORB Japan trial. *Circ J*. 2016;*80*(11):2317-2326.
24. Tanaka A, Latib A, Kawamoto H, et al. Clinical outcomes of a real-world cohort following bioresorbable vascular scaffold implantation utilising an optimised implantation strategy. *EuroIntervention*. 2017;*12*(14):1730-1737.
25. Sotomi Y, Onuma Y, Collet C, et al. Bioresorbable scaffold: The emerging reality and future directions. *Circ Res*. 2017;*120*(8):1341-1352.
26. Suwannasom P, Sotomi Y, Ishibashi Y, et al. The impact of post-procedural asymmetry, expansion, and eccentricity of bioresorbable everolimus-eluting scaffold and metallic everolimus-eluting stent on clinical outcomes in the ABSORB II trial. *J Am Coll Cardiol Interv*. 2016;*9*(12):1231-1242.
27. Rivero F, Bastante T, Cuesta J, Benedicto A, Restrepo JA, Alfonso F. Treatment of in-stent restenosis with bioresorbable vascular scaffolds: Optical coherence tomography insights. *Can J Cardiol*. 2015;*31*(3):255-259.

How to cite this article: Blachutzik F, Achenbach S, Tröbs M, et al. Effect of non-compliant balloon postdilatation on magnesium-based bioresorbable vascular scaffolds. *Catheter Cardiovasc Interv*. 2018;1–6. https://doi.org/10.1002/ccd.27794

Nr. 6: Major coronary evaginations following implantation of bioresorbable vascular scaffolds – Clinical and OCT characteristics

Cardiovascular Revascularization Medicine 20 (2019) 485–491

Contents lists available at ScienceDirect

Cardiovascular Revascularization Medicine

Major coronary evaginations following implantation of bioresorbable vascular scaffolds – Clinical and OCT characteristics

Florian Blachutzik [a,b,*], Stephan Achenbach [b], Mohamed Marwan [b], Jens Röther [b], Monique Tröbs [b], Reinhard Schneider [b], Holger Nef [a], Melissa Weissner [c,d], Christian Schlundt [b]

[a] Justus-Liebig University Giessen, Medizinische Klinik 1, Department of Cardiology, Giessen, Germany
[b] Friedrich-Alexander Universität (FAU) Erlangen-Nürnberg, University Hospital Erlangen, Department of Cardiology, Erlangen, Germany
[c] Zentrum für Kardiologie, University Hospital Mainz, Mainz, Germany
[d] German Center for Cardiac and Vascular Research (DZHK), Standort Rhein-Main, Mainz, Germany

ARTICLE INFO

Article history:
Received 27 April 2018
Received in revised form 27 July 2018
Accepted 1 August 2018

Keywords:
Percutaneous coronary intervention
Optical coherence tomography
Bioresorbable vascular scaffolds

ABSTRACT

Background: Coronary evaginations can occur after implantation of bioresorbable vascular scaffolds (BRS) and may be associated with scaffold thrombosis. Aim of this study was to clarify the clinical manifestation, extent and time course of coronary artery remodeling in vessel segments that develop angiographically detectable evaginations following BRS implantation through optical coherence tomography (OCT) analysis.
Methods: In 8 patients, 10 BRS (Absorb, Abbott Vascular, Santa Clara, CA, USA) which displayed coronary evaginations in clinically driven late invasive coronary angiograms were identified and findings were compared to 10 BRS in 8 patients without coronary evaginations. Vessel and device geometry was analyzed in serial OCT cross-sections at a spacing of 200 μm. Measured BRS dimensions were normalized to the reference vessel size at implantation.
Results: In OCT, major evaginations on average affected 24 ± 19% of the scaffold length. Scaffolds with major evaginations had a significantly larger lumen area than scaffolds without evaginations (mean normalized lumen area 1.19 ± 0.58 vs. 0.77 ± 0.38; $p < 0.001$), and also displayed a significantly larger scaffold area (mean normalized scaffold area: 1.36 ± 0.6 vs. 1.13 ± 0.43; $p < 0.001$), and scaffold diameter (mean normalized scaffold diameter: 1.17 ± 0.33 vs.1.04 ± 0.19; $p < 0.001$). Lumen area ($r = 0.47$; $p < 0.001$), scaffold area ($r = 0.52$; $p < 0.001$), and scaffold diameter ($r = 0.74$; $p < 0.001$) in the evagination group were positively correlated to the time since scaffold implantation.
Conclusion: Coronary evaginations following BRS implantation are associated with an increased scaffold area, indicating that the scaffold follows the outward remodeling of the artery. The process affects the entire scaffold length and seems to be continuously progressing following implantation.

1. Introduction

Bioresorbable vascular scaffolds (BRS) have been introduced into clinical practice in 2012. In contrast to conventional metallic stents, BRS are resorbed over the course of time and thus thought to restore vessel pulsatility, cyclical strain, physiological shear stress, and mechanotransduction [1,2]. Recent findings suggest that coronary evaginations may occur after implantation of BRS [3]. Coronary evaginations had initially been described as a specific optical coherence tomography (OCT) finding after implantation of first generation drug-eluting stents (DES). They have been assumed to be associated to vessel injury at implantation, display positive remodeling of the vessel wall during further course and correlate with uncovered stent struts, strut fractures and malapposition [4–7]. Coronary evaginations disturb laminar flow and have been reported as possible risk factor for late stent thrombosis [8,9]. Evaginations are nearly absent in newer generation DES, which may contribute to their lower rate of late stent thrombosis in comparison to first generation DES [4]. Recent publications report cases of coronary aneurysms following BRS implantation [10–12]. We hypothesize that these cases may be the end stage of evaginations in which the scaffold, due to loss of mechanical integrity, has expanded to follow extreme outward remodeling of the vessel wall. In this study, we therefore analyze clinical and morphological features of major evaginations associated with BRS and, to elucidate the dynamics of vessel remodeling and scaffold dimensions in patients who develop evaginations, we report the relationship of coronary evaginations, vessel dimensions, and scaffold geometry, as well as their development over time.

* Corresponding author at: University Hospital Giessen, Department of Cardiology, Klinikstrasse 33, 35392 Giessen, Germany.
E-mail address: florian.blachutzik@innere.med.uni-giessen.de (F. Blachutzik).

https://doi.org/10.1016/j.carrev.2018.08.001
1553-8389/

2. Materials and methods

2.1. Study design and population

We retrospectively analyzed all patients who underwent repeat coronary angiography after prior PCI with implantation of at least one BRS in our department between December 2014 and July 2016. All angiograms were clinically driven. In 8 out of 94 patients, evaginations were identified angiographically because of peri-stent contrast staining in the segment of previously implanted BRS and were confirmed by OCT. For the purpose of further analysis, evaginations were defined as "present" in OCT when the vessel contour extended beyond the outer border of well-apposed struts (see Fig. 1) [3]. If evaginations were identified angiographically, performance of OCT was obligatory per institutional protocol. In all other cases, performance of OCT was at the discretion of the operator. In 20 out of the 86 patients without coronary evaginations at the time of repeat angiography OCT was performed. 8 of these 20 patients, matched for the time since BRS implantation, served as control group. Baseline characteristics of the patients, including medical history as well as clinical, angiographic, and procedural data, were collected from the department's database.

2.2. Percutaneous coronary intervention

Baseline PCI with implantation of a BRS had been performed via transradial or transfemoral approach using 6 French guiding catheters and standard coronary guidewires (Runthrough™, Terumo Europe NV, Leuven, Belgium). All patients had received intravenous heparin and intracoronary nitrates. Pre-dilatation with a non-compliant balloon (NC balloon) had been performed in all lesions, with balloon size selected based on visual angiographic estimation to achieve a 1:1 ratio of vessel and balloon diameter. Lesions had been treated with everolimus-eluting BRS (Absorb BVS™, Abbott Vascular, Santa Clara, CA, USA). Deployment of Absorb BVS™ had been performed with an initial pressure of 2 bar and increasing pressure in increments of 2 bar every 10 s until fully deployed (minimum 8 bar). Further medication, techniques, and equipment for PCI were used in accordance with current clinical guidelines and were left to the responsible physician's discretion. NC balloon (NC Trek™, Abbott Vascular, Santa Clara, CA, USA) post-dilatation at a pressure of 16 bar was mandatory per institutional protocol and had been performed in all lesions.

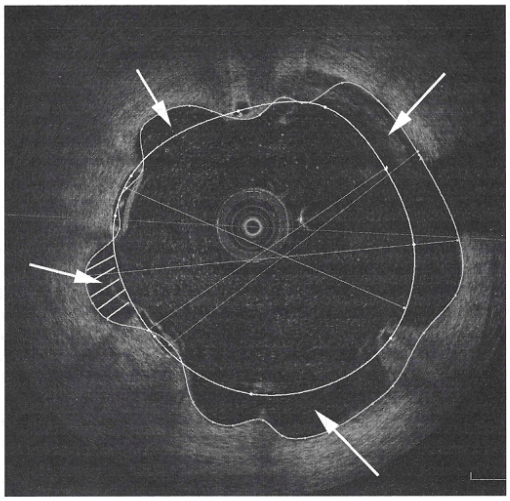

Fig. 1. Analysis of OCT cross section. Absorb BVS™ showing peri-scaffold evaginations (white arrows). The lumen area is contoured in green, the scaffold area is contoured in white. The area of one evagination is hatched in white. (For interpretation of the references to colour in this figure legend, the reader is referred to the web version of this article.)

2.3. Optical coherence tomography image acquisition

At follow-up, OCT was performed as part of the diagnostic angiogram and before any PCI. A 2.7 French Dragonfly™ intravascular imaging catheter (St. Jude Medical, Saint Paul, MN, USA) was used with a mechanical pullback speed of 18 mm/s over a distance of 54 mm. During pullback, 25 ml contrast agent (Ultravist™ 370, Bayer AG, Leverkusen, Germany) were injected at 4 ml/s with a maximum pressure of 400 psi using machine injection (Liebel-Flarsheim 903300 G, Liebel-Flarsheim Co, Cincinnati, OH, USA).

2.4. Optical coherence tomography image analysis

All OCT data sets were digitally recorded, stored, and analyzed. OCT image analysis was performed offline using the ILUMIEN™ OPTIS™ system (St. Jude Medical, Saint Paul, MN, USA) with manual calibration before each measurement. OCT cross sections were analyzed over the complete length of implanted BRS with a spacing of 200 μm. Malapposition was defined as any visible malapposition between the abluminal strut edge and the vessel wall. Strut fractures were defined as struts lying isolated in the lumen or the presence of one strut on top of another. Evaginations were defined as "present" when the vessel contour extended beyond the outer border of well-apposed struts [3]. Maximum evagination depth was measured between the direct connection line of the outer edge of two adjacent struts and the vessel wall. The area between the vessel wall and the above-mentioned connection line was measured by manual tracing and represented the evagination area (see Fig. 1). Evaginations can be differentiated from neointimal coverage of malapposed struts with abluminal connecting bridge since evaginations are usually visible all around the vessel circumference. Additionally, scaffold struts next to evaginations are usually well embedded into the vessel wall, whereas malapposed struts usually only have a thin layer of neointimal coverage. Eccentricity index was defined as the ratio between the minimum and maximum scaffold diameter. Lumen area was traced by following the vessel's intima. Scaffold area was traced by connecting the abluminal edges of the scaffold struts. OCT analysis was performed in accordance with previous publications [3,13]. All diameters and lumen or scaffold areas were normalized to the reference vessel size at implantation as determined by quantitative coronary angiography (QCA). Reference vessel size at baseline was obtained by QCA. Mean reference vessel size was calculated over the complete length of the coronary segment to be treated. Normalization was performed by dividing lumen and scaffold dimensions at follow-up through reference vessel size at baseline.

2.5. Statistical analysis

Continuous variables are summarized as mean ± standard deviation; categorical variables are provided as n (%). The Kolmogorov-Smirnov test was performed to test for non-parametric distribution. To test for statistical differences between two groups for comparison of continuous variables, either a t-test for unpaired samples (parametric distribution) or a Mann-Whitney-U test (non-parametric distribution) was used. For categorical variables, a Chi-squared or a Fisher's exact test was carried out. The Pearson correlation coefficient was calculated to analyze linear relationships. Statistical analyses were performed using SPSS version 21.0 (IBM SPSS Statistics, IBM Corporation, Armonk, New York, USA). A two-sided $p < 0.05$ was considered significant.

3. Results

3.1. Patients and clinical parameters

16 patients, 8 with and 8 without coronary evaginations after BRS implantation were included in this study. In one patient out of the evagination group, peri-scaffold evaginations were present in two BRS implanted in different vessels, in another patient out of the evagination group, peri-scaffold evaginations were present in two BRS implanted in the same vessel. The mean interval since BRS implantation was 17 ± 9 months for the evagination group and 18 ± 11 months for the control group. In all patients, follow-up had been clinically driven. Antiplatelet therapy with acetylsalicylic acid plus clopidogrel, ticagrelor or prasugrel had been prescribed for 12 months after the initial BRS implantation. There were no significant differences between the groups regarding baseline characteristics. For detailed patient characteristics see Table 1.

At follow-up, one patient out of the control group presented with non-ST-segment elevation myocardial infarction (NSTEMI), the other 7 patients because of stable angina. 5 of these 7 patients had a proven myocardial ischemia (stress echocardiography, SPECT myocardial perfusion or adenosine stress cardiac magnetic resonance). In the evagination group, one patient presented with NSTEMI, 7 patients presented with stable angina. 4 of these 7 patients had ischemia in noninvasive testing. In 10 of 16 patients, PCI was performed. In 5 of 8 patients in the evagination group and in 3 of 8 patients in the control group, this concerned the vessel in which a BRS had been implanted at baseline ($p = 0.62$). The index lesion was revascularized in 3 of 8 patients in the evagination group and in 3 of 8 patients in the control group ($p > 0.99$), in 2 cases DES and in 1 case Bare-metal stents (BMS) were implanted within the scaffold. In the evagination group, 2 of 3 stent implantations were performed specifically as an attempt to treat evaginations and 1 of 3 due to in-scaffold restenosis. In the control group, all 3 stent implantations were performed due to in-scaffold restenosis. For detailed outcome results see Table 2.

3.2. Baseline percutaneous coronary intervention

NC balloon pre-dilatation and post-dilatation had been performed in all cases during baseline implantation of a bioresorbable scaffold. Mean NC balloon diameter for pre-dilatation was 2.9 ± 0.5 mm. Mean scaffold diameter was 3.2 ± 0.4 mm in the evagination group and 3.1 ± 0.4 mm in the control group ($p = 0.92$). Mean NC balloon diameter for post-dilatation was 3.1 ± 1.2 mm. Bailout stenting was not necessary in any of the cases. In one patient of the control group, two BRS were implanted overlapping each over using the "marker to marker" method. For detailed procedural characteristics see Table 3.

3.3. Optical coherence tomography data – evagination vs. control group

As an effect of outward vessel expansion, mean lumen area normalized to baseline was significantly larger in BRS with evaginations as compared to BRS in the control group (1.19 ± 0.58 vs. 0.77 ± 0.38; $p < 0.001$). Scaffolds also displayed expansion: mean scaffold area normalized to the baseline value at implantation (1.36 ± 0.60 vs. 1.13 ± 0.43; $p < 0.001$), and scaffold diameter normalized to baseline (1.17 ± 0.33 vs. 1.04 ± 0.19; $p < 0.001$) were significantly larger in the evagination group as compared to the control group. Additionally, strut

Table 1
Patient characteristics.

Variable	All patients ($n = 16$)	Evagination group ($n = 8$)	Control group ($n = 8$)	p-Value
Age (years)	63 ± 7	63 ± 6	63 ± 7	0.93
Male/female	11/5	7/1	4/4	0.28
Body-Mass-Index (kg/m^2)	29.5 ± 7.2	29.4 ± 4.8	29.5 ± 6.6	0.78
Clinical presentation				
Stable angina	11 (69%)	5 (62.5%)	6 (75%)	0.72
Unstable angina	2 (12%)	1 (12.5%)	1 (12.5%)	
Non-ST-segment elevation myocardial infarction	3 (19%)	2 (25%)	1 (12.5%)	
Left ventricular ejection fraction (%)	47 ± 8	46 ± 6	48 ± 9	0.34
Left ventricular ejection fraction <30%	0 (0%)	0 (0%)	0 (0%)	>0.99
Hypertension	10 (63%)	4 (50%)	6 (75%)	0.22
Diabetes	4 (25%)	2 (25%)	2 (25%)	>0.99
Family history	8 (50%)	3 (37.5%)	5 (62.5%)	0.18
Hyperlipidaemia	15 (94%)	7 (87.5%)	8 (100%)	0.84
Active smoking	5 (31%)	3 (37.5%)	2 (25%)	0.74
Previous myocardial infarction	2 (12.5%)	1 (12.5%)	1 (12.5%)	>0.99
Previous percutaneous coronary intervention	5 (31%)	2 (25%)	3 (37.5%)	0.74
Previous coronary bypass surgery	2 (12.5%)	1 (12.5%)	1 (12.5%)	>0.99
Atrial fibrillation	2 (12.5%)	1 (12.5%)	1 (12.5%)	>0.99
Time since scaffold implantation (months)				
Mean	18	17	18	0.84
Minimum	4	4	9	
Maximum	33	33	33	
Target lesion				
Left anterior descending artery	5 (30%)	2 (22%)	3 (37.5%)	0.43
Circumflex artery	6 (35%)	3 (33%)	3 (37.5%)	
Right coronary artery	6 (35%)	4 (45%)	2 (25%)	
Lesion type (ACC/AHA-classification)				
A	0 (0%)	0 (0%)	0 (0%)	0.45
B1	2 (11%)	2 (20%)	0 (0%)	
B2	12 (67%)	7 (70%)	5 (62.5%)	
C	4 (22%)	1 (10%)	3 (37.5%)	
Antiplatelet therapy				
Acetylsalicylic acid	16 (100%)	8 (100%)	8 (100%)	>0.99
Clopidogrel	7 (37.5%)	3 (37.5%)	4 (50%)	0.80
Ticagrelor	6 (37.5%)	3 (37.5%)	3 (37.5%)	>0.99
Prasugrel	3 (25%)	2 (25%)	1 (12.5%)	0.74

Values are mean ± standard deviation or n (%).

Table 2
Outcome ($n = 16$).

Variable	Evagination group ($n = 8$)	Control group ($n = 8$)	p-Value
Clinical presentation			
Stable angina	7/8 (87.5%)	7/8 (87.5%)	>0.99
Non-ST-segment elevation myocardial infarction	1/8 (12.5%)	1/8 (12.5%)	
Target vessel myocardial infarction	1/8 (12.5%)	1/8 (12.5%)	>0.99
Any percutaneous revascularization	7/8 (87.5%)	3/8 (37.5%)	0.12
Target vessel revascularization	5/8 (62.5%)	3/8 (37.5%)	0.62
Target lesion revascularization	3/8 (37.5%)	3/8 (37.5%)	>0.99
Stent implantation over scaffold	3/8 (37.5%)	3/8 (37.5%)	>0.99
Reason for target lesion revascularization			
Evaginations	2/3 (67%)	0/3 (0%)	0.4
In-scaffold re-stenosis	1/3 (33%)	3/3 (100%)	0.14
Type of stent implanted over scaffold			
Bare-metal stent	1/3 (33%)	0/3 (0%)	0.82
Drug-eluting stent	2/3 (67%)	3/3 (100%)	0.79

Values are n (%).

fractures (0.08 ± 0.11 vs. 0.02 ± 0.18; $p = 0.03$) and malapposed struts (0.13 ± 0.24 vs. 0.03 ± 0.07; $p = 0.006$) were detected significantly more frequently in the evagination group. For detailed results see Table 4.

3.4. Optical coherence tomography data – BRS with evaginations

In the evagination group, peri-scaffold evaginations were visible over $24 \pm 19\%$ of the complete BRS length (minimum: 12%, maximum: 59%). Cross-sections with evaginations had a mean evagination area of 0.96 ± 1 mm^2 and a mean evagination depth of 0.48 ± 0.2 mm. Lumen area normalized to baseline was significantly larger in segments affected by evaginations as compared to those without (1.38 ± 0.49 vs. 1.13 ± 0.59; $p < 0.001$). Scaffold expansion was observed along the entire length of BRS affected by evaginations: scaffold diameter (1.18 ± 0.33 vs. 1.16 ± 0.20, $p = 0.33$) and consecutively, scaffold area normalized to baseline (1.37 ± 0.45 vs. 1.36 ± 0.64; $p = 0.41$), were only very slightly larger in areas with coronary evagination as compared to areas without. The frequency of strut fractures (0.23 ± 0.31 per cross-section vs. 0.07 ± 0.14 per cross-section; $p = 0.02$) as well as of malapposed struts (0.41 ± 0.36 vs. 0.13 ± 0.07 per cross-section; $p = 0.003$) was significantly higher in evagination areas. No significant differences regarding eccentricity index were observed between areas with and without evaginations. For detailed results see also Table 5.

Table 3
Procedural data of the index PCI.

Variable	All patients ($n = 16$)	Evagination group ($n = 8$)	Control group ($n = 8$)	p-Value
Scaffolds	20	10	10	>0.99
Non-compliant balloon pre-dilatation				
Performed	20 (100%)	10 (100%)	10 (100%)	>0.99
Balloon length (mm)	20 ± 6	19 ± 5	20 ± 6	0.83
Balloon diameter (mm)	2.9 ± 0.5	3 ± 0.4	2.8 ± 0.4	0.35
Inflation pressure (bar)	15 ± 4	15 ± 3	14 ± 4	0.74
Scaffold implantation				
Scaffold length (mm)	20 ± 7	21 ± 7	20 ± 6	0.65
Scaffold diameter (mm)	3.2 ± 0.4	3.2 ± 0.4	3.1 ± 0.4	0.92
Inflation pressure (bar)	12 ± 2	12 ± 2	11 ± 3	0.47
Non-compliant balloon post-dilatation				
Performed	20 (100%)	10 (100%)	10 (100%)	>0.99
Balloon length (mm)	14 ± 4	14 ± 3	14 ± 4	0.89
Balloon diameter (mm)	3.1 ± 1.2	3.2 ± 0.3	3.1 ± 1.3	0.54
Inflation pressure (bar)	16 ± 6	17 ± 4	16 ± 8	0.34

Values are mean ± standard deviation or n (%).

Table 4
Optical coherence tomography at follow-up: evagination vs. control group (all values normalized to nominal scaffold dimensions at implantation).

	Evagination group	Control group	p-Value
Mean scaffold area (mm^2)	15.8 ± 3.3	14.3 ± 3.4	0.09
Mean lumen area (mm^2)	16.3 ± 2.5	13.5 ± 3.1	0.03
Mean scaffold diameter (mm)	3.3 ± 0.5	3.1 ± 0.4	0.24
Normalized scaffold area	1.36 ± 0.60	1.13 ± 0.43	<0.001
Normalized lumen area	1.19 ± 0.58	0.77 ± 0.38	<0.001
Normalized scaffold diameter	1.17 ± 0.33	1.04 ± 0.19	<0.001
Mean eccentricity index	0.85 ± 0.05	0.85 ± 0.07	0.76
Sum of struts (n)	1242 ± 120	1326 ± 366	0.41
Strut fractures per frame	0.08 ± 0.11	0.02 ± 0.18	0.03
Malapposed struts per frame	0.13 ± 0.24	0.03 ± 0.07	0.006
Proximal edge dissection (n)	0	0	>0.99
Distal edge dissection (n)	0	0	>0.99

Values are mean ± standard deviation or n (%).

In BRS with evaginations, mean lumen area (Pearson correlation coefficient: 0.47; $p < 0.001$), scaffold area (Pearson correlation coefficient: 0.52; $p < 0.001$), and scaffold diameter (Pearson correlation coefficient: 0.74; $p < 0.001$) were significantly correlated with the time since scaffold implantation. Similar correlation could not be observed for the number of evaginations, evagination area or evagination depth. This strongly suggests that evaginations are progressive over time and that vessel and scaffold expansion (along the entire length of the scaffold) follow the process. In the control group, there was no significant correlation between lumen area, scaffold area or scaffold diameter and the time since scaffold implantation (see also Fig. 2). For detailed results see Table 6.

4. Discussion

BRS with evaginations are associated with significantly larger mean scaffold areas and scaffold diameters than BRS which do not develop evaginations. In addition, BRS with evaginations are associated with increased rates of strut fracture and malapposition as compared to those without.

One major finding of this study is that while peri-scaffold evaginations occur locally and not over the complete length of an affected scaffold, vessel and scaffold expansion occur not only in the segments affected by evaginations, but along the entire length of the implanted scaffold. Some extent of vessel remodeling after BRS implantation has been described in previous studies. However, this typically does not result in a significant lumen gain as compared to baseline lumen or scaffold dimensions [2,14]. As a second major finding, the enlargements of scaffold area, scaffold diameter, and lumen area in BRS with major

Table 5
Optical coherence tomography at follow-up: comparison of segments with and without evaginations within affected scaffolds.

	Scaffold segments with evaginations	Scaffold segments without evaginations	p-Value
Normalized scaffold area	1.37 ± 0.45	1.36 ± 0.64	0.41
Normalized lumen area	1.38 ± 0.49	1.13 ± 0.59	<0.001
Normalized scaffold diameter	1.18 ± 0.37	1.16 ± 0.20	0.33
Mean eccentricity index	0.86 ± 0.07	0.86 ± 0.08	0.58
Sum of struts (n)	202 ± 61	1023 ± 366	<0.001
Length (mm)	3.8 ± 1.6	16.7 ± 4.1	<0.001
Strut fractures per frame	0.23 ± 0.31	0.04 ± 0.19	0.02
Malapposed struts per frame	0.41 ± 0.36	0.13 ± 0.07	0.003
Proximal edge dissection (n)	0	0	>0.99
Distal edge dissection (n)	0	0	>0.99
Evagination area per cross-section (mm^2)	0.96 ± 1		
Evaginations per cross-section (n)	1.49 ± 0.76		
Evagination depth (mm)	0.48 ± 0.2		

Values are mean ± standard deviation or n (%).

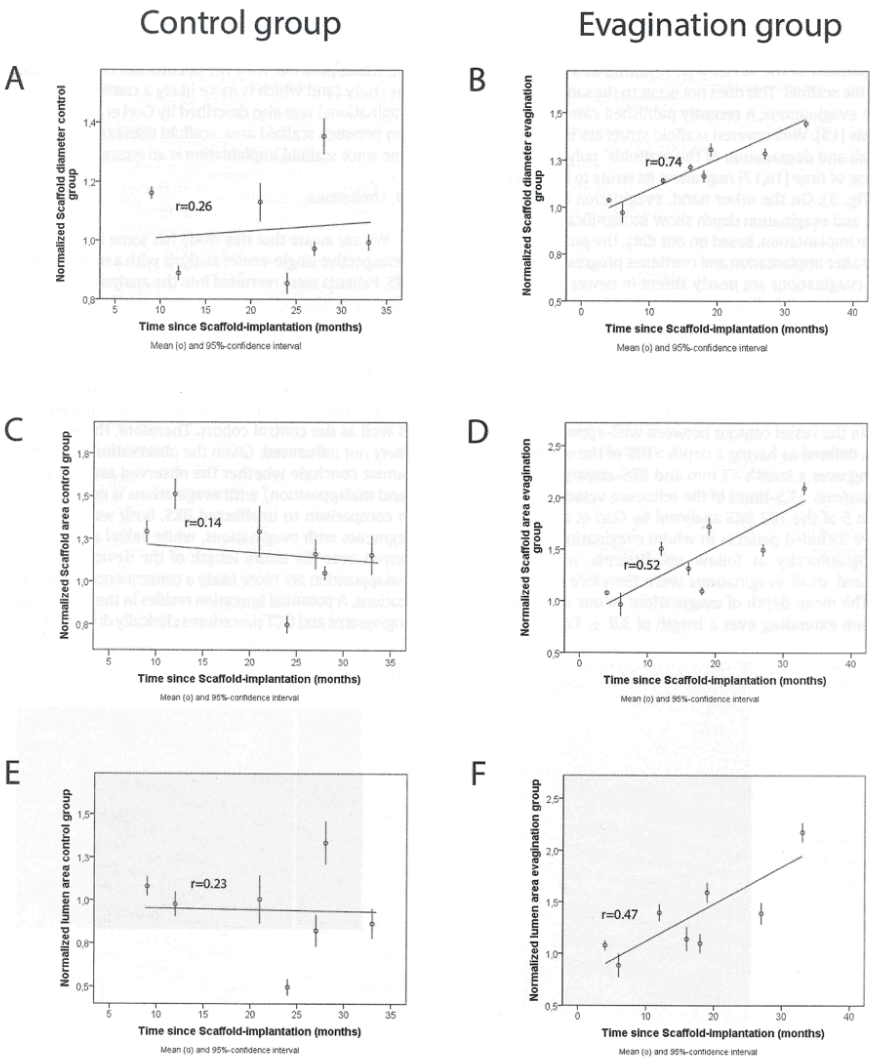

Fig. 2. Correlation of scaffold and vessel dimensions with the time since implantation. A and B. Normalized scaffold diameters relative to the time since scaffold implantation for the control (A) and evagination group (B). C and D. Normalized scaffold area relative to the time since scaffold implantation for the control (C) and evagination group (D). E and F. Normalized lumen area relative to the time since scaffold implantation for the control (D) and evagination group (E). Values are mean (o) and 95%-confidence interval. Line of best fit is shown for each graph; r = Pearson correlation coefficient.

Table 6
Correlation in the course of time since scaffold implantation.

	Evagination group		Control group	
	Pearson correlation coefficient	p-Value	Pearson correlation coefficient	p-Value
Lumen area	0.47	<0.001	0.23	0.54
Scaffold area	0.52	<0.001	0.14	0.32
Scaffold diameter	0.74	<0.001	0.26	0.63
Mean eccentricity index	0.08	0.22	0.13	0.72
Evaginations per cross-section (n)	0.03	0.60	0.23	0.43
Evagination area per cross-section (mm^2)	0.064	0.32	0.06	0.14
Evagination depth	0.025	0.701	0.32	0.87

evaginations significantly correlate with the time since scaffold implantation, which suggests that the process is continuous and progressive, with overexpansion of the vessel wall resulting in a consecutive enlargement of the scaffold. This does not occur to the same extent in scaffolds without evaginations. A recently published case report supports this hypothesis [15]. Well covered scaffold struts are incorporated into the vessel wall and degradation of the scaffolds´ poly-lactic structure over the course of time [16,17] may allow its struts to follow vessel enlargement (Fig. 3). On the other hand, evagination area, number of evaginations, and evagination depth show no significant correlation to the time since implantation. Based on our data, the process is likely initiated shortly after implantation and continues progressively thereafter.

Coronary evaginations are nearly absent in newer-generation DES, but frequently occurred in first-generation DES [4]. Gori et al. recently analyzed 102 BRS 12 months after implantation using OCT and reported that some extent of coronary evagination is present in about 54% of BRS [3]. However, Gori et al. performed OCT as part of a routine BRS follow-up protocol and used a definition of "evaginations" at a substantially lower threshold than we did. They defined evaginations as any "hollow" or outpouch in the vessel contour between well-apposed struts. Major evaginations, defined as having a depth >10% of the scaffold diameter and extending over a length >3 mm and BRS-aneurysms, defined as in-scaffold diameter >1.5-times of the reference vessel diameter, were only found in 5 of the 102 BRS analyzed by Gori et al. In contrast to this study, we included patients in whom evaginations had been detected angiographically at follow up. Patients with only minor outpouches and small evaginations were therefore not included in our cohort. The mean depth of evaginations in our study hence was 0.48 ± 0.2 mm extending over a length of 3.8 ± 1.6 mm. All of the BRS in our study fulfilled the criteria for the presence of major evaginations as defined by Gori et al. The association between strut fractures and malapposition with the occurrence of evaginations we found in our study (and which is more likely a consequence than a cause of the evaginations) was also described by Gori et al. Importantly, the correlation between scaffold area, scaffold diameter, and lumen area with the time since scaffold implantation is an entirely new finding of our study.

4.1. Limitations

We are aware that this study has some important limitations. It is a retrospective single-center analysis with a small number of patients and BRS. Patients were recruited into the analysis if evaginations were identified by angiography, which substantially favours large evaginations. OCT had not been performed in context with the baseline implantation. Therefore, reference vessel dimensions as determined by QCA at implantation were taken as baseline values for lumen and scaffold area. Baseline OCT would have been a better comparator. However, this systematic limitation affects both the group of patients with evaginations as well as the control cohort. Therefore, the main study findings are likely not influenced. Given the observational nature of our study, we cannot conclude whether the observed association of strut fractures (and malapposition) with evaginations is one of cause or effect. Since, in comparison to unaffected BRS, both were more frequent only in segments with evaginations, while vessel and scaffold expansion occurred over the entire length of the device, both strut fracture and malapposition are more likely a consequence of than a reason for evaginations. A potential limitation resides in the fact that with all follow-up angiograms and OCT procedures clinically driven, there is a bias towards

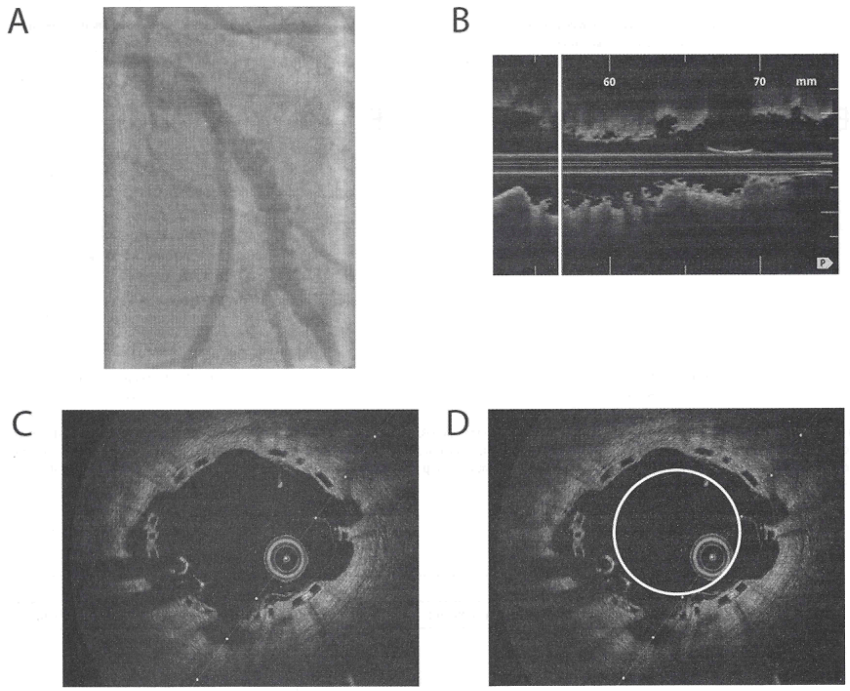

Fig. 3. Absorb BVS™ showing major coronary evaginations. A. Coronary angiogram of a 3.0/28 mm Absorb BVS™ 33 months after implantation into the circumflex artery. Evaginations are marked in white. B shows the longitudinal section of the affected BRS in the OCT. C shows an OCT cross-section (position: white mark in B) of the BRS with evaginations. In panel D the nominal scaffold size at implantation is indicated in white. Mean BRS-diameter (4.16 mm) is about 40% larger as compared to nominal size at implantation (3.0 mm).

the presence of in-scaffold restenosis in the control group. Our comparisons therefore are not comparisons to a "normal" control group. Finally, our analysis of time from baseline and extent of vessel enlargement rests on individual patients investigated at various intervals, and not the same patients imaged repetitively. However, effects are strong enough to at least be considered hypothesis-generating. Recently published reports of single cases support our findings [10–12,15].

4.2. Clinical implications

Coronary evaginations disturb laminar flow and may constitute a risk factor for late stent or scaffold thrombosis [8,9]. With some trials and analyses suggesting a slightly higher rate of scaffold thrombosis and target vessel major adverse cardiac events as compared to DES [18–23], coronary evaginations may be part of the underlying reason. Additionally, it is noteworthy that the observed overexpansion of the vessel may pose a particular challenge for future PCI of these segments, since in some cases diameters may grow too large to be treated with available devices.

Specific clinical and therapeutic implications of peri-scaffold evaginations and especially of the observed vessel overexpansion over the course of time will need further investigation.

5. Conclusion

Coronary evaginations as a consequence of PCI with bioresorbable vascular scaffolds are associated with progressive lumen enlargement that affects the entire scaffold length. Areas with evaginations are associated with higher rates of strut fracture and malapposed struts as compared to normal segments. The area of scaffolds affected by evaginations increases over time, suggesting that continuous degradation of the BRS allows its struts to follow the vascular expansion. "Coronary aneurysms" observed in patients late after BRS implantation may be a consequence of progressive vessel enlargement, followed by scaffold expansion, in the context of coronary evaginations.

Declaration of interests

None.

References

[1] Iqbal J, Onuma Y, Ormiston J, Abizaid A, Waksman R, Serruys P. Bioresorbable scaffolds: rationale, current status, challenges, and future. Eur Heart J 2014;35(12):765–76.
[2] Simsek C, Karanasos A, Magro M, et al. Long-term invasive follow-up of the everolimus-eluting bioresorbable vascular scaffold: five-year results of multiple invasive imaging modalities. EuroIntervention 2016;11(9):996–1003.
[3] Gori T, Jansen T, Weissner M, et al. Coronary evaginations and peri-scaffold aneurysms following implantation of bioresorbable scaffolds: incidence, outcome, and optical coherence tomography analysis of possible mechanisms. Eur Heart J 2016;37(26):2040–9.
[4] Radu MD, Räber L, Kalesan B, et al. Coronary evaginations are associated with positive vessel remodelling and are nearly absent following implantation of newer-generation drug-eluting stents: an optical coherence tomography and intravascular ultrasound study. Eur Heart J 2014;35(12):795–807.
[5] Joner M, Finn AV, Farb A, et al. Pathology of drug-eluting stents in humans: delayed healing and late thrombotic risk. J Am Coll Cardiol 2006;48(1):193–202.
[6] Cook S, Windecker S. Early stent thrombosis: past, present, and future. Circulation 2009;119(5):657–9.
[7] Guagliumi G, Sirbu V, Musumeci G, et al. Examination of the in vivo mechanisms of late drug-eluting stent thrombosis: findings from optical coherence tomography and intravascular ultrasound imaging. J Am Coll Cardiol Intv 2012;5(1):12–20.
[8] Räber L, Baumgartner S, Garcia-Garcia HM, et al. Long-term vascular healing in response to sirolimus- and paclitaxel-eluting stents: an optical coherence tomography study. J Am Coll Cardiol Intv 2012;5(9):946–57.
[9] Radu MD, Pfenniger A, Räber L, et al. Flow disturbances in stent-related coronary evaginations: a computational fluid-dynamic simulation study. EuroIntervention 2014;10(1):113–23.
[10] Cortese B, Silva Orrego P, Virmani R. Late coronary BVS malapposition and aneurysm: a time for appraisal. Catheter Cardiovasc Interv 2015;86(4):678–81.
[11] Timmers L, Lim YC, Tan HC, Low AF. Coronary aneurysm without malapposition after bioresorbable vascular scaffold implantation. EuroIntervention 2016;12(1):60.
[12] O'Gallagher K, Nerla R, Hill J, Byrne J. Acquired coronary artery aneurysm following treatment with bioresorbable vascular scaffolds. EuroIntervention 2016;12(9):1174.
[13] Gori T, Schulz E, Hink U, et al. Clinical, angiographic, functional, and imaging outcomes 12 months after implantation of drug-eluting bioresorbable vascular scaffolds in acute coronary syndromes. J Am Coll Cardiol Intv 2015;8(6):770–7.
[14] Diletti R, Farooq V, Girasis C, et al. Clinical and intravascular imaging outcomes at 1 and 2 years after implantation of absorb everolimus eluting bioresorbable vascular scaffolds in small vessels. Late lumen enlargement: does bioresorption matter with small vessel size? Insight from the ABSORB cohort B trial. Heart 2013;99(2):98–105.
[15] Nakatani S, Ishibashi Y, Suwannasom P, et al. Development and receding of a coronary artery aneurysm after implantation of a fully bioresorbable scaffold. Circulation 2015;131(8):764–7.
[16] Otsuka F, Pacheco E, Perkins LE, et al. Long-term safety of an everolimus-eluting bioresorbable vascular scaffold and the cobalt-chromium XIENCE V stent in a porcine coronary artery model. Circ Cardiovasc Interv 2014;7(3):330–42.
[17] Gomez-Lara J, Brugaletta S, Diletti R, et al. A comparative assessment by optical coherence tomography of the performance of the first and second generation of the everolimus-eluting bioresorbable vascular scaffolds. Eur Heart J 2011;32(3):294–304.
[18] Tröbs M, Achenbach S, Röther J, Klinghammer L, Schlundt C. Bioresorbable vascular scaffold thrombosis in a consecutive cohort of 550 patients. Catheter Cardiovasc Interv 2016. https://doi.org/10.1002/ccd.26569 [Epub ahead of print].
[19] Brugaletta S, Gori T, Low AF, et al. Absorb bioresorbable vascular scaffold versus everolimus-eluting metallic stent in ST-segment elevation myocardial infarction: 1-year results of a propensity score matching comparison: the BVS-EXAMINATION Study (bioresorbable vascular scaffold-a clinical evaluation of everolimus eluting coronary stents in the treatment of patients with ST-segment elevation myocardial infarction). J Am Coll Cardiol Intv 2015;8(1 Pt B):189–97.
[20] Gori T, Schulz E, Münzel T. Immediate, acute, and subacute thrombosis due to incomplete expansion of bioresorbable scaffolds. J Am Coll Cardiol Intv 2014;7(10):1194–5.
[21] Mukete BN, van der Heijden LC, Tandjung K, et al. Safety and efficacy of everolimus-eluting bioresorbable vascular scaffolds versus durable polymer everolimus-eluting metallic stents assessed at 1-year follow-up: a systematic review and meta-analysis of studies. Int J Cardiol 2016;221:1087–94.
[22] Lipinski MJ, Escarcega RO, Baker NC, et al. Scaffold thrombosis after percutaneous coronary intervention with ABSORB bioresorbable vascular scaffold: a systematic review and meta-analysis. J Am Coll Cardiol Intv 2016;9(1):12–24.
[23] Cassese S, Byrne RA, Ndrepepa G, et al. Everolimus-eluting bioresorbable vascular scaffolds versus everolimus-eluting metallic stents: a meta-analysis of randomised controlled trials. Lancet 2016;387(10018):537–44.

Nr. 7: Safety and effectiveness of coronary intravascular lithotripsy in eccentric calcified coronary lesions: a patient-level pooled analysis from the Disrupt CAD I and CAD II studies

Clinical Research in Cardiology
https://doi.org/10.1007/s00392-020-01737-3

ORIGINAL PAPER

Safety and effectiveness of coronary intravascular lithotripsy in eccentric calcified coronary lesions: a patient-level pooled analysis from the Disrupt CAD I and CAD II Studies

Florian Blachutzik[1] · Benjamin Honton[2] · Javier Escaned[3] · Jonathan M. Hill[4] · Nikos Werner[5] · Adrian P. Banning[6] · Alexandra J. Lansky[7] · Sophia Schlattner[1] · Bernard De Bruyne[8] · Carlo Di Mario[9] · Oliver Dörr[1] · Christian Hamm[1] · Holger M. Nef[1]

Received: 2 July 2020 / Accepted: 21 August 2020

Abstract

Background The aim of this study was to assess the safety and effectiveness of intravascular lithotripsy (IVL) in treating eccentric calcified coronary lesions.

Methods Between December 2015 and March 2019, 180 patients were enrolled in the Disrupt CAD I and CAD II studies across 19 sites in 10 countries. Patient-level data were pooled from these two studies ($n = 180$), within which 47 eccentric lesions (26%) and 133 concentric lesions were identified.

Results Clinical success, defined as residual stenosis < 50% after stenting and no in-hospital MACE, was similar between the eccentric and concentric cohorts (93.6% vs. 93.2%, $p = 1.0$). There were no perforations, abrupt closure, slow flow or no reflow events observed in either group, and there were low rates of flow-limiting dissections (Grade D–F: 0% eccentric, 1.7% concentric; $p = 0.54$). Final acute gain and percent residual stenosis were similar between the two groups. Final residual stenosis of 8.6 ± 9.8% in eccentric and 10.0 ± 9.0% ($p = 0.56$) in concentric stenosis confirms the significant effect of IVL in calcified coronary lesions.

Conclusion In this first report from a pooled patient-level analysis of coronary IVL from the Disrupt CAD I and CAD II studies, IVL use was associated with consistent improvement in procedural and clinical outcomes in both eccentric and concentric calcified lesions.

Keywords Lithotripsy · Clinical research · Calcified lesions · Percutaneous coronary intervention

✉ Florian Blachutzik
florian.blachutzik@innere.med.uni-giessen.de

[1] Department of Cardiology, Medical Clinic I, University Hospital Giessen, Justus Liebig University Giessen, Klinikstrasse 33, 35392 Giessen, Germany

[2] Clinique Pasteur, Toulouse, France

[3] Hospital Clínico San Carlos IDISSC, Complutense University of Madrid, Madrid, Spain

[4] King's College Hospital, London, UK

[5] Krankenhaus der Barmherzigen Brüder Trier, Trier, Germany

[6] Department of Cardiology, Oxford University Hospitals, Oxford, UK

[7] Yale University Medical Center, New Haven, USA

[8] Department of Cardiology, Cardiovascular Research Centre, OLV Hospital, Aalst, Belgium

[9] Structural Interventional Cardiology, Careggi University Hospital, Florence, Italy

Introduction

Severe calcification of coronary stenoses still provides a major challenge for percutaneous coronary intervention (PCI). To avoid a sub-optimal clinical outcome, it is important to achieve sufficient luminal gain during lesion preparation prior to stent implantation [1, 2]. Besides the risk of impaired stent expansion, severe coronary calcification may also lead to sub-optimal PCI outcomes by limiting lesion crossing, altering drug elution kinetics, and interfering with optimal stent expansion [3–7].

Intravascular lithotripsy (IVL) has been recently introduced to modify calcified coronary plaques and is useful in overcoming some of the limitations of the more commonly used techniques, e.g., percutaneous transluminal coronary angioplasty (PTCA) with non-compliant (NC) balloons, cutting-/scoring-balloons, and rotational atherectomy (RA). NC

Published online: 18 September 2020

balloon dilatation, even with high pressure, is often insufficient to apply the necessary force for disrupting calcifications. Due to the eccentricity of calcified lesions, balloon dilatation often results in disruption or dissection of healthy intima or fibrous plaques rather than modification of calcified segments within the artery [8]. Cutting and scoring balloons, though able to debulk the lesion more intensely than NC balloons suffer from the same limitation. Even rotational or orbital atherectomy (OA), the most effective techniques for modification of calcified plaques available prior to IVL, are limited due to guidewire bias, which may result in inhomogeneous ablation leaving significant areas of the calcified plaques unmodified, particularly in eccentric lesions [9]. Additionally, periprocedural complications including slow-/no-flow, coronary perforation, periprocedural myocardial infarction occur more frequently with atherectomy techniques as compared to balloon techniques [10, 11].

IVL catheters are equipped with emitters that deliver pulsatile sonic pressure waves circumferentially to the vessel wall. IVL catheters are equipped with emitters along with the balloon that delivers pulsatile shockwaves to the surrounding plaque after activation. An electrical discharge vaporizes the fluid within the balloon to generate a rapidly expanding bubble and collapses within a few microseconds afterward. Soft tissue transmits the pulsatile mechanical energy, while microfractures are induced in rigid calcified structures and thus break up the calcified plaques. The treatment sequence takes 10 s, during which shockwaves are emitted at a frequency of 80 Hz. 2–4 sequences are performed per vessel section. This provides the unique opportunity to modify the calcified plaque homogenously and reach calcification even in deeper vessel layers. The aim of this study was to assess the safety and effectiveness of IVL in treating eccentric calcified coronary lesions.

Methods

Study design and population

Between December 2015 and March 2019, 180 patients were enrolled in the Disrupt CAD I and Disrupt CAD II studies across 19 sites in 10 countries. Disrupt CAD I ($n = 60$) was a pre-market, prospective, single-arm, multi-center study designed to evaluate the safety and performance of the Shockwave (Shockwave Medical Inc., Santa Clara, CA, USA) coronary intravascular lithotripsy (IVL) system in the treatment of calcified coronary lesions for the purpose of optimizing the placement of stents and reducing the ultimate residual stenosis [12].

Disrupt CAD II ($n = 120$) was a post-market study evaluating the safety and performance of the coronary IVL system following expansion to a broader patient population and additional physician users [13]. The inclusion and exclusion criteria for both studies were identical and included patients with significant native calcified coronary artery disease suitable for PCI. In both studies, patients were required to have a single target lesion requiring PCI with diameter stenosis $\geq 50\%$, lesion length ≤ 32 mm in native coronary arteries, and severe calcification as determined by the operators, defined as calcification within the lesion on both sides of the vessel assessed by angiography. Primary endpoints of the Disrupt CAD I study were freedom from major adverse cardiac events (MACE) within 30 days of the procedure. MACE was defined as cardiac death, myocardial infarction or target vessel revascularization (TVR). IVL performance was defined as the ability of the IVL system to produce residual stenosis of $< 50\%$ after stenting without intra-hospital MACE [12]. The primary endpoint of the Disrupt CAD II study was the frequency of in-hospital MACE [13].

The same independent angiographic core lab was utilized for both studies and analyzed all procedural angiograms (Yale Cardiovascular Research Group, New Haven, CT, USA). The angiographic core lab defined an eccentric lesion as a stenotic lesion that had one of its luminal edges in the outer one-quarter of the apparent normal vessel lumen [14–16]. Concentric lesions were defined using the same criteria while involving both luminal edges. Whenever possible, multiple angiographic angles were used to confirm the lesion classification.

All patients gave written informed consent before enrollment. The study was conducted in accordance with the Declaration of Helsinki and applicable laws by all related governmental bodies. Studies were registered at https://www.clinicaltrials.gov; their unique identifiers: NCT02650128 and NCT03328949.

Study device

The coronary IVL system is a 6Fr compatible semi-compliant balloon catheter, containing two electrically charged lithotripsy emitters, inserted over a rapid exchange 0.014″ guidewire [11–13]. Balloon catheters are available in several diameters (2.5–4.0 mm in steps of 0.5 mm) with a length of 12 mm. The balloon is expanded to 4 atm by a fluid (50:50 mixture of NaCl 0.9% and contrast media) optimized to transmit circumferential sonic pressure waves through soft vascular tissue. A small electrical discharge at the emitters vaporizes this fluid, thereby generating a rapidly expanding and collapsing bubble within the balloon. The resulting mechanical energy (approximately 50 atm) selectively induces fractures in the calcium. The IVL system allows the manual application of individual therapy cycles, each comprising 10 pulses (one pulse per second) in series, with a maximum of eight cycles emitted by each catheter [13, 17, 18].

Study procedure

PCI was performed via 6Fr or larger femoral or radial access. The IVL catheter was inserted using a standard 0.014″ guidewire. If passing the IVL device was initially unable to cross the target lesion, preparation with a small NC balloon (1.5 mm diameter), buddy wire-technique or guidewire extension was allowed per protocol. Lithotripsy-balloon diameter was selected 1:1 according to the angiographically estimated reference lumen diameter. After positioning, the balloon was inflated to 4 atm to achieve proper contact with the vessel wall and one cycle was delivered; the balloon was inflated to 6 atm subsequently. Treatment cycles were repeated as necessary to cover the whole lesion. If the maximum of eight cycles (80 pulses) had been delivered without sufficient lesion preparation, the use of additional IVL catheters with the same or larger diameters was allowed per protocol. Stent implantation and post-dilatation were performed according to the standard of care in each institution. Post-procedure medication and selection of dual antiplatelet therapy were at the discretion of the operator. Clinical follow-up was conducted 30 days post-procedure by standardized telephone interview.

Statistical analysis

Patient baseline characteristics and procedural data were analyzed and represented using frequency, mean, SD, and median. In comparing two groups, the *t* test or Wilcoxon sum test was utilized for continuous variables and Fisher's exact test for dichotomous variables. All statistical tests were two-sided, with p values < 0.05 considered statistically significant. Statistical analyses were performed using SAS (SAS Institute, Cary, NC, USA), version 9.4.

Results

Patient data

Patient-level data were pooled from Disrupt CAD I and Disrupt CAD II study with eccentric lesions identified in 47 patients and concentric lesions in 133 patients. Mean patient age was 72.1 ± 9.7 years. There were no significant differences between patients with eccentric or concentric lesions regarding baseline characteristics (Table 1). There was a trend towards higher frequencies of previous myocardial infarction (40.4% vs. 27.1%; $p = 0.10$), arrhythmias (31.9% vs. 18%; $p = 0.06$) and renal insufficiency (14.9% vs. 6.8%; $p = 0.13$) in patients with eccentric stenoses as compared to patients with concentric stenoses.

Lesion characteristics

Target lesions were located in the left anterior descending artery in 57.2%, in the right coronary artery in 29.5%, in the circumflex artery in 12.2%, and in the protected left main in 1.1%. There were no significant differences between groups regarding the lesion location. However, patients with eccentric lesions demonstrated significantly larger reference vessel diameter (RVD, 3.2 ± 0.6 mm vs. 3.0 ± 0.5 mm; $p = 0.04$ and significantly shorter lesion length (16.7 ± 7.0 mm vs. 20.9 ± 10.7 mm; $p = 0.01$) as compared to patients with concentric lesions. For detailed lesion characteristics see also Table 2.

Procedural characteristics

Pre-dilatation was performed in 40% of patients and post-dilatation in 81.7%. Mean procedure time was 76.5 ± 37.0 min, mean fluoroscopy time 22.7 ± 15.9 min, and mean contrast load 207.3 ± 87.5 ml. The number of IVL treatment cycles delivered was heavily left-skewed, with a median of 68.5 [40, 80] IVL pulses delivered, translating to 3.5 [2.5, 5.8]

Table 1 Baseline characteristics

	Overall ($n = 180$)	Eccentric ($n = 47$)	Concentric ($n = 133$)	p value
Age	72.1 ± 9.7	73.0 ± 10.1	71.8 ± 9.6	0.35
Male	142 (78.9)	38 (80.9)	104 (78.2)	0.84
Diabetes	56 (31.1)	17 (36.2)	39 (29.3)	0.49
Hypertension	144 (80.0)	39 (83.0)	105 (78.9)	0.70
Hyperlipidemia	134 (74.4)	34 (72.3)	100 (75.2)	0.85
Renal Insufficiency	16 (8.9)	7 (14.9)	9 (6.8)	0.13
MI[a]	55 (30.6)	19 (40.4)	36 (27.1)	0.10
Arrhythmia	39 (21.7)	15 (31.9)	24 (18.0)	0.06

Values are mean ± standard deviation or *n* (%)

[a]*MI* myocardial infarction

Table 2 Lesion characteristics

	Overall ($n=180$)	Eccentric ($n=47$)	Concentric ($n=133$)	p value
Target vessel				
Protected LM[a]	2 (1.1)	2 (4.3)	0 (0.0)	0.10
LAD[b]	103 (57.2)	23 (48.9)	80 (60.2)	
Cx[c]	22 (12.2)	3 (6.4)	19 (14.3)	
RCA[d]	53 (29.4)	19 (40.4)	34 (25.6)	
RVD[e] (mm)	3.0 ± 0.5	3.2 ± 0.6	3.0 ± 0.5	0.03
MLD[f] (mm)	1.1 ± 0.4	1.2 ± 0.5	1.1 ± 0.4	0.11
DS[g] (%)	62.7 ± 12.9	61.7 ± 14.1	63.1 ± 12.5	0.44
Lesion length (mm)	19.8 ± 10.0	16.7 ± 7.0	20.9 ± 10.7	0.04
Calcified length (mm)	24.6 ± 12.5	24.2 ± 15.7	24.8 ± 11.3	0.18
Severe calcification	161 (89.4)	41 (87.2)	120 (90.2)	0.77

Values are mean ± standard deviation or n (%). Severe calcification was confirmed by angiography when radiopacity was noted without cardiac motion prior to contrast injection

[a]*LM* left main

[b]*LAD* left anterior descending artery

[c]*Cx* circumflex artery

[d]*RCA* right coronary artery

[e]*RVD* reference vessel diameter

[f]*MLD* minimum lumen diameter

[g]*DS* diameter stenosis

IVL pulses/mm of lesion length; this was consistent between patients with eccentric and concentric lesions. Intravascular imaging using optical coherence tomography was performed in 78 patients (43%). No procedural characteristics differed significantly between groups. See also Table 3.

Outcome

Clinical success, defined as final post-stent residual stenosis < 50% after stenting with no in-hospital MACE, was achieved in 93.3% of patients (Eccentric: 93.6% vs. concentric 93.2%; $p=0.80$). Angiographic success, defined as success in facilitating stent delivery with < 50% residual stenosis and without major angiographic complications (severe dissection impairing flow [type D–F], perforation, abrupt closure, persistent slow flow, or no reflow), was achieved in 98.9% of patients (Eccentric: 100% vs. concentric 98.5%; $p=0.97$). An exploratory goal of < 30% residual stenosis was achieved with high frequency in both groups (Eccentric: 97.9% vs. concentric 97.0%; $p=0.84$). Residual percent diameter stenosis (Eccentric: 61.7 ± 14.1% vs. concentric: 63.1 ± 12.5%; $p=0.44$) and acute gain (Eccentric: 1.8 ± 0.5 mm vs. concentric: 1.7 ± 0.5 mm; $p=0.47$) were similar between groups. Representative angiographic and optical coherence tomography images from eccentric and concentric lesions are shown in Fig. 1.

Table 3 Procedural characteristics

	Overall ($n=180$)	Eccentric ($n=47$)	Concentric ($n=133$)	p value
Procedure time (min)	76.5 ± 37.0	74.6 ± 40.1	77.2 ± 36.0	0.46
Fluoroscopy time (min)	22.7 ± 15.9	19.8 ± 13.5	23.8 ± 16.6	0.35
Contrast volume (ml)	207.3 ± 87.5	191.5 ± 87.7	212.8 ± 87.0	0.07
IVL[a] catheters (n)	1.5 ± 0.9	1.3 ± 0.6	1.5 ± 0.9	0.22
IVL[a] pulses (n)	68.5 [40, 80]	60 [50, 80]	70 [40, 80]	0.79
Pulses/mm lesion length	3.5 [2.5, 5.8]	3.7 [2.9, 6.5]	3.4 [2.3, 5.1]	0.13
Max IVL[a] inflation pressure	5.8 ± 0.8	6.0 ± 0.7	5.8 ± 0.8	0.15
Number of stents (n)	1.4 ± 0.7	1.3 ± 0.5	1.4 ± 0.7	0.12
Pre-dilatation	72 (40.0)	20 (42.6)	52 (39.1)	0.81
Post-dilatation	147 (81.7)	36 (76.6)	111 (83.5)	0.41

Values are mean ± standard deviation or median [Q1, Q3] or n (%)

[a]*IVL* intravascular lithotripsy

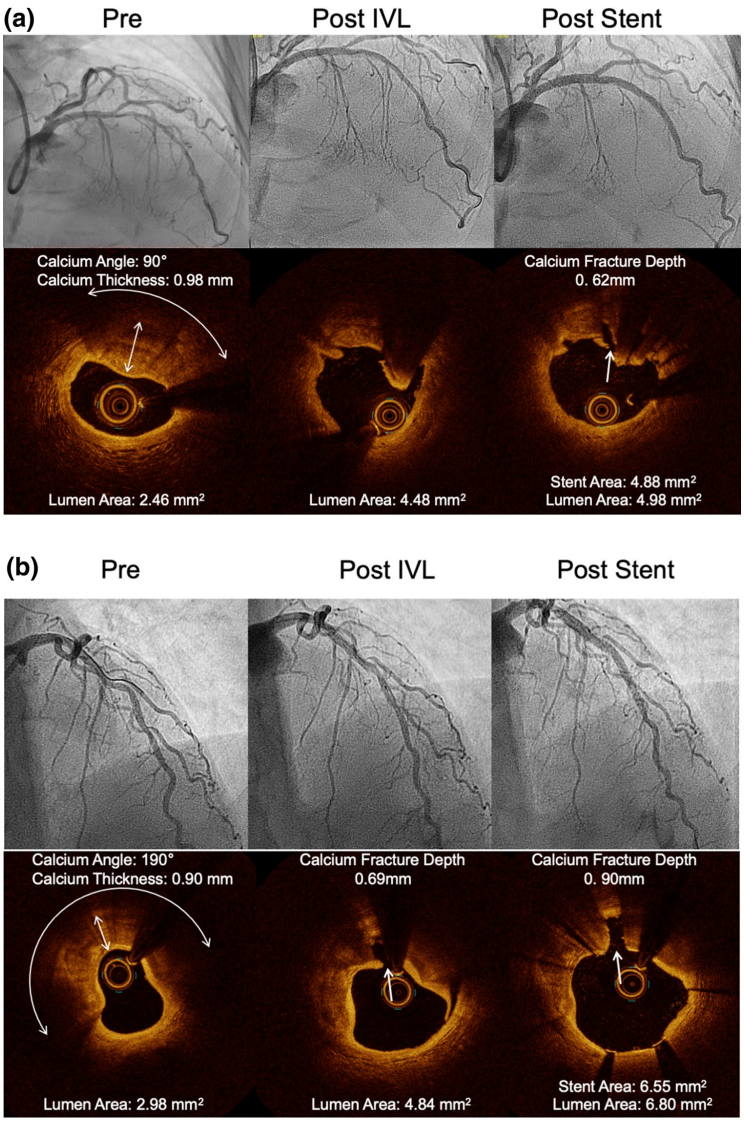

Fig. 1 IVL in eccentric and concentric coronary lesions. Representative angiography and optical coherence tomography images from cases involving an **a** eccentric lesion and **b** concentric lesion. Fractured calcium is visible within the intimal and medial vessel layers for both lesions. In each example, increased lumen area is notable post IVL treatment and again post stent

After IVL, no perforations, abrupt closure, slow-flow or no-reflow events were observed in either group, and low rate of flow-limiting dissections (Grade D–F: Eccentric 0% vs. concentric 1.7%, $p = 0.54$) occurred. All dissections were resolved with stent delivery.

During in-hospital follow-up, there were two cases (4.3%) of non-Q-wave myocardial infarction in patients with eccentric lesions and eight cases (6.0%) in patients with concentric lesions ($p = 0.93$). Neither group experienced cardiac death or target vessel revascularization during in-hospital follow-up.

The 30-day MACE rate was 8.7% in patients with eccentric lesions and 6.0% in patients with concentric lesions ($p = 0.80$). No new observations of non-Q-wave

myocardial infarction were observed following hospital discharge. There was one cardiac death in the group with eccentric lesions. The cardiac death occurred in a 70-year-old who originally presented with pre-syncope and died suddenly 14 days after treatment of a 95% lesion in the distal right coronary artery. The inclusion of this patient was a protocol deviation, as the patient met defined angiographic exclusion criterion (second lesion with ≥ 50% stenosis in the same target vessel) due to occluded posterior descending coronary artery and reference vessel diameter > 4.0 mm (quantitative coronary angiography: 4.57 mm) [15]. There were no significant differences in the frequency of 30-day MACE when comparing patients with eccentric and concentric lesions. For detailed outcome data see also Tables 4, 5, 6 and 7.

Discussion

The main findings of this pooled patient-level analysis are that IVL treatment of eccentric coronary lesions is associated with consistent outcomes including high procedure success and low vascular complications and that there are no significant differences regarding procedural and clinical outcome when comparing IVL treatment of eccentric with concentric lesions.

IVL provides a unique therapy to modify calcified coronary plaques even in deeper vessel layers [12, 13]. IVL mechanical pressure waves are transduced through the soft tissue of the vessel wall. Rigid calcifications cannot transduce this mechanical energy, so the energy selectively fractures calcified plaque. All other debulking techniques

Table 4 Performance outcomes

	Overall ($n=180$)	Eccentric ($n=47$)	Concentric ($n=133$)	p value
Clinical success	168 (93.3)	44 (93.6)	124 (93.2)	1.0
Angiographic success	178 (98.9)	47 (100.0)	131 (98.5)	1.0
Stent delivery	180 (100.0)	47 (100.0)	133 (100.0)	
Final in-stent angiographic outcomes				
MSD[a] (mm)	2.8 ± 0.5	3.0 ± 0.5	2.7 ± 0.5	0.004
Residual stenosis (%)	9.7 ± 9.2	8.6 ± 9.8	10.0 ± 9.0	0.56
Acute gain (mm)	1.7 ± 0.5	1.8 ± 0.5	1.7 ± 0.5	0.47
Residual stenosis < 50%	180 (100.0)	47 (100.0)	133 (100.0)	
Residual stenosis < 30%	175 (97.2)	46 (97.9)	129 (97.0)	0.84

Values are mean ± standard deviation or n (%)

[a]*MSD* minimum stent diameter

Table 5 Angiographic complications—Post-IVL

	Overall ($n=161$)	Eccentric ($n=44$)	Concentric ($n=117$)	p value
Dissections, type D–F	2 (1.2)	0 (0.0)	2 (1.7)	0.54
Perforation	0 (0.0)	0 (0.0)	0 (0.0)	
Abrupt closure	0 (0.0)	0 (0.0)	0 (0.0)	
Slow flow	0 (0.0)	0 (0.0)	0 (0.0)	
No reflow	0 (0.0)	0 (0.0)	0 (0.0)	

Values are n (%)

Table 6 Angiographic complications—Final

	Overall ($n=180$)	Eccentric ($n=47$)	Concentric ($n=133$)	p value
Dissections, type				
D–F	0 (0.0)	0 (0.0)	0 (0.0)	
Perforation	0 (0.0)	0 (0.0)	0 (0.0)	
Abrupt closure	0 (0.0)	0 (0.0)	0 (0.0)	
Slow flow	0 (0.0)	0 (0.0)	0 (0.0)	
No reflow	0 (0.0)	0 (0.0)	0 (0.0)	

Values are n (%)

Table 7 MACE

	Overall ($n=180$)	Eccentric ($n=47$)	Concentric ($n=133$)	p value
In-hospital	10 (5.6)	2 (4.3)	8 (6.0)	0.93
Cardiac death	0 (0.0)	0 (0.0)	0 (0.0)	
Non-Q-wave MI[a]	10 (5.6)	2 (4.3)	8 (6.0)	
Q-wave MI[a]	0 (0.0)	0 (0.0)	0 (0.0)	
TVR[b]	0 (0.0)	0 (0.0)	0 (0.0)	
30-day*	12 (6.7)	4 (8.7)	8 (6.0)	0.80
Cardiac death	1 (0.6)	1 (2.2)	0 (0.0)	
Non-Q-wave MI[a]	10 (5.6)	2 (4.3)	8 (6.0)	
Q-wave MI[a]	1 (0.6)	1 (2.2)	0 (0.0)	
TVR[b]	1 (0.6)	1 (2.2)	0 (0.0)	

Values are *n* (%)

[a]*MI* myocardial infarction

[b]*TVR* target vessel revascularization

*One subject with two events; one subject withdrew prior to the 30-day end-point

(Cutting-/Scoring-Balloon, atherectomy techniques) may suffer from guidewire bias leading to inhomogeneous plaque modification [9, 19–21]. OA and RA modify calcified plaque by generating a relatively smooth, circular channel, strictly following the guidewire [19, 21–24]. This facilitates balloon or stent delivery, although the gain in the cross-sectional area is modest [24]. Nevertheless, it must be kept in mind, that this atherectomy "tunnel" may not be located centrally in the coronary artery which can result in asymmetric stent expansion and undesirable clinical outcomes. Furthermore, in regions with tortuosity and eccentric lesions, there is a significant risk of coronary perforation with OA or RA [25] and damage to healthy portions of the vessel wall. Eccentric coronary calcifications are particularly difficult to modify by OA or RA atherectomy due to the guidewire being displaced away from the target lesion. In comparison, the IVL balloon inflated to 4 atm is in contact with all parts of the surrounding vessel and therefore has no guidewire bias. This provides the possibility for homogeneous plaque modification, in both the intima and the media, especially in eccentric coronary plaques that are usually associated with suboptimal outcomes after PCI [26, 27]. Patient age has continuously increased over the past years resulting in higher calcium burden of coronary plaques as well as more complex coronary stenoses, such as eccentric calcified coronary lesions. The increasing frequency of these complex lesions is associated with an impaired clinical outcome [28]. Therefore, promising treatment options for eccentric calcified lesions, such as IVL, need to be evaluated and established in clinical routine. IVL has demonstrated effective treatment of calcifications located in deeper vessel layers [13, 29]. Circumferential plaque modification results in increased vessel compliance, demonstrated by increasing vessel diameter during constant balloon pressure [18]. As a result, IVL facilitates full, symmetrical stent expansion [13].

As the utilization of IVL has increased, there has been much discussion as to which clinical cases the technology is best suited for. In this first comparison between eccentric and concentric lesions, as defined angiographically, it is instructive to observe high procedural success rates with IVL regardless of lesion type. Angiographic success was achieved in 100% of eccentric lesions and 98.5% of concentric lesions, which emphasizes the effectiveness of IVL in treating a wide range of stenoses. This clinical success was achieved using a similar number of pulses/mm lesions among the two groups in this study. Per protocol, the goal was to deliver lithotripsy until < 50% residual stenosis was achieved, but ending therapy was at physician's discretion and there were no limitations to the absolute number of pulses delivered. Regardless of the variability in the strategy of pulse delivery, the number of pulses delivered, and the pulses/mm lesion was similar between eccentric and concentric lesions. Accordingly, this analysis demonstrates no limitations in the efficiency or effectiveness of IVL treatment in eccentric lesions. Based on the results of this study, IVL should be considered as a valuable treatment option in both eccentric and concentric calcified lesions. This seems to be even more important when considering that rotational or orbital atherectomy, the most effective techniques prior to IVL, is limited due to guidewire bias, which may result in inhomogeneous ablation leaving significantly unmodified areas in eccentric lesions. Moreover, it may be suited to make safe and effective plaque modulation in calcified coronary stenoses available for a wider patient collective than it is at the moment since

atherectomy techniques are only used in a small part of patients in need due to their technical complexity [30, 31].

According to our results, Mattesini et al. reported similar results for IVL treatment of eccentric (Calcium arc > 180°) and concentric calcified stenosis (Calcium arc ≤ 180°) when comparing the acute results using intravascular imaging by optical coherence tomography in a prospective registry including 28 patients [32]. There were no significant differences regarding in-stent minimum lumen diameter, in-stent minimal lumen area, and the acute gain when comparing eccentric and concentric calcified stenoses. If this really translates into lower adverse event rates and better clinical outcome needs to be evaluated in future clinical trials.

Limitations

Our study has a number of limitations. First, this is a retrospective pooled analysis from two different studies that were designed for evaluating the safety and procedural success of IVL. Nevertheless, the inclusion and exclusion criteria of both studies were identical and data analysis was performed by the same independent core lab. Patient numbers were quite small with 180 patients being included in the aggregated studies. Nonetheless, this study includes the largest number of patients with coronary IVL treatment performed so far.

A further limitation is the angiographic endpoint of clinical success, defined as residual diameter stenosis of less than 50% after IVL and stenting, which is quite conservative. The endpoint was chosen as equivalent to the ORBIT II study which was used as a primary comparator for the Disrupt CAD I study [33]. Nonetheless, the final residual stenosis of 8.6 ± 9.8% in eccentric and 10.0 ± 9.0% ($p = 0.56$) in concentric stenosis confirms the significant effect of IVL on these lesions. Additionally, given the angiographic limitations in determining the exact arc of calcium within the lesions, further insights from planned OCT and IVUS analyses from the Disrupt CAD clinical program will add additional valuable insights.

Future clinical trials should focus on comparing IVL and other debulking techniques for the treatment of calcified coronary lesions to evaluate the technique in comparison to the current standards of care. No according data have been published so far.

Conclusion

In this first report from a pooled patient-level analysis of coronary IVL from the Disrupt CAD I and CAD II studies, IVL use was associated with high procedural success and consistent clinical outcomes in both eccentric and concentric calcified lesions.

Funding Open Access funding enabled and organized by Projekt DEAL. This analysis was funded by Shockwave Medical Inc. (Santa Clara, CA, USA).

Compliance with ethical standards

Conflict of interest Bernard De Bruyne reports that The Cardiovascular Center Aalst receives grant support from Abbott Vascular, Boston Scientific, and Biotronik AG, and receives consulting fees on his behalf Abbott Vascular and Boston Scientific outside of the submitted work. Bernard De Bruyne is a shareholder for Siemens, GE, Bayer, Philips, HeartFlow, Edwards Life Sciences, and Ceyliad. Carlo Di Mario received an institutional research grant to the institution from Shockwave Medical for the DISRUPT CAD 2 trial. Christian Hamm is Advisory Board Member for Medtronic. Holger Nef received an Institutional Research Grant from Shockwave Medical as well as speaker honorary from Shockwave Medical. All other authors report no relevant conflicts of interest.

References

1. Goto K, Zhao Z, Matsumura M, Dohi T, Kobayashi N, Kirtane AJ, Rabbani LE, Collins MB, Parikh MA, Kodali SK, Leon MB, Moses JW, Mintz GS, Maehara A (2015) Mechanisms and patterns of intravascular ultrasound in-stent restenosis among bare metal stents and first- and second-generation drug-eluting stents. Am J Cardiol 116(9):1351–1357
2. West NE, Ruygrok PN, Disco CM, Webster MW, Lindeboom WK, O'Neill WW, Mercado NF, Serruys PW (2004) Clinical and angiographic predictors of restenosis after stent deployment in diabetic patients. Circulation 109(7):867–873
3. Wiemer M, Butz T, Schmidt W, Schmitz KP, Horstkotte D, Langer C (2010) Scanning electron microscopic analysis of different drug eluting stents after failed implantation: from nearly undamaged to major damaged polymers. Catheter Cardiovasc Interv 75:905–911
4. Tzafriri AR, Garcia-Polite F, Zani B, Stanley J, Muraj B, Knutson J, Kohler R, Markham P, Nikanorov A, Edelman ER (2017) Calcified plaque modification alters local drug delivery in the treatment of peripheral atherosclerosis. J Control Release 264:203–210
5. Mori S, Yasuda S, Kataoka Y, Morii I, Kawamura A, Miyazaki S (2009) Significant association of coronary artery calcification in stent delivery route with restenosis after sirolimus-eluting stent implantation. Circ J 73:1856–1863
6. Kobayashi Y, Okura H, Kume T, Yamada R, Kobayashi Y, Fukuhara K, Koyama T, Nezuo S, Neishi Y, Hayashida A, Kawamoto T, Yoshida K (2014) Impact of target lesion coronary calcification on stent expansion. Circ J 78(9):2209–2214

7. Lee MS, Shah N (2016) The impact and pathophysiologic consequences of coronary artery calcium deposition in percutaneous coronary interventions. J Invasive Cardiol 28(4):160–167
8. Fitzgerald PJ, Ports TA, Yock PG (1992) Contribution of localized calcium deposits to dissection after angioplasty. An observational study using intravascular ultrasound. Circulation 86(1):64–70
9. Yamamoto MH, Maehara A, Karimi Galougahi K, Mintz GS, Parviz Y, Kim SS, Koyama K, Amemiya K, Kim SY, Ishida M, Losquadro M, Kirtane AJ, Haag E, Sosa FA, Stone GW, Moses JW, Ochiai M, Shlofmitz RA, Ali ZA (2017) Mechanisms of orbital versus rotational atherectomy plaque modification in severely calcified lesions assessed by optical coherence tomography. J Am Coll Card Intv 10:2584–2586
10. Abdel-Wahab M, Richardt G, Joachim Büttner H, Toelg R, Geist V, Meinertz T, Schofer J, King L, Neumann FJ, Khattab AA (2013) High-speed rotational atherectomy before paclitaxel-eluting stent implantation in complex calcified coronary lesions: the randomized ROTAXUS (Rotational Atherectomy Prior to Taxus Stent Treatment for Complex Native Coronary Artery Disease) trial. J Am Coll Card Intv 6:10–19
11. Matsuo H, Watanabe S, Watanabe T, Warita S, Kojima T, Hirose T, Iwama M, Ono K, Takahashi H, Segawa T, Minatoguchi S, Fujiwara H (2007) Prevention of no-reflow/slow-flow phenomenon during rotational atherectomy–a prospective randomized study comparing intracoronary continuous infusion of verapamil and nicorandil. Am Heart J 154:994
12. Brinton TJ, Ali ZA, Hill JM, Meredith IT, Maehara A, Illindala U, Lansky A, Götberg M, Van Mieghem NM, Whitbourn R, Fajadet J, Di Mario C (2019) Feasibility of shockwave coronary intravascular lithotripsy for the treatment of calcified coronary stenoses. Circulation 139(6):834–836
13. Ali ZA, Nef H, Escaned J, Werner N, Banning AP, Hill JM, De Bruyne B, Montorfano M, Lefevre T, Stone GW, Crowley A, Matsumura M, Maehara A, Lansky AJ, Fajadet J, Di Mario C (2019) Safety and effectiveness of coronary intravascular lithotripsy for treatment of severely calcified coronary stenoses: the Disrupt CAD II Study. Circ Cardiovasc Interv 12(10):e008434
14. Beig JR, Shah TR, Hafeez I, Dar MI, Rather HA, Tramboo NA, Lone AA, Rather FA (2017) Clinico-angiographic profile and procedural outcomes in patients undergoing percutaneous coronary interventions: the Srinagar registry. Indian Heart J 69(5):589–596
15. Zhu SG, Zhang RL, Liu WH, Yin Q, Zhou ZM, Zhu WS, Zhu YL, Xu GL, Liu XF (2010) Predictive factors for in-stent restenosis after balloon-mounted stent placement for symptomatic intracranial atherosclerosis. Eur J Vasc Endovasc Surg 40(4):499–506
16. Nair P, Gruberg L, Beyar R (2006) The eccentric lumenology. Acute Card Care 8(2):87–94
17. Forero MNT, Daemen J (2019) The coronary intravascular lithotripsy system. Interv Cardiol 14(3):174–181
18. Ali ZA, Brinton TJ, Hill JM, Maehara A, Matsumura M, Karimi Galougahi K, Illindala U, Götberg M, Whitbourn R, Van Mieghem N, Meredith IT, Di Mario C, Fajadet J (2017) Optical coherence tomography characterization of coronary lithoplasty for treatment of calcified lesions: first description. JACC Cardiovasc Imaging 10(8):897–906
19. Kini AS, Vengrenyuk Y, Pena J, Motoyama S, Feig JE, Meelu OA, Rajamanickam A, Bhat AM, Panwar S, Baber U, Sharma SK (2015) Optical coherence tomography assessment of the mechanistic effects of rotational and orbital atherectomy in severely calcified coronary lesions. Catheter Cardiovasc Interv 86:1024–1032
20. Tomey MI, Kini AS, Sharma SK (2014) Current status of rotational atherectomy. J Am Coll Card Intv 7:345–353
21. Oishi Y, Okamoto M, Sueda T, Hashimoto M, Karakawa S, Kambe M (2002) Guidewire bias in rotational atherectomy in the angled lesion: evaluation based on the thickness of the ablated intima and media. Circ J 66:659–664
22. Attizzani GF, Patrício L, Bezerra HG (2013) Optical coherence tomography assessment of calcified plaque modification after rotational atherectomy. Catheter Cardiovasc Interv 81(3):558–561
23. Mestre RT, Alegria-Barrero E, Di Mario C (2014) A coronary "tunnel": optical coherence tomography assessment after rotational atherectomy. Catheter Cardiovasc Interv 83(5):E171–173
24. Sotomi Y, Cavalcante R, Shlofmitz RA, Suwannasom P, Tateishi H, Tenekecioglu E, Zheng Y, Abdelghani M, de Winter RJ, Wykrzykowska JJ, Onuma Y, Serruys PW (2016) Quantification by optical coherence tomography imaging of the ablation volume obtained with the orbital atherectomy system in calcified coronary lesions. EuroIntervention 12(9):1126–1134
25. Cohen BM, Weber VJ, Relsman M, Casale A, Dorros G (1996) Coronary perforation complicating rotational ablation: the U.S. multicenter experience. Cathet Cardiovasc Diagn (Suppl 3): 55–59
26. Ellis SG, Guetta V, Miller D, Whitlow PL, Topol EJ (1999) Relation between lesion characteristics and risk with percutaneous intervention in the stent and glycoprotein IIb/IIIa era: an analysis of results from 10,907 lesions and proposal for new classification scheme. Circulation 100(19):1971–1976. https://doi.org/10.1161/01.cir.100.19.1971
27. Meier B, Gruentzig AR, Hollman J, Ischinger T, Bradford JM (1983) Does length or eccentricity of coronary stenoses influence the outcome of transluminal dilatation? Circulation 67(3):497–499
28. Räber L, Mintz GS, Koskinas K, Johnson T, Holm NR, Onuma Y, Radu MD, Joner M, Yu B, Jia H, Meneveau N, de la Torre Hernandez JM, Escaned J, Hill J, Prati F, Colombo A, di Mario C, Regar E, Capodanno D, Wijns W, Byrne RA, Guagliumi G (2018) Clinical use of intracoronary imaging. Part 1: guidance and optimization of coronary interventions. An expert consensus document of the European Association of Percutaneous Cardiovascular Interventions. Eur Heart J 39:3281–3300
29. Khan S, Li B, Salata K, Aljabri BA, Hussain MA, Khan M, de Mestral C, Verma S, Al-Omran M (2019) The current status of lithoplasty in vascular calcifications: a systematic review. Surg Innov 26(5):588–598
30. Généreux P, Redfors B, Witzenbichler B, Arsenault MP, Weisz G, Stuckey TD, Rinaldi MJ, Neumann FJ, Christopher Metzger D, Henry TD, Cox DA, Duffy PL, Mazzaferri EL Jr, Francese DP, Marquis-Gravel G, Mintz GS, Kirtane AJ, Maehara A, Mehran R, Stone GW (2017) Two-year outcomes after percutaneous coronary intervention of calcified lesions with drug-eluting stents. Int J Cardiol 231:61–67
31. Costopoulos C, Naganuma T, Colombo A (2014) Tools and techniques clinical: percutaneous intervention of calcific coronary lesions. EuroIntervention 9(9):1124–1126
32. Mattesini A, Nardi G, Martellini A, Sorini Dini C, Hamiti B, Stolcova M, Meucci F, Di Mario C (2020) Intravascular imaging to guide lithotripsy in concentric and eccentric calcific coronary lesions. Cardiovasc Revasc Med. https://doi.org/10.1016/j.carrev.2020.04.016**(Epub ahead of print)**
33. Chambers JW, Feldman RL, Himmelstein SI, Bhatheja R, Villa AE, Strickman NE, Shlofmitz RA, Dulas DD, Arab D, Khanna PK, Lee AC, Ghali MG, Shah RR, Davis TP, Kim CY, Tai Z, Patel KC, Puma JA, Makam P, Bertolet BD, Nseir GY (2014) Pivotal trial to evaluate the safety and efficacy of the orbital atherectomy system in treating de novo, severely calcified coronary lesions (ORBIT II). JACC Cardiovasc Interv 7:510–518

Nr. 8: Comparison of Coronary Intravascular Lithotripsy and Rotational Atherectomy in the Modification of Severely Calcified Stenoses

Comparison of Coronary Intravascular Lithotripsy and Rotational Atherectomy in the Modification of Severely Calcified Stenoses

Running title: Plaque modification by IVL and RA

Authors: Florian Blachutzik[a], MD; Sophie Meier[a] ; Melissa Weissner[b], MD; Sophia Schlattner[a], Tommaso Gori[c,g], MD; Helen Ullrich-Daub[c], MD; Luise Gaede[d], MD; Stephan Achenbach[d], MD; Helge Möllmann[e], MD; Bogdan Chitic[e], MD; Adem Aksoy[f], MD; Georg Nickenig[f], MD; Maren Weferling[b], MD; Oliver Dörr[a,g], MD; Niklas Boeder[a], MD; Matthias Bayer[a], MD; Albrecht Elsässer[h], MD; Christian Hamm[a,b,g], MD; Holger Nef[a,g], MD, on behalf of the ROTA.shock investigators

[a] Justus Liebig Universität Giessen, Medizinische Klinik 1, Giessen, Germany
[b] Kerckhoff-Klinik, Kardiologie, Bad Nauheim, Germany
[c] Universitätsmedizin Mainz, Kardiologie 1, Mainz, Germany
[d] Friedrich-Alexander-Universität Erlangen-Nürnberg (FAU), Erlangen, Germany
[e] St. Johannes-Hospital, Innere Medizin 1, Dortmund, Germany
[f] Universitätsklinikum Bonn, Medizinische Klinik 2, Bonn, Germany
[g] German Center for Cardiovascular Research (DZHK), Rhine-Main Partner Site, Germany
[h] Universitätsklinikum Oldenburg, Klinik für Innere Medizin - Kardiologie Oldenburg, Germany

Funding: This study was funded by the Else Kröner-Fresenius-Stiftung, Bad Homburg, Germany (Grant number: 2019_A17; Grant recipient: Florian Blachutzik)

Disclosures: Tommaso Gori received grant support and speaker´s honoraria from Abbott vascular and speaker´s honoraria from Boston Scientific and Shockwave Medical. Luise Gaede received speaker's honoraria from Abbott vascular, Boston Scientific and Shockwave Medical. Maren Weferling has received speaker's honoraria from Boston Scientific and Shockwave Medical. Helge Möllmann received speaker's honoraria from Boston Scientific and Shockwave Medical. Holger Nef received grant support and speaker's honoraria from Abbott vascular and Shockwave Medical. All other authors report no relevant conflicts of interest.

Address for correspondence:
Florian Blachutzik, MD
University Hospital Giessen – Department of Cardiology
Klinikstrasse 33
35392 Giessen
Germany
Tel: +49 641 98542212
Fax: +49 641 98542219
E-Mail: florian.blachutzik@innere.med.uni-giessen.de

Abstract

Debulking techniques are often necessary for successful lesion preparation in percutaneous coronary intervention. The aim of this study was to compare plaque modification of severely calcified lesions by coronary intravascular lithotripsy (IVL) vs. rotational atherectomy (RA) using optical coherence tomography (OCT). ROTA.shock was a 1:1 randomized, prospective, double-arm, multi-center non-inferiority trial designed to compare final minimal stent area after IVL vs. RA for lesion preparation in percutaneous coronary interventional treatment of severely calcified lesions. Based on OCT acquired before and immediately after IVL or RA in 21 of the 70 patients included, we performed detailed analysis of the modification of the calcified plaque. Following RA and IVL, calcified plaque fractures were present in 14 (67%) of the patients, with a significantly higher number of fractures after IVL (3.23± 0.49) than after RA (1.67 ± 0.52; $p<0.001$). Plaque fractures after IVL were longer than after RA (IVL: 1.67 ± 0.43 mm vs. RA: 0.57 ± 0.55 mm; $p=0.01$), resulting in a larger total volume of the fractures (IVL: 1.47 ± 0.40 mm^3 vs. RA: 0.48 ± 0.27 mm^3; $p=0.003$). Use of RA was associated with a larger acute lumen gain than use of IVL (RA: 0.46 ± 0.16 mm^2 vs. IVL: 0.17 ± 0.14 mm^2; $p=0.03$). In conclusion, we were able to demonstrate differences in plaque modification of calcified coronary lesions by OCT: whereas RA leads to a larger acute lumen gain, IVL induces more and longer fractures of the calcified plaque.

Key words: percutaneous coronary intervention, calcified coronary lesions, intravascular lithotripsy, rotational atherectomy, intravascular imaging

Introduction

Severe lesion calcification remains a challenge in percutaneous coronary intervention (PCI) and is associated with suboptimal procedural results and a consequently increased occurrence of adverse clinical events. (1,2) Furthermore, calcified morphology is associated with higher rates of acute complications such as dissections and slow-flow/low-flow situations, when compared to PCI in fibrotic coronary plaque. (2) To date, there is no standardized and evidence-based strategy for lesion modification of calcified coronary lesions. The decision to apply adjunctive techniques for plaque modification, such as rotational atherectomy (RA), orbital atherectomy, or intracoronary lithotripsy (IVL), is mainly based on visual estimation of lesion calcification by angiography, with its inherent limitations, or is driven by delivery and expansion failure of standard devices. (3) In order to make an informed decision regarding the use of plaque modification techniques, it is imperative to better understand their specific effects on the calcified plaque structure. Therefore, the aim of this study was to compare the acute effects of RA and IVL on severely calcified coronary stenoses using intravascular optical coherence tomography (OCT).

Methods

This is a retrospective substudy of the ROTA.shock trial. The ROTA.shock study was a randomized, prospective, double-arm, multi-center non-inferiority trial that compared the performance of the Shockwave™ coronary IVL system (Shockwave Medical Inc., Santa Clara, CA, USA) with RA regarding stent dimensions, lumen dimensions, and plaque modification as determined by OCT as well as procedural success. The primary endpoint was the minimal stent area at the end of the procedure.

From July 2019 until November 2021, 70 patients with clinically significant and severely calcified coronary lesions were included in ROTA.shock in six centers in Germany (Justus Liebig University Giessen, Medical Clinic I, Giessen; Kerckhoff Heart and Thorax Center, Department of Cardiology, Bad Nauheim; University of Mainz Medical School, Cardiology 1, Mainz; University Hospital Erlangen, Medical Clinic 2, Erlangen; St. Johannes Hospital, Internal Medicine 1, Dortmund; University Hospital Bonn, Medical Clinic 2, Bonn) and were randomly assigned to RA or IVL. The primary inclusion criterion was a clinically relevant coronary stenosis with proven myocardial ischemia and severe calcification as defined by coronary angiography showing radiopacities noted without cardiac motion before contrast injection, compromising both sides of the arterial lumen. (4,5) The main exclusion criteria were true bifurcation lesions requiring two-stent strategies and patients with cardiogenic shock requiring intravenous catecholamines. All patients in whom a native OCT as well as an OCT immediately after plaque modification by RA or IVL could be acquired were included in the current substudy.

All patients have given their written informed consent before enrolment. The study was conducted in accordance with the Declaration of Helsinki. The study protocol was approved by the ethics committee of the medical faculty of the Justus Liebig University Giessen, Giessen, Germany (protocol number 231/18). The study was registered at https://www.clinicaltrials.gov with the identifier NCT04047368.

After randomization to either IVL or RA, PCI was performed via radial or femoral access with a 6 or 7 Fr catheter. Prior to intervention, intraarterial or intravenous heparin was given to maintain an activated clotting time ≥250 seconds. In the first step, a native OCT scan of the lesion intended to treat was acquired using a 2.7Fr Dragonfly™ imaging catheter (Optis™, Abbott Vascular, Santa Clara, Ca, USA). The mechanical retraction speed was set to 18 mm/s over a length of 54 mm with automated OCT acquisition. Flushing of the vessel was performed using 20 ml of standard contrast media at an injection rate of 4 ml/s. Pre-dilatation with a non-compliant (NC) balloon up to a diameter of 2.0 mm was allowed if the imaging catheter could not be advanced through the stenosis.

If the patient was randomized to RA, a dedicated wire (Rotawire™, Boston Scientific, Marlborough, MA, USA) was advanced through the lesion. The burr size was selected according to a burr-to-angiographic reference vessel diameter ratio of 0.5. The rotational speed ranged from 140 000 - 180 000 rotations per minute.

If the patient was randomized to IVL, the IVL balloon catheter (Shockwave C2™, Shockwave Medical Inc., Santa Clara, CA, USA), with a diameter selected 1:1 in relation to the angiographic reference vessel diameter, was inserted using a standard coronary guidewire and positioned in the lesion. The balloon was then inflated to 4 atm for each treatment cycle of 10 pulses and briefly to 6 atm following each treatment cycle.

Treatment cycles were repeated as necessary to cover the whole target lesion with at least 2-3 cycles being applied in every segment of the calcified lesion.

Immediately after RA or IVL, a second OCT (post-IVL/RA OCT) was acquired to analyze plaque modification by the two techniques. OCT image analysis was performed at the core lab (Medizinische Klinik 1, Universitätsklinikum Giessen, Giessen, Germany) using dedicated OCT analysis software (QIVUS™ OCT Software, Medis, Leiden, Netherlands). OCT cross-sectional images were analyzed at 1-mm intervals using the methods recommended in the expert consensus report for OCT and previous publications. (6-13) The presence of calcium fracture was defined as discontinuity of the luminal surface in the calcified plaque (**Figure 1**). (14,15) Calcium fracture was considered to be a single calcium fracture when the frames with the fracture were connected longitudinally. (14,15) Post-IVL/RA OCT runs were analyzed in the first step to match the corresponding vessel segments in baseline OCT using anatomical landmarks (e.g. side branches, characteristic plaque structures). Additionally, the OCT-based calcium score described by Fujino et al., which includes a calcific arc >180°, calcified plaque length >5 mm, and calcific plaque thickness >0.5 mm, was assessed. (10) Representative OCT analyses are shown in **Figure 1** and **Figure 2**. For detailed description of OCT results see also **Supplemental Table 1**.

Continuous variables are summarized as mean ± standard deviation, and categorical variables are provided as n (%). The Kolmogorov–Smirnov test was performed to test for parametric distribution. To test for statistical differences between two groups for comparison of continuous variables, either a t-test for unpaired samples (parametric distribution) or a Mann–Whitney U-test (non-parametric distribution) was used. For categorical variables, a Chi-squared or Fisher's exact test was carried out. Statistical analyses were performed using SPSS version 28.0 (IBM SPSS Statistics, IBM Corporation, Armonk, NY, USA). A two-sided $P < 0.05$ was considered significant.

Results

A total of 21 patients from the ROTA.shock main study were identified who matched the inclusion criterion for this subanalysis, with available native OCT as well as OCT immediately after RA or IVL. Nine of the patients were treated by RA and 12 by IVL. The mean patient age was 78.1 ± 8.1 years and most patients were male (81.0%). There were no significant differences regarding baseline characteristics between the two groups (**Table 1**).

PCI was performed via radial access in the majority of the patients (76%), with most target lesions located in the left anterior descending artery (LAD) (52%) and in the right coronary artery (RCA) (38%). Pre-dilatation using NC balloons was performed in one third of the patients. The mean burr size for RA was 1.55 ± 0.25 mm, and the mean IVL balloon diameter was 3.04 ± 0.28 mm; for detailed procedural data see **Table 2**.

Native OCT analysis showed similar lumen dimensions and lesion eccentricity in RA and IVL groups. OCT revealed significant lesion calcification with a maximum plaque angle of 259.4 ± 81.3° and a total plaque volume of 49.23 ± 25.52 mm^3. Accordingly, most patients had an OCT-based calcium score of 3 (38.1%) or 4 (57.1%). There were no significant differences in lesion calcification between patients after RA or IVL (**Table 3**).

Fractures of the calcified plaque (**Figure 1**) were present in 14 patients (67%), with a higher number of fractures after IVL than after RA (IVL: 3.23 ± 0.49 vs. RA: 1.67 ± 0.52; p <0.001). In addition, plaque fractures after IVL were longer than those after RA (IVL: 0.57 ± 0.55 mm vs. RA: 1.67 ± 0.43 mm; p=0.01), resulting in a larger total volume of the fractures (**Figure 1**) (IVL: 1.47 ± 0.40 mm^3 vs. RA: 0.48 ± 0.27 mm^3; p = 0.003). RA was associated with a larger lumen gain than was IVL (RA: 0.46 ± 0.16 mm^2 vs. IVL: 0.17 ± 0.14 mm^2; p=0.03).

Dissections were present in 16 of the 21 patients (76%). Both techniques induced dissections with a similar frequency. The mean flap length (**Figure 2**) was greater after IVL than after RA (IVL: 1.26 ± 0.25 mm vs. RA: 0.83 ± 0.21 mm; p=0.03). All other lumen or plaque dimensions did not differ significantly when comparing the two techniques (**Table 4**). Representative OCT cross-sections showing severely calcified stenoses after RA and IVL are shown in **Figure 3**.

Discussion

The main findings of this first study to compare the acute effects of IVL and RA in the interventional treatment of severely calcified coronary lesions using OCT are the following: 1) IVL induces a higher number of fractures in the calcified plaque than RA; 2) IVL is associated with longer fractures of the calcified plaque than RA; 3) IVL leads to dissections with longer flaps than RA; 4) RA is associated with a larger acute lumen gain compared with IVL.

Analysis of lesions by native OCT showed severe calcification, with most patients having a calcium-based OCT score (including calcific arc >180°, calcific plaque length >5 mm and calcific plaque thickness >0.5 mm) of 3 or 4 (**Table 3**). (10) The lumen dimensions as well as the severity of calcification measured in this analysis are comparable to the observations in the PREPARE-CALC trial reported by Hemetsberger et al. (11) The PREPARE-CALC trial (Comparison of Strategies to Prepare Severely Calcified Coronary Lesions) evaluated the effect of lesion preparation using modified balloons (cutting/scoring) versus RA for interventional treatment of severely calcified coronary lesions. Native and post-procedural OCT were performed in 122 patients who made up the collective for the PREPARE-CALC trial. This OCT study showed that lesion preparation with either modified balloons (cutting/scoring) or RA resulted in similar stent expansion, asymmetry, and eccentricity. Identification of calcified lesions for the ROTA.shock trial was performed in the same way as in the PREPARE-CALC trial, by cineangiography (radiopacities noted without cardiac motion before contrast injection generally compromising both sides of the arterial lumen). (5,11) In contrast to the present study, which analyzed native OCT and OCT immediately after RA or IVL, the PREPARE-CALC trial investigated the effect of the lesion preparation on final OCT scans after stent implantation. Therefore, PREPARE-CALC trial did not analyze the mechanisms of acute effects of lesion preparation by modified balloon or RA but the effect on final stent implantation. To the best of our knowledge, our study is the first to provide high-resolution OCT images for comparison of the acute effects of lesion preparation using RA or IVL on calcified coronary plaques.

Both RA and IVL modify calcified plaques by producing acute luminal gain as well as fractures of the plaque (**Table 4**). The luminal gain achieved by RA, however, is larger than that produced by IVL, most likely due to the direct atherectomy effect of RA. (16,17) Thereby, RA might be better suited to facilitate stent deployment, since it generates a larger “working channel” for further steps of the PCI procedure.

On the other hand, IVL may induce fractures in the calcified plaque in more patients than does RA, although this numerical difference was not significant in the present study. IVL was associated with a significantly higher number, length, and area of fractures in the calcified plaque. This higher degree of plaque fracturing may translate into a better stent expansion, since more and longer fractures may allow an easier dilatation of the calcified plaque. Nevertheless, whether IVL is in fact associated with a better final stent expansion needs to be investigated in future trials and cannot be clarified from our data.

The application of RA or IVL for lesion preparation was associated with dissections in most patients (**Table 4**), which occurred in a similar frequency for the two techniques. The two-dimensional flap length of the dissections was greater after IVL than after RA, whereas the total flap area as well as the three-dimensional length of the dissections did not differ. It is doubtful whether the slightly but significantly longer flap observed here for IVL would be clinically relevant. It is conceivable that a longer flap may be a risk factor for a no-flow/slow-flow situation, since it could hinder the normal blood flow more, but this is speculative; clinical data from the DISRUPT CAD trials did not show a relevant increase in no-flow/slow-flow after application of IVL. (18-21)

This study has some important limitations. First, this is a retrospective analysis with a small number of patients. Despite the fact that ROTA.shock was a randomized study, this current subanalysis has a selection bias, since only patients in whom a native OCT scan as well as an OCT scan immediately after RA or IVL were available were included. Native OCT scans and OCT scans immediately after plaque modification were only available in 21 out of 70 patients. In most patients the imaging catheter could not be advanced through the lesion pre-procedurally. Therefore, it has to be assumed that fewer eccentric and fewer narrow lesions were selected. Nevertheless, pre-procedural OCT analysis confirmed severe lesion calcification with an extent comparable to other studies (5,11).

In addition, the reported rate of predilatation is biased by the fact that the study protocol allowed predilatation in order to acquire a native OCT and was therefore sometimes performed just in order to follow the protocol and acquire a native OCT. However, this bias would have affected both groups in the same way and should not have influenced the final results.

Other important limitations are the lack of outcome data as well as post-procedural OCT data, including stent analysis, since the aim of this analysis was to evaluate only the acute effects of RA and IVL on calcified

coronary plaques. Stent analysis in post-procedural OCT was the purpose of the ROTA.shock trial itself. Data from the ROTA.shock trial demonstrated the non-inferiority of IVL in comparison to RA regarding minimal stent area at the end of the procedure as determined by OCT, and there were no significant differences regarding stent expansion. Additionally, no significant association between the number of calcium fractures or the residual calcified area and the final stent expansion could be observed.

The present study demonstrated that RA and IVL are associated with a visible modification of calcified coronary plaques, as noted from the induction of plaque fractures and acute lumen gain in calcified vessel segments. However, the mechanisms by which the two techniques modify the calcified plaque are different to some extent. These differences should be considered when planning the interventional treatment of severely calcified coronary lesions. RA may be better suited in lesions with high eccentricity to facilitate subsequent balloon or stent deployment due to a larger lumen gain. However, we have to be aware that OCT for this study was acquired immediately after RA or IVL and not after ensuing NC balloon angioplasty, as routinely performed. Hence, we cannot evaluate in what way additional balloon angioplasty would have influenced the lumen gain, especially after IVL. Nevertheless, NC balloon deployment should be easier after RA, since the acute lumen gain is larger than with IVL alone.

IVL on the other hand, may be better suited in lesions with long calcifications, since IVL induces significantly longer fractures of the calcified plaques than RA. Also, the number of fractures induced is higher with IVL than with RA. Hence, calcified plaques with circumferential or nearly circumferential calcification may be better modified by IVL, since it induces a higher number of fractures, although we have to be aware that the fractures with IVL were not deeper or wider than with RA. These fractures of calcified plaques are commonly encountered after IVL therapy of calcified coronary lesions and are presumably one of the most important effects on the calcified plaque. (22-24)

It is obvious that there are differences in the acute mechanisms of plaque modification by RA and IVL, but further investigations will be necessary to evaluate whether the differences observed in this study translate into differences in stent expansion and clinical outcome. For precise planning of the PCI of calcified coronary lesions, the use of intravascular imaging is of great value in order to most accurately analyze the extent of lesion calcification and eccentricity. Nevertheless, the positioning of the imaging catheter may be impaired in lesions with especially extensive calcification and eccentricity, as we observed in the ROTA.shock trial.

Conclusion

RA and IVL are both effective techniques for the modification of calcified coronary plaques. Nevertheless, there are differences in the acute mechanisms of their effects: whereas RA leads to a larger acute lumen gain, IVL induces more and longer fractures of the calcified plaque. These differences should be considered when planning a PCI strategy.

References

1. Madhavan MV, Tarigopula M, Mintz GS, Maehara A, Stone GW, Généreux P. Coronary artery calcification: pathogenesis and prognostic implications. *J Am Coll Cardiol* 2014; 63(17): 1703-1714
2. Généreux P, Madhavan MV, Mintz GS, Maehara A, Palmerini T, Lasalle L, Xu K, McAndrew T, Kirtane A, Lansky AJ, Brener SJ, Mehran R, Stone GW. Ischemic outcomes after coronary intervention of calcified vessels in acute coronary syndromes. Pooled analysis from the HORIZONS-AMI (Harmonizing Outcomes With Revascularization and Stents in Acute Myocardial Infarction) and ACUITY (Acute Catheterization and Urgent Intervention Triage Strategy) TRIALS. *J Am Coll Cardiol* 2014; 63(18): 1845-1854
3. Maejima N, Hibi K, Saka K, Akiyama E, Konishi M, Endo M, Iwahashi N, Tsukahara K, Kosuge M, Ebina T, Umemura S, Kimura K. Relationship Between Thickness of Calcium on Optical Coherence Tomography and Crack Formation After Balloon Dilatation in Calcified Plaque Requiring Rotational Atherectomy. *Circ J* 2016; 80(6): 1413-1419
4. Mintz GS, Popma JJ, Pichard AD, Kent KM, Satler LF, Chuang YC, Ditrano CJ, Leon MB. Patterns of calcification in coronary artery disease. A statistical analysis of intravascular ultrasound and coronary angiography in 1155 lesions. *Circulation* 1995; 91: 1959–1965
5. Abdel-Wahab M, Toelg R, Byrne RA, Geist V, El-Mawardy M, Allali A, Rheude T, Robinson DR, Abdelghani M, Sulimov D, Kastrati A, Richardt G. High-Speed Rotational Atherectomy Versus Modified Balloons Prior to Drug-Eluting Stent Implantation in Severely Calcified Coronary Lesions. Circ Cardiovasc Interv 2018; 11: e007415
6. Tearney GJ, Regar E, Akasaka T, Adriaenssens T, Barlis P, Bezerra HG, Bouma B, Bruining N, Cho JM, Chowdhary S, Costa MA, Silva R, Dijkstra J, Di Mario C, Dudeck D, Falk E, Feldman MD, Fitzgerald P, Garcia H, Gonzalo N, Granada JF, Guagliumi G, Holm NR, Honda Y, Ikeno F, Kawasaki M, Kochman J, Koltowski L, Kubo T, Kume T, Kyono H, Lam CCS, Lamouche G, Lee DP, Leon MB, Maehara A, Manfrini O, Mintz GS, Mizuno K, Morel M, Nadkarni S, Okura H, Otake H, Pietrasik A, Prati F, Räber L, Radu MD, Rieber J, Riga M, Rollins A, Rosenberg M, Sirbu V, Serruys PW, Shimada K, Shinke T, Shite J, Siegel E, Sonada S, Suter M, Takarada S, Tanaka A, Terashima M, Troels T, Uemura S, Ughi GJ, van Beusekom HMM, van der Steen AFW, van Es G, van Soest G, Virmani R, Waxman S, Weissman NJ, Weisz G; International Working Group for Intravascular Optical Coherence Tomography (IWG-IVOCT). Consensus standards for acquisition, measurement, and reporting of intravascular optical coherence tomography studies: a report from the International Working Group for Intravascular Optical Coherence Tomography Standardization and Validation. *J Am Coll Cardiol* 2012; 59: 1058–1072
7. Suwannasom P, Sotomi Y, Ishibashi Y, Cavalcante R, Albuquerque FN, Macaya C, Ormiston JA, Hill J, Lang IM, Egred M, Fajadet J, Lesiak M, Tijssen JG, Wykrzykowskam JJ, de Winter RJ, Chevalier B, Serruys PW. The impact of post-procedural asymmetry, expansion, and eccentricity of bioresorbable everolimus-eluting scaffold and metallic everolimus-eluting stent on clinical outcomes in the ABSORB II trial. *J Am Coll Cardiol Intv* 2016; 9: 1231–1242
8. Ali ZA, Maehara A, Généreux P, Shlofmitz RA, Fabbiocchi F, Nazif TM, Guagliumi G, Meraj PM, Alfonso F, Samady H, Akasaka T, Carlson EB, Leesar MA, Matsumura M, Ozan MU, Mintz GS, Ben-Yehuda O, Stone GW. ILUMIEN III: OPTIMIZE PCI Investigators. Optical coherence tomography compared with intravascular ultrasound and with angiography to guide coronary stent implantation (ILUMIEN III: OPTIMIZE PCI): a randomised controlled trial. *Lancet* 2016; 388: 2618–2628
9. Suwannasom P, Sotomi Y, Asano T, Koon JN, Tateishi H, Zeng Y, Tenekecioglu E, Wykrzykowska JJ, Foin N, de Winter RJ, Ormiston JA, Serruys PW, Onuma Y, on behalf of the investigators of the ABSORB Cohort B study. Change in lumen eccentricity and asymmetry after treatment with Absorb bioresorbable vascular scaffolds in the ABSORB cohort B trial: a five-year serial optical coherence tomography imaging study. *EuroIntervention* 2017; 12: e2244–e2252
10. Fujino A, Mintz GS, Matsumura M, Lee T, Kim SY, Hoshino M, Usui E, Yonetsu T, Haag ES, Shlofmitz RA, Kakuta T, Maehara A. A new optical coherence tomography-based calcium scoring system to predict stent underexpansion. *EuroIntervention* 2018; 13: e2182–e2189
11. Hemetsberger R, Gori T, Toelg R, Byrne R, Allali A, El-Mawardy M, Rheude T, Weissner M, Sulimov DS, Robinson DR, Richardt G, Abdel-Wahab M. Optical Coherence Tomography Assessment in Patients Treated With Rotational Atherectomy Versus Modified Balloons: PREPARE-CALC OCT. *Circ Cardiovasc Interv* 2021; 14(3): e009819
12. Kini AS, Vengrenyuk Y, Pena J, Motoyama S, Feig JE, Meelu OA, Rajamanickam A, Bhat AM, Panwar S, Baber U, Sharma SK. Optical coherence tomography assessment of the mechanistic effects of rotational and orbital atherectomy in severely calcified coronary lesions. *Catheter Cardiovasc Interv* 2015; 86(6): 1024-1032
13. Tanimura K, Otake H, Kawamori H, Toba T, Nagasawa A, Sugizaki Y, Takeshige R, Nakano S, Matsuoka Y, Takahashi Y, Fukuyama Y, Hirata KI. Prediction of the debulking effect of rotational atherectomy using optical frequency domain imaging. *Heart Vessels* 2021; 36(9): 1265-1274

14. Amemiya K, Yamamoto MH, Maehara A, Oyama Y, Igawa W, Ono M, Kido T, Ebara S, Okabe T, Yamashita K, Hoshimoto K, Saito S, Yakushiji T, Isomura N, Araki H, Mintz GS, Ochiai M. Effect of cutting balloon after rotational atherectomy in severely calcified coronary artery lesions as assessed by optical coherence tomography. *Catheter Cardiovasc Interv* 2019; 94(7): 936-944
15. Karimi Galougahi K, Shlofmitz RA, Ben-Yehuda O, Généreux P, Maehara A, Mintz GS, Stone GW, Moses JW, Ali ZA. Guiding Light: Insights Into Atherectomy by Optical Coherence Tomography. *J Am Coll Cardiol Intv* 2016; 9(22): 2362-2363
16. Yamamoto MH, Maehara A, Karimi Galougahi K, Mintz GS, Parviz Y, Kim SS, Koyama K, Amemiya K, Kim SY, Ishida M, Losquadro M, Kirtane AJ, Haag E, Sosa FA, Stone GW, Moses JW, Ochiai M, Shlofmitz RA, Ali ZA. Mechanisms of Orbital Versus Rotational Atherectomy Plaque Modification in Severely Calcified Lesions Assessed by Optical Coherence Tomography. *J Am Coll Cardiol Intv* 2017; 10(24): 2584-2586
17. Attizzani GF, Patrício L, Bezerra HG. Optical coherence tomography assessment of calcified plaque modification after rotational atherectomy. *Catheter Cardiovasc Interv* 2013; 81(3): 558-561
18. Brinton TJ, Ali ZA, Hill JM, Meredith IT, Maehara A, Illindala U, Lansky A, Götberg M, Van Mieghem NM, Whitbourn R, Fajadet J, Di Mario C. Feasibility of Shockwave Coronary Intravascular Lithotripsy for the Treatment of Calcified Coronary Stenoses. *Circulation* 2019; 139(6): 834-836
19. Ali ZA, Nef H, Escaned J, Werner N, Banning AP, Hill JM, De Bruyne B, Montorfano M, Lefevre T, Stone GW, Crowley A, Matsumura M, Maehara A, Lansky AJ, Fajadet J, Di Mario C. Safety and Effectiveness of Coronary Intravascular Lithotripsy for Treatment of Severely Calcified Coronary Stenoses: The Disrupt CAD II Study. *Circ Cardiovasc Interv* 2019; 12(10): e008434
20. Hill JM, Kereiakes DJ, Shlofmitz RA, Klein AJ, Riley RF, Price MJ, Herrmann HC, Bachinsky W, Waksman R, Stone GW; Disrupt CAD III Investigators. Intravascular Lithotripsy for Treatment of Severely Calcified Coronary Artery Disease. *J Am Coll Cardiol* 2020; 76(22): 2635-2646
21. Saito S, Yamazaki S, Takahashi A, Namiki A, Kawasaki T, Otsuji S, Nakamura S, Shibata Y; Disrupt CAD IV Investigators. Intravascular Lithotripsy for Vessel Preparation in Severely Calcified Coronary Arteries Prior to Stent Placement - Primary Outcomes From the Japanese Disrupt CAD IV Study. *Circ J* 2021; 85(6): 826-833
22. Hlinomaz O, Tejc M, Sabbah M. Shockwave Lithotripsy vs Rotational Atherectomy: Mechanistic Differences From Optical Coherence Tomography. *J Invasive Cardiol* 2021; 33(2): E136-E137
23. La Manna A, D'Agosta G, Venuti G, Tamburino C. Cracking the Plaque With Coronary Lithotripsy: Mechanistic Insights From Optical Coherence Tomography. *J Invasive Cardiol* 2020; 32(1): E14
24. Ozdemir D, Karimi Galougahi K, Petrossian G, Ezratty C, Dominguez-Sulca D, Chowdhury E, Scheiner J, Thomas SV, Shlofmitz RA, Ali ZA. Calcific Plaque Modification by Acoustic Shockwaves: Intravascular Lithotripsy in Cardiovascular Interventions. *Curr Cardiol Rep* 2022; 24(5): 519-528

Legends for figures

Figure 1: Representative OCT analysis after IVL
OCT cross-section of a severely calcified coronary stenosis after treatment with IVL is shown on the left. Fractures of the calcified plaque are visible at 3, 7, and 10 o'clock. On the right the same cross-section is shown with representative analysis of a calcified plaque at 10 to 4 o'clock and a fracture at 3 o'clock.

Figure 2: OCT analysis of an intima dissection after RA
OCT cross-section of a severely calcified coronary stenosis after treatment with RA is shown on the left. Fractures of the calcified plaque are visible at 3 and 12 o'clock. An intima dissection is visible at 8 to 9 o'clock. On the right the same cross-section is shown with representative analysis of the dissection.

Figure 3: Comparison of plaque modification by IVL and RA
A, **B**, and **C** show OCT cross-sections of severely calcified lesions after treatment with IVL. **D**, **E**, and **F** show OCT cross-sections of severely calcified lesions after treatment with RA.
IVL = intravascular lithotripsy; RA = rotational atherectomy

Tables

Table 1: Baseline characteristics

	Overall (n = 21)	RA (n = 9)	IVL (n = 12)	P-value
Age (years)	78.1 ± 8.1	81.4 ± 6.9	76.3 ± 7.0	0.16
Male sex	17 (81)	7 (77.8)	10 (83.3)	0.51
BMI (kg/m^2)	27.2 ± 4.5	27.1 ± 3.5	27.7 ± 5.3	0.75
Previous MI	9 (42.9)	4 (44.4)	5 (41.7)	0.73
Previous PCI	15 (71.4)	6 (66.7)	9 (75.0)	0.69
Previous CABG	1 (4.8)	1 (11.1)	0 (0)	0.26
Hypertension	21 (100)	9 (100)	12 (100)	>0.99
Diabetes mellitus	7 (33.3)	3 (33.3)	4 (33.3)	>0.99
Hyperlipidemia	16 (76.2)	6 (66.7)	10 (83.3)	0.40
Active smoking	2 (9.5)	1 (11.1)	1 (8.3)	0.79
LVEF (%)	56.2 ± 6.9	57.5 ± 3.8	55.3 ± 8.4	0.12
Clinical presentation				
STEMI	0 (0.0)	0 (0.0)	0 (0.0)	>0.99
NSTEMI	2 (9.5)	1 (11.1)	1 (8.3)	0.79
Unstable angina	2 (9.5)	0 (0.0)	2 (16.7)	0.23
Stable CAD	17 (81.0)	8 (88.9)	9 (75.0)	0.59

Values provided as mean ± standard deviation or n (%).
Abbreviations: RA: rotational atherectomy; IVL: intravascular lithotripsy; BMI: body-mass index; MI: myocardial infarction; PCI: percutaneous coronary intervention; CABG: coronary artery bypass graft; LVEF: left ventricular ejection fraction; STEMI: ST-elevation myocardial infarction; NSTEMI: non- ST-elevation myocardial infarction; CAD: coronary artery disease.

Table 2: Procedural characteristics

	Overall (n=21)	RA (n=9)	IVL (n=12)	P-value
Target vessel				0.12
LM	0 (0.0)	0 (0.0)	0 (0.0)	
LAD	11 (52.4)	3 (33.3)	8 (66.7)	
Cx	2 (9.5)	1 (11.1)	1 (8.3)	
RCA	8 (38.1)	5 (55.6)	3 (25.0)	
Femoral access	5 (23.8)	2 (22.2)	3 (25.0)	0.89
Radial access	16 (76.2)	7 (77.8)	9 (75.0)	0.89
Maximum sheath size (french)	6.2 ± 0.4	6.2 ± 0.4	6.2 ± 0.4	0.77
Lesion length (mm)	18 ± 7	17 ± 9	18 ± 8	0.66
Predilatation	7 (33.3)	3 (33.3)	4 (33.3)	>0.99
Maximum pressure (atm)	15.4 ± 7.4	16.3 ± 8.2	15.0 ± 5.8	0.42
Maximum balloon diameter (mm)	2.67 ± 0.55	2.66 ± 0.50	2.70 ± 0.49	0.61
RA maximum burr size (mm)		1.55 ± 0.25		
RA number of runs		3.7 ± 1.1		
IVL balloon diameter (mm)			3.04 ± 0.28	
IVL number of treatment cycles			4.8 ± 3.0	

Values provided as mean ± standard deviation or n (%).
Abbreviations: RA: rotational atherectomy; IVL: intravascular lithotripsy; LM: left main artery; LAD: left anterior descending artery; Cx: circumflex artery; RCA: right coronary artery

Table 3: Native OCT analysis

	Overall (n=21)	RA (n=9)	IVL (n=12)	P-value
Number of frames	260 ± 108	275 ± 152	249 ± 65	0.63
Length of OCT run (mm)	28.7 ± 11.3	31.7 ± 15.3	26.4 ± 7.0	0.46
Mean lumen diameter (mm)	2.63 ± 0.53	2.75 ± 0.72	2.55 ± 0.35	0.28
Mean lumen area (mm^2)	5.90 ± 2.41	6.52 ± 3.21	5.44 ± 1.58	0.38
Minimum lumen diameter (mm)	1.68 ± 0.49	1.70 ± 0.60	1.66 ± 0.42	0.89
Minimum lumen area (mm^2)	2.39 ± 1.32	2.51 ± 1.65	2.29 ± 1.09	0.76
Maximum lumen diameter (mm)	3.62 ± 0.81	3.69 ± 0.83	3.57 ± 0.83	0.82
Maximum lumen area (mm^2)	10.77 ± 4.99	11.15 ± 4.34	10.48 ± 5.60	0.94
Maximum lumen eccentricity	0.36 ± 0.15	0.34 ± 0.22	0.37 ± 0.09	0.42
Maximum lumen asymmetry	0.77 ± 0.12	0.77 ± 0.13	0.77 ± 0.11	0.81
Mean reference area (mm^2)	6.62 ± 2.11	6.40 ± 2.39	6.78 ± 2.02	0.66
Mean reference diameter (mm)	2.90 ± 0.62	2.85 ± 0.61	3.01 ± 0.52	0.72
Mean lumen area stenosis (%)	66.4 ± 14.6	64.8 ± 12.2	67.3 ± 14.0	0.67
Calcified plaque				
Maximum angle (°)	259.4 ± 81.3	246.5 ± 66.7	269.6 ± 88.1	0.28
Mean angle (°)	119.9 ± 22.8	113.9 ± 12.4	124.9 ± 25.0	0.14
Mean thickness (mm)	0.62 ± 0.11	0.58 ± 0.14	0.64 ± 0.08	0.17
Maximum thickness (mm)	1.13 ± 0.17	1.13 ± 0.17	1.13 ± 0.18	0.86
Minimum thickness (mm)	0.22 ± 0.11	0.19 ± 0.12	0.24 ± 0.10	0.38
Minimum cap thickness (mm)	0.19 ± 0.16	0.15 ± 0.06	0.21 ± 0.20	0.65
Total length (mm)	16.14 ± 5.52	16.00 ± 4.67	16.25 ± 6.30	0.86
Total volume (mm^3)	49.23 ± 25.52	47.09 ± 27.20	50.20 ± 23.99	0.76
Plaque rupture	2 (9.5)	0 (0)	2 (16.7)	0.23
Plaque erosion	1 (4.8)	1 (11.1)	0 (0)	0.35
Red thrombus	0 (0)	0 (0)	0 (0)	>0.99
White thrombus	1 (4.8)	0 (0)	1 (8.3)	0.30
Dissection	0 (0)	0 (0)	0 (0)	>0.99

OCT-based calcium score				
1	0 (0)	0 (0)	0 (0)	0.89
2	1 (4.8)	1 (11.1)	0 (0)	
3	8 (38.1)	3 (33.3)	5 (41.7)	
4	12 (57.1)	5 (55.6)	7 (58.3)	
Number of calcified nodules	1.5 ± 2.4	2.5 ± 3.4	1.1 ± 1.1	0.81

Values provided as mean ± standard deviation or n (%).

Abbreviations: RA: rotational atherectomy; IVL: intravascular lithotripsy

Table 4: Post RA/IVL OCT analysis

	Overall (n=21)	RA (n=9)	IVL (n=12)	P-value
Number of frames	254 ± 99	265 ± 139	246 ± 61	0.71
Length of OCT run (mm)	28.2 ± 11.2	31.0 ± 15.3	26.1 ± 6.7	0.39
Mean lumen diameter (mm)	2.71 ± 0.60	2.83 ± 0.79	2.62 ± 0.41	0.48
Mean lumen area (mm^2)	6.20 ± 2.76	6.98 ± 3.68	5.61 ± 1.76	0.33
Minimum lumen diameter (mm)	2.00 ± 0.56	1.92 ± 0.76	2.05 ± 0.38	0.65
Minimum lumen area (mm^2)	3.37 ± 1.97	3.31 ± 2.80	3.41 ± 1.17	0.39
Maximum lumen diameter (mm)	3.62 ± 0.84	3.98 ± 1.04	3.36 ± 0.57	0.19
Maximum lumen area (mm^2)	10.84 ± 5.81	13.17 ± 6.29	9.09 ± 3.31	0.19
Maximum lumen eccentricity	0.42 ± 0.15	0.39 ± 0.19	0.45 ± 0.12	0.39
Maximum lumen asymmetry	0.67 ± 0.13	0.75 ± 0.13	0.62 ± 0.11	0.20
Mean reference area (mm^2)	6.65 ± 2.10	6.44 ± 2.40	6.78 ± 2.12	0.70
Mean reference diameter (mm)	2.93 ± 0.55	2.85 ± 0.65	3.05 ± 0.59	0.67
Mean lumen area stenosis (%)	60.7 ± 14.8	58.8 ± 13.9	61.5 ± 14.5	0.42
Luminal gain (mm^2)	0.31 ± 0.21	0.46 ± 0.16	0.17 ± 0.14	0.03
Calcified plaque				
Maximum angle (°)	238.4 ± 81.3	234.5 ± 66.7	241.6 ± 88.1	0.68
Mean angle (°)	114.4 ± 26.5	110.6 ± 21.6	116.5 ± 29.6	0.61
Mean thickness (mm)	0.63 ± 0.14	0.61 ± 0.18	0.65 ± 0.10	0.48
Maximum thickness (mm)	1.11 ± 0.19	1.11 ± 0.21	1.11 ± 0.18	0.97
Minimum thickness (mm)	0.25 ± 0.10	0.24 ± 0.10	0.26 ± 0.11	0.56
Minimum cap thickness (mm)	0.19 ± 0.10	0.20 ± 0.07	0.18 ± 0.07	0.54
Total length (mm)	16.18 ± 5.53	16.02 ± 4.67	16.27 ± 6.04	0.68
Total volume (mm^3)	47.42 ± 26.00	45.66 ± 29.29	49.13 ± 24.02	0.82
Red thrombus	0 (0)	0 (0)	0 (0)	>0.99
White thrombus	5 (23.4)	2 (22.2)	3 (25.0)	0.80
Fractures of calcified plaque present	14 (66.7)	4 (44.4)	10 (83.3)	0.15
Number of calcified plaque fractures	2.68 ± 0.50	1.67 ± 0.52	3.23 ± 0.49	<0.001

Fractures of calcified plaque				
Maximum depth (mm)	0.67 ± 0.36	0.63 ± 0.41	0.72 ± 0.47	0.96
Mean depth (mm)	0.52 ± 0.19	0.55 ± 0.22	0.47 ± 0.18	0.66
Maximum width (mm)	0.53 ± 0.26	0.50 ± 0.19	0.60 ± 0.21	0.73
Mean width (mm)	0.36 ± 0.24	0.36 ± 0.07	0.36 ± 0.10	0.99
Maximum length (mm)	2.32 ± 1.44	2.20 ± 2.22	3.81 ± 1.42	0.06
Mean length (mm)	1.19 ± 0.58	0.57 ± 0.55	1.67 ± 0.43	0.01
Maximum area (mm^2)	0.27 ± 0.24	0.21 ± 0.05	0.26 ± 0.25	0.80
Mean area (mm^2)	0.15 ± 0.19	0.16 ± 0.07	0.14 ± 0.09	0.78
Total volume (mm^3)	1.13 ± 0.74	0.48 ± 0.27	1.47 ± 0.40	0.003
Maximum angle (°)	22.5 ± 12.2	21.3 ± 16.8	23.4 ± 14.6	0.85
Mean angle (°)	14.5 ± 6.5	13.4 ± 5.6	15.5 ± 6.2	0.70
Mean angle of fractures/mean angle of calcified plaque (%)	6.49 ± 6.15	5.10 ± 4.05	8.13 ± 5.60	0.29
Dissections present	16 (76.2)	7 (77.8)	9 (75.0)	0.90
Dissections (n)	2.09 ± 1.52	2.00 ± 1.58	2.33 ± 1.78	0.60
Dissections				
Maximum flap length (mm)	1.75 ± 0.77	1.31 ± 0.65	2.12 ± 0.53	0.06
Mean flap length (mm)	1.08 ± 0.34	0.83 ± 0.21	1.26 ± 0.25	0.03
Mean length (mm)	3.21 ± 2.67	2.94 ± 2.09	3.48 ± 2.44	0.34
Maximum area (mm^2)	0.59 ± 0.36	0.47 ± 0.37	0.67 ± 0.35	0.12
Mean area (mm^2)	0.30 ± 0.15	0.26 ± 0.18	0.35 ± 0.14	0.26
Total volume (mm^3)	2.36 ± 1.82	1.80 ± 1.56	3.14 ± 2.18	0.19

Values provided as mean ± standard deviation or n (%).

Abbreviations: RA: rotational atherectomy; IVL: intravascular lithotripsy

Figures

Figure 1

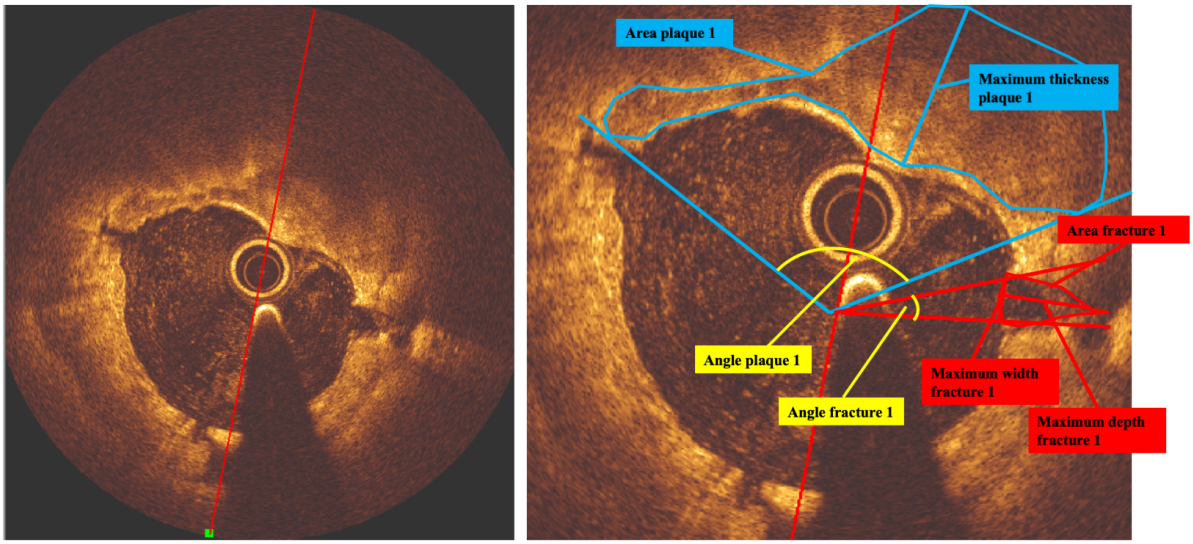

Figure 2

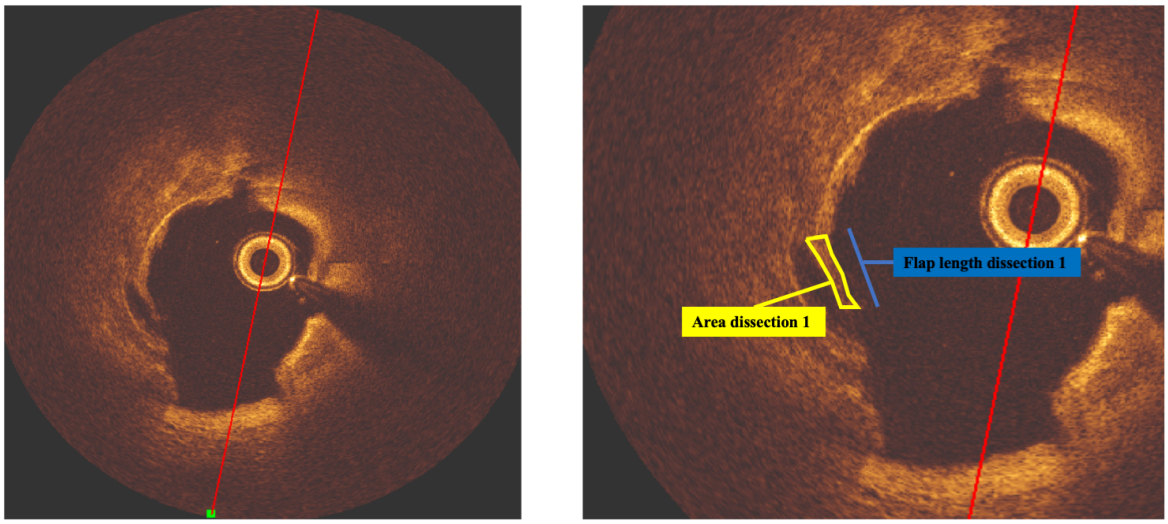

Figure 3